Using fruit fly eyes as membrane protein factories: Expression of rat P2X2 and pannexin-1 in *Drosophila melanogaster*

A thesis submitted for the degree of Doctor of Philosophy

By

Leanne Grimes

2015

Cardiff School of Biosciences

Cardiff University

Thesis summary – Leanne Grimes

P2X receptors and pannexins (Panx) are eukaryotic ion channels that are implicated in a range of diseases and conditions including cancer, inflammation and pain sensation and as a result, are important therapeutic targets. Deducing their 3D-structures would enable the use of structure-based drug design to identify novel agonists or antagonists. However, solving eukaryotic membrane protein structures is a significant challenge due to the requirement for high yields of purified folded, functional protein, which are not readily obtainable with conventional over-expression systems. By using P2X receptors and pannexins as model ion channel targets, this thesis aims to test *Drosophila melanogaster* as a system for the over-expression and functional analysis of eukaryotic ion channels. A number of epitope-tagged P2X and Panx protein constructs were generated and first expressed in HEK-293 cells (rat P2X2-GFP, human P2X4-GFP, rat Panx1-GFP and human P2X4-int-CBD (chitin binding domain)) to allow their expression, glycosylation and oligomeric states to be investigated as markers of protein folding and quality. Subsequently, rat P2X2-GFP and rat Panx1-GFP constructs were successfully expressed in the photoreceptor cells of *Drosophila melanogaster*, where the photoreceptive membrane in the visual system is organised into a densely packed brush of microvilli, the rhabdomere. This system provides a large surface area of membrane for protein expression. Although the yields of purified protein were lower than expected, rat Panx1-GFP was successfully purified and used for low resolution structural studies with transmission electron microscopy. Rat P2X2-GFP was also expressed in the nervous system of *Drosophila* under control of a pan-neural, *C155-Gal4* driver and was shown to be functional by measuring ATP-evoked action potentials using electrophysiological recordings of the *Drosophila* taste sensilla. This system was also used to test the activity of an adenosine nucleotide library of 80 compounds. Three nucleotides were identified that elicited responses similar to ATP; these were 2F-ATP, ATPαS and ATPγS.

Acknowledgements

Firstly, I would like to thank everyone I have worked with throughout my PhD for making it a fun and enjoyable time, particularly Clare, Jonathan, Marta, Stuart, Gordon and Alina.

Thank you to my supervisors Mark and Wynand for giving me this experience, and all their help and support throughout the last three years. I would also like to thank my advisor Pete for the assistance he has provided.

Thanks to Clare and Sonia for their help and input into my project, specifically with injecting constructs into flies and to my project student Hannah Garrard for all her hard work and contribution to this work.

I would also like to thank my Mum, Dad, Alex and Chris for all their support over the years. And I would like to thank my housemate Hannah for providing me with a glass of wine and a social life over the past year.

Abbreviations

2APB – 2-Aminoethoxydiphenyl borate

ADP – Adenosine diphosphate

AFM – Atomic force microscopy

AMP – Adenosine monophosphate

AMPA - α-amino-3-hydroxy-5-methyl-4-isoxazolepropionic acid

ATP – Adenosine triphosphate

BSA – Bovine serum albumin

CBD – Chitin binding domain

CIA – Collagen induced arthritis

CMC – critical micelle concentration

CNS – Central nervous system

COP-II – Coat-protein II

DAG – Diacyl glycserol

DDM – n-Dodecyl B maltoside

dNTP – deoxynucleotide triphosphate

DTT – Dithiothreitol

DRG – Dorsal root ganglion

EDTA – Ethylenediaminetetraacetic acid

EEA-1 – Early endosome antigen marker-1

Endo H – Endoglycosidase H

ER – Endoplasmic reticulum

FC-12 – Foscholine 12

FCS – Foetal calf serum

FSEC – Fluorescence size exclusion chromatography

GCUA – Graphical codon usage analyser

GDP – Guanosine diphosphate

GFP – Green fluorescent protein

GMR – Glass multimer reporter

GnTI – N-acetylglucosaminyltransferase I

GRN – Gustatory receptor neuron

GTP – Guanosine triphosphate

GPCR – G-protein-coupled receptor

HEK – Human embryonic kidney

HIV-1 – Human immunodeficiency virus type-1

IEC – Ion exchange chromatography

IMAC – Immobilised metal affinity chromatography

IL-1β – Interleukin 1 β

IP - Immunoprecipitation

IP_3 – inositol triphospate

LGIC – Ligand-gated ion channel

MCS – multiple cloning site

NMDA – N-methyl-d-aspartate

NO – Nitric oxide

N-OG – N-octyl glucosamine

NP40 – nonyl phenoxypolyethoxyethanol

Panx – Pannexin

PBS – Phosphate buffered saline

PCR – polymerase chain reaction

PDB – Protein Databank

PFO – Perfluoro-octanoic acid

PFO-PAGE - Perfluoro-octanoic acid polyacrylamide gel electrophoresis

PIP_2 – Phosphatidyl inositol 4, 5-bisphosphate

PLC – Phospholipase-C

PNGase F - Peptide-N4-(N-acetyl-beta-glucosaminyl)asparagine F

PPADS – Pyridoxal-phosphate-6-azophenyl-2'4'-disulfonic acid

SBDD - Structure based drug design

SD – Standard deviation

SDM – Site directed mutagenesis

SDS – Sodium dodecyl sulphate

SERT – Serotonin transporter

SEM – Standard error of the mean

SNP – single nucleotide polymorphisms

SOG – subesophageal ganglion

SRP – Signal recognition particle

TBS – Tris buffered saline

TCC – Tricholine citrate

TCS – Thrombin cleavage site

TCEP - Tris(2-carboxyethyl)phosphine

TM – Transmembrane

UAS – Upstream activating sequence

Table of Contents

Chapter 1 - Introduction

1.1 Membrane proteins

1.1.1 Classes of membrane proteins

Membrane proteins are embedded within or interact with the membrane lipid bilayer and are responsible for mediating many interactions between the cytoplasm of the cell and the extracellular environment. There are two main classes of membrane proteins; integral and peripheral proteins. Integral membrane proteins are embedded within the lipid bilayer, and are only displaced from the bilayer by the action of membrane-disrupting agents such as detergents (see section 1.2.1). Within the class of integral membrane proteins are the sub-classes of monotopic (partially embedded), bitopic (one transmembrane-spanning domain (TM) and polytopic (more than one TM) membrane proteins. Peripheral membrane proteins are not directly associated with the bilayer but interact with other membrane proteins (Lodish *et al*, 2000). There are many different types of membrane proteins including ion channels which gate the flow of ions across the membrane (Gadsby, 2009), G-protein coupled receptors (GPCRs) which activate intracellular signalling cascades in response to extracellular messages (Neer, 1995), receptor tyrosine kinases which respond to many growth factors and hormones (Lemmon and Schlessinger, 2010) and the Na^+/K^+ ATPase which pumps potassium and sodium ions into and out of the cell respectively by active transport (Morth *et al*, 2007). The variety in types and structures of ion channels reflects their involvement in almost all key cellular processes.

1.1.2 Membrane proteins as drug targets

Due to the importance of membrane proteins at the interface of the cell and the extracellular environment, they have many physiological roles in the body, impacting on a huge number of conditions including pain sensation (Tsuda et al, 2003), rheumatoid arthritis (Ardissone *et al*, 2011), cystic fibrosis (Taylor *et al*, 1999) and cancer (Di Virgilio *et al,* 2009; Arinaminpathy et al, 2009; Inoue et al, 2005; North and Jarvis, 2013). Therefore they are key therapeutic targets, representing over 60% of current drug targets (Arinaminpathy *et al*, 2009).

1.1.3 The use of structure based drug design

Many drugs have been developed against membrane proteins using high-throughput screening approaches, but this is expensive and time-consuming. The recent advances in membrane protein structure determination have opened up the possibility of using structure based drug

design (SBDD). 3D crystal structures of membrane proteins are vitally important for assisting SBDD. One of the first examples of the use of SBDD was the design of an inhibitor of the protease of human immunodeficiency virus type-1 (HIV-1) which was based on the 3D symmetry of the HIV-1 protease active site (Erickson *et al*, 1990). Three years later, in 1993, two potent inhibitors of influenza virus sialidase were designed based on its crystal structure (von Itzstein *et al*, 1993). More recently, drug discovery has vastly increased due to the development of docking tools and computer-aided resources that aide the rational design of drugs based on crystal structures (Mandal *et* al, 2009; Muller, 2009). The structure of AmpC β-lactamase was used in 2001 to design inhibitors useful for targeting antibiotic resistance (Tondi *et al*, 2001). In 2012, potent, selective antagonists of the adenosine A2A receptor were identified using SBDD to target molecules in the orthosteric binding cavity of the crystal structure for the potential treatment of Parkinson's disease (Congreve *et al,* 2012). Additionally, in 2014, the chromone antagonists of the adenosine A2A receptor were designed. Antagonists of A2A receptors may provide potential therapies for central nervous system (CNS) disorders (Andrews *et al*, 2014). These are just a small number of examples which represent the recent progress of drug discovery using SBDD.

It is clear that structure determination is necessary for SBDD but for membrane proteins this has proven to be difficult for a number of reasons. One significant problem is that when integral membrane proteins are removed from the membrane they often get degraded, misfold or aggregate due to their instability and the formation of hydrophobic interactions. To overcome these problems, membrane proteins must be solubilised in detergent (see section 1.2.1) (Carpenter *et al*, 2008). Additionally, conventional expression systems only enable membrane proteins to be expressed at low levels (see section 1.2.2) making obtaining a high enough yield of protein for 3D-crystallisation time-consuming and costly (Wuu and Swartz, 2008). This explains why membrane protein structures only account for approximately 2% of known protein structures (RCSB Protein Data Bank, accessed 12/05/14, Protein Data Bank of Transmembrane Proteins, accessed 12/05/14) despite accounting for 20 - 30% of all proteins in an organism (Stevens and Arkin, 2000).

1.1.4 Ion channels

Ion channels are an important class of integral membrane proteins that form pores and allow the passage of large numbers of specific ions across the membrane by passive diffusion along their electrochemical gradient. Ion channels can be opened by various means including changes in voltage, binding of ligands or by post-translational modifications (Alberts *et al*,

2002). In addition their expression at the membrane can be strictly regulated. Ion channels play major roles in the control of electrical excitability by regulating the flow of ions across the membrane of cells such as epithelial and secretory cells (Jentsch *et al*, 2004). Additionally, intracellular ion channels are responsible for calcium release from intracellular stores which can lead to various downstream signalling cascades important in cellular processes. Impairment of ion channel function can have extreme consequences leading to phenotypes such as hypertension, cardiac arrhythmias and neurological diseases (Jentsch *et al*, 2004).

Advancements in expression systems, crystal screening and data acquisition technology has led to a significant recent growth in publication of ion channel 3D-structures. Some of the published crystal structures include the CLC chloride channel from *Salmonella typhimurium* (3 Å – Protein Data Bank (PDB) 1KPL) (Dutzler *et al,* 2002) and *E. coli* (2.51 Å – PDB 1OTS) (Dutzler *et al*, 2003), the Torpedo nicotinic acetylcholine receptor (4 Å – PDB 2BG9) (Unwin, 2005) and the closed and open state structures of P2X4 from the zebrafish, *Danio rerio* at 2.9 and 2.8 Å respectively from *sf*9 cells (Hattori and Gouaux, 2012). More recently, a number of mammalian ion channel structures have been solved including the rat GluN1/GluN2B heterotetrameric NMDA (N-methyl-d-aspartate) receptor ion channel at a resolution of 4 Å from *sf9* insect cells (PDB – 4TLL/4TLM) (Karakas and Furukawa, 2014), and the mouse serotonin 5-HT_3 receptor at a resolution of 3.5 Å from the human T-Rex-293 cell line (PDB – 4PIR) (Hassaine *et al*, 2014). Thus the field of ion channel structure is rapidly growing due to their huge importance as targets for therapeutic drugs.

1.2 Challenges encountered in membrane protein structure determination

1.2.1 Solubilisation of membrane proteins

The membrane bilayer phospholipids are arranged with their polar head groups exposed to the cytoplasm and extracellular space, while the hydrophobic lipid chains fill the inside of the bilayer (Bretscher 1972). Membrane proteins comprise of hydrophobic transmembrane regions and hydrophilic intracellular and extracellular domains (Rees *et al*, 1989). Their unique protein topology makes them particularly difficult to solubilise due to aggregation of the hydrophobic regions in solution, thus membrane proteins must be successfully reconstituted in detergent in order for solubilisation to occur when they are removed from their native membrane environment (Garavito and Ferguson-Miller, 2001). Detergents are amphipathic molecules consisting of a polar head group and a hydrophobic carbon tail which form micelles in solution so that only polar residues are exposed to the aqueous environment. Their amphipathicity makes them ideal for membrane protein solubilisation as the non-polar tails surround the transmembrane protein regions, with the polar head groups exposed to the aqueous environment, see Fig 1.1 (Seddon *et al*, 2004). However, finding a detergent that can efficiently remove the protein of interest from the membrane and retain its native structure can prove challenging.

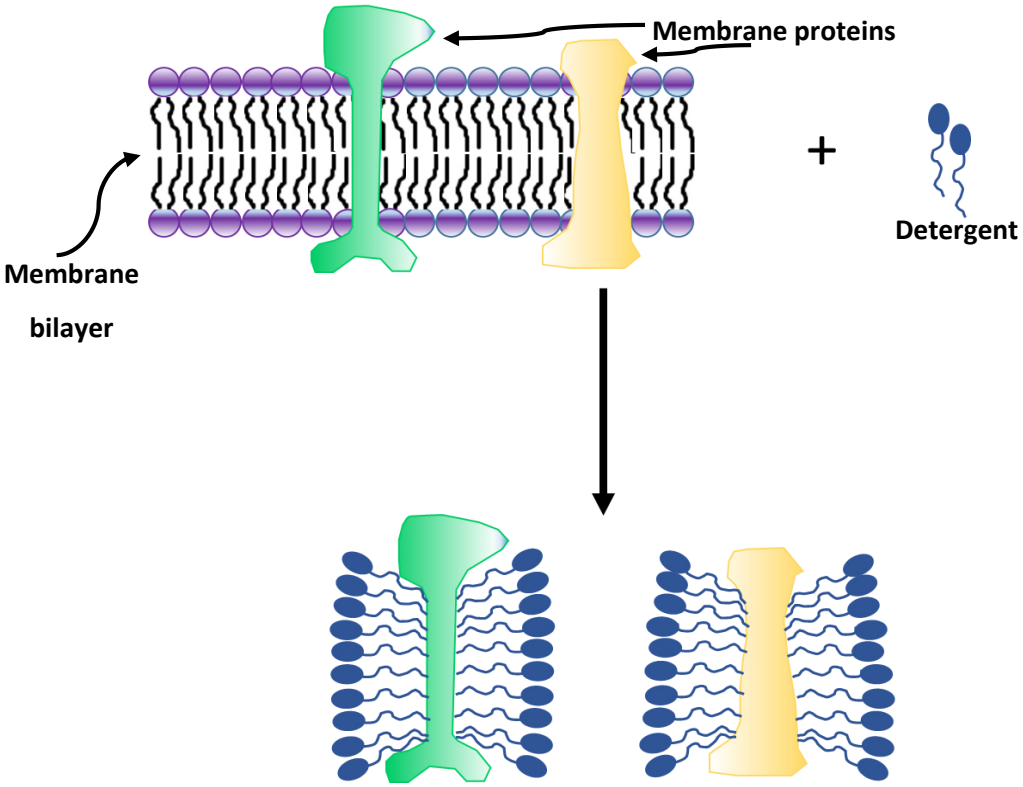

Figure 1.1 – Detergent solubilisation of membrane protein. (Top) Membrane proteins within the phospholipid bilayer of the membrane. Upon incubation with a concentration of detergent above the critical micelle concentration (CMC), the detergent disrupts the membrane and the hydrophobic detergent tails surround the hydrophobic regions of the protein, enabling solubilisation (bottom). Excess detergent forms pure detergent micelles and mixed lipid micelles.

1.2.2 Membrane protein expression systems

The majority of membrane proteins are only expressed at low levels in their endogenous environment, making it essential to overexpress these proteins in other systems to gain a high yield of protein. For example, the serotonin transporter (SERT) was overexpressed in both baculovirus systems and mammalian cells where expression levels did not exceed 250,000 copies/cell (Tate, 2001). Many of the membrane protein structures solved to date were successful, at least in part, due to their specialised, natural abundance in the membrane. For example, the structure of rhodopsin, which is naturally present at high levels in the eye (rhodopsin levels in mouse photoreceptor cells estimated to be approximately $8 \times 10^7 - 1.6 \times 10^8$ molecules per cell (Palczewski, 2006) and in *Drosophila* photoreceptor cells about 2×10^8 molecules per cell (Johnson and Pak, 1986)) was solved to 2.8 Å in 2000 (Palczewski *et al*, 2000). In addition, the first membrane protein structure solved was the photosynthetic reaction centre from *Rhodopseudomonas viridis* at 3Å resolution in 1985. The reaction centre

was naturally expressed at high levels and was purple in colour due to the presence of co-factors. The coloured nature of the protein not only assisted in purification procedures but was also useful in tracking protein quality; any changes in protein colour would have provided information on the cofactor environment of the protein and thus protein quality (Deisenhofer *et al*, 1985).

E. coli, yeast, insect cells and mammalian cells are commonly used systems for membrane protein over-expression. However there is no single system available which is suitable for the expression of all membrane proteins; each system has a number of limitations for membrane protein expression. Overexpression of membrane protein can often lead to protein aggregation, making it difficult to produce high levels of functional, folded protein in many systems (Mus-Veteau, 2010).

1.2.2.1 *E. coli*

Prokaryotic hosts such as *E. coli* are often used for exogenous protein expression due to their short generation time, simplicity and low maintenance costs. However, membrane proteins over-expressed in *E. coli* can encounter problems with protein folding and membrane targeting. A high level of heterologous membrane protein expression in *E. coli* frequently leads to the formation of inclusion bodies, which consist of highly aggregated protein. The unfolded, aggregated protein cannot be used directly for structural or functional experiments without complex refolding techniques (Palmer and Wingfield, 2004).

Inclusion bodies predominantly consist of recombinant protein (99%), chaperones and membrane fragments. An advantage to the formation of inclusion bodies is that these complexes can contain very high levels of membrane protein at high purity that would otherwise cause toxicity to the host. The aggregates can be separated from the cell using centrifugation and the protein is protected from proteolysis and degradation. High concentrations of a denaturing agent (e.g. urea) can be used to recover the recombinant protein and theoretically, specialised refolding methods can be used to refold the protein to make functional, folded protein for structural studies (Mus-Veteau *et al*, 2010). There are a small number of cases where mammalian membrane protein structures have been solved by over-expression in *E. coli* such as the integral membrane protein fatty acid amide hydrolase at a resolution of 2.8 Å (PDB – 1MT5) (Bracey *et al*, 2002) and human 5-lipooxygenase-activating protein with 2 leukotriene biosynthesis inhibitors at 4.0 and 4.2 Å resolution respectively (PDB – 2Q7M and 2Q7R) (Ferguson *et al*, 2007). However there has been no success with

determination of eukaryotic membrane protein structures refolded from inclusion bodies to date.

1.2.2.2 Yeast

Yeast (e.g. *Saccharomyces cerevisiae, Pichia pastoris*) is a eukaryotic host used for the exogenous expression of membrane proteins. An advantage of using yeast as an expression system is the capacity to implement many of the post-translational modifications native to eukaryotic membrane proteins, such as glycosylation. Furthermore, large volumes of yeast can be grown in a short period of time and is relatively cheap to culture. However, unlike mammalian membranes, yeast membranes contain ergosterol instead of cholesterol; this may have an effect on the correct trafficking and stability of membrane proteins (Baumann *et al*, 2011). Proteolytic degradation is also a common problem faced with yeast protein expression (Macauley-Patrick *et al*, 2005). Very few (3 – 4) mammalian membrane protein structures have been solved using the *S. cerevisae* expression system. Expression in *P. pastoris* has been slightly more successful with approximately 18-20 structures solved (Membrane Proteins of Known 3D Structure database, accessed 22/06/14). Some of the structures solved using yeast overexpression include human liver monoamine oxidase B (3 Å in *P. pastoris*) (Binda *et al*, 2002) and human liver monoamine oxidase B with bound Isatin (1.7 Å in *P. pastoris*) (Binda *et al*, 2003), rat monoamine oxidase A (3.2 Å in *S. cerevisiae*) (Ma *et al*, 2004), and the human AQP2 aquaporin kidney channel at 2.75Å (Frick *et al*, 2014).

1.2.2.3 Insect cells

Insect cells are widely used for eukaryotic protein expression due to their improved ability to express eukaryotic proteins, this is partially attributable to their similar codon usage to mammalian proteins, when compared with bacteria or yeast (Bernaudat *et al*, 2011). Insect cells are also cheaper, easier to maintain, culture and amplify compared with mammalian cells making them a rational choice for protein over-expression. However, insect cell membranes possess a lower level of cholesterol than mammalian cells which may interfere with the correct expression and localisation of mammalian membrane proteins. Additionally, they are capable of the post-translational modification of proteins; this is particularly important when studying membrane proteins. However, the modifications which take place in insect cells do not directly replicate what occurs in mammalian cells, for example complex glycosylation is rarely noted in insects (Bernaudat *et al,* 2011). Nevertheless, this can be considered to be advantageous for crystallisation due to the improved homogeneity of protein samples which lack complex glycan chains (see Section 1.2.3). Insect cells are commonly used for membrane protein expression as

they offer more comparable protein-processing machinery and membrane composition to mammalian cells than yeast or *E. coli* whilst they are much cheaper to culture and easier to maintain than mammalian cells (Mus-veteau, 2010). Fall armyworm, *Spodoptera frugiperda*, insect cells have been used for the expression and structure determination of approximately 60 membrane proteins including GPCRs and ion channels (Membrane Protein of Known 3D Structure databank, accessed 22/06/14). Some examples of structures solved following expression in *sf* insect cell lines include an AMPA-(α-amino-3-hydroxy-5-methyl-4-isoxasolepropionic acid) subtype glutamate receptor, rat GluA2 that was solved to a resolution of 3.6 Å (PDB – 3KG2) (Sobolevsky *et al*, 2009), connexin 26 gap junction channel that was solved at a resolution of 3.5 Å (PDB – 2ZW3) (Maeda *et al*, 2009) and zfP2X4.1 receptors in the *apo*, closed and ATP bound states at 2.9 and 2.8 Å respectively (PDB 4DW0 and 4DW1) (Hattori and Gouaux, 2012).

1.2.2.4 Mammalian cells

Although mammalian cells provide the most native environment for mammalian proteins, they also have many limitations in terms of their cost to maintain and low yield of protein production. To obtain enough protein for crystallisation and structural studies is very expensive and requires a large amount of labour-intensive work. Additionally, mammalian cells tend to produce a very heterogeneous population of protein. Heterogeneity of proteins can cause problems during crystallisation as a result of disorder and quality of crystals. Additionally the presence of certain glycan chains may hinder the formation of favourable crystal contacts (Grueninger-Leitch, 1996; Mus-veteau, 2010). There are some recent examples of membrane protein structures that have been solved using mammalian expression systems, for example, human ammonia transporter, Rh C glycoprotein (RhCG) was expressed and purified from HEK-293S GnTI- cells (GnTI- HEK-293 cell lines lack GnTI and thus cannot perform complex glycosylation) and the structure was solved at a resolution of 2.1 Å (Gruswitz *et al*, 2010). The *Xenopus laevis* GLuN1-GluN2B NMDA receptor was also expressed and purified from GnTI-HEK-293S cells; the structure was solved at a resolution of 3.7 Å (Lee *et al*, 2014). The crystal structure of a human β3 $GABA_A$ receptor was solved at a resolution of 3 Å, following expression and purification from GnTI- HEK-293S cells (Miller and Aricescu, 2014). The recent progression in the use of GnTI- cells for structure determination demonstrates the importance of obtaining homogeneous protein populations for crystallisation.

Due to the limitations of many of the currently available protein expression systems described above, a new membrane protein expression system that overcomes some of these problems

and enables the production of a high yield of homogeneous, quality protein would be very useful.

1.2.3 Post translational modifications

Post-translational modifications are extremely important for the correct expression and function of many proteins. In eukaryotes these modifications include the addition of methyl groups (methylation), phosphate groups (phosphorylation), ubiquitin groups (ubiquitination) and sugar groups (glycosylation). In summary, the addition of a methyl group to a protein from S-adenosylmethionine can be either reversible or irreversible and results in the formation of protein-protein interactions that may be important for processes such as protein repair, transport, differentiation and transcriptional regulation (Clarke, 1993; Willemsem *et al*, 2006). Ubiquitination is important for protein degradation thereby regulating protein turnover; the addition of a ubiquitin group to a protein causes the protein to be moved to the proteasome where it will be degraded (Lecker *et al*, 2006). Protein phosphorylation is the most widespread post-translational modification and is responsible for activating and deactivating proteins via protein kinases and phosphatases for phosphorylation and dephosphorylation respectively (Cielsa *et al*, 2011). Phosphorylation is important for many basic cell processes including cell division, cell growth, membrane transport and metabolism (Cielsa *et al*, 2011). Post-translational modifications are less extensive but still present in prokaryotes. There is some evidence for the existence of N-glycosylation and O-glycosylation in bacteria (Abu-Qarn *et al*, 2008). Additionally protein acetylation has been shown to happen in both gram-negative and gram-positive bacteria (Hayden *et al*, 2013). Although ubiquitination has not been established in prokaryotes, they have simpler versions of proteasome targeting systems that contain similar proteins labelled 'ubiquitin-like proteins' (Burroughs *et al*, 2012).

Protein glycosylation, the addition of sugar molecules to synthesised proteins, is an important post-translational modification that occurs ubiquitously in eukaryotes, predominantly to secreted and membrane-targeted proteins (Devasahayam, 2007). The added glycan structures can have essential roles in protein folding and targeting as well as in quality control (ensuring misfolded or aggregated proteins are targeted for degradation) (Moremen *et al*, 2012). N-linked glycosylation involves the attachment of an oligosaccharide to a nitrogen atom of an asparagine or arginine amino acid side chain. Dolichol phosphate acts as a membrane anchor for the formation of $Glc_3Man_9GlcNAc_2$ before the glycan is transferred to a developing amino acid chain in the ER (Burda and Aebi, 1999). N-linked oligosaccharides are often quite large with extensive chains (with a minimum of 5 sugar residues) and always contain mannose

residues, an N-acetylglucosamine residue as well as other sugar residues. O-linked glycosylation involves the addition of sugar residues to the hydroxyl group of hydroxylysine via galactose or a serine or threonine residue via N-acetylgalactosamine. O-linked saccharides tend to be short consisting of only one to four sugar residues (Freeman, 2000).

The majority of membrane proteins and secreted proteins are translated and processed in the endoplasmic reticulum (ER) and many of them are consequently N-linked glycoproteins. Problems are encountered during membrane protein structure determination due to the large number of N-linked glycans. The glycan chains take form in a variety of conformations, chemical structures and can be mobile; therefore in conventional expression systems, glycosylated membrane proteins are often very heterogeneous making X-ray crystallography particularly difficult as a result of disorder and quality of crystals (Grueninger-Leitch, 1996; Mus-veteau, 2010). As a result of this, the majority of protein structures obtained using x-ray crystallography have their glycosylation sites removed using site directed mutagenesis or are treated with deglycosylases (Nagae and Yamaguchi, 2012).

1.2.4 N-linked glycosylation in vertebrates

In vertebrates, the sequence of events that occur during glycosylation is highly complex leading to a mixture of high mannose, hybrid and complex N-glycosylated proteins (Fig 1.2). High mannose glycoproteins have 3 or more mannose residues attached to the chitobiose core which consists of 2 N-acetylglucosamine ($GlcNAc_2$) molecules. Complex glycoproteins have a mixture of other glycans such as fucose and galactose attached to the initial 3 mannose residues in the chain and have no terminal mannose residues, whereas hybrid glycoproteins are complex glycoproteins with one or more terminal mannose residues (Fig 1.2) (Freeman, 2000). In eukaryotes, the transfer of an assembled $Glc_3Man_9GlcNAc_2$ saccharide to the asparagine residue of an Asn-X-Ser, Asn-X-Cys or Asn-X-Thr motif to initiate glycosylation is relatively well conserved (Katoh and Tiemeyer, 2012; Burda and Aebi, 1999).

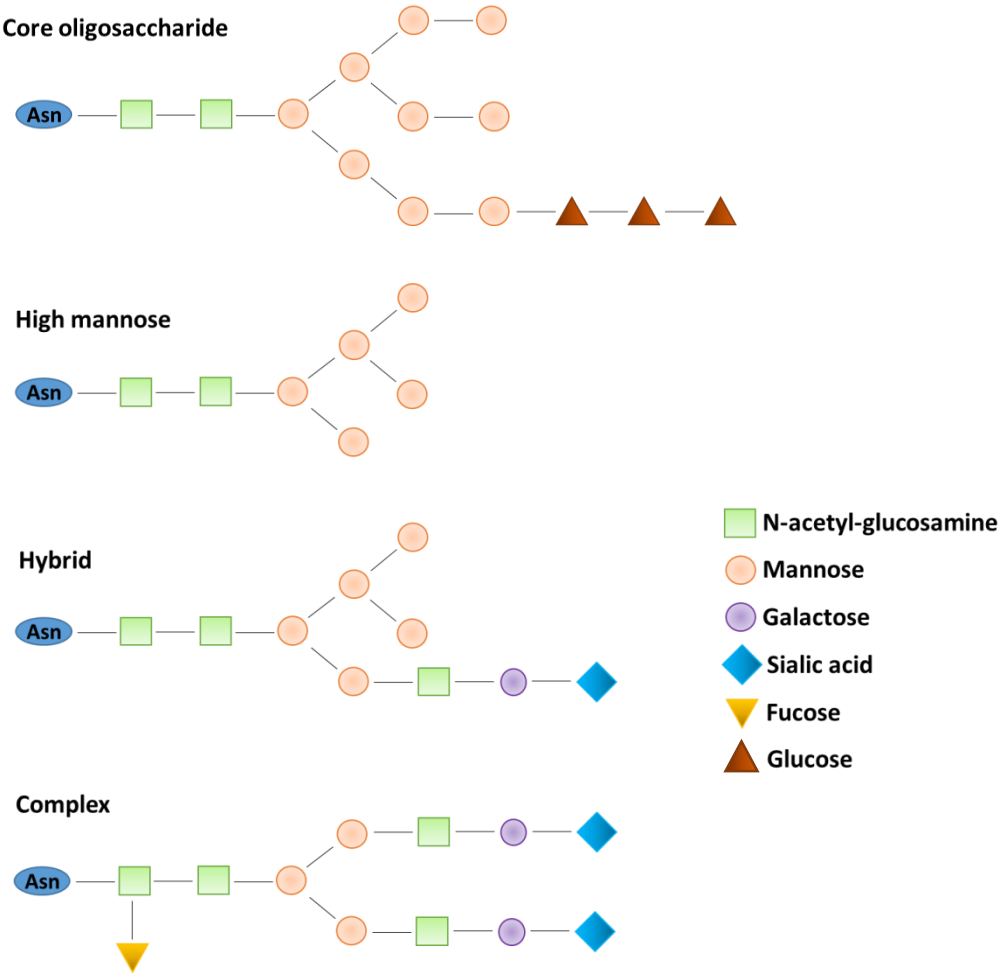

Figure 1.2 – Glycosylation. Representations of the core oligosaccharide ($Glc_3Man_9GlcNAc_2$) and high mannose, hybrid and complex glycosylated proteins. See key for individual symbols.

Animal systems contain approximately 200 glycosyltransferases, the enzymes involved in extending the glycan chain; local enzyme availability is equally as important as the abundance and localisation of glycoprotein substrates and sugar donors during glycosylation (Moreman *et al,* 2012).

The first step of N-linked glycosylation is the transfer of a $Glc_3Man_9GlcNAc_2$ glycan to the emerging amino acid chain in the ER. Subsequently 2 of the Glc residues are removed resulting in a $GlcMan_9GlcNAc_2$ structure, which acts as a substrate for the lectin chaperones, calnexin and calreticulin (Helenius and Aebi, 2004). Calnexin and calreticulin are linked to another protein, ERp57, which together protect developing polypeptide chains from hydrophobic aggregation and misfolding (Lederkremer, 2009). Correctly folded proteins that pass quality control dissociate from the lectins and the final Glc is cleaved, they are sent for export to the Golgi apparatus where further glycan processing may take place (Fig 1.3) (Moremen *et al*,

2012). In the Golgi, several trimming steps occur by α-mannosidase I to generate an intermediate ($Man_5GlcNAc_2$). At this stage, the high mannose-type glycoprotein can be converted to a hybrid type glycoprotein via the action of N-acetylglucosaminyl transferase I (GnTI). Hybrid glycans can then be remodeled further by a number of enzymes to form complex N-glycans. These processes that occur in the Golgi can vary in nature and can result in the addition of large numbers of sugar residues to the protein which add significant mass. In addition, these processes can result in the formation of a very heterogeneous protein population causing great problems for crystallization as described above (Nagae and Yamaguchi, 2012). Ideally these processes should be avoided in order to help achieve protein crystallization.

In vertebrate differentiated cells, very few glycoproteins at the high mannose stage can successfully reach the cell surface and require further modification in the Golgi apparatus. This is in contrast to what occurs in stem cells where cell surface glycoproteins appeared to consist mostly of the high mannose type (An *et al,* 2012).

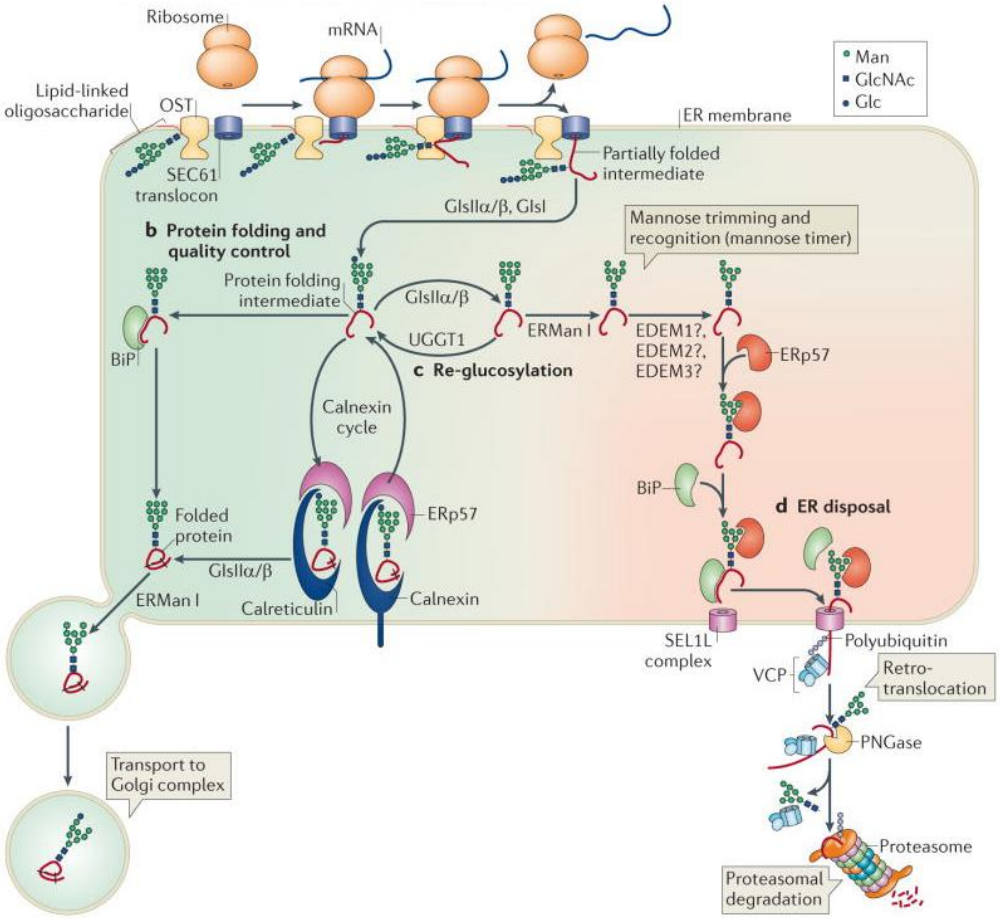

Figure 1.3 – N-glycsoylation and quality control of proteins. Schematic showing the post-translational events that occur in the cell to form mature functional, folded proteins. Reprinted by permission from Macmillan Publishers Ltd: [Nature] (Moremen *et al*), copyright (2012).

1.2.5 Glycosylation in insect cells

The process of glycosylation in insects is markedly different from that in vertebrates. There is some evidence to suggest that mannose containing O-glycans are present in insect species although only one has been described, the dystroglycan protein in *D. melanogaster* (Ichimiya *et al*, 2004). It is well established that the majority of glycoproteins synthesised are paucimannosidic or oligomannosidic N-linked glycan structures (Rendic *et* al, 2008) whereas complex and hybrid N-linked glycoproteins are uncommon in insects. This was initially accredited to the fact that either no or very low levels of appropriate glycosyltransferase activity needed for the production of complex glycans were present. However, more recently a β-*N*-acetylglucosaminidase enzyme (*fused lobes*) involved in removing the terminal GlcNAc structure from a polypeptide chain was identified. Removal of the GlcNAc residue thereby blocks further elongation of the chain, suggesting that the production of hybrid and complex glycoproteins in insects is impeded (Rendic *et al,* 2008). Despite the activity of *fused lobes,*

there is evidence of primary production of a complex glycoprotein on the bee venom phospholipase A, which contains 2 fucose residues linked to the proximal GlcNAc residue. In addition, it contains an additional GlcNAc residue linked to a fucose residue and a GalNAc residue (Fig 1.4) (Rendic *et al,* 2008). This was the first indication of the initial phases of complex-type glcyosylation occuring in insects.

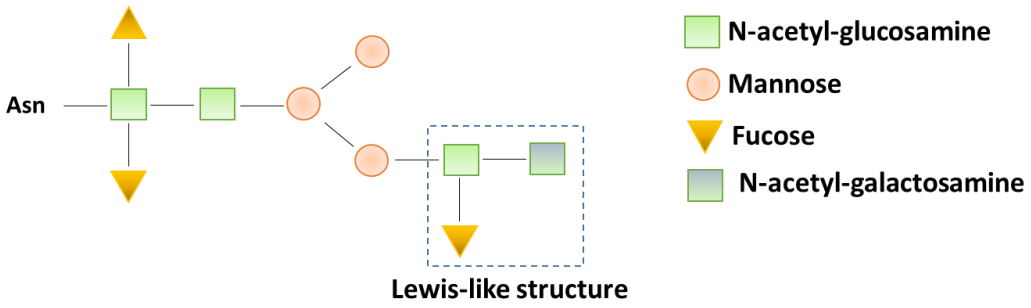

Figure 1.4 – Complex glycosylation-like moiety observed in insects. Lewis-like structure observed on phospholipase A represents the initial stages of complex glycosylation, indicating that insects have some of the enzymes required to perform complex glycosylation.

Therefore, although insect cells are commonly used as expression systems for mammalian proteins due to their ability to perform eukaryotic post-translational modifications, the specific modifications that take place may differ considerably from the modifications that occur in native systems. However these differences can be advantageous in terms of membrane protein structure determination. When a mammalian protein is expressed in an insect system, the protein can still be glycosylated which is important for protein function and quality control. However the nature of the glycosylation that will occur in an insect system will be different to that occurring in mammalian cells as they will be less likely to contain long, heterogeneous complex sugar chains (Rendic *et* al, 2008). This is beneficial as expressing proteins in insect systems will reduce the large degree of protein heterogeneity acquired with other systems and this will have less of an impact on crystal formation. For this reason, a novel insect expression system would be particularly valuable for eukaryotic membrane protein studies and biologically relevant ion channels.

1.3 Purinergic receptors

1.3.1 Purinergic signalling – summary

Purinergic signalling may be defined as cell-signalling activity induced by the action of adenosine and purine nucleotides such as adenosine diphosphate (ADP) and adenosine triphosphate (ATP). Three families of purinergic receptors have been identified in mammals,

the adenosine P1 receptors (GPCRs), P2Y receptors (GPCRs) and P2X receptors (ligand gated ion channels -LGICs) (Burnstock 2006). P1 adenosine receptors are activated by adenosine, P2X receptors by ATP and P2Y receptors by ADP, ATP and a variety of other nucleotide-based ligands (Table 1.1). ATP is released by gentle mechanical stress such as an increase in fluid flow (Bodin and Burnstock, 2001; Jensen *et al*, 2007), at synapses, and at sites of cell damage, injury and inflammation where it activates P2X and P2Y receptors. Subsequently the ATP is broken down by a family of ectonucleotidase enzymes to form ADP, adenosine monophosphate (AMP) and adenosine, which can in turn act on P2Y and adenosine receptors accordingly (see Table 1.1 for summary) (Zimmermann, 2000). Each receptor family now has a representative crystal structure(s), which has been instrumental in the interpretation of structure-function data, but, at least in the case of P2X receptors, not without its limitations.

1.3.2 Brief history of purinergic signalling

ATP was first postulated to act as a neurotransmitter in 1953 (Holton, 1953) and in 1954 it was shown that ATP injection caused a similar effect on vasodilatation of the rabbit ear artery as that induced by antidromic stimulation of the nerves supplying it. This led to the hypothesis that stimulation of nerves causes release of ATP, resulting in vasodilatation of the ear (Holton and Holton, 1954). Further work in 1959 demonstrated that ATP does indeed act as a neurotransmitter where Holton showed that ATP is released upon stimulation of the great auricular nerve (Holton, 1959).

In the early 1960s, a novel component of the autonomic nervous system was acknowledged that was both nonadrenergic and noncholinergic (Eccles, 1964). This component was later termed ‘purinergic’ by Burnstock who suggested that ATP was the substance released from these nerves (Burnstock *et al*, 1970). In 1978, two types of purinergic receptors (termed P1 and P2) activated by adenosine and ADP/ATP respectively were distinguished according to a number of criteria: (i) the agonist potency of adenosine, AMP, ADP and ATP; (ii) antagonist action e.g. methylxanthines which inhibit adenosine actions; (iii) changes in intracellular cAMP levels in response to adenosine and (iv) the induction of prostaglandin synthesis by ATP (Burnstock and Kennedy, 1985). This P1/P2 classification of receptors is now well-established and is widely used.

P2 receptors were further reclassified into two distinct subtypes – the P2X and the P2Y receptors. Burnstock and Kennedy discriminated between the two classes by their differential response profiles to a range of ATP analogs and antagonists (Burnstock and Kennedy, 1985). P2X and P2Y receptors can also be discriminated by their transduction mechanisms. P2X

receptors form a cation selective ion channel permeable to Na^+, Ca^{2+} and K^+ (Benham and Tsien, 1987) whereas P2Y receptors are G-protein coupled receptors (Abbrachio and Burnstock, 1994). The first P2X receptor was subsequently cloned from the rat vas deferens and characterised in mammalian cells and *Xenopus* oocytes where it was shown to be a cation-selective ion channel with high calcium permeability (Valera *et al*, 1994).

Table 1.1 – Summary of purinergic receptor types and associated ligands (Khakh and North, 2006).

Receptor	Receptor type	Ligand(s)	No. mammalian subtypes	Crystal structure
P1	G-protein coupled receptor	Adenosine	4	Human A2A receptor bound to ZM241385 – **PDB 3EML** (Jaakola *et al*, 2008) and adenosine – **PDB 2YDO** (Lebon *et al*, 2011)
P2Y	G-protein coupled receptor	ADP ATP UDP UDP-glucose UTP	8	P2Y12 in complex with 2MeSADP – **PDB 4PXZ** P2Y12 in complex with 2MeSATP – **PDB 4PY0** (Zhang *et al*, 2014)
P2X	Ligand gated ion channel	ATP	7	zfP2X4.1 closed state – **PDB 4DW0** zfP2X4.1 open state – **PDB 4DW1** (Hattori and Gouaux, 2012)

1.3.3 P2X receptors - Expression and topology

P2X receptors are a family of ligand-gated ion channels that open when ATP binds to the extracellular domain resulting in the non-selective influx of cations including sodium and calcium. This ion flow plays a key part in many signalling pathways due to changes in membrane potential and local ion concentrations (Khakh and North, 2006; Young MT, 2009).

P2X receptors have been identified in a large range of species from the slime mold, *Dictyostelium discoideum*, to more complex organisms such as the rat, *Rattus norvegicus* and humans, *Homo sapiens*. However they are absent from the genomes of insects such as the fruit fly, *Drosophila melanogaster* and the nematode, *Caenorhabditis elegans* (North, 2002; Fountain and Burnstock, 2009). Seven subtypes have been identified in mammals that vary considerably in length; P2X4 is the shortest (388 amino acids) and P2X7 the longest, with a long intracellular C-terminal domain (approximately 240 amino acids in length; total protein length 595 amino acids) (Khakh and North, 2006). Each P2X subunit consists of 2

transmembrane, hydrophobic α-helical domains, intracellular N and C termini and a large extracellular domain (Fig 1.5) (Khakh and North, 2006).

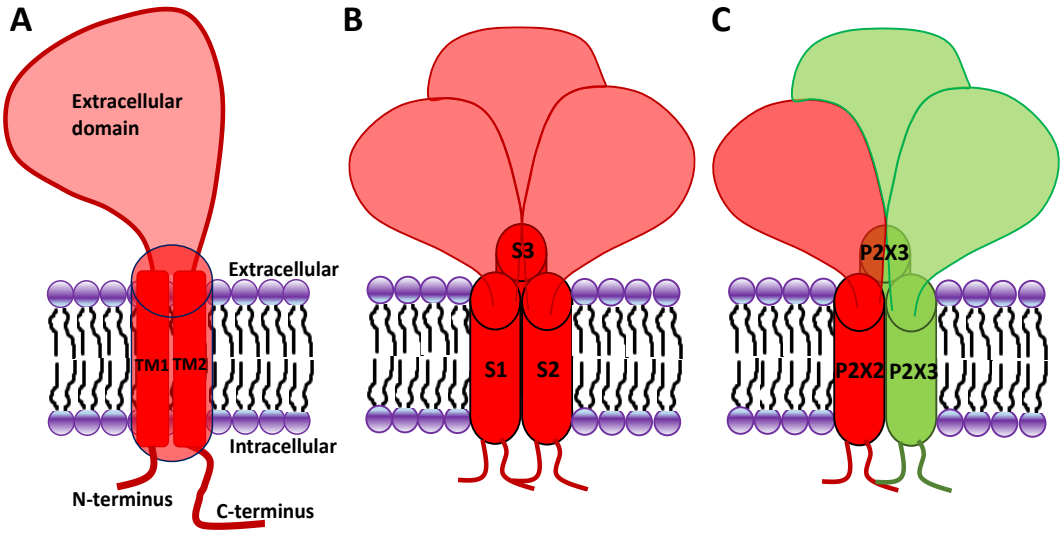

Figure 1.5 – Schematic representations of a P2X receptor. (A) Schematic showing topology of a single P2X subunit with intracellular N- and C- termini, 2 transmembrane domains (TM1 and TM2) and large extracellular domain. (B) Schematic showing the clustering of 3 subunits to form a functional channel in the membrane (S=subunit) where ATP would bind at the intersubunit interface. (C) Schematic showing an example of a heterotrimer, in this case a P2X2/3 heteromer made up of two P2X3 (green) subunits and one P2X2 (red) subunit. TM = transmembrane domain. S = subunit.

Functional P2X channels are formed from 3 subunits, which move relative to one-another upon ATP binding, resulting in the opening of a lateral portal just above the transmembrane domains and cation influx through the transmembrane domains (see Section 1.3.8) (Hattori and Gouaux, 2012). Channels can be either homomeric (made up of 1 subtype) or heteromeric (made up of 2 subtypes) depending on the particular subtype/s involved. In addition, a heteromeric receptor made up of 3 subtypes (P2X2/4/6) has also been suggested to form according to co-immunoprecipiation and atomic force microscopy (AFM) imaging experiments in tsa-201 cells (Antonio *et al,* 2014).

P2X6 cannot form homomeric channels but can form functional heteromeric channels with P2X2 or P2X4 (Barrera *et al*, 2005; Barrera *et al*, 2007). The remaining subtypes (with the exception of human P2X5 – hP2X5) are able to form functional homomeric channels at the cell surface. The full-length hP2X5 protein is able to traffic to the cell surface; however the majority of hP2X5 contains a deletion of exon 10 (Δ328 – 349) and lacks part of the TM2 and pre-TM2 domains (Le *et al*, 1997; Duckwitz *et al*, 2006). As a result the majority of the protein appeared to be retained in the ER (Bo *et al*, 2003; Kotnis *et al*, 2010). Conversely, more recently, a functional role has been identified for this hP2X5 splice variant. Abramowski and

colleagues showed that hP2X5 gene expression in human T lymphocytes was upregulated and receptors were trafficked to the cell membrane during activation of CD4+ T cells. In addition, in hP2X5 knockdown cells, there was a two-fold higher production of IL-10 indicating that the hP2X5 variant might play a role in T-cell activation and thus immunoregulation (Abramowski *et al*, 2014).

1.3.4 P2X receptors – N-linked glycosylation

All P2X receptors studied so far undergo N-linked glycosylation, however the number of glycosylation sites varies between subtypes. Each P2X monomer contains a minimum of 2 N-glycosylation consensus sequences (Asn, X, Ser/Thr, where X denotes any amino acid except proline), all of which are relatively well conserved across species (North, 2002). The number of glycosylation sites in the various subtypes can be referred to in Table 1.2.

Table 1.2 – Summary table showing the number of glycosylation sites in each P2X receptor subtype and the effects caused by mutagenesis of these sites.

P2X Subtype	No. of consensus sequences	Effects of mutagenesis of glycan sites
1	5	Increases/decreases in channel function. Reduction in ATP potency. Abolition of channel function upon mutation of 3 sites (Rettinger *et al*, 2000b).
2	3	Effects on channel function and trafficking to the surface (Newbolt *et al*, 1998).
3	4	Effects on channel function, trimer formation and trafficking to the membrane (Vacca *et al*, 2011).
4	6	Abolition of P2X4 resistance to degradation in lysosomes. Effects on cell surface trafficking (Qureshi *et al*, 2007).
5	2	Not studied
6	3	Not studied
7	5	Effects on channel function, pore formation and cell surface trafficking (Lenertz *et al*, 2010).

Four of the five glycosylation sites in rat P2X1 (rP2X1) undergo glycosylation when expressed in *Xenopus* oocytes. However, only one of these sites (N300) acquires complex glycosylation.

Removal of the N210 site using site-directed-mutagenesis significantly altered channel function. Electrophysiological recordings demonstrated that mutation at this site resulted in increased channel currents, but a threefold decrease in potency for ATP. In contrast, elimination of N153 resulted in a 30% decrease in the current response to ATP. If more than 2 of the glycan sites were eliminated, rP2X1 channel formation was severely affected or completely abolished. Therefore rP2X1 glycosylation is implicated in both channel function and trafficking (Rettinger *et al*, 2000b).

N-linked glycosylation has been well studied in rat P2X2 (rP2X2), which contains 3 consensus sequences (N182S, N239S, and N298S). Mutagenesis studies show that all three of these sites undergo glycosylation in the wild type receptor (Newbolt *et al*, 1998). Additionally, glycosylation of 2 sites gave a fully functional channel that was successfully trafficked to the cell membrane. However upon removal of 2 of the sites by mutagenesis or tunicamycin treatment, which inhibits GlcNAc phosphotransferase (GPT) (Doroghazi, *et al*, 2011*)*, very low levels of protein reached the membrane and currents in response to ATP were almost undetectable. Removal of all three consensus sites resulted in a non-functional channel (Torres *et* al, 1998; Newbolt *et al,* 1998). In addition, cysteine substitution of residues Arg304, Leu306, Lys308 and Ile312 in the N-terminal half of the pre-TM2 led to channels with a loss of function due to the loss of complex glycosylation at Asn298. This work suggested that the glycosylation site at Asn298 has an important role in sensing receptor conformational changes in this pre-TM2 region, which was shown to be important for the correct conformation of the receptor at the extracellular face of the membrane (Young *et al*, 2008).

A minimum of 2 successfully glycosylated consensus sites was shown to be required for cell-surface trafficking of P2X1, P2X3 and P2X7 subtypes (Kaczmarek-Hajek *et al*, 2012). The N170 glycosylation site in P2X3, located close to the ATP binding site, is the most well conserved, this may be due to its critical role in receptor function (Vacca *et al*, 2011). Mutation of this P2X3 consensus site resulted in a loss of P2X3 cell surface expression, an inability to form trimeric complexes and a loss of inward currents detected in response to ATP in HEK-293 cells (Vacca *et al*, 2011).

Experiments with chick P2X4 (cP2X4) demonstrated that only the glycosylated form of cP2X4 was detectable at the cell surface (Hu *et al,* 2002). Furthermore, Endoglycosidase-H (Endo-H) digestion experiments showed that rP2X4 underwent complex glycosylation, with partial resistance to Endo-H digestion. Removing the N-glycans from the 6 glycosylation sites by incubation with DMJ (an inhibitor of Golgi α-mannosidase I) followed by Endo H did not affect

protein trafficking to lysosomes. However the receptors were rapidly degraded in the lysosomes, suggesting that glycosylation of P2X4 plays an important role in receptor resistance to degradation (Qureshi *et al*, 2007). Additionally Valente and colleagues published work showing that each of the 6 glycosylation sites in hP2X4 underwent N-linked glycosylation in HEK cells, where abolition of any one site had no effect on channel function (Valente *et al*, 2011).

P2X5 receptors contain 3 N-glycosylation sites in the extracellular domain, 2 of which undergo complex glycosylation and 1 that undergoes high mannose glycosylation (Duckwitz *et al*, 2006). P2X6 receptors are unable to form functional homomeric receptors at the cell surface. However data by Jones and colleagues showed that there was an increased level of glycosylation of P2X6 in functional HEK-293 cells expressing P2X6 receptors compared to non-functional cells suggesting that the glycosylation state of the protein is essential in the production of functional P2X6 channels (Jones *et al*, 2004).

Human P2X7 contains 5 N-linked glycosylation consensus sequences and Lenertz and colleagues showed that the wild type receptor is glycosylated at all 5 sites (N187, N202, N213, N241 and N284) using site directed mutagenesis; when each site was mutated to alanine, a reduction in molecular weight was observed using sodium dodecyl sulphate (SDS)-PAGE. Mutation of N187 had a significant effect on downstream channel function, cell surface expression and pore formation. Furthermore this glycan site is conserved across six of the seven P2X subtypes, suggesting that it is vitally important to P2X channel function (Lenertz *et al*, 2010).

These results highlight the importance of glycosylation for P2X receptor trafficking which in turn is necessary for protein function. However, whether or not glycosylation itself is necessary for P2X protein function has not been determined, thus those channels that reach the membrane may be fully functional.

1.3.5 P2X receptors - Trafficking

P2X receptors undergo core N-linked glycosylation in the endoplasmic reticulum, where they assemble into trimeric complexes (see below). Subsequently they are transported to the Golgi complex for further modification and packaging before transportation to the cell membrane. Depending on the P2X subtype, the receptors may be internalised and returned to the cell surface via endosomes or may be targeted for degradation in lysosomes (Robinson and Murrell-Lagnado, 2013). A non-canonical, conserved YXXXK trafficking motif present in the C-terminus of all P2X receptor subtypes was shown to be responsible for the regulation of cell surface expression. Mutation of this motif resulted in a decrease of cell surface expression of all P2X subtypes; furthermore it increased internalisation of P2X2 receptors (Chaumont et al, 2004).

The only P2X subtype that is fully retained within the ER and unable to form functional homomeric channels is P2X6 (Ormand *et al*, 2006). However, P2X6 was shown to be able to form functional heterotrimers with P2X2 or P2X4 (Bobanovik *et al*, 2002). The heteromeric receptor complexes were successfully trafficked to the cell surface and their localisation resembled that of homomeric P2X2 or P2X4 receptors respectively (Robinson and Murrell-Lagnado, 2013). The transportation of P2X6 to the cell surface from the ER only in assembly with other subunits indicates that the assembly of trimeric complexes takes place in the ER.

P2X2 channels often appear to be localised mostly within intracellular compartments in heterologous expression systems, due to the slow progression of P2X2 through the secretory pathway (Bobanovik *et al*, 2002). However upon reaching the cell membrane, P2X2 is stably expressed at the surface. P2X7 shows a similar expression pattern to P2X2, experiencing slow but stable accumulation of expression at the cell surface. However the trafficking of P2X7 receptors is cell-type specific and localisation can vary from being largely within the cell (monocytes and lymphocytes) to being largely at the plasma membrane (macrophages) (Gu *et al*, 2000; Gudipaty *et al,* 2001).

P2X4 is principally located in intracellular organelles, in a distinct punctate pattern surrounding endosomes and lysosomes. A small level of expression can also be seen at the periphery of the cell (Fig 1.6) (Bobanovik *et al,* 2002). Upon further investigation, it was found that the majority of P2X4 protein co-localised with the early endosomal marker, EEA-1, suggesting it is recycled to and from the cell surface. Localisation to the membrane is largely influenced by the extracellular concentration of ATP; an increase in extracellular ATP caused increased

internalisation of P2X4 receptors. This is in contrast to P2X2, which did not undergo any changes in protein internalisation upon ATP application (Bobonavik *et al*, 2002).

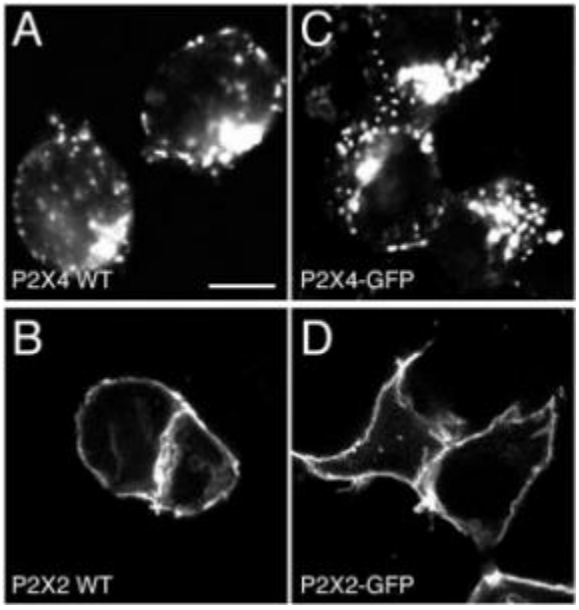

Figure 1.6 – **P2X2 and P2X4 localisation in HEK-293 cells.** (A,C) Expression of P2X4 and P2X4-GFP in HEK-293 cells. Confocal images show that the majority P2X4 clusters are intracellular. (B,D) Expression of P2X2 and P2X2-GFP in HEK-293 cells. P2X2 is localised predominantly at the cell membrane. Cells expressing untagged P2X2 and P2X4 were visualised using Anti P2X2/Cy3 or Anti P2X4/Cy5 respectively (Figure reused with permission, Bobanovik *et al*, 2002). GFP tagging of protein had little or no effect on protein localisation. Scale bar: 10 µM.

Co-expression of a dominant negative form of dynamin-1 (K44A), which is responsible for the inhibition of dynamin-dependent endocytosis, resulted in a P2X4 distribution similar to that of P2X2 i.e. a uniform distribution at the cell surface. These results imply that P2X4 internalisation is a dynamin-1 dependent mechanism (Bobanovik *et al,* 2002). Furthermore, two endocytic motifs were identified in the P2X4 C-terminus. The first is a non-canonical tyrosine based sorting C-terminal YXXGL motif (where X is any amino acid). Mutation of this motif resulted in a dramatic increase in P2X4 expression at the cell membrane due to a decrease in both constitutive and agonist-induced internalisation. The YXXGL motif is conserved across all mammalian P2X4 receptors, however it is not present in the C-terminus of any other P2X subtype (Royle *et al,* 2002). The second C-terminal motif is the canonical YXXØ (where X is any amino acid and Ø is an amino acid with a bulky hydrophobic side chain) motif, but this motif appears to be less accessible to AP2, the clathrin adaptor complex responsible for receptor inclusion into clathrin-coated vesicles. Hence internalisation is predominantly mediated by the YXXGL motif (Royle *et al,* 2005). Lysosomal targeting of P2X4 is further determined by a dileucine motif located in the N-terminus (Quereshi *et al*, 2007).

P2X3 also undergoes constitutive internalisation and re-insertion into the membrane and contains a C-terminal dileucine motif with a DSGØXS (where X is any amino acid and Ø is an amino acid with a bulky hydrophobic side chain) ubiquitination consensus sequence, which has been suggested to be partly responsible for its internalisation and degradation. However, it does not share any of the described trafficking motifs associated with P2X4 (Vacca *et al*¸ 2009).

The trafficking pathways of each of the P2X subtypes is summarised in Fig 1.7.

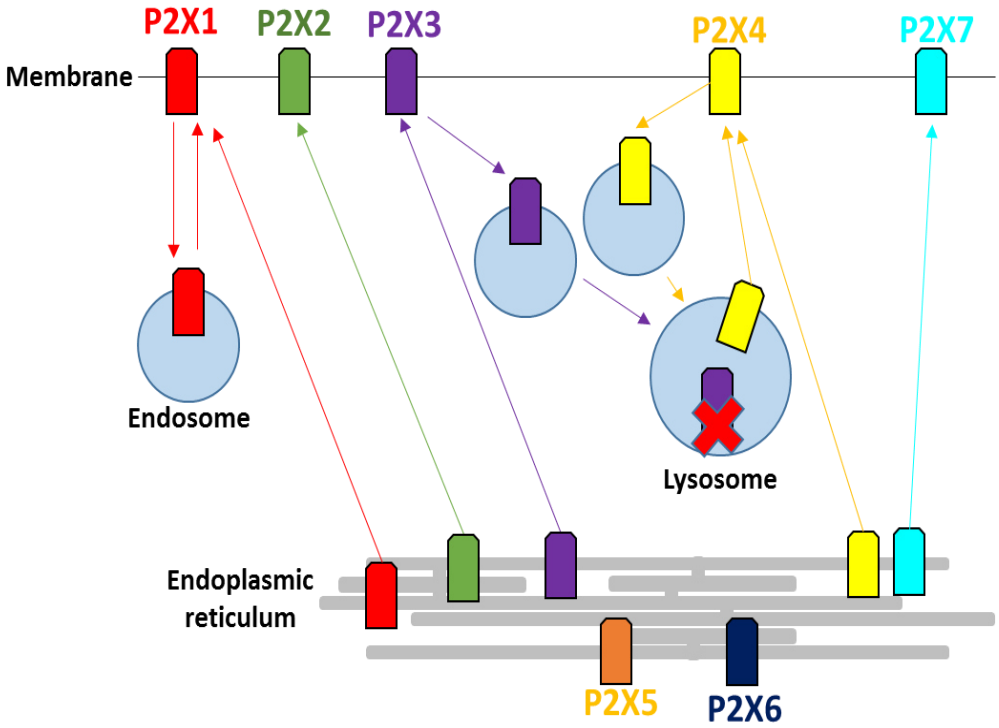

Figure 1.7 – Summary of the trafficking pathways of P2X receptors. P2X1 is internalised and stored in endosomes and recycled to the cell surface. P2X2 and P2X7 are stably expressed at the cell membrane and are not recycled. P2X3 can be internalised by endosomes and is sent to lysosomes for degradation. P2X4 is rapidly internalised by endosomes and lysosomes, but resists degradation and is recycled to the cell surface. The majority of P2X5 and P2X6 receptors are retained in the endoplasmic reticulum and do not form functional homomers. However P2X6 can form various heteromers with other subtypes. These heteromers will acquire the trafficking properties of the second subtype.

1.3.6 P2X receptors - Expression, distribution and roles in health and disease

ATP plays a definitive role in excitatory transmission at synapses within many areas of the CNS via activation of P2X receptors (Holton, 1959). P2X receptors are largely involved with neuropathic pain; this can be partially attributed to their abundant expression in neurons and glial cells of the nervous system (North, 2002; Rubio and Soto, 2001). Specifically P2X2, P2X4 and P2X6 are the most widely expressed in neurons. P2X2 and P2X4 were identified at the

edge of the postsynaptic membrane of excitatory synapses of the brain, indicating that ATP release into synapses during stints of action potential firing may activate the receptors (Rubio and Soto, 2001).

Further evidence has also implicated P2X receptors with a function at the presynaptic membrane as well as the postsynaptic membrane. For example, P2X receptors are expressed on the presynaptic membrane of dorsal root ganglion (DRG) neurons. Upon activation at these synapses, action potentials were evoked that resulted in glutamate release and downstream signalling, which may lead to pain sensation (Gu and MacDermott, 1997).

1.3.6.1 P2X receptors in pain

P2X2 homomers and P2X2/P2X3 heteromers are critical mediators of pain sensation. Both P2X2-/- and P2X2/P2X3 (dbl-/-) mice experienced a reduction in pain-response behaviour following formalin injection, an established method for assessing nociception in mice (Cockayne *et* al, 2005; Hunskaar and Hole, 1987). P2X4 receptors are also largely implicated in nociception. Wild type mice experienced tactile allodynia following peripheral nerve damage. Upon reducing P2X4 protein expression levels by intraspinal administration of P2X4 antisense oligodeoxynucleotide, the tactile allodynia response was reversed (Tsuda *et al*, 2003). This data highlighted the importance of P2X receptors in pain sensation, and their therapeutic potential for anti-analgesic drugs.

1.3.6.2 P2X receptors in blood pressure

Vigorous exercise or changes in environmental conditions can influence changes in blood flow through the body (Hudlicka *et al*, 1992). These changes in conditions are sensed by endothelial cells, which in turn respond by releasing vasodilators such as nitric oxide (NO) (Davies *et al*, 1995). P2X4 is expressed on these endothelial cells and has a significant role in the dilation of blood vessels. Endothelial cells of P2X4 (-/-) mice did not experience calcium influx or subsequent NO release in response to changes in blood flow, contrary to wild type mice. Consequently, vessel dilation was substantially reduced in response to increases in blood flow and this caused an increase in blood pressure. This data suggested that P2X4 plays a significant role in the mechanisms involved in regulating blood pressure and vascular remodelling (Yamamoto *et al*, 2006).

1.3.6.3 P2X receptors in inflammation

P2X7 receptors are largely involved in the inflammatory response. P2X7 activation is implicated in the release of the pro-inflammatory cytokine, interleukin - 1β (IL-1β). Le Feuvre

and colleagues demonstrated that prolonged ATP and lipopolysaccharide (LPS) stimulation of macrophages isolated from wild type mice led to IL-1β release. However cells obtained from P2X7 (-/-) mice (Pfizer) did not release IL-1β (Le Feuvre *et al*, 2002). The inflammatory response of wild-type and P2X7 (-/-) mice was investigated in response to the induction of monoclonal anti-collagen-induced arthritis. Wild type mice suffered from severely inflamed and swollen paws, collagen degradation products and lesions on joint cartilage following lipopolysaccharide stimulation. However P2X7 deficient mice showed a much lower level of response with the disease severity markedly reduced (Labasi *et al*, 2002). This data implicated P2X7 receptors as important mediators of pain and inflammation, serving them as possible targets for anti-inflammatory drugs and anti-arthritic drugs.

P2X2, P2X3 and P2X4 channels are also important mediators of inflammation. Inflammation was induced in rats via hindpore injection with Freund's adjuvant (CFA). ATP responses in DRG neurons isolated from the rats were examined. CFA-induced inflammation caused an increase in ATP-activated currents and an increase in expression of P2X2 and P2X3 receptors. As a result of the increased ATP responses, large depolarisations were elicited and action potentials were fired in DRG neurons. The increase in P2X receptor expression following inflammatory injuries may account for the high levels of pain responses experienced (Xu and Huang, 2002). P2X4 inhibition was shown to affect the development of arthritis in a collagen-induced arthritis (CIA) mouse model. Inhibition of P2X4 using P2X4 antisense oligonucleotide reduced the clinical score of CIA of mice, inhibited joint inflammation and suppressed inflammasome activation (Li *et al*, 2014).

1.3.6.4 P2X receptors in taste sensation

In 2005, ATP was identified as the key neurotransmitter involved in the transduction of information from taste receptor cells to taste nerves (Finger *et al*, 2005). Furthermore P2X2 and P2X3 are expressed in taste nerves and were recognised as the receptors involved in the taste transmission pathway. P2X2/P2X3 (dbl-/-) mice showed abolition of any taste evoked neural responses following chemical stimulation in the taste nerves of the oral cavity. However responses to touch, temperature and menthol were unaffected. In a further experiment it was shown that P2X-knockout mice also have reduced behavioural responses to specific taste substances including sweeteners and bitter compounds using bottle preference tests. Single knockouts of either P2X2 or P2X3 in mice resulted in a slight decrease in taste behavioural responses, but these changes were moderate in comparison to those experienced by double knockout mice (Finger *et al,* 2005). More recently, it was shown that in P2X2/P2X3 (-/-) mice,

stimulation by tastants still mobilises calcium ions in taste receptor cells but their taste cells do not release ATP when stimulated (Huang *et al*, 2011).

1.3.6.5 P2X receptors in cancer

P2X receptors have been associated with a variety of cancer types, which is unsurprising considering their importance in many biological processes. P2X receptors are not only expressed in excitable cells such as neurons and smooth muscle, but have also been identified in tissues such as the lungs, skin, kidneys and endothelium (White and Burnstock, 2006). Upon prolonged application of a high concentration of ATP to P2X7 receptors, a large pore is formed, possibly via interactions with other proteins such as Pannexin (Panx) 1, which allows the passage of both cations and small molecules up to 900 daltons (Ralevic and Burnstock, 1998). Opening of P2X7 and this large pore leads to intracellular potassium efflux which is associated with activation of the inflammasome and caspase 1. However the mechanisms underlying these processes are not fully understood. Potassium efflux is dependent upon pore formation and IL-1β processing is dependent upon this potassium efflux (Wewers and Sarkar, 2009). Caspase 1 cleaves pro-IL-1β to form mature IL-1β which is subsequently released from the cell. IL-1β activates immune cells and contributes to the induction of cell apoptosis (Fig 1.8) (Pelegrin and Surprenant, 2007). Targeting mediators of apoptosis is a keen area of research for the development of new cancer therapies. Furthermore, P2X7 receptors are expressed and functional in many different cancer types including human melanoma cancers and non-melanoma skin cancers (White *et al*, 2005; Greig *et al,* 2003). Incubation of malignant melanoma cells with a highly potent and partially selective P2X7 agonist, BzATP, led to a reduction in cell number whereas antagonism of P2X7 activation using KN-62 (1-N,O-bis-[5-isoquinoline-sulfonyl]-N-methyl-L-tyrosyl)-4-phenyl-piperazine) caused a reverse in this cell reduction (White *et al,* 2005). This data indicates that P2X7 may be a key anti-cancer therapeutic target.

P2X5 is expressed in a variety of tissues such as the skin, bladder and skeletal muscle, and has roles in cell differentiation and the inhibition of cell proliferation making them attractive targets for anti-cancer drugs. Additionally P2X5 receptors have been identified in skin carcinomas and prostate cancers. Application of ATP and ATPγS (P2X5 agonists) to these carcinogenic cells caused a decrease in cell number (Greig *et al,* 2003).

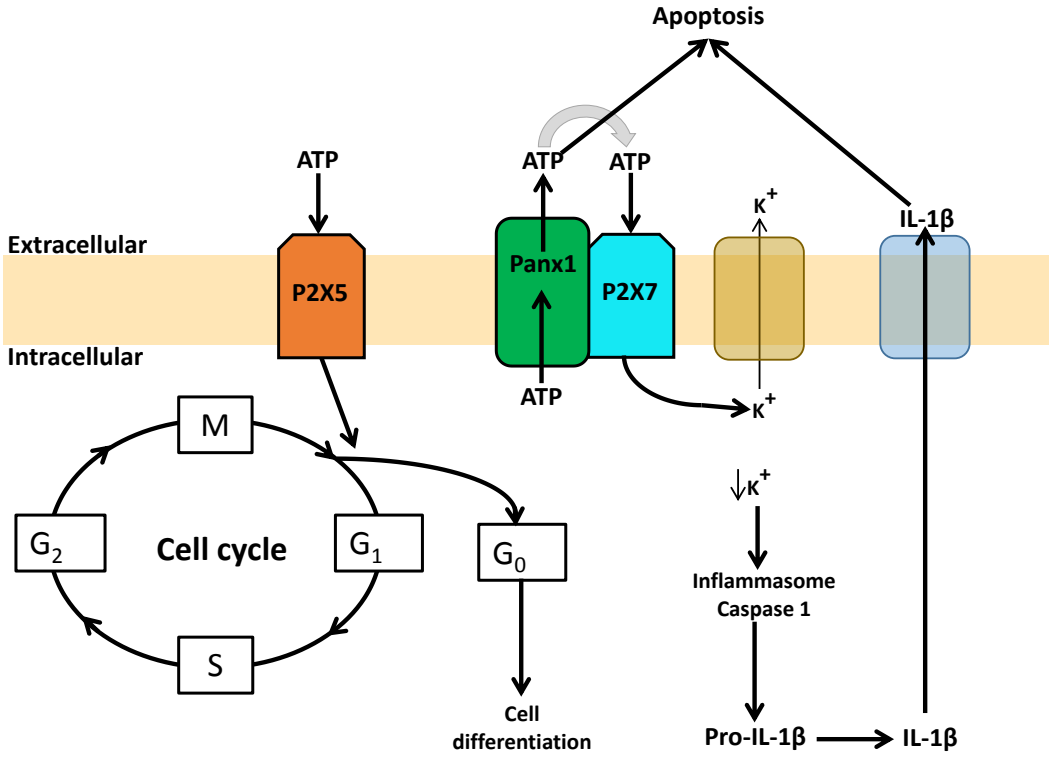

Figure 1.8 – Implications of P2X receptors in the cell cycle and apoptotic pathways. P2X5 is involved in regulation of the cell cycle, affecting the proliferative ability of cancer cells upon application of P2X5 agonists (Greig *et al*, 2005). Upon P2X7 activation, potassium ions are exported from the cell; the decrease in intracellular potassium concentration induces activation of the inflammasome and IL-1β release, thereby mediating apoptosis. Panx1 channels, speculated to form the large pore associated with P2X7, releases ATP which acts as a 'find-me' signal for apoptotic machinery. At high concentrations this ATP can reactivate P2X7 in a feed-forward mechanism (Pelegrin and Surprenant, 2007; Wewers and Sakar, 2009).

1.3.6.6 P2X receptors in platelet aggregation

Platelets express 3 P2 subtypes – P2Y1, P2Y12 and P2X1. Experiments have been done both *in vivo* and *in vitro* to study the role of P2X1 receptors in platelet function. *In vitro*, selective activation of P2X1Rs led to a fast, reversible change in platelet shape, temporary centralisation of secretory granules and low level activation of $\alpha_{IIb}\beta_3$ integrin that led to weak platelet aggregation (Rolf *et al*, 2001; Toth-Zsamboki *et al*, 2003; Erhardt *et al*, 2003). Additionally in a mouse model with acute vascular occlusion where mice were injected with adrenaline and collagen, P2X1 (-/-) mice displayed a lower level of thrombus formation compared to wild type mice. The loss of P2X1 caused a 50% reduction in the number of mice deaths as a result of blocked pulmonary circulation (Hechler *et al,* 2003; Mahaut-Smith *et al*, 2011). The calcium influx via P2X1 receptors was shown to amplify the P2Y1-evoked calcium response in platelets whereby activation of P2X1 alone did not cause significant platelet aggregation but co-

stimulation of both P2X1 and P2Y1 increased the aggregation response (Jones *et al*, 2014). P2X1 is promising as a potential new drug target to reduce thrombotic events in diseases such as atherosclerosis.

1.3.6.7 P2X receptors in hearing loss

P2X2 receptors are expressed in the sensory and supporting cells of the cochlea. A P2X2 mutation (V60L) was identified in inherited, progressive sensorineural hearing loss in families studied over six generations. The mutation was associated with fully penetrant hearing loss in two families and was absent from controls. The V60L mutation was shown to abolish the P2X2 ATP-evoked inward current response and ATP stimulated macropore permeability. In addition, P2X2-null mice acquired severe progressive hearing loss (Yan *et al*, 2013).

1.3.6.8 P2X receptors in mood disorders

A number of single nucleotide polymorphisms (SNPs) have been identified in P2X7 receptors that have been associated with affective mood disorders. For example, a strong association was observed in families with bipolar disorder and the SNP E13A (P value = 0.000708) (Barden *et al*, 2006). P2X7 SNPs have also been associated with other mood disorders such as major depressive disorder and anxiety disorder (Lucae *et al*, 2006; Hejjas *et al*, 2009; Erhardt *et al*, 2007). In a study by Roger and colleagues, twelve P2X7 SNPs that have been linked with mood disorders were tested for function in HEK-293 cells. Eleven of the mutations had a significant effect on channel function and pore formation. Using a P2X7 structural model (based on the zfP2X4.1 crystal structure), it was suggested that the functional effects of the SNPs are caused by changes in agonist binding, channel gating and subunit interactions (Roger *et al*, 2010). In addition, more recently, it was shown that the changes in protein function of P2X7 are associated with changes in protein expression levels (Ursu *et al*, 2014).

1.3.6.9 P2X receptors in CNS diseases

Recent evidence has implicated P2X7 receptors in CNS diseases such as stroke, epilepsy, Alzhiemer's disease and Parkinson's disease. Genetic deletion or antagonism of P2X7 receptors led to changes in the responsiveness of animal models of neurological diseases. For example, in animal models with induced epileptic like seizures, BzATP was shown to prolong the activity of brain neurons caused by seizures whereas P2X7 antagonists were shown to have neuroprotective effects (Jimenez-Pacheco *et al*, 2013). The β-amyloid peptide (Aβ) present at high concentrations in the plaques found in the brains of Alzheimer's patients, was shown to generate a rise in intracellular calcium, ATP release and interleukin-1 β release in wild-type but not P2X7(-/-) mice indicating that Aβ initiates a purinergic activation loop involving P2X7

receptors. In addition, inhibition of P2X7 in mice expressing mutant human amyloid precursor protein resulted in a decrease in the number of plaques (Sanz *et al*, 2009; Diaz-Hernandez *et al*, 2012).

1.3.6.10 P2X receptors in male fertility

P2X1 receptors are expressed in the vas deferens smooth muscle cells where they play a role in the contractile response of the vas deferens to nerve stimulation. This response is essential for propelling sperm into the ejaculate and is largely mediated by P2X receptors. It has been shown that a P2X1 mutation with a targeted deletion causes a reduction in fertility in male mice by 90% due to a reduction in sperm in the ejaculate, whereas female mice were unaffected. Responses to P2XR agonists were abolished in these mice and contraction of the vas deferens in response to nerve stimulation was dramatically reduced. Due to the role of P2X1 receptors in male infertility, selective antagonists may provide potential therapies in the development of a male contraceptive pill (Mulryan *et al*, 2000). In addition, more recently a study by White *et al* showed that α_{1A}- adrenoceptor and P2X1 double knockout mice experienced 100% infertility without affecting sexual behaviour or function (White *et al*, 2013).

1.3.6.11 P2X receptors in health and disease: Summary

With critical roles in many conditions including pain sensation, blood pressure, cancer, rheumatoid arthritis, mood disorders, male fertility and atherosclerosis, finding selective agonists and antagonists for P2X receptors will be greatly beneficial for future drug development against a range of conditions. However, as many of the receptors are implicated in more than one disorder, problems may arise when using the receptors as drug targets. For example, development of a selective P2X7 agonist as a therapeutic agent against cancer may have implications for inflammation in patients. Similarly, using a selective P2X7 antagonist to target inflammation for a condition such as rheumatoid arthritis may cause affect the patients' mood causing anxiety or depression. P2X4 was shown to be implicated in blood pressure and a selective agonist may be useful for reducing blood pressure. However, like P2X7, P2X4 agonists may cause problems with both pain and inflammation in patients. P2X2/3 receptors have been shown to be involved in pain sensation and antagonists may act as anti-analgesics; however they may also affect the patients' tastant responses and hearing. P2X1 receptors were shown to be involved in platelet aggregation and antagonists were thus suggested to be used to reduce thrombotic effects. However they may have an effect on the fertility of the male patients. These results show that although P2X receptors are key drug targets, there are many

factors that need to be considered for agonists or antagonists to be used as therapeutic agents.

1.3.7 P2X receptors - agonists and antagonists

1.3.7.1 Agonists

Although all P2X receptors are activated by ATP, their sensitivity to ATP and the kinetics of the current passing through the channel varies considerably for each subtype. The order of channel sensitivity to ATP is: P2X1R = P2X3R < P2X2R < P2X4R = P2X5R < P2X6R << P2X7R (Zemkova *et al*, 2004).

P2X1 and P2X3 undergo rapid desensitisation following application of 30 µM ATP (Fig 1.8), while P2X2 and P2X4 desensitise at a much slower rate. P2X5 does not desensitise (Ralevic and Burnstock, 1998). P2X7 requires a higher concentration of ATP for activation compared with other subtypes, experiencing full activation at 1mM ATP (North, 2002). Fig 1.9 illustrates the differing responses elicited by each homomeric receptor.

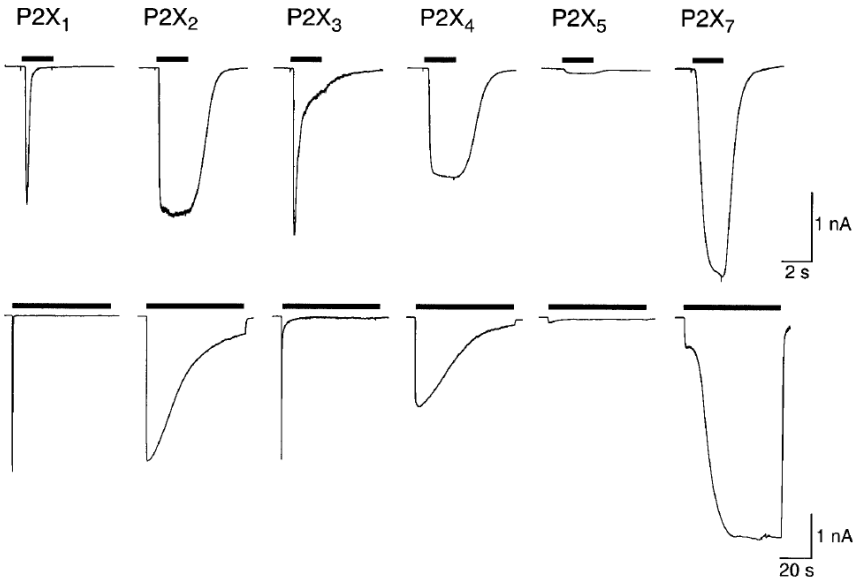

Figure 1.9 – Comparison of fast (top) and slow (bottom) desensitisation of homomeric rat P2X receptors transfected in HEK-293 cells, in response to 30 µM ATP (1mM for P2X7). Fast desensitisation is observed for P2X1 and P2X3 in response to a 2 second application of ATP. Slow desensitisation is observed for P2X2 and P2X4 in response to a 60 second application of ATP. P2X7 transfected cells experienced a 2 minute pre-application of ATP before the recorded application shown (Image: North, 2002).

As well as exhibiting differing responses to ATP, the subtypes display variable sensitivities to a number of other compounds. Many P2X subtypes are activated by ATP analogues; however the exact activation profile is subtype-specific.

P2X1, P2X3 and P2X5 subtypes are activated by the synthetic ATP analogue, αβ-methylene ATP (αβ-meATP). Their sensitivity to low micromolar concentrations of αβ-meATP distinguishes P2X1, P2X3 and P2X5 from the remaining homomeric receptors that are activated by significantly higher concentrations of αβ-meATP (Waldron and Sawynok, 2004, North, 2002). αβ-meATP and ATP are equally potent at human P2X1, with an EC_{50} in HEK-293 cells of 0.8- 1 μM (Evans *et al*, 1995).

2'(3')-*O*-(4-Benzoylbenzoyl)adenosine-5'-triphosphate (BzATP) is an ATP analogue with the addition of a benzoyl-benzoyl group to either the 2'- or 3'-position of the ribose moiety. BzATP acts as an agonist at all P2X subtypes with the exception of P2X3 and is highly potent at human P2X1 and P2X2 receptors (EC_{50} – 1-2 μM and 6 μM respectively) (Evans *et al*, 1995; Lynch *et al*, 1999). However it is much less effective at rat P2X1 and P2X2 receptors (EC_{50} - 24 μM and 23 μM respectively) (Wildman *et al*, 1999; Kew and Davies, 2010). BzATP is also active at human P2X4 (EC_{50} – 9.4 μM) and at human and rat P2X5 (EC_{50} – 1.3 μM and 5.7 μM respectively). Importantly, P2X7 is considerably more sensitive to BzATP (EC_{50} - 7 μM) than ATP (EC_{50} - 2.62mM) (Surprenant *et al,* 1996).

Adenosine 5'-O-(3 thiotriphosphate) (ATPγS) contains a sulphide group attached to the gamma phosphate group of ATP and is active at P2X1, P2X2, P2X3 and P2X5 receptors with variable potency (EC_{50} ranging from 0.29 μM [rP2X5] to 8 μM [rP2X2]) (Wildman *et al*, 2002; Evans *et al*, 1995; Lynch *et al*, 1999; Liu *et al*, 2001).

βY-methylene-ATP (βγmeATP) is an ATP derivative with a methyl group substitution for the oxygen between the β and ϒ phosphate groups. This compound is relatively insensitive at P2X2, P2X3 and P2X4 receptors. However it displays a relatively high potency at P2X1 (EC_{50} - 2 - 8.7 μM) and P2X5 (EC_{50} - 11.8 μM) (Evans *et al*, 1995; Wildman *et al*, 2002; Liu *et al,* 2000; Garcia-Guzman, 1997; Chen *et al*, 1995; Coddou *et al*, 2011).

2-Methylthioadenosine triphosphate (2MeSATP) contains a methylthio group attached to the adenosine ring of ATP. 2MeSATP is a full agonist of P2X1 and P2X2 (EC_{50} = 0.1 - 8 μM respectively) expressed in *Xenopus* oocytes (Evans *et al*, 1995; Lynch *et al*, 1999; Wildman *et al,* 2002). Additionally it activates P2X3, P2X4, P2X5 and P2X7 (EC_{50} – 0.3 μM, 10-100 μM, 0.44 μM and 200 μM respectively) (Garcia Guzman, 1997; Liu *et al*, 2001; Coddou *et al*, 2011; Wildman *et al*, 2002; Surprenant *et al*, 1996).

A summary of agonist activity of the compounds mentioned above and other agonists at all P2X subtypes can be referred to in Table 1.3.

Table 1.3 – P2X receptor agonists. Values given represent approximate EC_{50} values for compound at each subtype.

Compound	P2X1	P2X2	P2X3	P2X4	P2X5	P2X7
ATP	**0.8 µM** (human) (Evans *et al*, 1995) **0.1 -0.3 µM** (rat) (Wildman *et al*, 1999)	**8 µM** (rat) (Grubb and Evans, 1999)	**0.8 µM** (human) (Garcia-Guzman, 1997) **1.2 µM** (rat) (Chen *et al*, 1995)	**10 µM** (rat) (Buell *et al*, 1996) **5.5 µM** (human) (Jones *et al*, 2000)	**0.44 µM** (rat) (Wildman *et al*, 2002) **4 µM** (human) (Bo *et al*, 2003)	**2.62 mM** (mouse), **3.89 mM** (rat), **4.13 mM** (human) (Surprenant, 1996)
αβ-methylene ATP	**1 µM** (human) (Evans *et al*, 1995), **3 µM** (rat) (Wildman *et al*, 2002)	**Inactive** (rat) (Liu *et al*, 2001)	**2.5 µM** (human) (Garcia-Guzman, 1997) **1 -2 µM** (rat) (Lewis *et al*, 1995)	**Inactive** (human) Norenberg and Illes, 2000) **Acts as an antagonist IC50 – 4.6** (rat) (Jones *et al*, 2000)	**1.1 µM** (rat) (Wildman *et al*, 2002) **12.2 µM** (human) (Kotnis *et al*, 2010)	-
BzATP	**1-2 µM** (human) [Evans *et al*, 1995, **24 µM** (rat) (Wildman *et al*, 1999)	**6 µM** (human) (Lynch *et al*, 1999) **23 µM** (rat) (Kew and Davies, 2010)	Not determined (Coddou *et al,* 2011)	**9.4 µM** (human) (Stokes *et al*, 2011)	**1.3 µM** (rat) (Wildman *et al*, 2002) **5.7 µM** (human) (Bo *et al*, 2003)	**7 µM** (rat) (Surprenant *et al*, 1996),
ATPYS	**1 µM** (human) (Evans *et al*, 1995) **0.6 µM** (rat) (Wildman *et al*, 2002)	**6 µM** (human) (Lynch *et al*, 1999) **8 µM** (rat) (Liu *et al*, 2001)	**1.5 µM** (rat) Liu *et al*, 2001	-	**0.29 µM** (rat) (Wildman *et al*, 2002)	-
βY-methylene-ATP	**2 µM** (human) (Evans *et al*, 1995) **8.7 µM** (rat) Wildman *et al*, 2002)	**>300 µM** (rat) (Liu *et al*, 2000)	**> 100 µM** (human) (Garcia-Guzman, 1997) **>300 µM** (rat) (Chen *et al*, 1995)	**> 300 µM** (rat and human) (Coddou *et al*, 2011)	**11.8 µM** (rat) (Wildman *et al*, 2002)	-
2-meSATP	**0.8 µM** (human) (Evans *et al,* 1995), **0.1 µM** (rat) (Wildman *et al*, 2002)	**1 µM** (human) (Lynch *et al*, 1999) **8 µM** (rat) (Grubb and Evans, 1999)	**0.3 µM** (human) (Garcia-Guzman, 1997) **0.3 µM** (rat) (Liu *et al,* 2001)	**10 – 100 µM** (Coddou *et al*, 2011)	**0.44 µM** (rat) (Wildman *et al*, 2002)	**200 µM** (rat) (Surprenant *et al*, 1996)
Other agonists	Ap_3A, Ap_4A, Ap_5A**,** Ap_6A (rat) **– >100, 0.04, 0.9, 0.72 µM** respectively (Wildman *et al*, 1999)	Ap_4A - **15 µM** (rat) (Pintor *et al*, 1996))	Ap_3A, Ap_4A, Ap_5A**,** Ap_6A (rat) – **1, 0.8, 1.3, 1.6 µM** respectively (Wildman *et al*, 1999)	Ap4A**,** Ap_6A (rat) – **3, >100 µM** respectively (Wildman *et al*, 1999)	ADP – **3.6 µM** (rat), UTP – **8.2 µM** (rat), Ap_3A, Ap_4A, Ap_5A, Ap_6A **– 5, 0.3, 0.69, 5 µM** respectively (Wildman *et al*, 2002)	-

1.3.7.2 Antagonists

Pyridoxal-phosphate-6-azophenyl-2',4'-disulfonic acid (PPADS) and suramin are non-selective P2 receptor antagonists (Lambrecht *et al,* 1992). PPADS is relatively potent at P2X1, P2X2, P2X3 and P2X5 with an IC_{50} in the low micromolar range. It is also effective at blocking P2X7 with a slightly higher IC_{50} of 45-60 μM. However PPADS has no effect on P2X4 receptors. Similarly suramin is highly potent at P2X1-3 and P2X5 and is inactive at P2X4. Suramin exhibits a variable potency at the different mammalian P2X7 receptors (IC_{50} at rat P2X7 = 285 μM, IC_{50} at human P2X7 = 52 μM); these differences are likely to be caused by small variations in channel structure. The insensitivity of P2X4 to PPADS and suramin distinguishes P2X4 from the rest of the P2XR subtypes (Wildman *et al*, 2002; Evans *et al*, 1995; Lynch *et al*, 1999; Lewis *et al*, 1995; Buell *et al*, 1996; Bo *et al*, 2003; Surprenant *et al*, 1996)

8,8 - carbonylbis imino- 4,1-phenylenecarbonylimino-4,1-phenylenecarbonylimino.bis 1,3,5-naphthalenetrisulfonic acid (NF279), a suramin-related compound, is a potent antagonist at P2X1 receptors (IC_{50} – 19-50 nM). It is also active at P2X2, P2X3 and P2X7 receptors, but is inactive at P2X4 receptors (Damer *et* al, 1998; Rettinger *et al*, 2000a]; Klapperstuck *et al*, 2000). Brilliant Blue-G (BBG) shows potent antagonist effects at P2X7 (IC_{50} – 10 – 200nM) and also blocks P2X4 and P2X5 receptors. However it is less effective at the other P2X subtypes (Jiang *et al*, 2000a). 2'(3')-O-(2,4,6-trinitrophenyl)adenosine 5'-triphosphate (TNP-ATP) is a potent antagonist at all P2X subtypes (IC_{50} at P2X1 – 1-6 nM, IC_{50} at P2X7 - 30 μM). (Virginio *et al*, 1998; Wildman *et al*, 2002). These antagonists and other P2X antagonists can be referred to in more detail in table 1.4.

Despite the many non-selective P2 antagonists described here, there are still relatively few selective antagonists available for specific P2X subtypes, including P2X4 and P2X2, which are key drug targets in pain and inflammation. N-(benzyloxycarbonyl)phenoxazine (PSB-12054) is a recently developed selective hP2X4 antagonist. PSB-12054 (IC_{50} – 0.189 μM) was identified following a screen of N-substituted phenoxazine and acridone derivates in hP2X4 stably transfected 1321N1 astrocytoma cells. However, although PSB-12054 significantly reduced P2X4 channel activation, it did not completely block the response. Additionally, more potent compounds are still required for use as therapeutic agents against P2X4 (Hernandez-Olmos *et al*, 2012).

A series of anthraquinone derivatives were screened in *Xenopus* oocytes expressing rP2X2 in a search for selective P2X2 antagonists. Two potent P2X2 antagonists were identified. Sodium 1-amino-4-[3-(4,6-dichloro[1,3,5]triazine-2-ylamino)phenylamino]-9,10-dioxo-9,10-

dihydroanthracene-2-sulfonate (PSB-10211) displayed an IC_{50} of 86nM. Disodium 1-amino-4-[3-(4,6-dichloro[1,3,5]triazine-2-ylamino)-4-sulfophenylamino]-9,10-dioxo-9,10-dihydroanthracene-2-sulfonate (PSB-1011) displayed an IC_{50} of 79nM. However the latter was only 5-fold more selective at P2X2 compared with P2X1 and P2X3 (Baqi *et al*, 2011). The search for potent and selective P2X2 and P2X4 antagonists is still ongoing.

4,4',4",4"'-(carbonylbis(imino-5,1,3-benzenetriylbis(carbonylimino)))tetrakis-benzene-1,3-disulfonic acid (NF449) is a suramin analogue which is a highly potent antagonist at P2X1 receptors (IC_{50} – 0.05nM) with significant selectivity of human P2X1 over human P2X7, rP2X2, rP2X3 or rP2X4 receptors (IC_{50} – 40 μM, 47 μM, 1.82 μM and >300 μM respectively) (Braun *et* al, 2001; Hulsmann *et al*, 2003; Rettinger *et al*, 2005).

A number of selective P2X7 antagonists have been identified. Nelson and colleagues tested a series of disubstituted tetrazole compounds for P2X7 antagonist activity and identified 3-((5-(2,3-dichlorophenyl)-1H-tetrazol-1-yl)methyl pyridine (A-438079) as a reversible and competitive blocker at rat and human P2X7 receptors (IC_{50} of 100 and 300 nM respectively). Additionally it appeared to have little activity at other P2 receptor types (Nelson *et al*, 2006). N-(1-{[(cyanoimino)(5-quinolinylamino) methyl]amino}-2,2-dimethylpropyl)-2-(3,4-dimethoxyohenyl)acetamide (A-740003) is also a cyanoguinidine compound shown to have highly specific antagonistic activity at rat and human P2X7 receptors (IC_{50} of 18 and 40 nM respectively) (Honore *et al*, 2006).

A-317491 is a potent antagonist of P2X3 and P2X2/3 receptors (IC_{50} – 22 – 92 nM) and was shown to be highly selective over other P2 receptors. However A-317419 is not selective of P2X3 over P2X2/3 receptors (Jarvis *et al*, 2004). Similarly, Spinorphin, an endogenous antinociceptive peptide (LVVYPWT), which is a potent P2X3 antagonist (IC_{50} – 8.3 pM), does not distinguish between the two receptor complexes (Jung *et al,* 2007). More recently reports of a selective and potent P2X3 antagonist, RO-85, have been published (rat P2X3 IC_{50} = 31 – 32 nM, human P2X3 IC_{50} =0.4 μM) which is selective for P2X3 homozygous receptors over other P2X receptors tested (IC_{50} > 10 μM) (Brotherton-Pleiss *et al*, 2010).

The chemical structures of a selection of P2X antagonists are shown in Fig 1.10 for reference and show the diversity between the structures.

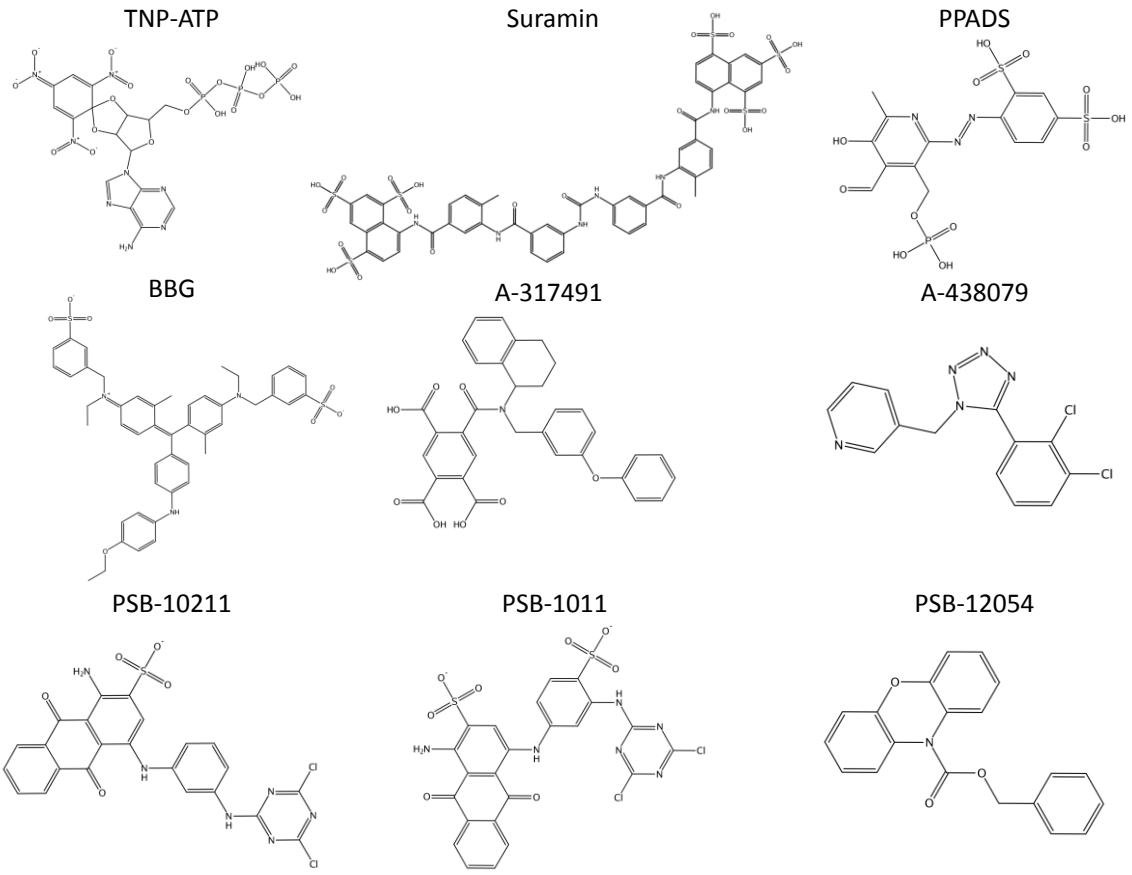

Figure 1.10 – Chemical structures of P2X antagonists. Non-selective P2X antagonists – TNP-ATP, Suramin, PPADS, BBG. P2X2/3 antagonist - A-317491. P2X7 selective antagonist – A-438079. P2X2 selective antagonists – PSB-10211, PSB-1011. P2X4 selective antagonist – PSB-12054.

Table 1.4 – P2X receptor antagonists. Values given represent approximate IC_{50} values for compound at each subtype.

Compound	P2X1	P2X2	P2X3	P2X4	P2X5	P2X7
PPADS	**0.12 µM** (Rat) (Wildman *et al*, 2002)	**1-6 µM** (human and rat) (Evans *et al*, 1995, Lynch *et al*, 1999)	**0.2 - 1.5 µM** (rat) (Lewis *et al*, 1995, Liu *et al*, 2001)	**Insensitive** (Buell *et al*, 1996)	**0.2 µM** (rat and human) (Wildman *et al*, 2002; Bo *et al*, 2003)	**45 - 60 µM** (rat) (Surprenant *et al*, 1996)
Suramin	**1.7 µM** (Rat) (Wildman *et al*, 2002)	**1-5 µM** (human and rat) (Evans *et al*, 1995; Lynch *et al*, 1999)	**3 -4 µM** (rat) (Lewis *et al*, 1995, Liu *et al*, 2001)	**Insensitive** (Buell *et al*, 1996)	**1.5 µM** (rat) (Wildman *et al*, 2002) **2.9 µM** (human) Bo *et al*, 2003)	**70 µM** (human) (Chessel *et* al, 1998)
NF279 (Suramin analogue)	**50 nm** (human) (Klapperstuck *et* al, 2000) **19 nm** (with pre-incubation) (rat) (Rettinger *et al*, 2000a)	**0.76 µM** (rat) (Rettinger *et al*, 2000a)	**1.62 µM (**with pre-incubation) (rat) (Rettinger *et al*, 2000a)	**Insensitive** (Rettinger *et al*, 2000a)	-	**4.8 µM** (mouse),**2.8 µM** (human) (Klapperstuck *et al,* 2000*)* **<4 µM** (rat) (Donnelly-Roberts *et al*, 2009)
BBG	-	-	-	**>10 µM** (rat), **3.2 µM** (human) (Jiang *et al*, 2000a)	**0.53 µM** (human) (Bo *et al*, 2003)	**10 nm** (rat), **200nm** (human) (Jiang *et al*, 2000a)
TNP-ATP	**1 nM** (Rat) (Wildman *et al*, 2002b) **6 nM** (human) (Virginio *et al*, 1998)	**1-2 µM** (rat) (Virginio *et al*, 1998, Liu *et al*, 2001)	**0.9 µM** (rat) (Virginio *et al*, 1998)	**15 µM** (rat/human) (Virginio *et al*, 1998)	**0.45 µM** (Rat) (Wildman *et al*, 2002)	**>30 µM** (rat) (Virginio *et al*, 1998)
RB-2	**2.3 µM** (Rat) (Wildman *et al*, 2002)	**0.4 µM** (rat) (Liu *et al*, 2001)	-	**-**	**18.3 µM** (Rat) (Wildman *et al*, 2002)	**-**
IP_5I	**0.003 µM** (Rat) (King *et al*, 1999)	**Insensitive** (King *et al*, 1999)	**2.8 µM** (rat) (King *et al*, 1999)	**0.002 µM** (rat) (King *et al*, 1999)	**>30 µM** (Rat) (Wildman *et al*, 2002)	**-**
Other antagonists	**NF449 (0.05 nM)** (human) (Hulsmann *et al*, 2003), **IP4I (0.56 µM)** (rat) (King *et al*, 1999) **NF023 (0.24 µM, 0.21 µM)** (rat, human) (Soto *et al*, 1999)	**NF770, NF776, NF778 (19 nM, 97 nM, 1.4 µM respectively)** (rat) (Wolf *et al*, 2011) **PSB1011, PSB10211 (79 nM, 86 nm respectively)** (rat) (Baqi *et al*, 2011)	**A-317491 (20 nM)** (Jarvis *et al*, 2002) **IP4I (1 µM)** (King *et al*, 1999) **RO-85 (6.4-7.5 nM)** (Brotherton-Pleiss *et al*, 2010) **Spindorphin (8.3 pM)** (Jung *et al*, 2006)	**PSB-12054 (0.189 µM)** (Hernandex-Olmos *et al*, 2012) **5-BDBD (0.5 µM)** (Donnelly-Roberts *et al*, 2008) **IP4I (1.69 µM)** (King *et al*, 1999)	**-**	**KN-62 (12.7 nM)**(Gargett and Wiley, 1997)**, o-ATP** (Di Virgilio, 2003), **AZ11645373 (90nM)** (human) (Stokes *et al*, 2006) **A-438079 (100nM and 300nM at rat and human)** (Nelson *et al*, 2006) **A-740003 (18-40nM at rat and human)** (Honore *et al*, 2006)

1.3.8 P2X receptors – Structure

The first crystal structure of a P2X receptor was solved in 2009 by Kawate *et al* at a resolution of 3.1 Å. This structure represented the closed state of zfP2X4.1. Additionally, in 2012, the ATP bound structure was solved at a resolution of 2.8 Å and the *apo,* closed structure was corrected and solved to a resolution of 2.9 Å (Hattori and Gouaux, 2012). zfP2X4.1 shares significant sequence similarity with mammalian P2X receptors. It is most similar to hP2X4 with 59% sequence identity and least similar to hP2X6 with 40% sequence identity (Fig 1.11; sequence alignment).

1.3.8.1 Zebrafish P2X receptors

Nine P2X receptor genes have been identified in the zebrafish, *Danio rerio*, 6 of which are orthologs of mammalian P2X subtypes – *zfP2X1, zfP2X2, zfP2X3.1, zfP2X4.1, zfP2X5* and *zfP2X7*. Two of the other identified receptors correspond to *zfP2X3.1* and *zfP2X4.1* paralogs (*zfP2X3.2* and *zfP2X4.2* respectively), the final receptor has not been classified (Kucenas *et al*, 2003). zfP2X4.1 displays significant sequence similarity to the mammalian P2X4 receptors, with an amino acid identity of 59% with rat P2X4 (rP2X4) and 58% with human P2X4 (hP2X4) (Figure 1.11). Additionally zfP2X4.1 is able to form functional homomeric channels, with properties comparable to the respective mammalian orthologs (Diaz-Hernandez *et al*, 2002).

When expressed in HEK-293 cells, zfP2X4.1 channels display a similar electrophysiological and pharmacological profile to rP2X4 (North, 2002), exhibiting a slow, incomplete desensitisation in response to ATP, and little or no response to the ATP derivatives 2'(3')-O-(4-Benzoylbenzoyl) adenosine-5'-triphosphate (BzATP) and α,β-Methylene adenosine 5’-triphosphate (αβmeATP). Additionally, zfP2X4.1 is not inhibited by the non-selective P2X antagonists, pyridoxalphosphate-6-azophenyl-2',4'-disulfonic acid (PPADS) and suramin, which are also ineffective at mammalian P2X4 receptors (Diaz-Hernandez *et al*, 2002; Buell *et al*, 1996). However, ATP is significantly less potent at zfP2X4.1 (EC_{50} = 275 – 800 μM [4, 22]) compared with the equivalent mammalian channels (rP2X4 EC_{50} = 10 μM (Buell *et al*, 1996; Khakh *et al*, 2001a); hP2X4 EC_{50} = 5.5 μM (Jones *et al*, 2000)).

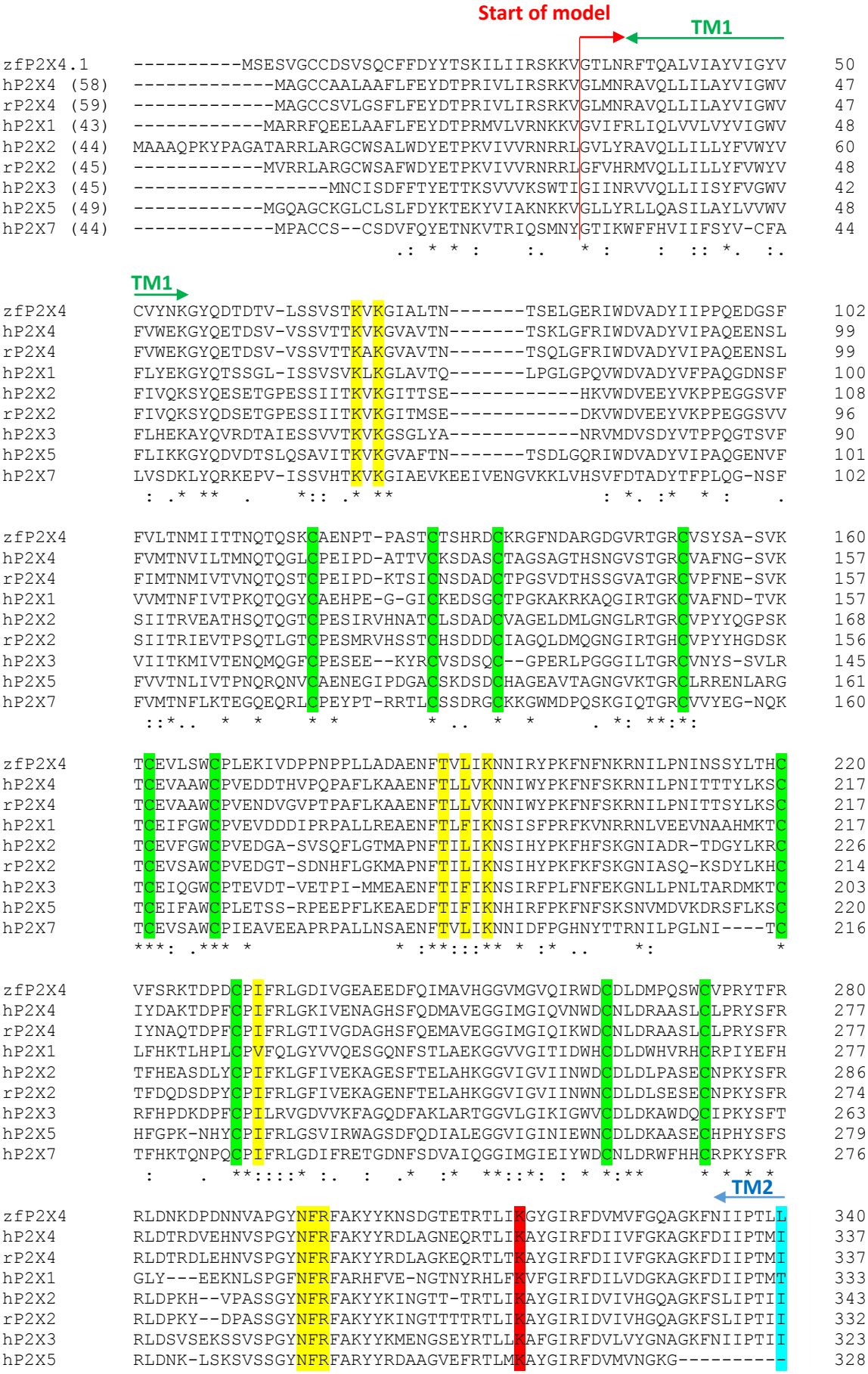
Start of model
TM1
TM1
TM2

Figure 1.11. Sequence alignment of selected mammalian P2X receptors with zfP2X4.1. The start and the end of the *zfP2X4.1* sequence present in the crystal structure (PDB ID 3H9V) are indicated with red arrows. The percentage amino-acid identities are indicated by the numbers in brackets next to the sequence names at the start of the alignment. TM1 and TM2 are indicated by green and blue double-headed arrows respectively. The ten conserved cysteine residues in the extracellular domain are indicated in green, the amino-acids which contribute to the ATP binding site are indicated in yellow, the amino-acids contributing to the channel pore are indicated in cyan, and the conserved lysine which contributes to both ATP binding and channel gating is indicated in red. The long C-terminal domains of P2X2 and P2X7, for which there is no structural information, are omitted.

1.3.8.2 Zebrafish P2X4.1 crystal constructs

zfP2X4.1 was chosen for structural studies following a screen of 35 different green fluorescent protein (GFP)-tagged P2X receptor homologs using fluorescence size exclusion chromatography (FSEC) following transient transfection in HEK-293 cells. The screen showed that zfP2X4.1 was capable of forming stable trimers in detergent and displayed a sharp, symmetrical elution profile following FSEC, which favoured it as a candidate for further structural studies. However, the addition of a GFP tag to the C-terminus of zfP2X4.1 had a significant effect on receptor function. According to Kawate *et al* the EC_{50} of ATP at wild type zfP2X4.1 was 800 µM, while the EC_{50} at zfP2X4.1-GFP was increased to 1.73 mM (Kawate *et al*, 2009).

To improve the crystallisation behaviour of zfP2X4.1, a number of modifications were made to the wild-type receptor. Firstly the N- and C-termini were truncated; 26 and 8 residue segments were removed from the N- and C-termini respectively to yield a crystal structure solved by single-wavelength anomalous diffraction in the presence of gadolinium (zfP2X4.1-A), which diffracted to 3.5 Å resolution (PDB ID - 3I5D). Additionally, 3 further point mutations (C51F, N78K and N187R) were introduced to the extracellular domain to reduce both non-native disulphide bond formation and heterogeneity due to glycosylation (zfP2X4.1-B). The structure of zfP2X4.1-B was solved by molecular replacement, yielding crystals that diffracted to 3.1 Å resolution (PDB ID - 3H9V). Although the mutated receptors were still responsive to ATP, the peak current amplitude was markedly reduced (by approximately 95% and 99% for zfP2X4.1-A and zfP2X4.1-B respectively) (Fig 1.12) when compared to the wild type GFP-tagged channel. Additionally, the agonist sensitivity was markedly increased with reported EC_{50} values of 27.4 µM and 3.4 µM for zfP2X4.1-A-GFP and zfP2X4.1-B-GFP respectively. The return of current to baseline on washout of agonist was significantly delayed in both crystal constructs (Kawate *et al*, 2009). These observations demonstrate that there are large differences in channel function between the wild-type and crystal constructs.

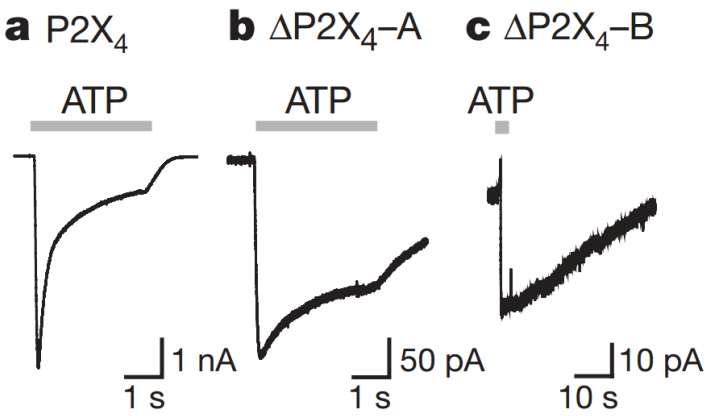

Figure 1.12 – Peak current amplitude in response to ATP for wild type zfP2X4 (a), zfP2X4.1-A (b) and zfP2X4.1-B (c) constructs. The peak current amplitude is reduced by approximately 95% for zfP2X4.1-A and 99% for P2X4.1-B compared to wild type. Reprinted by permission from Macmillan Publishers Ltd: [Nature] (Kawate *et al*), copyright (2009).

To solve the ATP bound structure of zfP2X4.1, additional mutagenesis of the receptor was required to improve crystallisation behaviour. Further truncation of the C-terminus (zfP2X4.1 final model, residues 36 – 359) and reversal of the initial C51F mutation gave rise to P2X4.1-C, which also gave a sharp, symmetrical elution profile following FSEC. The P2X4.1-C structure was solved by molecular replacement, using P2X4.1-B as a search probe, at a resolution of 2.8

Å (PDB ID - 4DW1; Fig 1.13B,D). Furthermore the structure of the *apo*-state zfP2X4.1-B construct was re-solved using new crystals which diffracted to a higher resolution of 2.9 Å (referred to as zfP2X4.1-B2; PDB ID 4DW0; Fig 1.13A,C) (Hattori and Gouaux, 2012). Electron density maps from the new *apo*-state structure (PDB ID 4DW0) showed an incorrect assignment of electron density in the region encompassing residues 88 – 97 in the previously published structures (PDB IDs 3H9V and 3I5D). The functional properties of GFP-tagged zfP2X4.1-C were measured using two-electrode voltage clamp of *Xenopus* oocytes; the authors stated that the functional properties of this receptor were similar to that recorded for wild-type zfP2X4.1, yet their EC_{50} value was significantly different (2.1 µM compared to 1.73 mM for the wild-type GFP-tagged construct (Hattori and Gouaux, 2012)). They did not report peak current values for wild-type zfP2X4.1 in their experiments, so it is not known how much peak current amplitudes were impaired by the introduced mutations, but it is clear from the current traces that zfP2X4.1-C also displayed delayed return of current to baseline values on washout of agonist, so from this evidence it is reasonable to assume that the function of zfP2X4.1-C was impaired in a similar fashion to the zfP2X4.1-A and zfP2X4.1-B crystal constructs. While the crystal structure derived from the zfP2X4.1-C construct clearly represents an ATP-bound structure, because of the impairment of function, it may well represent an artificially stabilised open state for the channel (because of the delayed return of current to baseline on washout of agonist).

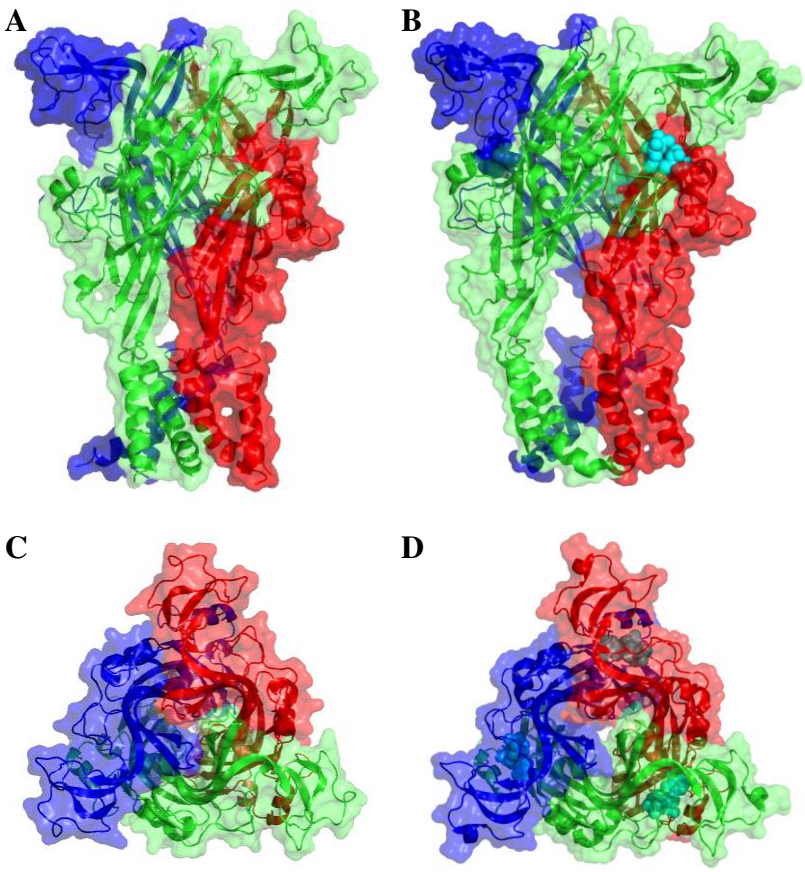

Figure 1.13 - Representation of the crystal structures of zfP2X4.1. The *apo*-, closed state zfP2X4-B2 (PDB ID - 4DW0) crystal structure viewed from the side (A) and the top (extracellular side) (C). The ATP bound, open state zfP2X4-C (PDB ID - 4DW1) crystal structure viewed from the side (B) and the top (extracellular side) (D). Each subunit is represented by a different colour. ATP in the binding pocket between 2 adjacent subunits is shown in cyan.

1.3.8.3 The ATP binding site

Preceding determination of the crystal structure of zfP2X4.1, mutagenesis and functional experiments were used to ascertain key residues involved in ATP binding of P2X receptors. P2X receptors do not contain any of the previously identified ATP binding motifs associated with other ATP binding proteins, such as the Walker motif (Walker *et al*, 1982). It was hypothesized that polar and positive amino acids conserved across P2X subtypes may play a role in ATP binding and activity. Site-directed mutagenesis has been used to assess the function of some of these highly conserved residues at a number of P2X subtypes.

Residues thought to contribute to the ATP binding pocket have been identified in hP2X1, rP2X2, hP2X3 and rP2X4. An alanine-scanning mutagenesis study in rP2X2 performed by Jiang *et al* identified Lys-69, Lys-71 and Lys-308 as critical residues for ATP binding. K69A and K308A

mutations in rP2X2 gave rise to non-functional channels, K71C channels experienced a marked reduction in function, with a 1000-fold reduction in affinity for ATP (Jiang *et al*, 2000b). Additionally, Leu-186 was shown to be involved in the binding of the adenine base of ATP (Jiang *et al*, 2011).

Similarly Ennion *et al* studied the effect of mutating 11 conserved positive residues in the extracellular loop of hP2X1. K69A and K308A (rP2X2 numbering) mutations led to a dramatic reduction (< 1,400 fold) in ATP potency. Upon mutation of Lys-308 to arginine, another positively charged amino acid, the channel was 25 fold less sensitive to ATP. These results indicate the individual chemical properties of the amino acid, as well as the charge, contribute to the binding of ATP. Lys-71 and Arg-290 were also proposed to contribute to the ATP binding pocket of hP2X1 (Ennion *et al*, 2000).

The conserved Lys-69 and Lys-71 residues have been shown to be highly important for ATP recognition in hP2X1, hP2X2, rP2X2, hP2X3, rP2X4 homomers and rP2X2/P2X4 heteromers (Roberts *et al*, 2008; Jiang *et al,* 2000b; Allsopp *et al*, 2011; Bodnar *et al*, 2011; Wilkinson *et al*, 2006). Lys-188 and Lys-308 have also been implicated in agonist recognition in hP2X1, hP2X2, rP2X2, hP2X3, rP2X4 and hP2X7 receptors (Ennion *et al*, 2000; Roberts and Evans, 2007; Roberts *et* al, 2008; Bodnar *et* al, 2011; Jiang *et al*, 2000b]; Worthington *et al*, 2002). Arg-290 is also understood to interact with the phosphate group of ATP in hP2X1, rP2X2, hP2X3 and rP2X4 receptors (Ennion *et al*, 2000; Jiang *et al*, 2000b; Fischer *et al*, 2007; Zemkova *et al*, 2007).

ATP was proposed to bind at the interface between 2 adjacent subunits, as opposed to within one subunit, using a disulphide cross-linking approach in hP2X1. Mutation of Lys-69 and Phe-289 to cysteine residues leads to cross-linking between neighbouring subunits, indicating them to be in close proximity between 2 adjacent subunits. Furthermore these channels showed a reduction in ATP potency. However upon application of dithiothreitol (DTT), which disrupts disulphide bond formation, these currents were increased 60 fold, indicating an inter-subunit ATP binding site at hP2X1 receptors (Marquez-Klaka *et al*, 2007). These results were later replicated with P2X2 receptors. However cross-linking between equivalent residues was less efficient in P2X3 and P2X4 receptors, signifying one of these residues may not play a role in ATP binding in these subtypes (Marquez-Klaka *et al*, 2009).

In zfP2X4.1, the ATP binding site is embedded in the receptor between the upper body domain of subunit A and the lower body and dorsal fin of subunit B (Fig 1.14A) (Hattori and Gouaux,

2012). The site is lined by a number of positively charged residues that form extensive hydrophilic interactions with ATP. ATP assumes a U-shaped conformation in the binding pocket; the phosphate groups form salt bridges and hydrogen bonds with surrounding polar and basic amino acids. In agreement with previous data, Lys-69 is shown to have a crucial role in ATP binding, forming critical interactions with all 3 phosphate groups. Additionally Asn-288 and Lys-308 form further contacts with the β-phosphate. The γ phosphate further interacts with Lys-71, Arg-290 and Lys-308 residues (rP2X2 numbering) (Fig 1.14) (Hattori and Gouaux, 2012; Chataigneau *et al*, 2013).

The extensive number of interactions the γ-phosphate forms with surrounding residues gives partial insight into why P2XRs are responsive to ATP, but not to ADP or AMP (Coddou *et al*, 2011). However the β- and γ- phosphate groups are not fully submerged in the binding pocket, raising a possible explanation for why rP2X receptors are activated by diadenosine polyphosphates (Wildman *et al*, 1999).

The adenine base is buried deep within the binding pocket and forms a number of interactions with highly conserved residues. The side chain of Thr-184 forms 3 hydrogen bonds with the adenine base. The adenine base also undergoes interactions with the carbonyl oxygen groups in the main chain of Lys-71 and Thr-184. Furthermore, hydrophobic interactions are formed with Leu-186 and Ile-226 (rP2X2 numbering) (Fig 1.14) (Hattori and Gouaux, 2012).

Many of the key residues identified in zfP2X4.1 involved in ATP binding are conserved across the mammalian P2X receptors studied, and molecular modelling implies that a similar agonist binding site is likely to exist in mammalian channels (see Fig 1.14B for example). Differences in the non-conserved residues lining the ATP binding cavity are likely to reflect differences in sensitivity to agonists and competitive antagonists. More detail on the key residues involved in ATP binding can be found in (Chataigneau *et al*, 2013).

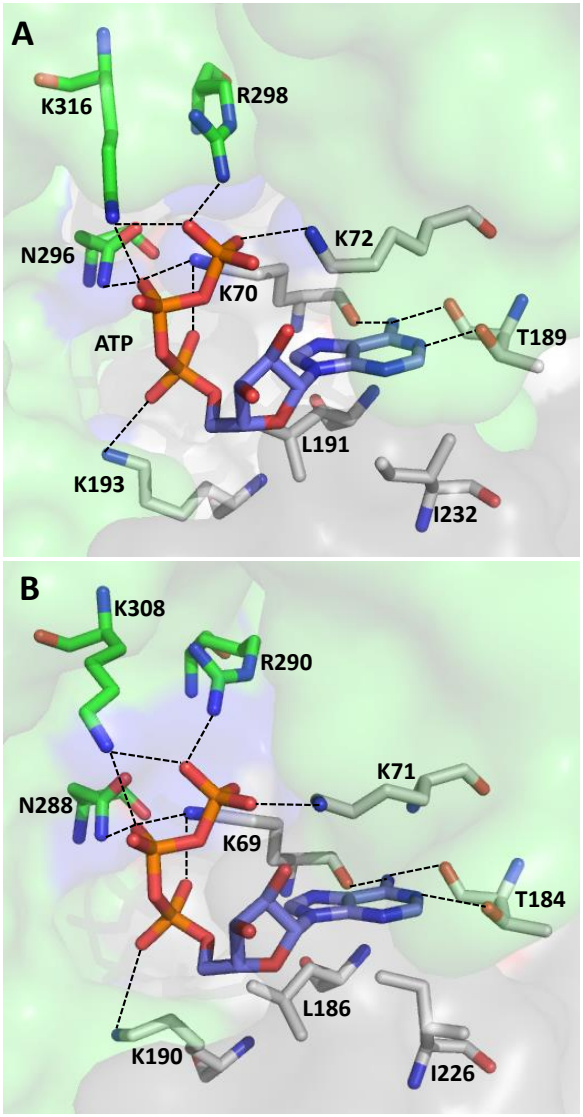

Figure 1.14 - The ATP binding site of P2X receptors. (A) ATP-binding site of zfP2X4.1 (PDB ID - 4DW1). (B) ATP binding site in a molecular model of rP2X2. Black dashed lines designate hydrogen bonds. ATP is shown in orange and blue with nitrogen and oxygen atoms represented in dark blue and red respectively. Residues from chain A are shown in green. Residues from chain B are shown in grey.

1.3.8.4 Pore lining residues and the transmembrane domains

Mutational analysis has been used extensively to study the transmembrane pore-lining residues of P2X receptors. P2X receptors show differential preference towards certain cations. For example, P2X2 has a much higher affinity for calcium over sodium (Virginio *et al*, 1998). Additionally, P2XRs demonstrate a specific selectivity sequence to alkali metal cations (K(+) > Rb(+) > Cs(+) > (Na(+) > Li(+)). This differs from the ions' relative mobility in water, indicating that the receptors are able to distinguish between a selection of cations, regardless of size,

and that cations are likely to undergo weak interactions with the interior of the channel pore (Ding and Sachs, 1999; Migita *et al*, 2001).

The second transmembrane domain of rP2X2 contains a number of polar amino acids that are hypothesized to line the pore and form a hydrated surface for cation conductivity, regulating the current by solvating ions within the pore (Egan *et al*, 1998; Rassendren *et al*, 1997). Three of these polar residues in rP2X2, Thr-336, Thr-339 and Ser-340, are thought to be important for cation selectivity. Mutation of Thr-336, Thr-339 or Ser-340 to the hydrophobic amino acid tyrosine leads to a substantial change in calcium permeability and the alkali metal cation selectivity sequence (i.e. the receptor could no longer distinguish between the different ions). This data suggests the permeability sequence of P2X2 is partly composed of these 3 polar amino acids in TM2 interacting with permeating cations (Migita *et al*, 2001).

In addition, mutation of Thr-339 in rP2X2 (T339S) gave rise to a channel with spontaneous opening activity. ATP was also ten times more potent at rP2X2 T339S compared to wild-type rP2X2, suggesting that the T339S mutation causes destabilisation of the closed channel. Lys-308 and Lys-69 are conserved residues, likely to be involved in ATP binding, as previously described. A K69A/T339S double mutant channel gave the same phenotype as the T339S single mutant. However a K308A/T339S mutant channel underwent no spontaneous activity, implying that Lys-308 may be involved in channel gating as well as ATP binding (Cao *et al*, 2007).

The crystal structure of zfP2X4.1 revealed that interactions between Leu-332, Leu-338 and Ile-347 are important for stabilizing the closed pore conformation. These interactions are broken upon activation of the channel as the transmembrane domains move apart. Additionally, new interactions are formed between Leu-338 and Ile-347. The ion permeation pathway pore of zfP2X4.1 is lined by Leu-332, Ala-336, Ala-339, Leu-343 and Ile-347 (rP2X2 numbering) (Hattori and Gouaux, 2012). It is noteworthy that the majority of the pore-lining residues possess hydrophobic side chains. This is in contrast to the key residues hypothesized to line the mammalian P2X2 pore, which predominantly consists of polar amino acids. For example, in rP2X2, the equivalent amino acid to the hydrophobic isoleucine residue at position 347 is the polar residue tyrosine. In the mammalian P2X2 receptor, the polar side chains lining the pore may interact directly with the hydrated cations. These significant differences in pore lining residues imply there may be dissimilarities in the way cations pass through the transmembrane domains in the zfP2X4.1 receptor and the mammalian receptors. Clearly this

observation has implications for interpretation of the pore function of mammalian P2X receptors based upon the zfP2X4.1 crystal structure.

1.3.8.5 The N-terminus

The roles of the N- and C-termini of P2X receptors in channel desensitization kinetics has been extensively studied in P2X1 and P2X2 receptors. The N-terminus of P2XRs contains a highly conserved protein kinase C (PKC) binding site, TX(K/R). Two conserved N-terminal residues – Thr-18 and Lys-20 in rP2X2 – are important for its slow rate of desensitisation compared to P2X1. Abolition of the PKC consensus site via T18A, T18N and K20T mutations in rP2X2 gave rise to a change in channel kinetics, with channels undergoing fast desensitization in response to ATP. A P19A mutation gave rise to channels with similar desensitisation kinetics to wild type P2X2 channels. These results implicate the TX(K/R) PKC consensus site as a critical determinant of P2X2 kinetics (Boué-Grabot *et al*, 2000). Similarly P2X1 Y16C, T18C and R20C mutants experienced a reduction in peak current amplitude and changes in desensitization kinetics, demonstrating an important role for these residues in specific channel kinetics (Wen and Evans, 2009).

In 2013, Allsopp and colleagues used P2X1/2 N- and C- terminal chimeric proteins to investigate the effects of the intracellular termini on channel kinetics. They noted that mutating the N-terminus affects partial agonist efficacy without altering agonist potency. Additionally, the first 16 amino acids of the N-terminus predominantly control agonist efficacy, whereas the N-terminal region adjacent to TM1 is likely to fine-tune these effects (Allsopp *et al*, 2013). Specifically, residues 21-23 were suggested to affect desensitization in P2X1 and P2X2 receptors. (Allsopp *et al*, 2011).

The zfP2X4.1 construct used for crystallization contained an N-terminal truncation (28 amino acids), therefore all the residues identified above with roles in channel kinetics of P2X1 and P2X2 were removed prior to protein expression, purification and structure determination. This N-terminal truncation may account for the large reduction in peak amplitude in response to ATP observed for the zfP2X4.1 crystal constructs. It may also play a role in delayed return of current to baseline after washout of agonist.

1.3.8.6 The C-terminus

The C-terminal domains are the most variable domains among the P2X receptors; P2X2 and P2X7 receptors have long intracellular C-termini for which no structural information is available. However these domains are thought to play important roles in channel kinetics, with

certain residues regulating recovery from desensitization. The partial agonist efficacy at a P2X1-2C chimeric channel was intermediary between efficacy at wild-type P2X1 and P2X2 receptors. However unlike the N-terminus, the C-terminal domain was also associated with a decrease in agonist potency. Residues 360-364 are involved in regulation of channel recovery from desensitisation (Allsopp *et al*, 2013).

Additional potential PKC sites are present in the C-terminus of rP2X2 at Thr-372 and Thr-464. Elimination of these sites from rP2X2 via a truncation of the receptor at His-375 and mutation of Thr-372 gave rise to channels that experience rapid desensitisation in response to ATP. Additionally, truncated channels in combination with N-terminal PKC site mutations (T18A, K20T) displayed peak currents with a significant smaller amplitude. This data indicates that in addition to the PKC site in the N-terminus, P2X2 receptors require specific intracellular interactions between the 2 cytoplasmic domains for complete cell surface expression of slowly desensitising channels (Boué-Grabot *et al*, 2000).

The C-terminal domain of zfP2X4.1 was truncated at position 359 in zfP2X4.1-C so the YXXXK trafficking motif responsible for plasma membrane targeting was absent and this may have had a significant effect on receptor function (described in section 1.3.5). Additionally the mammalian P2X4 tyrosine based, endocytic motif (YEQGL) (described in section 1.3.5) is not present in zfP2X4.1; the equivalent residues following the tyrosine (GLLH) were truncated in the zfP2X4.1 construct used for crystallisation. Therefore if wild type zfP2X4.1 undergoes rapid internalisation and reinsertion into the membrane, disruption of these residues may have had an effect on channel trafficking and function.

1.3.8.7 Apo, closed vs open state structures

Publication of the crystal structures of the *apo*- and ATP-bound states of zfP2X4.1 receptors has provided valuable insight into the structure and mechanism of action of P2X receptors. The structures have enabled us to identify key residues involved in agonist binding and pore-lining residues with roles in cation selectivity (Kawate *et al*, 2009; Hattori and Gouaux, 2012).

Kawate *et al* liken the receptor monomer to a leaping dolphin and the various domains have been named accordingly (Fig 1.15A). The transmembrane domains are referred to as the tail or fluke domain of the dolphin. The extracellular domain is made up of the upper body, lower body, dorsal fin, the left and right flippers and the head region. The body region of the dolphin is made up of β-sheets to form a β sandwich domain. The trimeric form of the closed-state receptor is represented as 3 dolphin monomers wrapped around one-another. The majority of

subunit-subunit interactions are found in the upper body domain, with fewer interactions found in the lower body domain, proximal to the TM domains, which is consistent with a structure that permits movement (transmission of a conformational change induced by agonist binding to the channel pore) (Hattori and Gouaux, 2012).

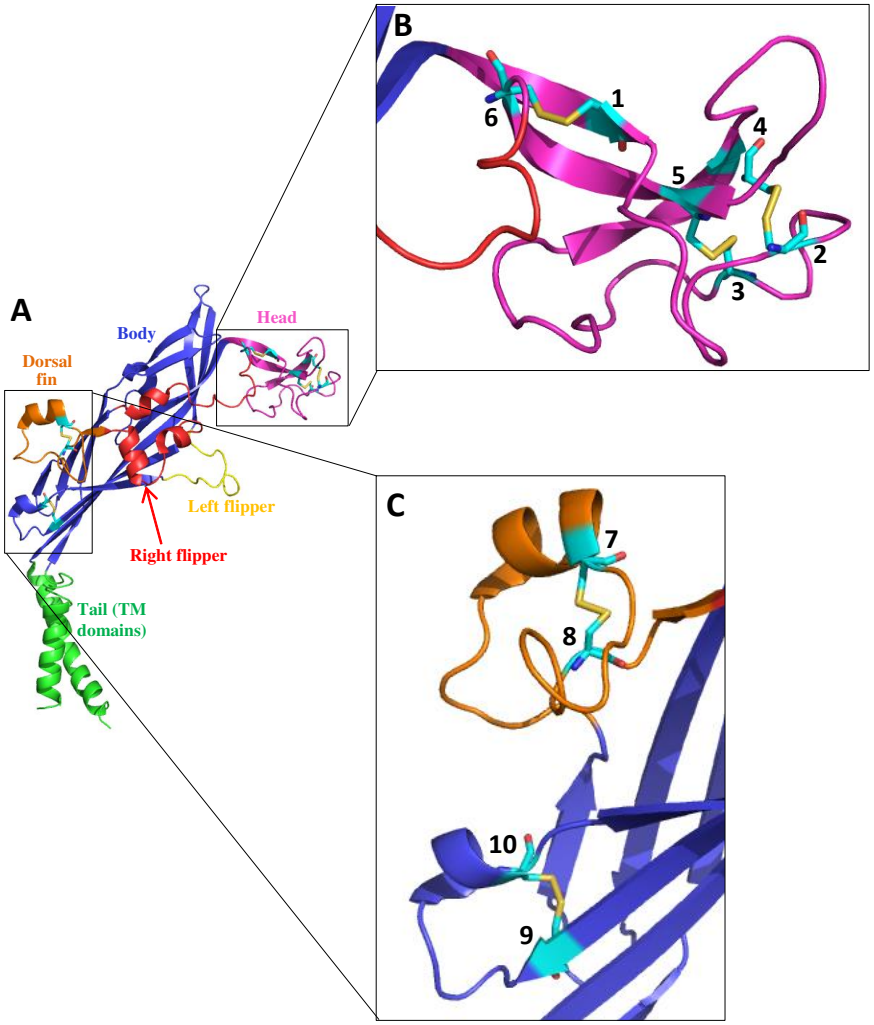

Figure 1.15 - Schematic of a zfP2X4.1 monomer and location of disulphide bonds. (A) Schematic structure of a zfP2X4.1 monomer, showing the analogy of the receptor monomer to a dolphin with labelled domains. (B) Close-up of the head domain showing the location of the disulphide bond pairs 1-6, 2-4 and 3-5. Disulphides are shown in yellow. (C) Close-up of the body and dorsal fin domains showing the location of the disulphide bond pairs 7-8 and 9-10. Disulphides are shown in yellow.

Mammalian P2X receptors contain 10 extracellular conserved cysteine residues that form 5 disulphide bond pairs; 1-6 (Cys-119-Cys-168), 2-4 (Cys-129-Cys-152), 3-5 (Cys-135-Cys-162), 7-8 (Cys-220-Cys-230), and 9-10 (Cys-264-Cys-273), (Corresponding to rP2X2 Cys-113, Cys-164, Cys-124, Cys-147, Cys-130, Cys-158, Cys-214, Cys-224, Cys-258 and Cys-267 respectively) confirmed by the zfP2X4.1 crystal structure (Fig 1.15B and 1.15C). Disulphide pairs 1-6, 2-4 and 3-5 are located in the head region of the receptor, 7-8 is situated in the dorsal fin region and 9-10 in the lower body region, proximal to the TM domains (Kawate *et al*, 2009). Disulphide bonds have important roles in the formation and maintenance of ion channel structure. Although in hP2X1, all single cysteine residue mutants gave rise to functional channels, some of the mutants (C264A, C273A, C135A, C162A corresponding to the 3-5 and 9-10 disulphide

bond pairs (zfP2X4.1 numbering)) caused a reduction in current amplitudes. Additionally C264A and C273A channels are not efficiently trafficked to the cell surface. These results indicate that Cys-264 and Cys-273 are involved in the formation of a disulphide bond and disruption has implications on the tertiary structure of the protein, thereby preventing it from being trafficked to the cell membrane (Ennion and Evans, 2002). In addition, *Dictyostelium discoideum* P2XA (DdP2XA) does not contain any of the conserved disulphide bonds stated above, however it is still functional and low resolution structural studies indicate that it has a similar architecture to zfP2X4.1 (Valente *et al*, 2011).

The extracellular domain of zfP2X4.1 appears to be shaped like an equilateral triangle, extending approximately 70 Å above the membrane. The transmembrane domain is 28 Å long and adopts a chalice-like shape through the membrane. The transmembrane helices show a left-handed twist orientation and are anti-parallel to one another, approximately 45° from the membrane plane (Kawate *et al*, 2009). The transmembrane pore is predominantly lined by the TM2 domains, with the TM1 helices positioned peripheral to the TM2 helices. The pore is open and continuous with the narrowest part of the pore marked by Ala-347 and Leu-351 (Thr-339 and Val-343 in rP2X2) (Hattori and Gouaux, 2012).

Superposition modelling of the two channel states shows that ATP binding does not greatly affect the conformation of the upper body domain, inferring that this part of the structure stays relatively rigid upon activation. Conversely, the lower body domain undergoes substantial conformational changes upon agonist binding, resulting in an outward 'flexing' of the lower body domain (Fig 1.13B). Movement of these domains results in an expansion of the transmembrane helices. The transmembrane domains undergo conformational changes in an iris-like movement when ATP binds to the extracellular domain. TM1 and TM2 rotate anticlockwise by 10° and 55° respectively proximal to an axis perpendicular to the membrane plane. Their tilt angle is also increased by 8° and 2° respectively about an axis parallel to the membrane. These movements result in the helices moving away from the central axis, allowing expansion of the ion conducting pore to a width that would permit the flow of ions through the channel, consistent with a transition from closed- to open-state (Hattori and Gouaux, 2012).

Inspection of the electron density of both the *apo*- and ATP-bound states reveals that it is of poorest quality in the transmembrane regions, which is not unusual for membrane proteins.

Several side chain positions within the TM domains cannot be assigned, and so care must be taken when interpreting data for the TM domains with these structures (Wang *et al*, 2012).

Lateral fenestrations present in the extracellular vestibule of the receptor open wide upon ATP binding and provide a pathway for the influx of cations into the channel. Once the ions have entered through the fenestrations, the highly acidic residues of the central vestibule attract only cations and repel anions, which is thought to contribute to the cation selectivity of the channel (Kawate *et* al, 2011; Samways *et al*, 2011; Hattori and Gouaux, 2012; Kracun *et al*, 2010; Samways *et al*, 2012).

The structure determination of zfP2X4.1 represents the first major breakthrough in high resolution imaging of a P2X receptor, providing great insight into the mechanism of action of the receptor and how the receptor is designed to open upon ATP binding. However, as noted above, zfP2X4.1 has some significantly different characteristics to most mammalian P2X receptors (relatively low ATP potency, hydrophobic residues lining the channel pore), and the function of the crystal constructs was significantly different to wild-type zfP2X4.1 and so it is still important to strive for high-resolution structures of mammalian P2X receptors, both for comparative structural biology and structure based drug design.

1.3.9 P2Y receptors

P2Y receptors are metabotropic membrane proteins activated by ATP and ADP. Upon ATP binding to P2X and P2Y receptors, there is an increase in intracellular calcium either from the extracellular environment (P2X) or from intracellular stores (P2Y). Unlike P2X receptors, P2Y receptors, of which there are 8 subtypes (P2Y1, P2Y2, P2Y4, P2Y6, P2Y11, P2Y12, P2Y13 and P2Y14), are G-protein coupled receptors. Their activation by ATP induces downstream signalling via intracellular second messengers that lead to calcium release from stores (Burnstock, 2007; Burnstock and Verkhratsky, 2010). P2Y activation induces activation of phospholipase C (PLC) by exchanging guanosine diphosphate (GDP) for guanosine triphosphate (GTP) on G_{α} subunits. PLC cleaves phosphatidylinositol 4,5-bisphosphate (PIP_2) into inositol triphosphate (IP_3) and diacylglycerol (DAG). IP_3 binds to its cognate receptor in the endoplasmic reticulum and calcium is released from thapsigargin-sensitive stores (Fig 1.16) (Wu et al, 2007). 2-Aminoethoxydiphenyl borate (2-APB), a membrane-penetrable modulator, can block P2Y signaling by preventing IP_3 induced calcium release (Maruyama *et al*, 1997).

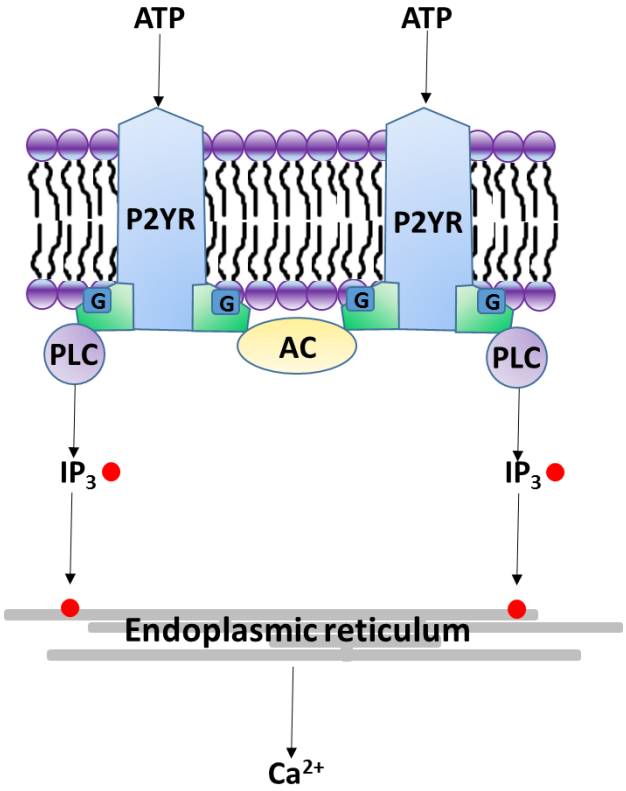

Figure 1.16 – Calcium signalling pathway of P2Y receptors. ATP couples to the receptor inducing exchange of GDP for GTP. The release of Gα leads to activation of PLC. PLC cleaves PIP2 to form IP3 and DAG. IP3 binds to IP3 receptors in the endoplasmic reticulum leading to the release of calcium into the cell from intracellular stores (image adapted from Burnstock and Verkhratsky, 2010).

1.4 Pannexin channels

1.4.1 Introduction to Pannexin channels

Pannexin (Panx) channels are non-selective ion channels that allow the passage of small molecules up to 1kDa in size (Wicki-Stordeur and Swayne, 2014). The family of pannexin proteins was first identified due to their restricted sequence homology (25 – 33% identity) to the invertebrate family of Innexin gap junction proteins (Panchin *et al,* 2000). The pannexin family consists of 3 subtypes – Panx1, Panx2 and Panx3. Panx1 is expressed across a large range of cell and tissue types in mammals, whereas Panx2 and Panx3 have a more restricted pattern of expression (Baranova *et al,* 2004). Panx2 has a role in neuron differentiation (Swayne *et al,* 2010) and is found predominantly in brain tissues including the cerebellum and the cerebral cortex. Although low levels of Panx3 expression have also been detected in human hippocampus extracts (Baranova *et al,* 2004), it is predominantly expressed in bone and skin tissues (Penuela *et al,* 2012).

Multiple factors can contribute to channel opening of Panx1, the most extensively studied of the pannexin family. Panx1 is activated by membrane depolarisation and increased extracellular potassium concentrations (Silverman *et al,* 2009). However it can also be modulated by mechanical stresses such as osmolarity and pressure changes (Bao *et al*, 2004). Panx1 is activated by Gαq coupled receptors via Rho and downstream kinase activity, however the exact mechanisms regulating this pathway are poorly understood (Sandilos and Bayliss, 2012). Panx1 channel currents and ATP release are inhibited at multiple sites (Cys 40 and Cys346) by S-nitrosylation (Lohman *et al*, 2012).

1.4.2 Pannexins - Expression and topology

Pannexin channels are formed by multiple subunits; Panx1 is predicted to assemble into hexameric channels at the cell membrane, according to cross-linking and SDS-PAGE experiments performed by Boassa and colleagues (2007). Additionally, low resolution electron microscopy studies of protein purified from Madin-Darby canine kidney (MDCK) cells show that Panx1 and Panx2 form channel-like structures, similar in appearance to Connexin26 (Cx26) (Ambrosi *et al*, 2010). Panx1 and Panx2 were also expressed and purified from Sf9 insect cells and electron microscopy was used to determine the channel size of the proteins. Due to different orientations of the proteins, 2 diameter averages were obtained for each subtype – 120 and 160 Å for Panx1, 183 and 190 Å for Panx2. These results agree with the hypothesis that Panx2 forms a higher oligomeric structure than Panx1. The predicted pore sizes of Panx1

are 17 and 21 Å, and for Panx2 29.5 and 30.5 Å. These pores are considerably larger than that noted for Cx26 which has a pore size of 12.5 Å. However these measurements were taken from averaged 2D projection images and pore size may vary across the axis of the pore (Ambrosi *et al,* 2010).

Despite the structural homology of Panx channels to connexin channels, multiple groups have shown that Panx receptors do not form gap junctions. For example, Ambrosi and colleagues (2010) used immunogold labelling experiments to show Panx1 expressing membranes were labelled on one side of the membrane, presumed to be the cytoplasmic side, whereas connexin expressing membranes were labelled on both sides of the membrane indicating the formation of gap junctions (Ambrosi *et al,* 2010).

Due to the significant sequence similarity between Panx1 and Panx3, Panx3 is also predicted to form hexameric channels. On the other hand, cross linking experiments have predicted that Panx2 forms octameric channels (Ambrosi *et al,* 2010). Each monomeric subunit of all pannexin channels consists of 4 α-helical transmembrane domains, 2 extracellular loops, 1 intracellular loop and intracellular N- and C- termini (Fig 1.16). Although the vertebrate gap junction family, connexins, share little sequence homology with pannexins, all three families of proteins (Pannexins, Connexins, Innexins) are predicted to have the same subunit topology (Yen *et al,* 2007; Baranova *et al*, 2004).

1.4.3 Pannexins - Trafficking

Trafficking of pannexin channels to the cell surface is vital for channel function and is regulated by cells in a number of ways. Both a fully intact C-terminal domain and appropriate N-linked glycosylation are required for Panx expression at the cell surface (Gehi *et al*, 2011). In addition, the number of channels expressed at the membrane is regulated by COP II (Coat-protein II), which has a role in the ER-to-Golgi trafficking transition. Pannexin channels can also be internalised independently of clathrin/calveolin/dynamin II mechanisms, regulating the level of protein expressed at the membrane (Gehi *et al*, 2011).

Sequencing and site directed mutagenesis work by Penuela and colleagues in 2007 revealed that both Panx1 and Panx3 subunits contain one N-linked glycosylation site, Asn-254 in the second extracellular loop of Panx1 and Asn-71 in the first extracellular loop of Panx3. Panx2 also contains a potential N-linked glycosylation site at Asn-86 in the first extracellular loop; however glycosylation at this site has not been ascertained (Fig 1.17) (Penuela *et al,* 2013).

Three glycosylation states of Panx1 have been identified, the non-glycosylated, core form of Panx1, the high mannose glycosylated form which is mostly located at the ER and the fully functional, complex glycosylated form of Panx1 (Penuela *et al*, 2009). Glycosylation of Asn254 is important for trafficking of Panx1 to the plasma membrane. Upon mutagenesis of this residue (N254Q) there is a significant reduction in levels of Panx1 protein expressed at the cell surface, suggesting glycosylation plays an important role in protein trafficking (Boassa *et al*, 2007). However glycosylation does not affect the function of the channels; the few receptors that are trafficked to the surface are fully functional (Penuela *et al,* 2009). The glycosylation of Panx1 at the extracellular domain (N254) is suggested to be responsible for interfering with the possible docking of 2 channels to form gap junctions, increasing the likelihood of the proteins forming singular membrane channels (Boassa *et al*, 2008).

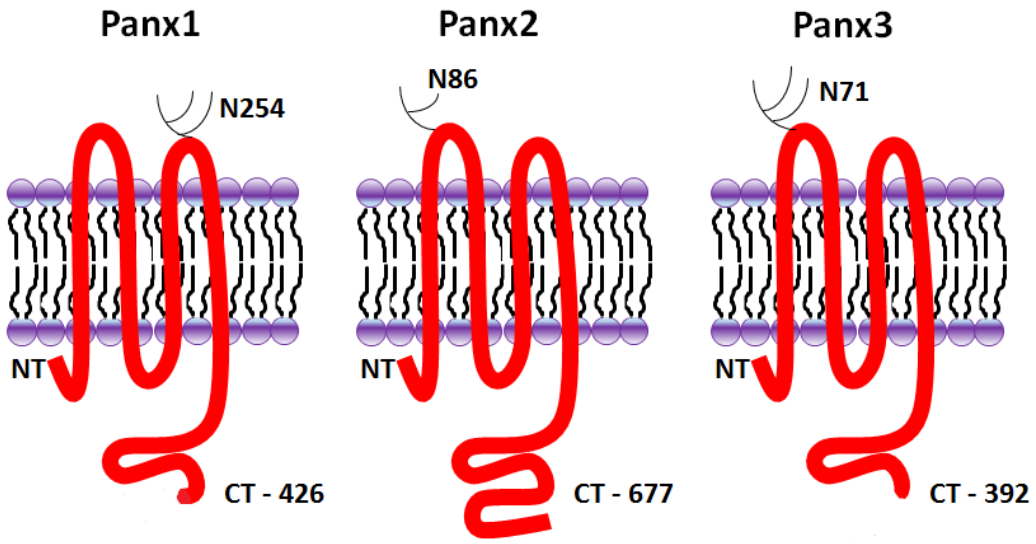

Figure 1.17 – Membrane topology of Panx1, Panx2 and Panx3. Each subunit consists of intracellular N- and C- termini, 4 transmembrane domains and 2 extracellular loops. Panx2 is the largest of the pannexin subtypes, with an extensive C-terminus; Panx3 is the smallest. Panx1 contains a glycosylation site on its second extracellular loop (N254), Panx2 and Panx3 each contain an N-glycosylation site on the first extracellular loop (N86 and N71 respectively) (Penuela *et al*, 2013).

Co-expression of wild-type Panx1 channels with N254Q mutated channels in Madin-Darby canine kidney cells rescues the expression of Panx1 at the cell surface. This was one of the first pieces of evidence indicating the oligomerisation of Panx1 proteins (Boassa *et al*, 2008).

1.4.4 Pannexin channels - Function

The open Panx1 channel has been shown to be capable of ATP efflux, which may then go on to activate P2X and P2Y receptors (Romanov *et al*, 2012). This leads to downstream signalling and cell-cell communication, implicating Panx1 with roles in biological functions such as taste sensation, inflammatory conditions, immunity and tumorigenesis (Wicki-Stordeur and Swayne, 2014; Penuela *et al,* 2013). The exact mechanism regarding the opening and functioning of pannexin channels is poorly understood. However there is evidence to suggest Panx1 is implicated in early stages of cell death to begin recruitment of immune cells via the release of ATP, a classic 'find-me' signal. Panx1 has been shown to be capable of activation by caspase 3/7 cleavage at a specific DVVD site (residues 376-379) located in its C-terminal domain leading to efflux of ATP. Panx1 knockdown was shown to cause a decrease in recruitment of monocytes by apoptotic cells demonstrating that ATP release is important in early apoptotic signalling (Chekeni *et al*, 2010).

P2X7 has been reported to interact with Panx1 during the immune response resulting in the formation of large pores that allow the passage of dye molecules (up to 900 Da) into the cell and release of the pro-inflammatory cytokine, IL-1β (Pelegrin and Surprenant, 2006). Upon activation of P2X7 by ATP, caspase-1 was activated inside the cell which in turn activated the NLRP inflammasome leading to production of active IL-1β. Activated IL-1β is released and secreted from the cell leading to activation of immune cells and destruction of the cell (Fig 1.7). This shows that both P2X7 receptors and pannexin channels play important roles in the immune response (Pelegrin and Surprenant, 2006).

As well as having a role in immunity, pannexins are implicated in taste perception. Pannexins are expressed in the receptor cells of the taste buds, alongside the presynaptic cells. Upon activation of pannexin, ATP is released and acts on the neighbouring presynaptic cells to induce the release of serotonin (Dando and Roper, 2009).

Determining the structure of a pannexin channel would help to understand the underlying mechanism behind apoptotic induction by P2X7, and the role Panx1 may play in this process. It will also enable the design of new therapies targeting cancer and various other diseases. Additionally, if Panx1 is a hexamer, it will be a good candidate for low resolution structural studies using electron microscopy for which only a low yield of protein is required, as higher symmetry enables more accurate 3D-reconstructions. An expression system from which we

can successfully purify high quality protein, even at low yield, will be useful for low resolution studies.

1.5 *Drosophila* as a model organism

The fruit fly, *Drosophila melanogaster,* has served as a highly important model organism in biological research for many years. In addition to a short life cycle (10-18 days) and their ability to lay up to 100 eggs per day, they are easy and economical to culture, making them suitable for genetic and biomedical studies. Additionally, in 2000, the full genome of *Drosophila melanogaster,* with approximately 13,600 protein coding genes, was sequenced using whole genome shotgun sequencing (Adams *et al*, 2000). More recently the genomes of many other *Drosophila* species have been sequenced (*D. ananassae, D. erecta, D. Grimshawi, D.mojavensis, D. persimilis, D, sechellia, D. simulans, D. virilise, D. willistoni, D. yakuba* (Clark *et al*, 2007*), D. biarmipes, D bipectinata, D. elegans, D. eugracillis, D. ficusphila, D. kikkawai, D. rhopaloa, D. takahashii,* (Flybase website) *D. pseudoobscura* (Richards *et al*, 2005). The well characterised *Drosophila* genome makes it suitable for a variety of genetic analyses. One of the most crucial biological discoveries of inheritance was solved by Thomas Hunt Morgan who won a Nobel Prize in 1933 for his work concerning the use of *Drosophila* to discover that genes were contained within chromosomes (Jennings, 2011).

Although the fruit fly and humans are considerably different organisms, many key developmental processes and biological mechanisms are highly conserved between species. Furthermore, following analysis of the sequenced human and *Drosophila* genomes, it was discovered that 75% of known human disease genes have an equivalent orthologous gene in the fruit fly, further validating their role as a model organism (Reiter *et al*, 2001).

1.5.1 The Life cycle of *Drosophila melanogaster*

The fruit fly goes through a 4-stage life cycle that lasts approximately 10 – 18 days dependent upon temperature, allowing *Drosophila* geneticists a good control over fly generation times. Once a fertilised egg is laid by a female, it develops for approximately 1 day before hatching into a larva. The larva lives in the fly food for approximately 5 days (at 25°c) before pupation. Following pupation, much of the larval tissue undergoes histolysis and the adult tissues develop from the imaginal discs as the fly undergoes metamorphosis. Emergence or eclosion of the fly from the pupal case marks the end of metamorphosis (Jennings, 2011).

1.5.2 The use of insect cells for P2X and Pannexin expression

Insect cells have been widely used for expression of P2X receptors. As mentioned previously, zP2X4.1 was expressed in *Sf*9 insect cells for purification and structural studies (Kawate *et al*, 2009; Hattori and Gouaux, 2012). *Sf*9 cells were also used to express rP2X2, which was purified and used for negative-stain TEM. The receptor was presented as an inverted three sided pyramid, with the extracellular domain described as a crown shaped structure. However, their data estimated the volume of the receptor to be 1200 nm^3 (Mio *et al*, 2005; Mio *et al*, 2009), which is significantly larger than what has been reported for the rP2X2 receptor using AFM (Barrera *et al*, 2005) or the zfP2X4.1 crystal structure (Kawate *et al*, 2009), indicating that it is likely that small protein aggregates were imaged as opposed to trimeric receptors (Fig 1.18).

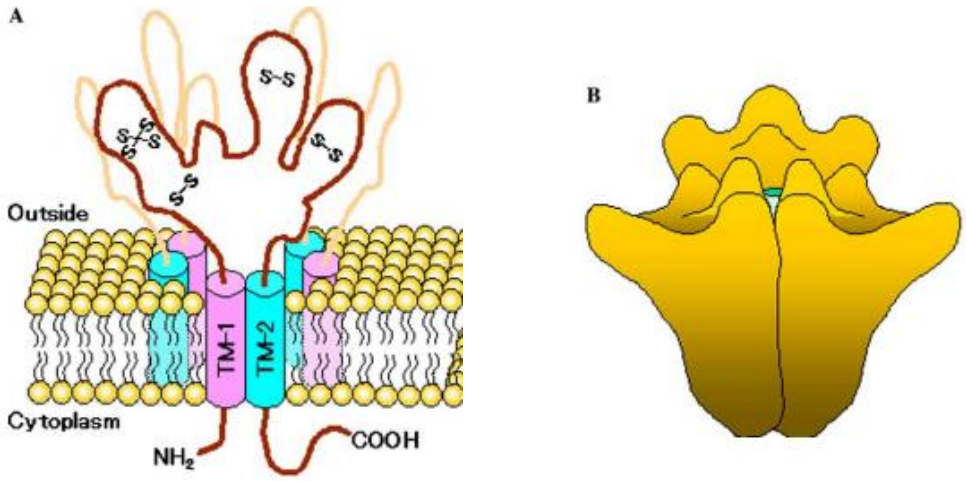

Figure 1.18 – Low resolution structures of rP2X2. (A) A schematic drawing of the rP2X2 receptor model. (B) A cartoon showing the estimated pyramid, crown like shape of the extracellular domain of rP2X2. Reprinted from Biochemical and Biophysical Research Communications, 337(3), Mio *et al*, Visualization of the trimeric P2X2 receptor with a crown-capped extracellular domain, p998-1005., Copyright (2005), with permission from Elsevier.

P2X2 and P2X3 receptors were also shown to be functional and respond to ATP in *Sf*9 cells using electrophysiological whole cell recordings (Radford *et al*, 1997). Additionally, hP2X4 and *Dictyostelium discoideum* P2XA (DdP2XA) were expressed in *sf*9 insect cells by Valente and colleagues, the latter of which was purified and used for low resolution electron microscopy structural studies. The DdP2XA structure was solved to a resolution of 21 Å. (Valente *et al*, 2011). Therefore the capacity for insect cells to successfully express, fold and traffic P2X receptors is well documented. Similarly, Panx1 and Panx2 channels have been successfully

expressed using a baculovirus *sf*9 expression system. The expressed protein was purified and used for low resolution electron microscopy (described in section 1.4.2) (Ambrosi *et al*, 2010).

Furthermore, P2X receptors have been expressed in the fruit fly (*Drosophila melanogaster*) itself by various groups. Hu *et al* (2010) ectopically expressed rP2X2 receptors in the Kenyon cells of *Drosophila* mushroom bodies with the intention of studying functional feedback from mushroom bodies of the fly brain to antennal lobes. Due to the small size of Kenyon cells, it is difficult to specifically activate these cells using electrophysiological methods; expressing rP2X2 in specific neurons of the fly brain using the *Gal4-UAS* system (see section 4.1.2) enabled precise activation of individual neurons. The effective activation of these neurons in *Drosophila* provided evidence that rP2X2 could indeed by expressed, folded and is functional in parts of the *Drosophila* nervous system (Hu *et al,* 2010).

Lima and Meisenbock expressed rP2X2 in parts of the giant fiber (GF) system of *Drosophila*, which is responsible for escape movements such as jumping (Koto *et al*, 1981), under control of the driver lines *GAL4-C17 or shakB-GAL4*. ATP was chemically modified with photoremovable groups rendering it inactive and was microinjected into the CNS of flies. A flash of 355 nm laser light which released the active agonist (ATP) from the caged precursor resulted in typical GF-mediated escape movements. In addition, laser pulses repeated at 2.5 s intervals caused repeated escape responses. As well as showing that P2X2 is functional when expressed in the *Drosophila* nervous system, this work implied that P2X2 did not noticeably desensitise and ATP was rapidly cleared from the extracellular space (Lima and Miesenbock, 2005).

In a third series of experiments, concatenated rP2X2 was introduced into *Drosophila melanogaster* as a novel method for measuring functional connectivity between separate, defined neuronal subsets in the fly brain. Yao and colleagues developed a system where they used stimulation of rP2X2 in a defined set of neurons via application of ATP and simultaneously imaged calcium and cAMP responses in potential target neurons in order to study neuronal interactions. Again, their data confirms the functional response of rP2X2 to ATP in this system (Yao *et al*, 2012).

1.6 Aims and Objectives

The three main aims of this project are:

1. To develop the eye of the fruit fly as a new expression system for mammalian ion channels, specifically P2X2 and Pannexin 1 receptors, in order to gain a high yield of homogenous, folded protein for structural studies.
2. To further develop the system by expressing P2X2 in the taste system of *Drosophila* allowing us to test the function of the protein expressed in this system and determine whether or not the protein is folded and targeted correctly in *Drosophila*.
3. To use the expression of P2X2 in the *Drosophila* taste system to screen compounds from both compound libraries and compounds designed using structure based drug design as potential new agonists and antagonists of P2X receptors.

Chapter 2 – Materials and Methods

2.1 Cloning

2.1.1 Site directed mutagenesis

Mutagenesis was performed using the Quikchange Lightning site-directed mutagenesis kit according to manufacturer's instructions [Agilent – Cat No. 210519]. Complementary primers that contained the chosen mutation flanked by unmodified sequence were designed and used to amplify the plasmid using the following conditions.

Segment	No. of Cycles	Temperature (°c)	Time (seconds)
1	1	95	120
2	18	95	20
		60	10
		68	30/kb plasmid length
3	1	68	300

Each polymerase chain reaction (PCR) reaction was made up according to the Quikchange manufacturer's instructions in 50 µl reactions with 10 ng double stranded DNA template and 125 ng of each primer.

The PCR products were treated with 2 µl Dpn1 enzyme to digest any remaining parental DNA and incubated at 37°c for one hour. 45 µl XL-10 gold ultracompetent cells [Agilent] were transferred to a 14 ml BD polypropylene round-bottom tube. 2 µl β-mercaptoethanol was added to the cells and the mixture was incubated on ice for 2 min. 2 µl of DNA was transferred to an aliquot of ultracompetent cells, tubes were gently swirled and incubated on ice for 30 min. Cells were heat pulsed at 42°c for 30s, placed on ice for 2 min and placed in a shaking incubator at 37°c for 1 hour. Cells were then plated onto ampicillin agar plates and incubated overnight at 37°c.

Colonies from agar plates were inoculated in 5ml of liquid medium containing the appropriate antibiotic. Tubes were placed in a 37°c shaking incubator overnight. Minipreps were performed using the Qiagen Spin miniprep kit [Qiagen] according to manufacturer's instructions (below). The presence of mutations was verified by DNA sequencing.

2.1.2 Minipreps

Minipreps were performed using QIAprep spin miniprep kit (Qiagen – Cat No. 27104). Bacterial cultures were centrifuged at 6,800 g for 3 min at room temperature. The pellet was resuspended in 250 µl buffer P1 and transferred to a 1.5 ml tube. 250 µl buffer P2 was added and mixed thoroughly by inversion. 350 µl buffer N3 was added and immediately mixed by inversion. The tube was centrifuged at 13,000 rpm in a table top microcentrifuge.

The supernatant was transferred to a QIAprep spin column and centrifuged at 13,000 rpm for 1 min. The flowthrough was discarded, 500 µl buffer PB was added to the spin column and centrifuged for 1 min. 750 µl of buffer PE was added to the column, centrifuged at 13,000 rpm for 1 min and flowthrough discarded. The spin column was centrifuged for a further minute to discard any residual wash buffer and transferred to a new 1.5 ml tube; 30-50 µl Buffer EB was added to the centre of the column. After one min standing, the tube was centrifuged for 1 min at 13,000 rpm and DNA was collected in the microcentrifuge tube.

2.1.3 Midipreps

Midipreps were performed using Qiagen Plasmid Midi Kit (Qiagen - Cat no. 12143). 50 ml bacterial culture was centrifuged at 6000 g for 15 min at 4°c. The bacterial pellet was resuspended in 6 ml buffer P1. 6 ml buffer P2 was added and tubes were inverted 6 times and incubated at room temperature for 5 min. Following the incubation, 6 ml buffer P3 was added and mixed thoroughly by inversion. The lysate was poured into the QIAfilter cartridge barrel and incubated at room temperature for 10 min.

4 ml buffer QBT was added to a HiSpeed tip and filtered through the resin. The cell lysate was then filtered into the HiSpeed tip using a plunger and pushing it through the Qiafilter cartridge. The HiSpeed tip was washed with 20 ml buffer QC. DNA was eluted by adding 5 ml buffer QF to the HiSpeed tip. The eluted DNA was collected into a 15 ml falcon tube, 3.5 ml isopropanol was added and the tubes were incubated for 5 min.

A QIAprecipitator module was added to the end of a 20 ml syringe. The isopropanol-eluate mixture was filtered through the precipitator using the plunger under constant pressure. The precipitator was washed with 2 ml 70% ethanol and then air dried by pushing air through the filter twice. The precipitator was attached to a 5 ml syringe and 1 ml buffer TE was added to elute the DNA which was collected in a 1.5 ml microcentrifuge tube. The eluate was transferred back to the 5 ml syringe and re-filtered through the precipitator and collected in the 1.5 ml microcentrifuge tube.

2.1.4 Ligation reactions

Quick stick ligase [Bioline – Cat No. Bio27027] was used for ligations according to manufacturer's instructions. Ligation mixtures were left for 5-10 minutes at room temperature.

2.1.5 Bacteria transformation

1. DNA was transformed into 10-beta competent *E coli* cells [NEB – Cat No. C3019H] according to the manufacturers' high efficiency transformation protocol and as described above for XL-10 ultracompetent cells.
2. Z competent cells were made using the Z competent *E coli* transformation buffer set [Zymo Research – Cat No. T3002]. 50 µl aliquots of cells were thawed on ice and 1 µl DNA was added and mixed. Cells were incubated on ice for 5 minutes. 30 µl of the mixture was then spread on an appropriate antibiotic agar plate.

2.1.6 PCR

All PCR reactions were carried out using Velocity polymerase [Bioline – Cat No. BIO-21098], Phusion High fidelity polymerase [NEB – Cat No. M0530] or Platinum taq polymerase [Invitrogen – Cat No. 10966034] according to standard conditions stated in manufacturer's instructions. Details of specific melting temperatures and primers used can be found in Table 2.1 (p80-83).

2.1.7 Agarose Gel electrophoresis

1% agarose [Bioline – Bio 41025] was added to 1 x Tris Acetate EDTA (Ethylenediaminetetraacetic acid) buffer (40 mM Tris, 20 mM acetic acid, 1mM EDTA) and heated in a microwave oven until fully dissolved. When the mixture had sufficiently cooled, 5 µl SafeView [nbsbio] was added and the mixture was poured into gel holders until set. Following loading of DNA, gels were run at 60-70V for approximately 1 hour. Gels were visualised under UV light using the ChemiDoc MP Imaging system [Biorad] and Image lab software.

2.2 Cell culture

2.2.1 Culture of HEK-293 cells

Human embryonic kidney (HEK) 293 cells were maintained at 37°c, 5% CO_2 in Dulbecco's modified Eagle's medium containing 10% foetal calf serum (FCS), 1% penicillin/streptomycin and 1% L-glutamine. Trypsin-EDTA 0.05% [Life technologies – Cat No. 25300-054] was added to

cells when they reached approximately 80% confluency. Cells were diluted and transferred to new flasks every 4 – 7 days.

2.2.2 Transfection of HEK-293 cells

DNA was transfected into HEK-293 cells using Lipofectamine 2000 [Life technologies – Cat No. 11668-027] according to manufacturers' recommendations. Cells were grown in 6 well plates to 60 – 80 % confluency. 1 µg DNA was mixed with 100 µl Optimem [Life technologies – Cat No. 31985-070]. 3 µl Lipofectamine reagent was incubated with 100 µl Optimem and incubated at room temperature for 5 minutes. The DNA-Optimem mixture was then mixed with the Lipofectamine-Optimem mixture and incubated at room temperature for 20 minutes. The solution was added drop wise to the cells.

Cells were incubated for 48 hours at 37°C following transfection and media was changed after 16 – 24 hours.

2.2.3 Confocal microscopy

HEK-293 cells were transfected with Lipofectamine 2000 [see Section 2.2.2 for details] and incubated at 37°c for 48 hours. Cells were plated onto glass-bottomed 35 mm plates at approximately 20% confluency. These cells were left to grow overnight and visualised after 18 hours using the Leica TCS SP2 AOBS spectral confocal microscope system with a Leica DMIRE2 inverted microscope. GFP was excited at 495 nm and emission detected at 550 nm. Media was removed and 2 drops of DAPI-containing antifade reagent were added to visualise nuclei of the cells. DAPI was excited at 410 nm and emission detected at 480 nm.

2.3 *Drosophila* techniques

Fly stocks were stored at 18 °c in food vials, sealed with a cotton wool plug. The food vials were changed every 4 weeks. Flies were raised on a standard corn meal agar/yeast diet (yeast powder, corn flour, dextrose, plant agar, Nipagen (10% p-hydroxy benzoic acid methyl ester) and propanoic acid).

Virgin female flies and male flies for crosses were anaesthetised using CO_2 and were stored at room temperature or 25°c in food vials. The food vials were changed regularly (every 2 – 3 days) until enough flies were obtained. Each cross contained approximately 4 – 8 virgin female flies and 2 – 3 male flies.

To amplify stocks for large scale purification, approximately 100 – 200 flies were added to bottles and these were changed 3 times a week. Flies were collected from all bottles once a

week; flies were anaesthetised using CO_2, stored in 1.5 ml microcentrifuge tubes and frozen in liquid nitrogen. Flies were stored at -80°C until required.

2.3.1 Imaging flies

Whole flies - Flies were anaesthetised using carbon dioxide gas and placed in a chamber containing FlyNap [Carolina – Cat No. 173010]. GFP was visualised with an Olympus BX50 microscope and an ultraviolet light arc lamp.

Fly heads - heads were removed using tweezers and mounted onto a microscope slide. GFP was visualised with an Olympus BX50 microscope and an ultraviolet light arc lamp.

2.3.2 Injecting *Drosophila* embryos

hP2X4-his and hP2X4-GFP DNA constructs were cloned into the multiple cloning site (MCS) of pUAST-attB (Bischoff *et al*, 2007). rP2X2-GFP and rPanx1-GFP were cloned into the MCS of a modified version of pUAST-attB containing 19 UAS sites (kindly supplied by Sonia Lopez de Quinto, Cardiff University). See Table 2.1 (p80-83) for details.

The Phi31C integrase system involves the use of a site specific integrase (PhiC31) to mediate recombination between *attB* and *attP* recognition sites (Thorpe *et* al, 1998; Groth *et al*, 2004). Constructs flanked by *attB* sites in specialised vectors (e.g. pUAST-attB) are injected into white eyed fly lines containing known intergenic *attp* landing sites and with endogenous sources of PhiC31 integrase for targeted and efficient integration. The vector also contains a mini-white gene that allows for efficient selection of transgenic progeny (Bateman *et al*, 2006; Bischof *et al*, 2007; Markstein *et al*, 2008).

Approximately 60 flies from a Phi31C fly stock were placed in a laying cage at 18°c containing apple juice agar plates (Agar, sucrose, Nipagen, ethanol and apple juice) 4 days before microinjection. One day before microinjection these cages were moved to a 25°C incubator. The agar plates were changed every hour the morning prior to microinjection until the afternoon when microinjection was carried out. Method A was used for hP2X4-his construct, Method B was used for remaining constructs. All constructs were injected into flies with the attp40 on the second chromosome or attP2 landing site on the third chromosome (Markstein *et al*, 2008).

a) A soft paintbrush was used to gently remove the embryos from the apple agar plates. Microscope slides were coated with a small layer of glue which was obtained by soaking brown packaging tape in N-heptane. The embryos were placed on the glue and

the membrane was peeled from the embryos using a needle. They were then aligned on the slide so all the embryos were in the same orientation.

b) Embryos were washed in 50% bleach for 1 min to remove the outer, chorion membrane surrounding the embryo. Embryos were washed and placed on a fresh apple juice agar plate and aligned for injection. A glue coated coverslip was gently pressed over the embryos to transfer them onto the coverslip. Coverslips were placed over silica beads allowing embryos to dry for 14 minutes before being coated with Halocarbon oil 700 [Sigma].

DNA for injection was diluted to 100 ng/µl and briefly centrifuged to sediment particulates that could clog the injection pipette and the supernatant was transferred to a new tube. Using a microloader tip [Eppendorf] 2 µl DNA solution was loaded into microinjection needles, pulled on a Sutter Puller, whereupon the tip of the needle was broken to 1-2 µm diameter. DNA was injected into the posterior pole of fly embryos using a Narishige IM-30 micro injector and Nikon Eclipse T5100 microscope, until minor movement of the cytoplasm was observed in phase-contrast microscopy.

Following injection the embryos were placed on apple juice agar plates and 1st instar larvae were transferred to food vials. When the flies emerged from pupal cases, they were crossed to *W^{1118}* flies that have a white eye colour. Transgenic flies were distinguished from siblings by selection for an orange eye colour marker (*mini-white*) present in the construct. Transgenic flies were balanced by crossing with *If/CyO* balancer fly stocks.

2.3.3 *Drosophila* DNA extraction

50 µl squishing buffer (10 mM Tris base, 1 mM EDTA, 25 mM NaCl, 0.5 µL proteinase K [Sigma – Cat No. P4850], adjusted to pH8) was used to homogenise fly tissue (single fly) using a pipette tip in a 1.5 ml tube. The tube was incubated at 25°c for 20 min and then heated at 95°c for 2 min. The tube was then centrifuged at 2000 g for 1 min to pellet fly debris and the supernatant was transferred to a new tube. The DNA was then ready for use or stored at -20°c.

2.3.4 *Drosophila* RNA extraction

1 ml Trizol was used to homogenise fly tissue (single fly) using a micro pestle in a 1.5 ml tube, all RNAse free. The tubes were incubated at room temperature for 5 min. 0.2 ml chloroform was added; tubes were incubated for a further 10 min at room temperature and centrifuged at 12,000 g for 15 min, 4°c. Approximately 400 µl of the colourless, upper-phase was transferred

to a fresh RNAse free tube. An equal volume of 70% ethanol was added to give a final ethanol concentration of 35% and tubes were thoroughly mixed by vortexing and inversion.

The RNA was prepared and purified using the GeneJET RNA purification kit according to manufacturer's instructions [Thermoscientific]. RNA was stored at -80°c.

cDNA synthesis was performed using the superscript III First Strand synthesis system [Life technologies]. 180 – 850 ng of RNA was added to a tube with 7.7 µM oligo $(dT)_{18}$ [Fermentas] and 0.77 mM dNTPs [NEB N0447S], made to a final volume of 13 µl with H_2O. The tubes were heated to 65°c for 5 min and on ice for 1 min. 50 mM Tris-HCl, 75mM KCl, 3 mM $MgCl_2$ (1 x FS buffer), 5 mM DTT, 20 units RNasin and 200 units Superscript III RT [Life technologies] were added to each tube and tubes were centrifuged briefly before being incubated at 50°c for 30 – 60 min. The enzyme was then inactivated by heating to 70°c for 15 min. To remove RNA, 5 units RNase H [NEB – M0297S] was added and tubes were incubated at 37°c for 20 min.

2.4 Protein extraction and analysis techniques

2.4.1 Cell lysis and protein extraction (HEK-cells)

Cells were washed twice in phosphate buffered saline (PBS), resuspended in PBS, transferred to a microcentrifuge tube and centrifuged at 4,000 g for 3 min. The supernatant was removed and the pellet was resuspended in 50 µl of Radioimmunoprecipitation assay (RIPA) buffer (20 mM Tris-HCl [pH7.4], 150 mM NaCl, 1 mM $MgCl_2$, 1 mM $CaCl_2$, protease inhibitors mixture [complete-EDTA free, Roche]), 1% n- Dodecyl B maltoside (DDM) was also added. Cell lysis was completed for 30 min on ice with regular agitation. The mixture was centrifuged at 13,000 rpm in a table top centrifuge for 2 min to discard insoluble material and the supernatant was collected.

2.4.2 Membrane protein extraction (*Drosophila*)

2.4.2.1 50 – 100 flies

50 – 100 whole flies were frozen in liquid nitrogen and transferred to -80°c. Upon removal from the freezer, flies were placed on ice. 500 µL of sucrose buffer [50mM Tris-HCl, 250mM sucrose, 180mM NaCl, 2mM $MgCl_2$ plus protease inhibitors] was added to each tube and a micro-pestle was used to homogenise fly tissue thoroughly. Tubes were centrifuged at 5000 rpm for 1 min in a table top centrifuge to collect fly debris. The supernatant was transferred to a collection tube and centrifuged at 60,000 g, 4°c for 30 min. The supernatant was discarded and the pellet was resuspended in sucrose buffer. Detergent was added to a final

concentration of 1% DDM (rP2X2-GFP) or 7.5mM FC-12 (rPanx-GFP). These tubes were placed on ice, regularly agitated for 30 min and centrifuged at 13,000 rpm in a table top centrifuge for 2 min. The supernatant (solubilised protein) was collected and ready to use or stored at -20°c for up to a month.

2.4.2.2 2000 – 5000 flies

2000 - 5000 whole flies were frozen in liquid nitrogen and transferred to -80°c. Upon removal from the freezer, flies were placed on ice. Glass homogeniser, falcon tubes, glass beads and sucrose buffer were also cooled on ice prior to experiment.

4 ml glass beads (5 mm) were added to a falcon tube. 600 – 1,200 flies were also added and placed in liquid nitrogen. Tubes were quickly inverted, briefly vortexed and placed back in liquid nitrogen. This was repeated 3 – 4 times until the heads became detached from the fly body.

A 710 micron sieve was stacked above a 425 micron sieve to collect fly heads. Liquid nitrogen was briefly poured onto the sieves to keep them cool. The contents of the falcon tube were transferred straight from liquid nitrogen to the sieve stack and the sieves were shaken to help the heads pass through the 710 micron sieve. The wings remained attached to the outside of the falcon tube, the fly bodies were retained on the 710 micron sieve, the heads were retained on the 425 micron sieve and the legs fell through to be collected underneath.

The heads collected by the smaller sieve were brushed into a 50 ml glass homogeniser using a funnel. 5 ml of sucrose buffer was added to the homogeniser and the heads were thoroughly homogenised using a drill attached to the homogeniser. The homogenised material was then transferred to a 15 ml falcon tube. Tubes were centrifuged at 2000 g for 10 min to collect fly debris. The debris was re-homogenised in 5 ml sucrose buffer and centrifuged at 2000 g. This was repeated 3 times. The supernatants were pooled, transferred to a Beckmann tube and centrifuged at 100,000 g, 4°c for 1 hour. The supernatant was discarded and the pellet was resuspended in 100 – 500 µl sucrose buffer. Detergent was added to a final concentration of 1% DDM (rP2X2-GFP) or 7.5mM FC-12 (rPanx1-GFP). Tubes were placed on ice, regularly agitated for 30 min and centrifuged at 13,000 rpm in a table top centrifuge for 2 min. The supernatant (solubilised protein) was collected and ready to use or stored at -20°c for up to a month.

2.4.3 Protein quantification

1. A series of bovine serum albumin (BSA) protein standards were made from 0 mg/ml to 1 mg/ml. 900µl Bradford ultra [Expedeon – BFU1L] was added to 60 µl protein standard and the absorbance was measured using the Beckman DU530 Lifescience UV/vis spectrophotometer at 595nm. Absorbance was plotted to produce a protein standard curve. 54µl of PBS and 900 µl Bradford Ultra were added to 6µl of protein sample in a macro cuvette [VWR]. Samples were briefly vortexed to ensure thorough mixing. The absorbance of each sample was measured at wavelength 595nm. Concentrations were determined using the standard curve (See Appendix I)
2. Biorad protein assay reagent [Biorad – Cat No. 500-0006] was diluted 1 in 5 with ddH_2O. 1 ml diluted reagent was added to 10 µl protein sample in a macro-cuvette and the absorbance was measured using the Beckman DU530 Lifescience UV/vis spectrophotometer at 595nm (See Appendix I).

2.4.4 Western Blotting

1. 6 x Sample buffer (100mM Tris-HCl [pH7.6], 10mM EDTA, 10% glycerol, 12% sodium dodecyl sulphate (SDS), 0.04% Bromophenol blue, 50mM TCEP and NaOH to pH7.6) was added to protein at a 5:1 v:v ratio. Protein samples were heated at 100°c for 2 min followed by centrifugation at 13,000 rpm, 2 min in a table top centrifuge. Samples were run on a 10% polyacrylamide gel (separating gel- 10% acrylamide [Sigma – Cat No. A3699], 0.26M Tris-HCl, 0.05% SDS, 0.05% APS and 0.08% TEMED, made up to 4 ml with H_2O, pH8.8. Stacking gel – 8% acrylamide, 0.56M Tris HCl, 0.1% SDS, 0.1% APS and 0.1% TEMED, made up to 4 ml with H_2O, pH 6.6) at 100-200V for 1 hour (Running buffer – TGS [25 mM Tris, 192 mM glycine, 0.1% SDS]) and transferred to a nitrocellulose membrane at 40 V for 1 hour (transfer buffer – 1 x NuPAGE transfer buffer [Invitrogen], 20% methanol).
2. 6 x Sample buffer (100mM Tris-HCl, 10mM EDTA, 10% glycerol, 12% SDS, 0.04% Bromophenol blue, 50mM TCEP and NaOH to pH7.6) was added to protein sample at a 5:1 v:v ratio. Protein samples were heated at 100°c for 2 min followed by centrifugation at 13,000 rpm for 2 min in a table top centrifuge. Samples were run on 4-15% mini-PROTEAN TGX stain free gels [BioRad – Cat No. 456-8085] at 250 - 300V for 20 minutes. The gel was UV illuminated for 5 minutes before being imaged on the Chemidoc MP imaging system [Biorad] to test for equal loading. Gels were blotted

onto Trans-blot turbo mini PVDF transfer packs [Biorad – Cat No. 170-4156] at 25V for 3 minutes using BioRad Trans-blot turbo transfer system.

Membranes were blocked in 3% Bovine Serum Albumin [PAA] in TBS (Tris Buffered Saline – 20 mM Tris, pH7.5, 150 mM NaCl) or 5% dried milk [Marvel] in TBST (Tris Buffered Saline with Tween – 50 mM Tris, 150 mM NaCl, 0.05% Tween 20) depending on the antibody used [See section 2.4.4.1]. Primary antibodies were applied in 3% BSA or 5% milk and tubes rotated overnight at 4°c. Membranes were washed in TBST 3 x 5 min and incubated with the secondary antibody in 3% BSA or 5% milk for 45min-1hour. Membranes were washed 4 x 5 min in TBST and developed with ECL prime kit [Amersham Biosciences] and viewed using ChemiDoc MP Imaging system [Biorad] and Image lab software.

2.4.4.1 Antibodies

Mouse monoclonal primary antibodies: Tetra-his antibody was used at 1:2000 [Qiagen – Cat No. 34670] in 3% BSA. β-actin antibody was used at 1:1000 [Abcam – Cat No. ab8224] in 3% BSA. *Drosophila* Rhodopsin antibody was used at 1:300 in 3% BSA [DSHB – Cat No. 4C5].

Rabbit polyclonal primary antibodies: P2X2 antibody was used at 1:2000 in 5% milk [Alomone labs – Cat No. APR-003]. GFP antibody was used at 1:1000 in 5% milk [Invitrogen – Cat No. A11122].

Secondary antibodies: Polyclonal goat anti rabbit IGg / HRP [Dako – Cat No. P0448] was used at 1:2000 in 5% milk. Mouse IgG HRP-linked antibody [Cell signalling – Cat No. 70765] was used at 1:5000 in 3% BSA.

2.4.5 Perfluorooctanoate-polyacrylamide gel electrophoresis

For perfluorooctanoate-polyacrylamide gel electrophoresis (PFO-PAGE), 2 x sample buffer (100 mM Tris base, 1% (w/v) NaPFO, 20% (v/v) glycerol, 0.005% Bromophenol Blue, adjusted to pH 8 with NaOH) was added to protein in a 1:1 v:v ratio. SDS free 6 % polyacrylamide gels were run at 140 V at room temperature in PFO-containing buffer (25 mM Tris, 192 mM glycine, 0.5% PFO (w/v), adjusted to pH 8.5 With NaOH). Membranes were blocked and antibodies added as described in section 2.4.4 Membranes were developed with ECL prime kit [Amersham Biosciences] and viewed using ChemiDoc MP Imaging system [Biorad] and Image lab software.

2.4.6 Coomassie gels

6 x Sample buffer (100mM Tris-HCl, 10mM EDTA, 10% glycerol, 12% SDS 0.04% Bromophenol blue, 50mM TCEP and NaOH to pH7.6) was added to protein sample at a 5:1 v:v ratio. Protein samples were heated at 100°c for 2 minutes followed by centrifugation at 13,000 rpm for 2 min in a table top centrifuge. Samples were run on 4-15% mini-PROTEAN TGX stain free gels [BioRad – Cat No. 456-8085] at 250 - 300V for 20 min. Gel was then covered in Quick Coomassie Stain [Generon – Cat No. Gen-QC-Stain] for 1h – 16h at room temperature. Gels were washed 4 x 5 min with water prior to visualisation.

2.4.7 Deglycosylation assays

Endoglycosidase H (Endo H) [NEB – Cat No. P0702] – Approximately 35 – 45 µg (12.5 µl) of total extracted protein from HEK-293 cells or membrane protein extracted from approximately 18 -20 flies (18 µl) was incubated with 2 µl denaturing buffer and H_2O to make a final volume of 20 µl at 100°c for 10 min. Following the incubation 4 µl G5 buffer, 2 µl Endo H and 14 µl H_2O were added and the protein was incubated for 1 hour at 37°c.

Peptidyl -*N*-Glycosidase F (PNGase F) [NEB – cat# P0704] - Approximately 35 – 45 µg (12.5 µl) of total extracted protein from HEK-293 cells or membrane protein extracted from approximately 18 -20 flies (18 µl) was incubated with 2 µl denaturing buffer and H_2O to make a final volume of 20 µl at 100°c for 10 min. Following the incubation 4 µl G7 buffer, 2 µl 10% nonyl phenoxypolyethoxyethanol (NP40), 2 µl PNGase F and 12 µl H_2O were added and the protein was incubated for 1 hour at 37°c.

2.5 Protein purification techniques

2.5.1 Nickel affinity purification (HEK)

Protein was extracted from 4 x transfected T75 flasks (section 2.4.1). 0.5 ml Tris binding wash buffer (20 mM Tris HCl, 150 mM NaCl, 25 mM Imidazole, 0.2% DDM, protease inhibitors, pH7.4) and 25 µl nickel sepharose beads [GE Life Science – Cat No. 17-5268-01] were added to the protein sample. Samples were rotated for 1 hour at room temperature and centrifuged at 5000 rpm for 1 min. The supernatant was removed and 0.5 ml wash buffer was added to the beads. Tubes were centrifuged at 5000 rpm for 1 min in a table top centrifuge and supernatant removed. This wash step was repeated 4 times. 50 µl elution buffer (20mM Tris-HCl, 150 mM NaCl, 1 mM TCEP, 500 mM Imidazole, 0.1% DDM, 1 x protease inhibitors, adjusted to pH7.9) was added to the pellet and mixed for 1-2 min. Tubes were centrifuged for 1 min at 5000 rpm

in a table top centrifuge for protein elution. The supernatant (elution) was transferred to a new tube.

2.5.2 Nickel affinity purification (*Drosophila*)

Protein samples were rotated with 0.5 – 1 ml sepharose beads [Nickel beads stripped with EDTA] for 2 to 3 hours at room temperature. Samples were then centrifuged at 5000 rpm in a microcentrifuge for 1 min. The supernatant was transferred to a fresh tube and the beads were discarded or kept for a western blot control. 25 µl nickel sepharose beads [GE Life Sciences] were added to the supernatant. Tubes were rotated overnight at 4°.

The tubes were centrifuged at 5,000 rpm for 1 min. The supernatant was collected and stored (flowthrough). 500 µl wash buffer was used to resuspend the nickel beads. Tubes were centrifuged for 1 min at 5000 rpm, the supernatant was discarded. This wash step was repeated 5 times (retaining the wash 1 and wash 5 samples for western blotting purposes). 50 – 100 µl elution buffer was added to the beads and mixed thoroughly for 1 – 2 min. Tubes were then centrifuged for 1 min at 5000 rpm. The supernatant (elution) was collected and transferred to a new tube. The beads were resuspended in sample buffer for western blotting.

2.5.3 GFP TRAP

The GFP-TRAP system [Chromotek] was developed to enable efficient one-step isolation of fluorescent fusion proteins. GFP TRAP involves the use of small recombinant alpaca antibody fragments covalently coupled to the surface of agarose beads which bind to fluorescent labels (e.g. GFP, YFP, CFP) and allow purification by immunoprecipitation.

The GFP TRAP purification was performed using the GFP TRAP-A kit [Chromotek]. Total membrane protein was extracted from 1,500 fly heads and solubilised in 300 µl of sucrose buffer plus detergent (concn. 3 mg/ml) (see section 2.4.2 for details). The protein sample was further diluted to a total volume of 600 µl with ice-cold dilution buffer (10 mM Tris-HCl, pH 7.5, 150 mM NaCl, 0.5 mM EDTA).

20 µl bead slurry was resuspended in 500 µl ice-cold dilution buffer and centrifuged at 2500 g for 2 min at 4°c. The supernatant was discarded. This wash step was repeated twice. The diluted protein sample was added to the washed GFP-TRAP beads, mixed for 1 hour at 4°c under constant mixing and centrifuged at 2500 g for 2 min at 4°c. The supernatant was discarded 500 µl ice-cold dilution buffer was used to resuspend the beads. The beads were

centrifuged at 2500 g for 2 min at 4°c and supernatant discarded. This wash step was repeated twice.

The beads were resuspended in 50 µl 0.2 M glycine, mixed for 30 sec and centrifuged at 2,500 g for 2 min. Following centrifugation, the supernatant was transferred to a new microcentrifuge tube and immediately neutralised with 5 µl 1 M Tris base. This elution step was repeated and the supernatants pooled.

2.5.4 Immunoprecipitation

Total membrane protein was extracted from 1,800 fly heads and solubilised in 200 µl PBS + detergent (see section 2.4.2 for details). Immunoprecipitation was performed using Pierce classic IP kit [Pierce – Cat No. 26146] and the Invitrogen GFP antibody [Invitrogen – Cat No. A11122]. 10 µg anti-GFP was added to the protein sample. IP lysis/wash buffer was added to make a total volume of 500 µl and incubated overnight at 4°c.

20 µl protein A/G agarose resin was added to a spin column placed in a collection tube and centrifuged at 1000 g for 1 minute. The flowthrough was discarded and the column was washed twice with 100 µl IP lysis/wash buffer. The bottom plug was inserted into the spin column and the antibody/protein sample mix was added to the tube and sealed with a screw cap. This was incubated under constant mixing for 1 hour at 4°c. The plug was removed and the spin column was placed in a fresh collection tube. The tube was centrifuged at 2000 g for 1 minute and washed 4 times with 200 µl IP lysis/wash buffer followed by centrifugation. The tube was then further washed with 100 µl conditioning buffer.

To elute the protein, the spin column was placed in a new collection tube. 50 µl elution buffer was added to the tube and incubated at room temperature for 10 min. The tube was then centrifuged at 2000 g for 1 min and the supernatant was collected [elution].

2.5.5 Ion exchange chromatography

Membrane protein pellets prepared from 2000 – 5000 flies were solubilised in 1 – 1.5 ml low salt sucrose buffer (50 mM Tris-HCl, 250 mM sucrose, 20 mM NaCl, pH 7.4). Detergent was added to a final concentration of 1% DDM (rP2X2-GFP) or 7.5 mM FC-12 (rPanx1-GFP) (see section 2.4.2). After solubilisation, samples were made up to a total volume of 2 ml with start buffer (20 mM Tris-HCl, 20 mM NaCl and detergent [3 mM FC-12 for rPanx1-GFP and 0.2% DDM for rP2X2-GFP]). Protein was loaded onto a 5 ml HiTrap Q column [GE healthcare] using a 2 ml sample loop and 5 ml syringe. A salt gradient was set up from 20 mM to 500 mM NaCl

using the standard ion exchange protocol for the Akta Prime. The gradient was set up over a 20-minute period between start buffer and elution buffer (20 mM Tris-HCl, 500 mM NaCl, 3 mM FC-12 (rPanx1-GFP) or 0.2% DDM (rP2X2-GFP) pH 7.4) at a flow rate of 1 ml per minute and 1 ml fractions were collected.

2.5.6 Chitin bead protein purification

HEK-293 cells were transfected with P2X4-int-CBD in 6 x 35 mm dishes (see section 2.2.2 for details). The protein pellets solubilised in 400 µl RIPA buffer plus detergent (see section 2.4.1) and were diluted to a total volume of 800 µl with column buffer (20 mM Tris-HCl, 500 mM NaCl, 1 mM EDTA, 0.1% DDM, pH 8.5).

500 µl column buffer was added to 100 µl chitin bead slurry and centrifuged at 5000 rpm in a microcentrifuge for 1 min. The supernatant was removed and this wash step repeated. The diluted protein sample was added to the washed beads and incubated under constant mixing for 1 hour at 4°c. Following the incubation, samples were centrifuged at 5000 rpm for 1 min and the supernatant [flowthrough] was collected. The beads were washed 5 times with 1 ml column buffer. 100 µl cleavage buffer (20 mM Tris-HCl, 500 mM NaCl, 1 mM EDTA, 50 mM DTT, 0.2% DDM, pH8.5) was added to the beads and incubated overnight at 4°c.

Tubes were then centrifuged at 5000 rpm for 2 min and supernatant [elution] was collected.

2.5.7 Gel filtration chromatography

300 - 450 µl of wash buffer (20 mM Tris-HCl, 150 mM NaCl, 25 mM Imidazole, 0.2% DDM or 3 mM FC-12, pH 7.9) was added to 50 µl partially purified protein (HEK) or 200 µl purified protein (*Drosophila*) and centrifuged at 13,000 rpm, 2 min in a table top centrifuge to pellet protein aggregates. The column was washed with filtered, degassed ultrapure water and titration buffer (20mM Tris-HCl, 50mM NaCl, 0.05% DDM or 3mM FC-12, pH 7.9). The supernatant was injected into a Superdex 200 column [GE healthcare] using a 1ml syringe. The column was run at 0.5ml/minute and separated into 1 ml fractions according to size. A gel filtration standard [BioRad – Cat No. 151-1901] was used to calibrate the column (see appendix I).

2.5.7.1 Fluorescence measurements

200 µl of each fraction collected during gel filtration was transferred to a black 96 well plate and the fluorescence of each well was measured using the Fluoroskan Ascent FL [Thermo labsystems], excitation: 485 nm, Emission: 538 nm, integration time: 100 ms.

2.6 Electron microscopy

Purified protein samples obtained after gel filtration were concentrated using a 50 kDa MWCO viva-spin-column to a volume of 200 µl. Protein samples were adsorbed onto a glow-discharged carbon-coated grid and negatively stained with 2% uranyl acetate. Transmission electron microscopy images were recorded at a specimen level increment of 2.43 Å/pixel using a Jeol JEM-2100 LaB_6 electron microscope at 200 kV. Samples were prepared for electron microscopy by Dr Mark T Young at the School of Biosciences, Cardiff University and images were taken by Dr Georgi Lalev at the School of Chemistry, Cardiff University. EMAN software was used to manually select, process and measure particles.

2.7 Electrophysiology of the *Drosophila* taste system

Taste recordings were performed on flies 5 – 15 days old following the protocol published by Benton and Dahanukar (2011). A high input-impedance (>$10^{15}\,\Omega$) amplifier was used to record action potentials, and signals were digitised at 10000 sample/s in a Syntech A/D converter, and band-pass filtered between 50 and 5000 Hz. The rig was placed in a Faraday cage on a stabilized base plate. The fly was observed under 240x magnification using an Olympus SZ-70 binocular. Electrodes were fashioned using chloride silver wire sheathed with 1 mm borosilicate glass micropipettes, which had been pulled to a fine tip. The tip of the recording electrode was broken to an approximately 5-10 µm opening.

The reference electrode was filled with Beadle-Ephrussi Ringer solution using a syringe and tapped to dislodge any air bubbles. The electrode was placed in the reference electrode holder.

A single fly and the microscope base plate were placed on ice for a minimum of 5 minutes. The fly was then placed on the base plate under the microscope and the forelegs of the fly were removed using forceps. The tip of the reference electrode was inserted into the dorsal side of the thorax. The electrode was pushed through the neck of the fly and into the proboscis until movement of the proboscis was minimal.

The recording electrode was filled with the test solution using a syringe and was placed onto the recording electrode holder. All test compounds were dissolved in water and tricholine citrate (TCC) was added as an electrolyte to a final concentration of 0.03M. Using the microscope and micro-manipulator the recording electrode was carefully placed over the tip of the sensillum, with the tip just breaking the meniscus of the solution. Action potentials were recorded using Autospike 32 software.

Consecutive stimuli applied to the same sensillum were applied at a minimum of one minute intervals. For changing solutions, the recording electrode was washed 15 times with water following by 6 washes with the new solution before filling the electrode.

2.7.1 Testing the function of rP2X2-GFP in *Drosophila*

100 mM sucrose was applied to each sensillum used to ensure the sensillum was still responsive. The solvent control (TCC), 100 µM ADP and 100 µM ATP were then applied to each sensillum in turn for 30 seconds and action potentials recorded. This was repeated on 10 – 12 sensilla from a minimum of 3 different flies for each genotype tested (control: *w; UAS-rP2X2-GFP;+,* panneural expression: *C155-Gal4; UAS-rP2X2-GFP,* and sugar neuron expression: *w; UAS-rP2X2-GFP; Gr5a-Gal4*). The number of action potentials was counted between 10 and 15 s after compound application.

2.7.2 Dose response curves

100 mM sucrose was applied to each sensillum used to ensure the sensillum was still responsive. The solvent control TCC was then applied to each sensillum for 30 seconds and action potentials recorded. 1 µM, 3 µM, 10 µM, 30 µM, 100 µM and 300 µM ATP solutions were then applied to each sensillum in turn for 30 seconds. An additional concentration of 1 mM was tested on *w; rP2X2-GFP; Gr5a-Gal4* flies. The number of action potentials was counted between 10 and 15 s after compound application. This was repeated on 6 – 9 sensilla from a minimum of 3 different flies for each genotype tested (*C155-Gal4; rP2X2-GFP, w; rP2X2-GFP; Gr5a-Gal4*).

2.7.3 Testing the adenosine nucleotide compound library

100 mM sucrose was applied to each sensillum (*C155-Gal4; UAS-rP2X2-GFP* flies) to ensure it was still responsive after mounting. TCC and 100 µM ATP were then applied to each sensillum in turn for 20 seconds and action potentials were recorded. The sensillum was only used if the ATP response was more than 3 times greater than the TCC response. Each nucleotide from the adenosine nucleotide library [Jena Biosciences] was diluted in TCC to make a 100 µM stock in a final concentration of 0.03M TCC. Each nucleotide was then applied to one sensillum per fly for 20 seconds on a total of 3 different flies (n=3) and action potentials recorded. One compound was tested per sensillum, up to 4 compounds were tested per fly. Action potentials were counted between 10 and 15 s after compound application. The compound responses and the TCC responses were normalised to the ATP response (100%). The four most effective

compounds were tested on an additional 3 flies to give an n of 6. These compounds were also tested on 3 control flies.

Table 2.1 – Cloning of DNA constructs. Primers are located below table and maps of vectors/constructs in Appendix II.

Construct	Cloned from:	Cloned into:	Restriction enzymes:	Primers:	Tm	Details
pE-GFP-C1_int_CBD (with SapI site)	PTXB1 (Contains intein-chitin binding domain region)	pE-GFP-C1	Nhe1, BamHI	1, 2	66°c	GFP removed from pE-GFP-C1 by restriction digest and replaced with int-CBD obtained from PTXB1 using PCR (Phusion), restriction digest and ligation.
pE-GFP-C1_int_CBD	-	-	-	3, 4	60°C	SapI sites removed from pE-GFP-C1-int-CBD using Quikchange lightning SDM kit.
hP2X4-int-CBD	pL118 (hP2X4 full coding sequence in pcDNA3.1) Gift from Mark Young.	pE-GFP-C1_int_CBD	NheI, SapI	5, 6	54°C	hP2X4 amplified from pL118 by PCR (Phusion). PCR product and pE-GFP-C1-int-CBD digested with NheI and SapI and ligated.
hP2X4-GFP	pL118	pE-GFP-C1 (zfP2X4.1-thr-GFP-his)	XhoI, EcoRI	7, 8	54°C	zfP2X4.1 removed from vector using XhoI and EcoRI. hP2X4 amplified from pL118 using PCR (Phusion DNA pol), restriction digest and ligation.

rPanx1-GFP	rPanx1 full coding sequence in pcDNA3.1. Gift from Pablo Pelegrin.	pE-GFP-C1 (zfP2X4.1-thr-GFP-his)	XhoI, EcoRI	9, 10	54°C	zfP2X4.1 removed from vector using XhoI and EcoRI. rPanx1 amplified from Panx1 vector using PCR (Phusion DNA pol), restriction digest and ligation.
rP2X2-GFP	P698 (rP2X2 full coding sequence in pcDNA3.1) Gift from Alan North.	pE-GFP-C1 (zfP2X4.1-thr-GFP-his)	NheI, EcoRI	11, 12	48°C	zfP2X4.1 removed from vector using NheI and EcoRI. rP2X2 amplified from p698 using PCR (Phusion DNA pol), restriction digest and ligation.
rP2X7-GFP	P927 (rP2X7 full coding sequence in pcDNA3.1)	pE-GFP-C1 (zfP2X4.1-thr-GFP-his)	XhoI, EcoRI	13, 14	54°C	zfP2X4.1 removed from vector using XhoI and EcoRI. rP2X7 amplified from p927 using PCR (Phusion DNA pol), restriction digest and ligation.
UAS-hP2X4-his	pL118	pUAST-attB (from Basler lab in Zurich, Switzerland)	XhoI, XbaI	15, 16	60°C	PCR was used to amplify hP2X4-his from pL118. PCR product was cleaved with XhoI and XbaI and ligated into pUAST-attB cut with XhoI and XbaI.
UAS-hP2X4-GFP	hP2X4-GFP	pUAST-attB	XhoI, XbaI	n/a		hP2X4-GFP cut out of vector with XhoI and XbaI and ligated into pUAST-attB cut with XhoI and XbaI.

UAS-rP2X2-GFP	rP2X2-GFP	pUAST-attB	XbaI	17, 18	60°C	PCR used to insert XbaI sites to each end of P2X2-GFP. Both PCR product and pUAST-attB cut with XbaI and ligated. Orientation checked with NotI digestion.
UAS-rPanx1-GFP	rPanx1-GFP	pUAST-attB	XhoI, XbaI	n/a		rPanx1-GFP cut out of vector with XhoI and XbaI and ligated into pUAST-attB cut with XhoI and XbaI.
UAS19-rP2X2-GFP	UAS-rP2X2-GFP	pUAST19-attB (pUAST-attB with 19 UAS sites) Gift from Sonia Lopez de Quinto.	XbaI	n/a		rP2X2-GFP removed from UAS-rP2X2-GFP using XbaI and purified by gel extraction. pUAST19-attB cut with XbaI and ligated to rP2X2-GFP. Orientation checked with NotI digestion.
UAS19-rPanx1-GFP	UAS-rPanx1-GFP	pUAST19-attB	XhoI, XbaI	n/a		rPanx1-GFP removed from UAS-rPanx1-GFP using XhoI and XbaI and purified by gel extraction. pUAST-attB19 cut with XhoI and XbaI and

						ligated to rPanx1-GFP.
UAS19-rP2X2-LTS-1	UAS19-P2X2-GFP	UAS19-P2X2-GFP	a) EcoRI b) NotI and BglII	19,20	60°c	LTS sequence from Gr64a was amplified by PCR from w1118 flies using primers 19 and 20. P2X2-GFP was removed from UAS19-P2X2-GFP by cutting with EcoRI and religating the vector. GFP was removed by cutting with NotI and BglII. The LTS-1 PCR product was ligated into the vector using Not I and BglII. Vector was cut with EcoRI and P2X2-GFP was re-ligated into the vector.
UAS19-rP2X2-STS-10	UAS19-P2X2-GFP	UAS19-P2X2-GFP	a) EcoRI b) NotI and BglII	21,20	60°c	STS sequence from Gr64a was amplified by PCR from w1118 flies. Vector was prepared as above for rP2X2-LTS-1. (STS cloned in instead of LTS)

Primers:

1. AGCGCTAGCTCGCGAGTCGACGGC
2. AAGGGATCCCCTTCCTGCAGTCATTG
3. CAGGATGATCTGGACGAGGAGCATCAGGGGCTC
4. GAGCCCCTGATGCTCCTCGTCCAGATCATCCTG
5. TATGCTAGCCCACCATGGCGGGCTGCTGC
6. GGTGGTTGCTCTTCCGCACTGGTCCAGCTCACTAG
7. TATCTCGAGCCACCATGGCGGGCTGCTGC
8. ATAAGAATTCGCCTGGTCCAGCTCACTAG
9. TATCTCGAGCCACCATGGCCATCGCCCAC
10. ATAAGAATTCGCGCAGGATGAATTCAGAAG
11. TATGCTAGCGCCACCATGGGCCGGCGCTTG
12. ATAAGAATTCGCCAGTTGGGCCAAACC
13. TATCTCGAGCCACCATGCCGGCTTGCTGCA
14. ATAAGAATTCGCGTAGGGATACTTGAAGC
15. TATCTCGAGAAGCTTATGGCGGGCTGCT
16. ATATCTAGACTATCAGTGATGGTGGTG
17. CTATTCTAGACAAAATGGGCCGGCGCTTGGC
18. TATATCTAGACTATCAGTGATGGTGGTGATG
19. AAAGCGGCCGCAGAGGAGCAGAAGCTGATCTCGGAGGAGGATCTGCTGAAGATGTGCGAGCTACTGGA
20. TTTAGATCTTCAGGAGCACAGTGGCTG
21. AAAGCGGCCGCAGAGGAGCAGAAGCTGATCTCGGAGGAGGATCTGCTGTTCCAGATGACCACACAGAC

Table 2.2 – Primers used during site directed mutagenesis of hP2X4. Altered amino acids are underlined.

Mutation	Sense primer	Antisense primer	vector	Tm of PCR reaction	Reagent
F81E	ACCAACACTTCTAAACTTGGAGAGC GGATCTGGGATGTGGCGGAT	ATCCGCCACATCCCAGATCCGCTCT CCAAGTTTAGAAGTGTTGGT	pL118	60 °c	Phusion DNA Polymerase (NEB)
A93P	GCGGATTATGTGATACCACCTCAG GAGGAAAACTCCCTC	GAGGGAGTTTTCCTCCTGAGGTGG TATCACATAATCCGC	pL118	60 °c	Quikchange lightning SDM kit (Agilent)
N97G	ATACCAGCTCAGGAGGAAGGCTCC CTCTTCGTCATGACC	GGTCATGACGAAGAGGGAGCCTTC CTCCTGAGCTGGTAT	pL118	60 °c	Quikchange lightning SDM kit (Agilent)
A162L	AAGACGTGTGAGGTGCTGGCCTGG TGCCCGGTG	CACCGGGCACCAGGCCAGCACCTC ACACGTCTT	pL118	60 °c	Quikchange lightning SDM kit (Agilent)
W194R	CTTTTGGTTAAGAACAACATCCGGT ATCCCAAATTTAATTTCAGC	GCTGAATTAAATTTGGGATACCGG ATGTTGTTCTTAACCAAAAG	pL118	60 °c	Quikchange lightning SDM kit (Agilent)
H286N	GATACACGGGACGTTGAGAACAAC GTATCTCCTGGCTAC	GTAGCCAGGAGATACGTTGTTCTCA GTCCGTGTATC	pL118	60 °c	Quikchange lightning SDM kit (Agilent)

Table 2.3 – Fly stocks and genotypes.

Stock name	Source	Reference	Genotype
BL8121 – GMR-Gal4	Bloomington *Drosophila* stock center	Freeman, M, MRC lab of molecular biology	*y^1 w^*; wg^{Sp-1}/CyO; P{longGMR-GAL4}3/TM2*
BL458 – Elav-Gal4	Bloomington *Drosophila* stock center	Lin and Goodman, 1994	*P{GawB}$elav^{C155}$*
BL8691 – Rh1-Gal4	Bloomington *Drosophila* stock center	Treisman, J, NYU Langone medical centre	*P{rh1-GAL4}3, ry^{506}*
Gr5a-Gal4	Gift from Anupama Dahanukar (UCR)	Ueno *et al*, 2006	*w ; Gr5a-GAL4 ; Gr5a-GAL4*
nanos-phic31 ; attP40 (Stock 13 – 18)	Cambridge Stock Collection	Markstein *et al*. 2008	*y w M(eGFP, vas-int, dmRFP)ZH-2A; P{CaryP}attp40*
nanos-phiC31 ;; attP2 (Stock 13 -20)	Cambridge Stock Collection	Markstein *et al*. 2008	*y w P{y[+t7.7]=nos-phiC31\int.NLS}X #12;; P{y[+t7.7]=CaryP}attP2*
Double balancer stock	Gift from Helen White Cooper (Cardiff University)	n/a	*w* ; If / CyO ; TM3 / TM6
X-chromosome balancer stock	Gift from Helen White Cooper (Cardiff University)	n/a	*w*-Lethal/FM7b; Sco/CyO
UAS-eGFP	Lab stock	Spana, E, Harvard Universityf	*w; UAS-eGFP; UAS-eGFP*
W^{1118}	Gift from Helen White Cooper (Cardiff University)	n/a	*w-;+;+*

Chapter 3 - Expression of membrane protein constructs in mammalian cells

3.1 Chapter 3 - Introduction

3.1.1 Translation of membrane proteins

P2X receptors and pannexin channels (Panx) are eukaryotic membrane proteins which play roles in many physiological processes, and are implicated in a number of diseases including cancer, arthritis, male fertility and mood disorders (Labasi *et al*, 2002; Xu and Huang, 2002; Li *et al*, 2014; White and Burnstock, 2006; Ralevic and Burnstock, 1998; Pelegrin and Surprenant, 2007; White *et al*, 2005; Greig *et al*, 2003; Barden *et al*, 2006; Lucae *et al*, 2006; Hejjas *et al*, 2009; Erhardt *et al*, 2007; Roger *et al*, 2010; White *et al*, 2013; Mulryan *et al*, 2000).

Eukaryotic membrane protein biosynthesis occurs on the membrane of the ER. As the protein chain emerges from the ribosome, it is recognised by a signal recognition particle (SRP) that transfers the ribosome-chain complex to the translocon machinery; the extracellular portions of the membrane proteins are extruded into the lumen of the ER and the transmembrane domains (TMs) exit laterally through the translocon into the ER lipid bilayer (Geest and Lolkema, 2000; Ott and Lingappa, 2003). Evidence from co-expression studies with complementary fragments of rP2X2 indicates that the first transmembrane domain (TM1) 'waits' in the translocon pore for the second transmembrane domain (TM2), and will not exit without it (Cross and High, 2009). Several chaperone proteins are present in the ER lumen, including protein disulfide isomerase A3, calreticulin and calnexin to aid the correct folding and oligomerisation of the newly synthesised protein (Moremen *et al*, 2012). It is thought that, for P2X receptors, oligomerisation occurs in the ER, because the P2X6 subunit (which is incapable of forming homotrimers, but can form heteromeric receptors with P2X2 or P2X4 receptors) does not exit the ER, but when co-expressed with either P2X2 or P2X4, is found at the cell surface in heteromeric receptors (Ormond *et al*, 2006).

3.1.2 Post-translational modification; N-linked glycosylation

P2X receptors and Panx channels contain consensus N-glycosylation sequences (N-X-S/T, where X represents any amino acid except proline (Burda and Aebi, 1999), and several members of both protein families have been shown to be post-translationally modified by N-

glycosylation (Rettinger *et* al, 2000b; Newbolt *et* al, 1998; Young *et* al, 2008; Vacca *et* al, 2011; Qureshi *et* al, 2007; Jones *et al,* 2004; Lenertz *et al*, 2010; Boassa *et* al, 2007; Penuela *et al*, 2009). N-glycosylation is a post-translational modification that is added to a protein in the ER (core, high-mannose) by oligosaccharyl transferase (OST) which is embedded in the ER membrane with its catalytic site facing the lumen (Geest and Lolkema, 2000). The saccharide chain is then subsequently modified (complex) as the protein traffics to the cell surface *via* the Golgi apparatus (see Section 1.2.4). Protein glycosylation has been demonstrated to be important for correct eukaryotic membrane protein trafficking to the cell surface, and P2X receptors and Panx channels are no exception; abolition of the N-glycan acceptor sequences by mutagenesis in P2X receptors leads to a loss of trafficking to the cell surface and thus a loss of protein function (Rettinger *et al*, 2000b; Newbolt *et al*, 1998; Vacca *et al*, 2011; Lenertz *et al*, 2010). Furthermore, in P2X4 receptors, N-glycosylation has been shown to protect the protein from degradation in the lysosome which is essential for regulation of P2X4 expression at the cell surface (Qureshi *et al*, 2007). Conversely, although there is a preference for complex glycosylated species of Panx1 and Panx3 to be trafficked to the cell surface, non-glycosylated forms of both mouse channels were also shown to be able to reach the membrane (Penuela *et* al, 2009). Similarly, mutated rPanx1, which lacks a glycosylation site, showed a reduction but not abolition of cell surface expression (Boassa *et al,* 2008). Analysis of the N-glycosylation state of a eukaryotic membrane protein can provide information about protein quality in a heterologous expression system. N-glycosylation is also a potential problem for structural studies of membrane proteins because it adds unstructured regions to the protein and can increase heterogeneity, both of which inhibit crystallisation and reduce the obtainable resolution in particle averaging techniques (Chang *et al*, 1993). For these reasons it is often desirable to remove N-glycosylation by either mutagenesis (problematic for P2X receptors and Panx channels (see above)) or enzymatic treatment post-purification.

Endoglycosidase H (Endo H) and Peptidyl-*N*-Glycosidase F (PNGase F) are glycosidase enzymes commonly used to study the N-glycosylation state of proteins. Endo H, isolated from *Streptomyces plicatus,* specifically cleaves asparagine-linked mannose-rich oligosaccharides from glycoproteins, cleaving between the 2 GlcNAc subunits adjacent to the asparagine residue (Maley *et al*, 1989) (see Fig 1.4). Hence following digestion with Endo H, a reduction in molecular weight of a glycoprotein indicates the protein undergoes high mannose glycosylation. PNGase F, isolated from *Flavobacterium meningosepticum,* cleaves between the innermost GlcNAc subunit and the asparagine residue of all high mannose, hybrid and complex

glycoproteins (Maley *et al, 1989*). If a further reduction in molecular weight of a glycoprotein is observed upon digestion with PNGase F, this signifies that the protein undergoes complex glycosylation. A reduction in molecular weight of approximately 2.5 kDa would be expected when an oligosaccharide chain is cleaved from a single glycosylation site (Geest and Lolkema, 2000). For the removal of N-glycosylation for structural work, Endo H is the preferred treatment, because it cleaves efficiently under native conditions, as opposed to PNGase F, which works best on denatured protein. If any remaining complex glycosylation following deglycosylation with Endo H is still problematic for structure determination, the expression system can be changed (insect expression systems are not capable of complex glycosylation (see Introduction and Chapter 4)), or specialised mammalian cell lines deficient in complex glycosylation (GnTI- HEK-293 cell lines) (Reeves *et al,* 2002; Chaudhary *et al*, *2012*) can be used.

3.1.3 Mammalian protein expression: purification tags

It is often the case with mammalian protein over-expression systems that the relative yield of protein (protein of interest as a percentage of total protein) is much lower than with other over-expression systems (approximately 0.1% in mammalian cells versus 20-30% in *E. coli* (Bernaudat *et al,* 2011; Gan *et al*, 2006)). For this reason it is important to use affinity purification tags which have high binding capacity and low non-specific binding. There are a large variety of purification tags available. Some of the techniques that can be employed for protein purification include ion-exchange chromatography, size-exclusion chromatography, affinity chromatography and immunoprecipitation. More than one of these methods is often required for efficient protein purification (Hagel, 2001).

Immobilised metal affinity chromatography (IMAC) is very commonly used to purify proteins which contain an N- or C- terminal small poly-histidine (approximately 6-10 residues) affinity tag (His-tag), because of its low cost and ease of use. Transition metal ions (commonly Co^{2+}, Ni^{2+}) are immobilised to a solid matrix; these ions interact with the side chains of histidine residues upon contact with the protein of interest. Electron-donor groups of the histidine imidazole ring form bonds with the metal ion (Fig 3.1). Other proteins should not bind to the solid matrix and can be eluted (Bornhorst and Falke, 2000). Following immobilisation of the protein to the matrix, a change in pH or the addition of imidazole can be used to elute the protein. However, a drastic change in pH can cause protein denaturation and so low pH elution is unsuitable for purification if protein structure is to be retained.

This method has been successfully used to purify proteins expressed in a number of systems including *E. coli*, *S. cerevisae*, mammalian cells and baculovirus-infected insect cells (Van-Dyke *et al*, 1992; Kaslow and Shiloach, 1994; Janknecht and Nordheim, 1992; Kuusinen *et al*, 1995), with up to 95% purity (Janknecht *et al*, 1991). Although it is possible that the His-tag can impede protein activity, this is unlikely due to the small size and charge of the tag. Additionally the folded protein may cause occlusion of the tag and nickel affinity purification would not be useful when trying to maintain protein structure.

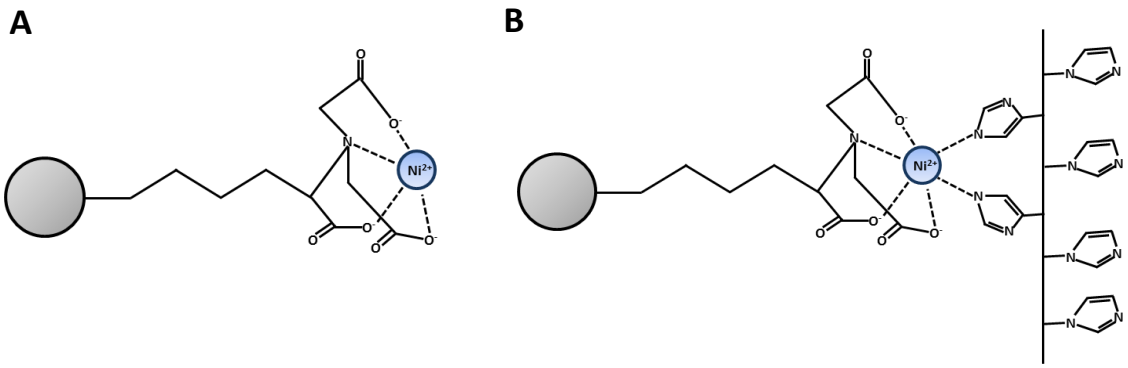

Figure 3.1 – Nickel affinity chromatography. (A) Schematic of sepharose bead (grey sphere) bound to nickel (blue sphere). (B) Nickel sepharose bead bound to hexa-histidine tag.

An additional system which allows purification in a single chromatographic step is the IMPACT (Intein mediated purification with an affinity chitin-binding tag) system. This system is a tandem-tag consisting of a self-cleaving protein (intein) and a chitin binding domain (CBD) affinity tag, which can be cloned onto the N- or C- terminus of a protein construct, and which enables purification of the protein by affinity purification on a chitin resin. The addition of thiol reagents such as DTT (dithiothreitol) activates the intein and enables release of the target protein from the intein-CBD tag (Watanabe *et al*, 1994; Chong *et al* 1998).

Similarly the addition of other tags such as a strep-tag, which is an 8 residue peptide sequence (Trp-Ser-His-Pro-Gln-Phe-Glu-Lys) or a myc-tag which is a 10 residue peptide sequence (Fly-Gln-Lys-Leu-Ile-Ser-Glu-Glu-AsP-Leu), to the N- or C-terminus of a protein will allow protein purification using immobilised streptavidin or a high affinity anti-myc antibody respectively (Schmidt and Skerra, 1994; Zhao *et al*, 2013).

Removal of the purification tag before structural studies is often desirable, and one way to achieve this is to introduce a thrombin cleavage site (TCS) (Leu-Val-Pro-Arg-Gly-Ser) between a protein and its tag. Upon the addition of thrombin under native conditions, the tag is cleaved between the Arg and Gly residues. In addition, appropriately tagged thrombin can be used as

the final purification step (i.e. instead of imidazole during metal affinity chromatography) to remove the protein from the resin (Hefti *et al*, 2001).

Immunoprecipitation is another method which can be used for the purification of an individual protein from a protein mixture or cell lysate, providing a relevant antibody which binds to the protein of interest is available. The antibody is often coupled to a solid substrate such as protein A- or protein G- (immunoglobulin binding proteins)-agarose. Upon contact with the protein antigen, the antibody-substrate complex will bind to the protein enabling physical separation from the rest of the protein mixture using centrifugation (Fig 3.2) (Bonifacino *et al*, 2001).

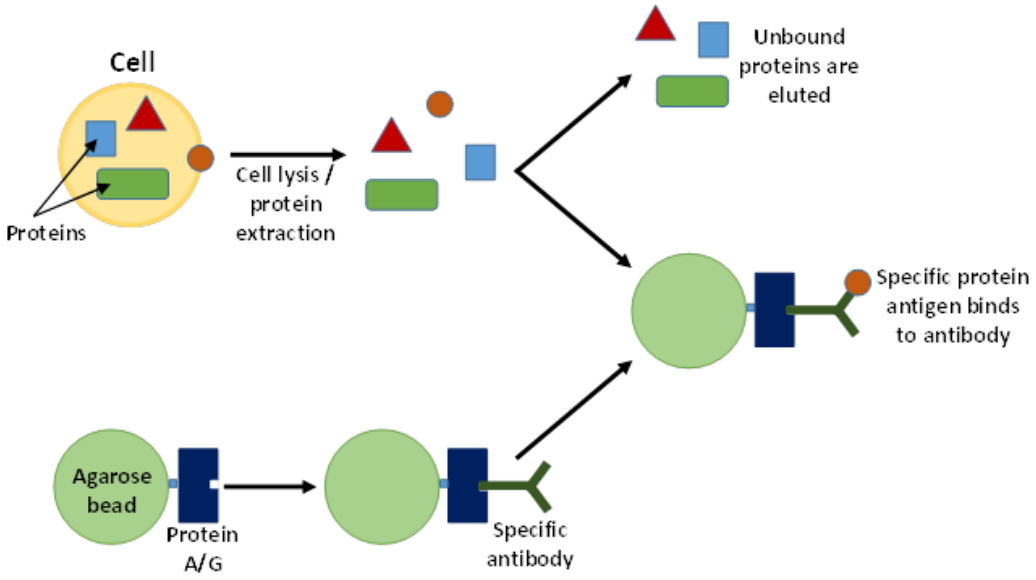

Figure 3.2 – Immunoprecipitation. Cell lysates or protein extractions can be purified using a specific antibody in Immunoprecipitation. The antibody is bound to a protein A/G-agarose substrate and incubated with a cell lysate or protein preparation. The protein with the antigen specific to the antibody will bind to the beads and can be separated from the remaining, unbound proteins. The protein of interest can then be eluted by low pH elution or antigen competition.

Gel filtration chromatography is a technique used to separate proteins according to their molecular size by passing the protein mixture through a porous column. Large molecules elute first due to exclusion from the matrix and small molecules elute later due their penetration into a larger number of pores within the matrix. Gel filtration is often used as an additional purification step following IMAC or immunoprecipitation. Additionally gel filtration can be used to assess the oligomeric state of a protein and separate monomers from protein oligomers (Hagel, 2001).

3.1.4 Aims of this chapter

The aims of this chapter were to construct and express a series of membrane protein constructs, which were fused to purification tags, in HEK-293 cells. It also aimed to study the glycosylation, localisation and purification of the constructs. The membrane protein constructs generated were rP2X2-GFP, rPanx1-GFP, rP2X7-GFP, hP2X4-GFP and hP2X4-int-CBD. These constructs were transfected into HEK-293 cells to determine whether or not they could be expressed. In addition, their glycosylation state, oligomeric state and expression pattern within the cell was studied to help assess protein quality. Two purification strategies were tested; metal affinity chromatography and the IMPACT system.

3.2 Chapter 3 – Results

3.2.1 Mutagenesis of hP2X4 receptors

zfP2X4.1 was chosen for structural studies by Kawate and colleagues due to its stability and ability to form trimers in detergent solution (Kawate *et al*, 2009). Previous work (Valente *et al*, 2011) used non-denaturing PFO-PAGE to analyse the degree of trimer formation of both hP2X4 and *Dictyostelium discoideum* P2XA (DdP2XA), finding that wild-type hP2X4 did not form stable trimers when assessed using this technique, whereas DdP2XA did. The authors concluded that improving the trimer stability of hP2X4 was a prerequisite for successful structure determination.

For this reason, I introduced a number of mutations into hP2X4 based upon amino-acid sequence differences between hP2X4 and zfP2X4.1 to try and increase the strength of the subunit-subunit interactions and hence the stability of hP2X4 trimers in detergent solution. Amino-acid residues positioned at the subunit interface of zfP2X4.1 were compared with the equivalent residues in a molecular model of hP2X4 based upon the zfP2X4.1 crystal structure. I identified six differences which gave rise to significant changes in the amino-acid properties and used site-directed mutagenesis to mutate these residues to their corresponding residue in zfP2X4.1 (Phe81Glu, Ala93Pro, Asn97Gly, Ala162Leu, Trp194Leu and His296Asn) (shown in magenta in Fig 3.3A).

Mutant constructs were expressed in HEK-293 cells by transient transfection and their expression was confirmed by western blotting (Fig 3.3A). Notably, the expression level of zfP2X4.1-GFP was considerably lower than that of hP2X4 and the mutant constructs.

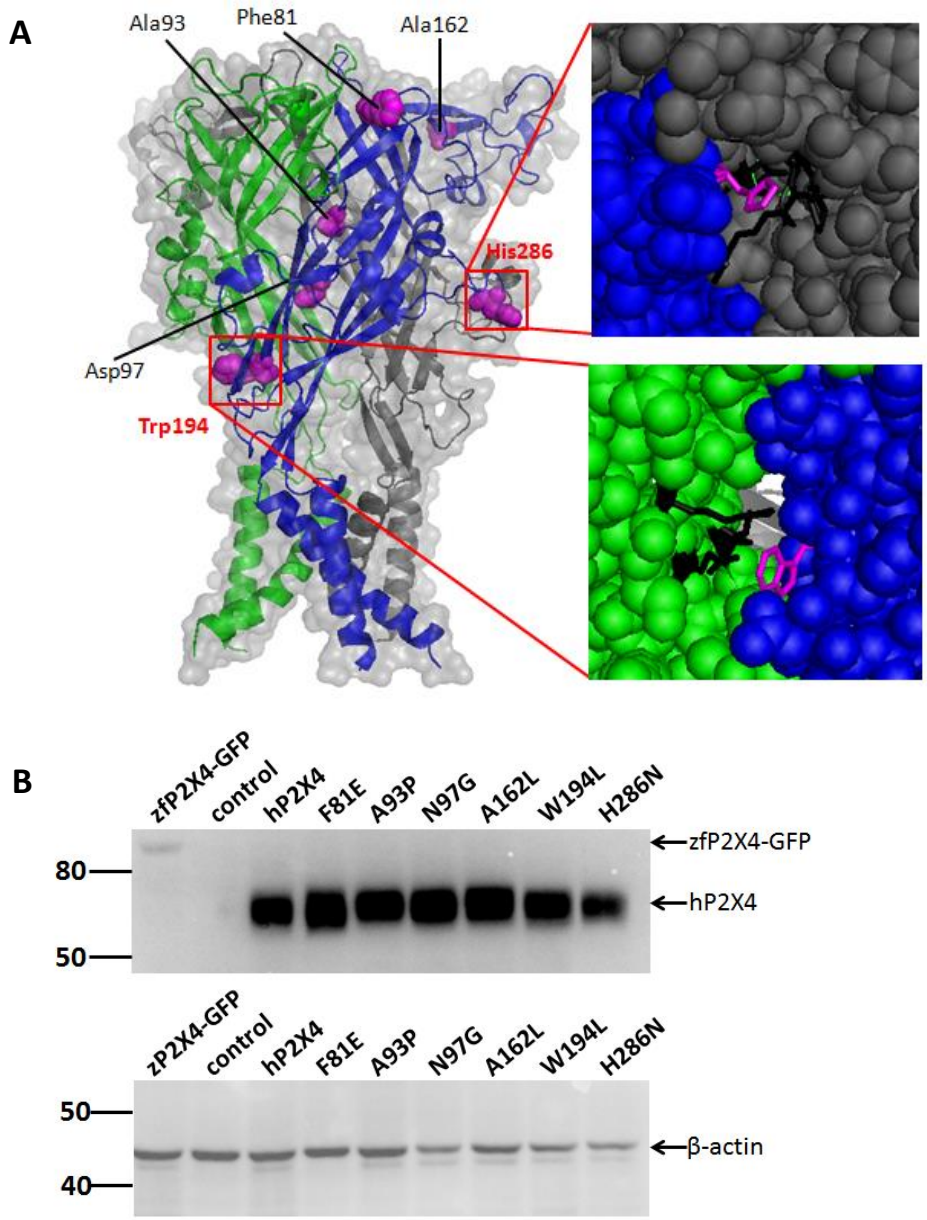

Figure 3.3 – Site directed mutagenesis of hP2X4. (A) Homology model of hP2X4, based on zfP2X4.1. Green, blue and grey cartoons represent the different subunits. Amino acid residues modified using site directed mutagenesis (SDM) are shown by fuchsia spheres. Inset – close up of the location of 2 modified amino acids acting at the subunit interface. Black shows the surrounding location in the adjacent subunit. (B) [top] Western blot of zfP2X4-GFP, hP2X4-his and the 6 mutant hP2X4-his constructs in HEK-293 cells. Proteins were detected using a tetra-his primary antibody [Qiagen]. hP2X4 and the 6 mutants show a high level of expression. zfP2X4-GFP is expressed at a much lower level in HEK-293 cells. [Bottom] Western blot of the same protein set probed with anti-β-actin [Abcam] to ensure equal loading. All cells were transfected for 48 hours using Lipofectamine 2000 [Invitrogen].

PFO-PAGE was used to assay the oligomeric state of hP2X4 and the 6 hP2X4 mutants to see if any of the mutations had a significant effect on trimer stability in detergent. However the protein for all P2X4 constructs formed a mixture of monomers, dimers and trimers but the

majority was monomeric (Fig 3.4A). zfP2X4-GFP was shown to form strong trimers in detergent using fluorescence size exclusion chromatography (FSEC) (Kawate *et al*, 2009). DdP2XA, a P2X receptor expressed in the slime mould, *Dictyostelium discoideum*, was also shown to form stable trimers, by PFO PAGE (Valente *et al*, 2011). Consequently the oligomeric state of zfP2X4-GFP and DdP2XA were investigated to use as controls in PFO PAGE. DdP2XA formed stable trimers (MW approximately 125kDa). However zfP2X4-GFP did not form stable trimers in PFO detergent (MW approximately 80kDa); the majority of the protein was monomeric (Fig 3.4B).

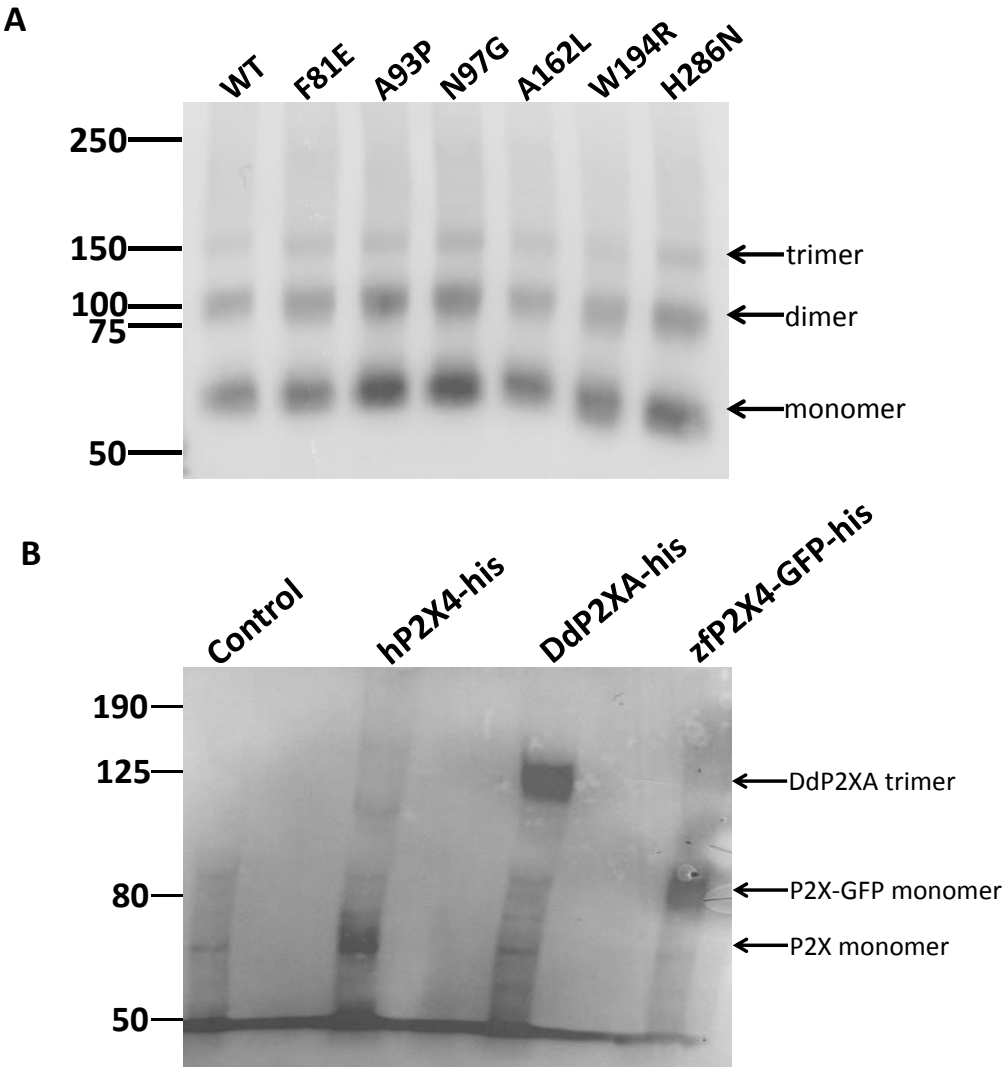

Figure 3.4 – PFO PAGE of constructs in HEK-293 cells. (A) Western blot analysis of hP2X4-his and the 6 mutant proteins following PFO-PAGE [anti-His, Qiagen]. HEK-293 cells were transfected with P2X4 receptor constructs carrying a C-terminal his-tag. All constructs formed a mixture of monomers, dimers and trimers. The result shown is representative of 3 assays. (B) Western blot analysis of hP2X4-his, DdP2XA and zfP2X4.1-GFP following PFO-PAGE [anti-His, Qiagen]. The majority of DdP2XA formed stable trimers, whereas hP2X4-his and zfP2X4-GFP were mostly monomeric (Note: the size of zfP2X4 is slightly larger than hP2X4-his due to the addition of GFP). The result shown is representative of 2 assays.

As zfP2X4-GFP did not form stable trimers using the PFO-PAGE assay as expected, FSEC was used to further investigate its oligomeric state to distinguish between the two possibilities that; (1) the protein is being denatured or the oligomer is not stable in PFO detergent or (2) the protein was not forming trimers in HEK-293 cells. The hP2X4 construct was cloned into the zfP2X4.1-GFP vector which allowed the his-tag to be replaced with a thrombin-cleavable GFP his-tag for visualisation and comparative purposes (Fig 3.6). The proteins were purified via their C-terminal his-tag using nickel affinity chromatography. The partially purified protein was applied to a Superdex 200 size exclusion column and the protein was separated into fractions according to size. The GFP fluorescence of a sample from each fraction was subsequently measured in a fluorescence plate reader.

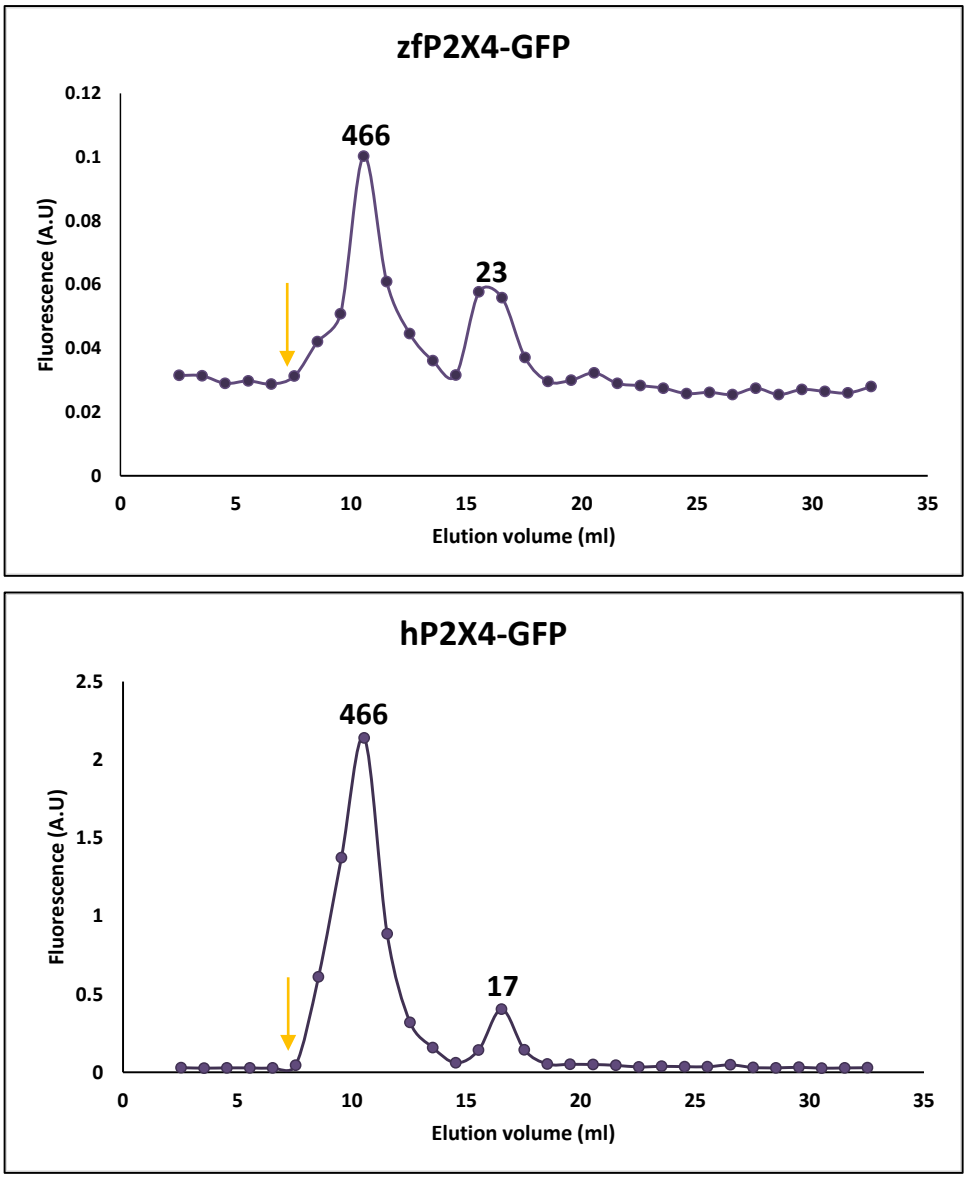

Figure 3.5 – Fluorescence size exclusion chromatography elution profiles. FSEC profiles of zfP2X4-GFP (top) and hP2X4-GFP (bottom) protein extracted and purified from HEK-293 cells. Yellow arrow indicates the void volume. Numbers adjacent to peaks show the estimated molecular weight of the protein elution (kDa). Expected size of hP2X4-GFP and zfP2X4-GFP monomer approximately 80 kDa + 60 kDa detergent micelle.

The FSEC results show that purified zfP2X4-GFP protein forms an oligomeric structure in DDM detergent with a molecular weight of approximately 466 kDa; the purified protein is made up of a mixture of a large oligomer (possibly a trimer) and a smaller band of approximately 23 kDa which may represent free GFP (Fig 3.5). Purified hP2X4-GFP also formed an oligomer of the same molecular weight (466 kDa) in DDM detergent and free GFP (17 kDa) (Fig 3.5). The data for the column calibration standards can be found in Appendix I. Taking these results into account it was decided to continue working with wild type hP2X4 as both proteins (hP2X4-GFP and zfP2X4-GFP) gave similar FSEC profiles but hP2X4 was expressed at a higher level with less GFP degradation.

3.2.2 Construction of membrane protein constructs

Three other membrane protein DNA constructs were cloned into the zfP2X4-GFP vector – rP2X2, rP2X7 and rPanx1 giving rise to rP2X2-GFP, rP2X7-GFP and rPanx1-GFP protein constructs, each of which has a thrombin cleavable GFP his-tag (Fig 3.6).

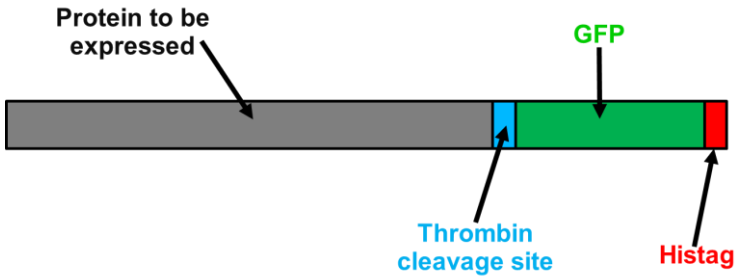

Figure 3.6 – Protein construct schematic – Each protein (rP2X2, hP2X4, rP2X7 and rPanx1) was cloned into the zfP2X4.1-GFP vector. Each protein was fused to a GFP tag (for visualisation purposes), C-terminal his-tag (for purification) and a thrombin cleavage site (to enable removal of the tag).

Additionally, a hP2X4 construct with an intein chitin-binding-domain tag to enable protein purification using a chitin column was cloned. The intein allowed for straightforward tag removal using thiol reagents such as DTT.

3.2.3 Expression and purification of protein constructs in HEK cells

The constructs were expressed in HEK-293 cells and their expression was analysed using western blotting. hP2X4-GFP, rP2X2-GFP, rPanx1-GFP and hP2X4-int-CBD constructs were successfully expressed in HEK cells and detected by western blotting with anti-GFP and anti-P2X4 antibodies appropriately. However, rP2X7-GFP was not expressed in HEK-293 cells (Fig

3.7). Due to the lack of expression of rP2X7-GFP in HEK-293 cells, no more work was performed with this construct.

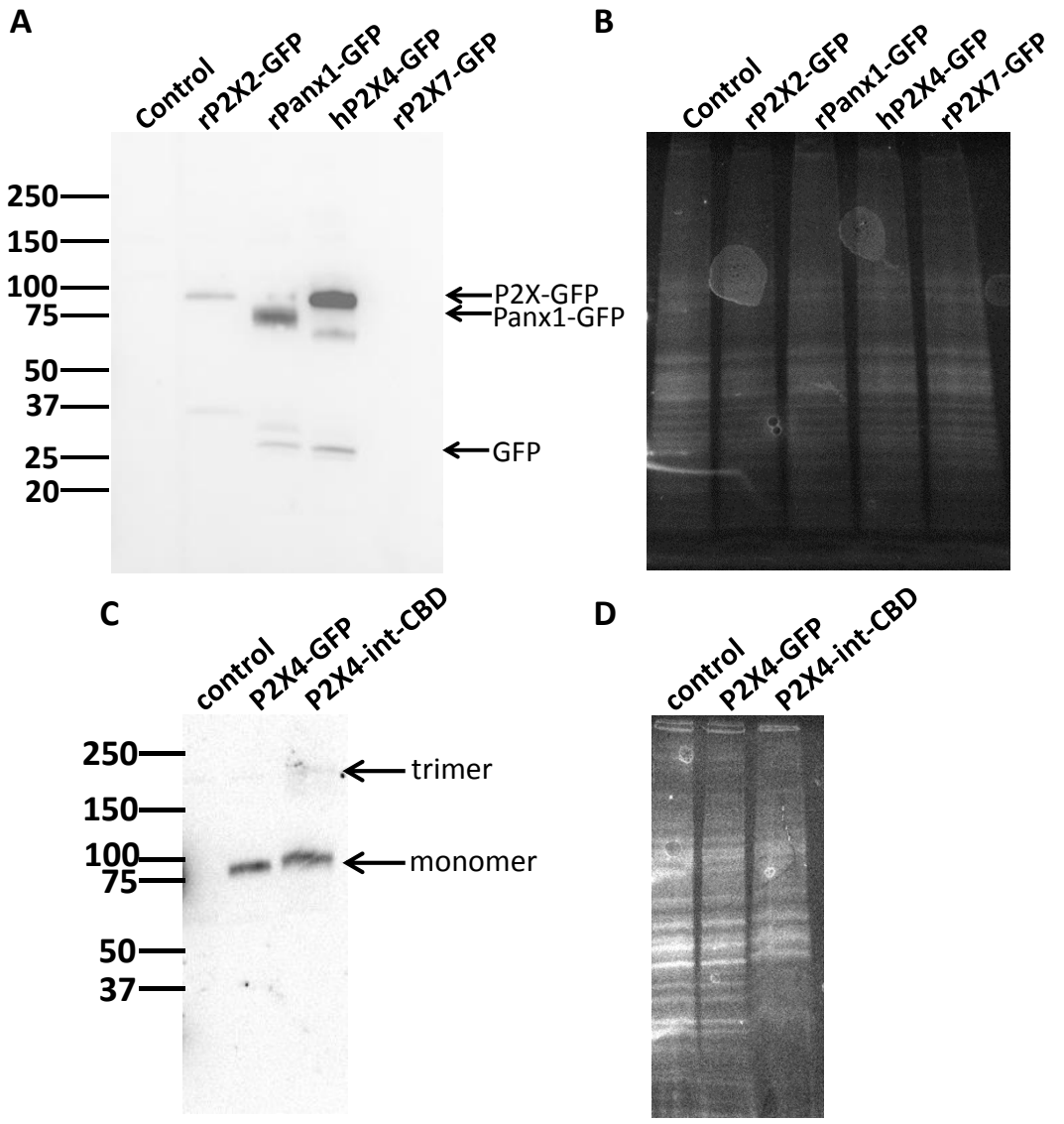

Figure 3.7 – Expression of protein constructs in HEK-293 cells. (A) Western blot of rP2X2-GFP, rPanx1-GFP, hP2X4-GFP and rP2X7-GFP protein constructs expressed and extracted from HEK-293 cells (anti-GFP, Invitrogen). 10 µg protein loaded/lane. (B) Stain-free gel (blotted in A) visualised under UV light following SDS PAGE to ensure equal loading. (C) Western blot of hP2X4-GFP and hP2X4-int-CBD protein constructs expressed and extracted from HEK-293 cells (anti P2X4, Alomone). 10 µg loaded per lane. (D) Stain-free gel (blotted in C) visualised under UV light following SDS PAGE to ensure equal loading.

rP2X2-GFP and rPanx1-GFP were purified from HEK-293 cells using nickel affinity chromatography. Fractions were taken at each stage of the purification process to assess binding and elution of protein to nickel beads (see Fig 3.8). The majority of the protein bound

successfully to the nickel beads with a small amount observed in the nickel flowthrough fraction. Most of the protein was eluted upon the addition of 1M imidazole. However some remained bound to the nickel beads (Fig 3.8 B/C).

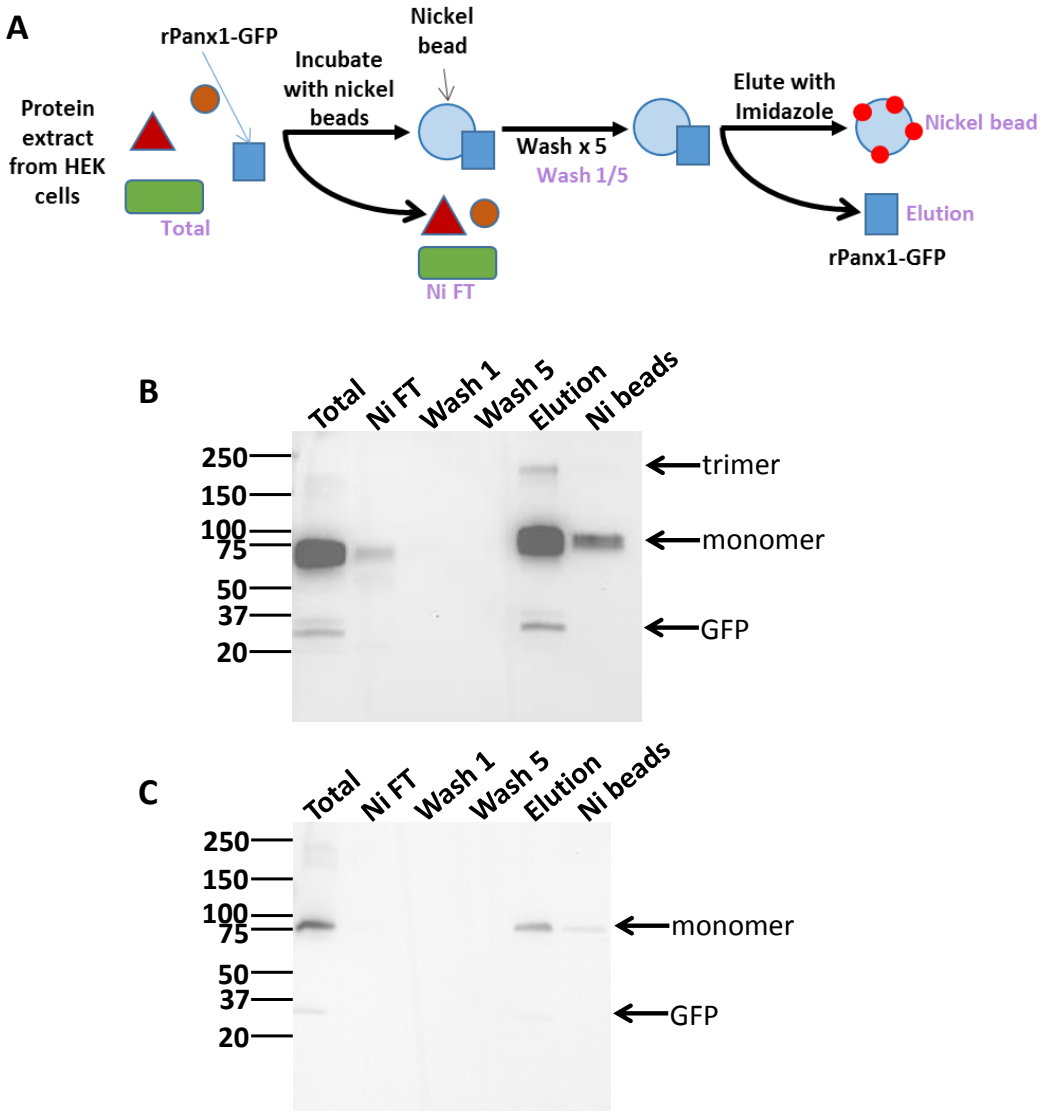

Figure 3.8 – Purification of rPanx1-GFP and rP2X2-GFP from HEK-293 cells. (A) Schematic showing steps undertaken during rPanx1-GFP purification. (B/C) Western blots showing purification of rPanx1-GFP (B) and rP2X2-GFP (C) from HEK cell extracts using nickel affinity chromatography (anti GFP, Invitrogen). Each blot shows the 'Total' starting fraction, the nickel flowthrough (Ni FT), wash 1 and wash 5, the elution and what remains on the nickel beads after elution (as shown in purple in A). The majority of the protein successfully bound to nickel beads and was eluted with 1M imidazole. rPanx1-GFP is shown as an example in (A).

hP2X4-int-CBD was purified by binding to a chitin resin and eluting with DTT. Most of the protein did not bind to the chitin beads and washed out in the flowthrough. Additionally more

protein became displaced during washing steps. Cleaved protein can be observed in both the elution and remaining on the chitin beads (Fig 3.9).

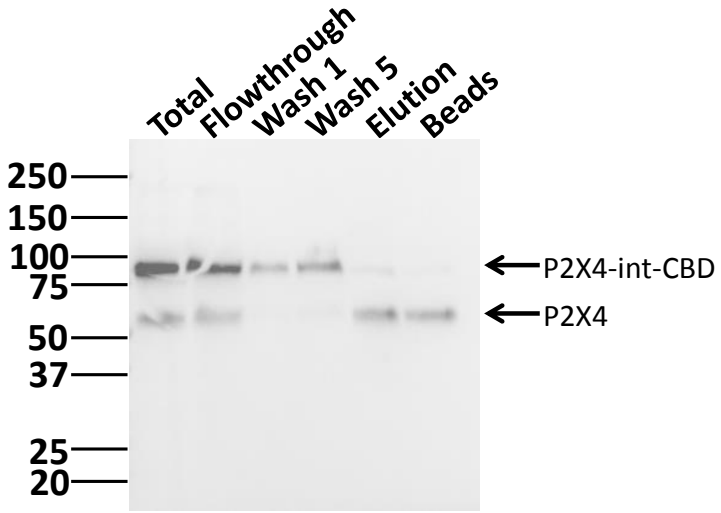

Figure 3.9 – Purification of hP2X4-int-CBD – Western blot showing purification of hP2X4-int-CBD extracted from transfected HEK cells using chitin beads [anti P2X4, Alomone]. Little protein bound to the chitin beads and some was also displaced during the washing steps. A small amount of protein was successfully eluted following cleavage and some remained bound to the beads after cleavage of the tag.

The oligomeric state of purified rP2X2-GFP and rPanx1-GFP was investigated using FSEC. rPanx1, suggested to form hexamers based on results from cross-linking experiments and SDS-PAGE, where a protein band of approximately 290 kDa was observed (Boassa *et al*, 2007), did not appear to form hexamers under these conditions (expected molecular weight of Panx1-GFP hexamer with a DDM detergent micelle – 450 – 490 kDa). The majority of the protein, separated by FSEC gave peaks corresponding to molecular weights of 156 kDa and 17 kDa, which are likely to represent dimeric protein and free GFP respectively. Unlike hP2X4, rP2X2 did not form a stable oligomer in detergent; the majority of the protein corresponded to a molecular weight of 30 kDa, indicating that the GFP is largely cleaved from the protein during FSEC. There is also a peak in the void volume which is aggregated protein (Fig 3.10).

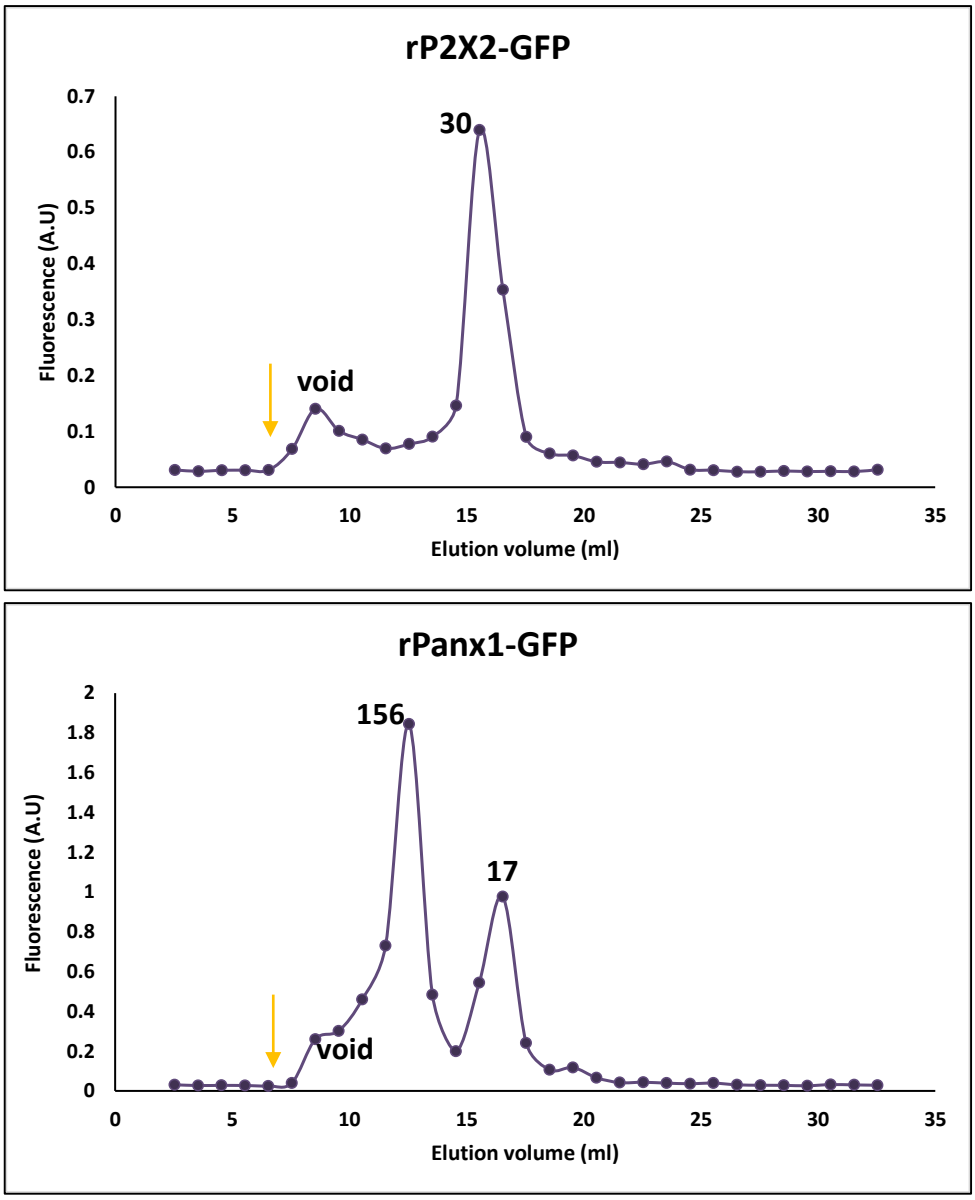

Figure 3.10 – Fluorescence size exclusion chromatography elution profiles. FSEC profiles of rP2X2-GFP (top) and rPanx1-GFP (bottom) protein extracted and purified from HEK-293 cells. Yellow arrow indicates the void volume. Numbers adjacent to peaks show the estimated molecular weight of the protein elution (kDa). Expected size of rP2X2-GFP monomer – approximately 85 kDa + 60 kDa detergent micelle. Expected size of rPanx1-GFP monomer – approximately 70 kDa + 60 kDa detergent micelle.

3.2.4 Localisation of constructs in HEK-293 cells

The localisation of membrane proteins is very important for correct protein function. The distribution of hP2X4-GFP, rP2X2-GFP and rPanx1-GFP was investigated in HEK-293 cells using confocal microscopy. hP2X4-GFP displayed a punctate distribution throughout the cell with the majority expressed inside the cell (Fig 3.11). rPanx1-GFP expression was more defined to the cell surface with a lower level of intracellular expression than hP2X4-GFP (Fig 3.11). rP2X2-GFP displayed a similar expression distribution in HEK-293 cells to hP2X4-GFP. However the

localisation of rP2X2-GFP is less punctate but still predominantly intracellular, possibly being retained at the ER or Golgi (further experiments would be required to confirm the exact localisation).

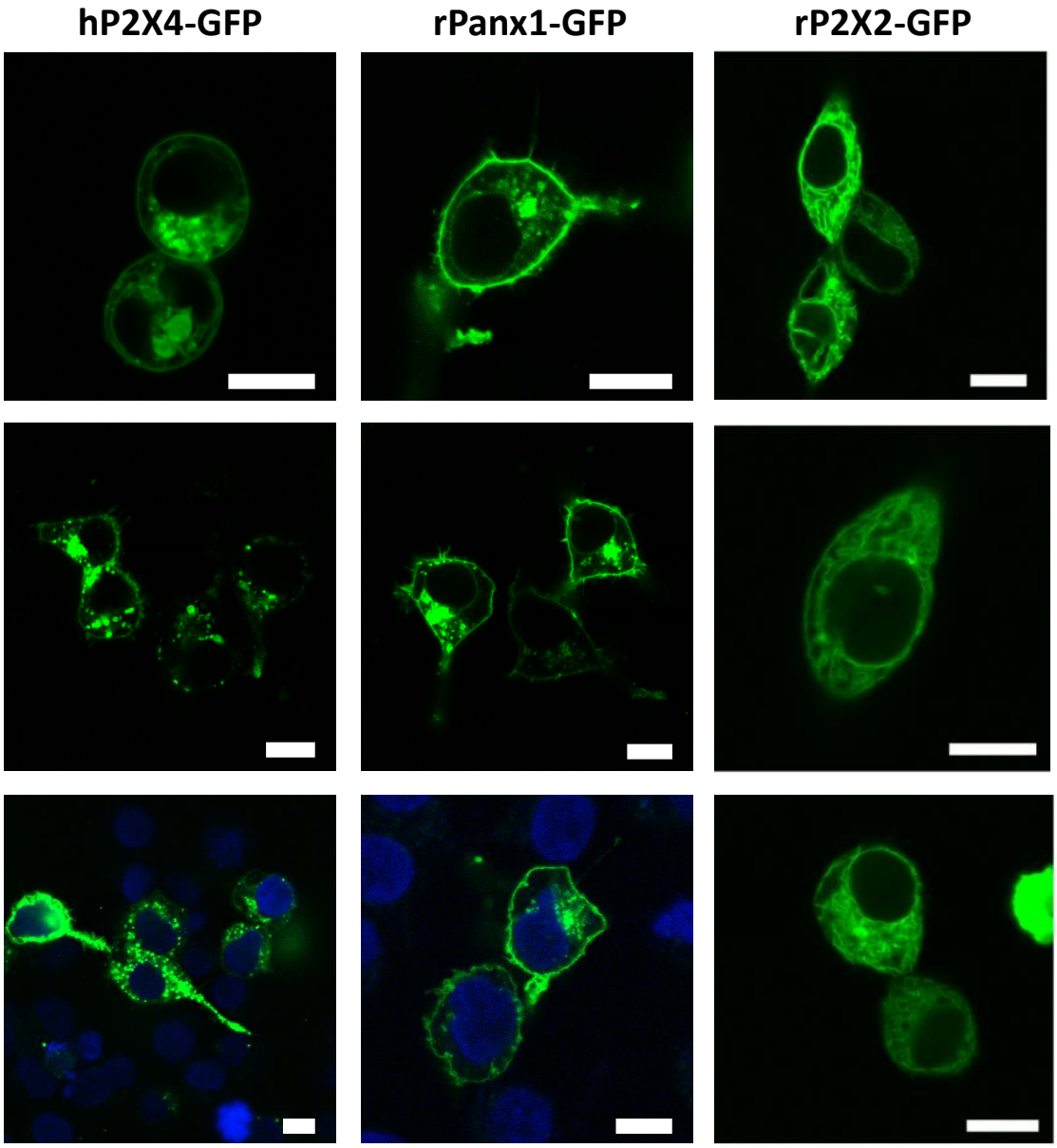

Figure 3.11 – Confocal Images of protein constructs expressed in HEK-293 cells. Images taken using a Leica confocal microscope. Protein-GFP constructs are shown in green – hP2X4-GFP (left), rPanx1-GFP (middle) and rP2X2-GFP (right). The nuclei were stained using dapi and are shown in blue in the bottom images for hP2X4-GFP and rPanx1-GFP. Scale bar = 10µm.

3.2.5 Glycosylation of hP2X4-GFP, rP2X2-GFP and rPanx1-GFP in HEK-293 cells

As explained in the introduction, correct glycosylation of membrane proteins is important for protein targeting and/or function. To investigate the glycosylation state of rP2X2-GFP and rPanx1-GFP protein constructs in HEK-293 cells 2 deglycosylation enzymes were used; PNGase F which is capable of deglycosylating all glycoproteins including complex and hybrid glycoproteins and Endo H which only deglycosylates high-mannose glycoproteins.

rP2X2-GFP underwent high mannose glycosylation in HEK cells as shown by the reduction in molecular weight by western blotting following incubation with Endo H. However following digestion with PNGase F, the protein did not undergo a further reduction in molecular weight (Fig 3.12B). This data suggests that rP2X2-GFP does not undergo complex glycosylation in this system. rPanx1-GFP protein underwent high mannose glycosylation in HEK cells; the lower molecular weight band is reduced upon digestion with Endo H. Additionally rPanx1-GFP underwent hybrid/complex glycosylation in HEK cells; the band of higher molecular weight was reduced to a basal size upon digestion with PNGase F (Fig 3.12A). Like rP2X2-GFP, hP2X4-GFP underwent high mannose but no complex glycosylation in HEK cells (Fig 3.12C).

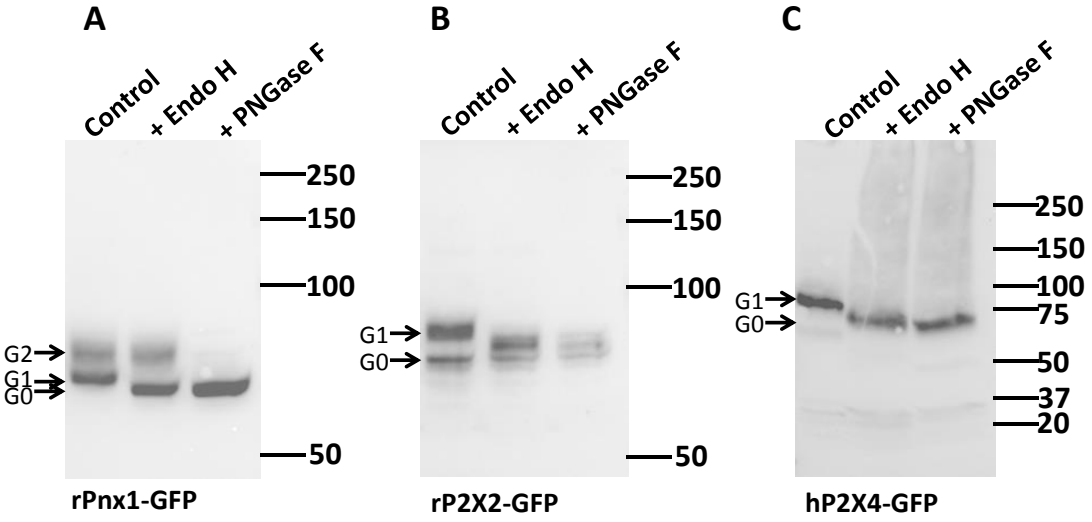

Figure 3.12 – Glycosylation of protein constructs in HEK-293 cells. – (A) Western blot showing deglycosylation of rPanx1-GFP extracted from HEK cells with Endo H and PNGase F. (B) Western blot showing deglycosylation of rP2X2-GFP extracted from HEK cells with Endo H and PNGase F. (C) Western blot showing deglycosylation of hP2X4-GFP extracted from HEK cells with Endo H and PNGase F. (All blots detected with anti-GFP, Invitrogen). G0 = non-glycosylated protein, G1 = high mannose glycosylated protein, G2 = complex glycosylated protein. All blots representative of 2 assays.

3.3 Chapter 3 – Discussion

3.3.1 PFO-PAGE and FSEC of zfP2X4-GFP and hP2X4-GFP

zfP2X4-GFP formed stable trimers following FSEC according to Kawate *et al*, 2009, when the closed state crystal structure was solved to a resolution of 2.9 Å. Although the data was not shown, they also assessed the oligomeric state of 34 other P2X receptors following solubilisation in detergent and stated that zfP2X4.1 was chosen as a candidate for crystallisation due to its sharp and symmetrical elution profile. They also showed that rP2X4 largely dissociates following solubilisation in detergent without the use of high concentrations of cross-linkers (Kawate *et al*, 2009). Using this knowledge, I sought to improve the solubilisation behaviour of hP2X4 based on the zfP2X4 structural data. As previously stated, residues acting at the subunit interfaces were analysed and 6 residues with significantly different properties in zfP2X4 and hP2X4 were identified (F81, A93, N97, A162, W194 and H286). These residues were mutated to the equivalent residues present in zfP2X4.1. The oligomerisation state of the mutated proteins was then analysed using PFO PAGE to allow the assessment of the native quarternary structure of membrane proteins in the presence of the mild detergent, PFO (Fig 3.4) (Ramjeesingh *et al*, 1999). Wild type hP2X4 dissociated in the presence of PFO and the majority of the protein was monomeric. In addition, none of the 6 mutations had a significant effect on trimer formation (Fig 3.4). Two control proteins were also assessed using this method; DdP2XA, which was previously shown to form stable trimers in PFO detergent (Valente *et al*, 2011) and zfP2X4.1 (Fig 3.4B). Although DdP2XA formed trimers (with an approximate molecular weight of 120 kDa) following PFO PAGE, the majority of zfP2X4-GFP protein formed monomers (with an approximate molecular weight of 80 kDa). As the control protein, zfP2X4-GFP, did not form trimers with PFO solubilisation, the oligomerisation state was further investigated using FSEC.

hP2X4-GFP and zfP2X4-GFP constructs were purified using nickel affinity purification and the purified protein was analysed using FSEC. Contrary to PFO results, both protein constructs formed an oligomer of approximately 466 kDa in the presence of the detergent, DDM. DDM was chosen for protein solubilisation due to its previous successful use with P2X receptors (Sim *et* al, 2004; Mio *et al*, 2005; Kawate *et al*, 2009; Valente *et al*, 2011). DDM is a mild, non-ionic detergent commonly used for membrane protein solubilisation due to its ability to readily solubilise many membrane proteins in a functional state (Seddon *et al*, 2004). The calculated molecular weights of both hP2X4-GFP and zfP2X4-GFP are higher (466 kDa) than the expected molecular weight of a hP2X4-GFP trimer with a DDM micelle (300 kDa), and the peak is more

comparable to that of a P2X4 tetramer than a trimer. The peaks are not likely to represent aggregated protein as aggregates would be observed in the void volume of the column. Although it cannot be ascertained, column calibration may have been inaccurate as the molecular weight markers were run in the presence of detergent and so could have affected the molecular mass of the individual protein standards; if this was the case, it is possible that both proteins were forming stable trimers in DDM. The gel filtration results showed that a larger proportion of hP2X4-GFP formed stable oligomers compared to zfP2X4-GFP (Fig 3.5). In light of this result I decided to discontinue working with the 6 hP2X4 mutant constructs.

The PFO-PAGE and gel filtration results differed from one-another significantly for both the hP2X4 and zfP2X4 protein constructs; PFO-PAGE indicated that the proteins all formed a mixture of monomers, dimers and trimers and gel filtration indicated formation of an oligomer with a molecular weight higher than would be expected for a trimer. As zfP2X4-GFP was previously shown to form strong trimers in the presence of DDM, it was expected to form a trimer in both assays. It may be that although PFO-PAGE appeared to be a valid technique for assessing the oligomerisation state of DdP2XA, it is not valid for studying other P2X receptors. One possible reason for this is that while PFO preserves some oligomeric protein structures, it may destabilise and cause dissociation of others. In this case, PFO appears to destabilise the P2X4 oligomer and so is not sufficient for the solubilisation of hP2X4 or zfP2X4.1. However, Compan and colleagues have shown that in contrast, the oligomeric states of P2X2 and P2X5 are efficiently preserved by PFO detergent with dimers and trimers observed with PFO-PAGE (Compan *et* al, 2012). This suggests that small differences between the different P2X receptors can affect the stabilising effect of PFO on oligomer structure preservation.

3.3.2 rP2X7-GFP was not expressed in mammalian cells

As well as hP2X4-GFP, the rP2X2-GFP, rPanx1-GFP and rP2X7-GFP constructs were transfected into HEK-293 cells and their expression was assessed using western blotting. The western blots showed that of these constructs, rP2X2-GFP, rPanx1-GFP and hP2X4-GFP were expressed successfully at varying levels in HEK cells. However the rP2X7-GFP construct was not expressed (Fig 3.7). The reasons underlying the inability of HEK cells to express the rP2X7-GFP construct are unclear. The addition of a tag to a protein can have significant effects on protein expression. However, the fusion of a His-tag to a protein is unlikely to have an effect on protein expression or activity due to its small size and charge (Terpe *et al*, 2003). In addition, Mohanty and Weiner looked into the effects of the size and position of the His-tag on many aspects of protein expression; they concluded that all combinations that were tested yielded

similar expression levels indicating that the His-tag is unlikely to be the underlying cause of P2X7 not being expressed (Mohanty and Weiner, 2004).

The GFP tag is a much larger tag that was added to each of the protein constructs. Although it is possible that the GFP tag is responsible for interfering with protein expression, previous work has demonstrated the expression of rP2X7 with a C-terminal GFP tag in HEK-293 cells (Ferrari *et al*, 2007). However the linker sequences which were cloned between the protein of interest and the GFP sequence could have a significant effect on protein expression (Zhang, 2009; Minskaia and Ryan, 2013). The number of linker amino acids can be critical for correct protein expression and membrane targeting (Tavoularis *et al*, 2001). Therefore it is possible that the linker sequences used in the rP2X7-GFP construct may have affected expression of the protein. This would have to be further investigated by testing a range of linker sequences to determine if the linker sequences are problematic. In addition, the linker sequence used in previous work where P2X7-GFP expression was successful could be cloned into the rP2X7-TCS-GFP-His construct and expressed in HEK cells to see if there is an improvement in expression levels.

Another difference between other expressed P2X7 constructs and the rP2X7-TCS-GFP-His construct is the addition of the TCS and the His-tag to the C-terminus of the protein resulting in a very lengthy C-terminus. Thus one possibility is that the extensive C-terminus of rP2X7, 244 amino acids in length, and is extended by the addition of the TCS, GFP tag and His-tag, caused the protein to become unstable and degraded by the cell. The C-terminus of the rP2X2-GFP and hP2X4-GFP protein constructs are considerably smaller consisting of 124 and 35 amino acids respectively, before the addition of the tag. In addition, the larger of the two (rP2X2-GFP) is expressed at significantly lower levels than hP2X4-GFP. It is possible that a lengthy C-terminus has a negative effect on protein expression levels.

3.3.3 Expression, glycosylation and localisation of hP2X4-GFP, rP2X2-GFP and rPanx1-GFP in HEK cells

The confocal images of HEK-293 cells transiently transfected with hP2X4-GFP showed that the protein had a punctate distribution throughout the cytoplasm with low levels at the plasma membrane (Fig 3.11). The intracellular localisation of hP2X4 was previously shown to correspond to localisation at endosomes and lysosomes where it is thought to be continuously recycled to and from the plasma membrane due to its roles in synaptic transmission (Bobanovik *et al,* 2002). hP2X4-GFP underwent high mannose glycosylation in HEK-293 cells

(Fig 3.12) with a reduction in molecular weight observed upon incubation with Endo H. However it did not display complex glycosylation. These results are in contrast to a previous report where P2X4 was shown to possess both high mannose and complex glycosylation in NRK (normal rat kidney epithelial) cells (Qureshi *et al*, 2007). Glycosylation of P2X4 is known to be important to protect the receptor from degradation when localised to endosomes and lysosomes (Qureshi *et al*, 2007). However whether or not high mannose glycosylation is sufficient to prevent degradation in lysosomes has not been determined.

In contrast, FSEC showed that the majority of the purified rP2X2-GFP protein formed protein aggregates and a smaller peak at 30 kDa that may represent free GFP following purification from HEK-293 cells suggesting that the protein is not forming trimers and functioning correctly in these cells. If the gel filtration protein standards are correct, one possible explanation for these results is that the GFP was degraded/cleaved from the P2X2 receptor during gel filtration, this may explain why a larger oligomer cannot be observed. Unfortunately, the yield was too low for peaks to be observed on the UV trace and thus we cannot determine the oligomeric state of P2X2 from these experiments. Imaging of HEK-293 cells transiently transfected with rP2X2-GFP showed that the protein was localised mostly within the cell with some expression at the cell membrane. This is not typical of rP2X2 localisation in HEK-293 cells according to previous experiments. For example, wild type P2X2 and P2X2-GFP constructs were expressed in HEK-293 cells and olfactory bulb neurons by Bobanovik and colleagues; both constructs were localised predominantly to the cell surface in both cell types (Bobanovik *et al*, 2002). In addition, an experiment by Vulchanova *et al*, 1996 showed that P2X2 was expressed at the cell periphery in HEK cells. The deglycosylation assays show that rP2X2-GFP underwent high mannose glycosylation but not complex glycosylation in HEK-293 cells. This is in contrast to previous work that showed that rP2X2 underwent complex glycosylation in HEK cells (Young *et al*, 2008). Removal of 2 out of the 3 glycosylation sites located on the extracellular domain of P2X2 led to a large reduction in channel function and trafficking to the cell surface (Newbolt *et al*, 1998). Additionally, P2X receptors are synthesised and undergo core glycosylation in the endoplasmic reticulum before being transported to the Golgi apparatus for further glycosylation to allow transportation to the cell surface. The differences observed in P2X2 distribution in this study and others may have been as a result of the incomplete glycosylation of this rP2X2-GFP protein construct, and this may have, in turn, had an effect on the oligomeric state of the protein. However, the gel filtration results are particularly difficult to interpret because western blotting showed that GFP remained bound to the P2X2 protein following

extraction from cells and solubilisation in detergent throughout the purification process with no free GFP observed with a GFP antibody (Fig 3.7, 3.8). This would indicate that the 30 kDa peak could not represent free GFP and as it smaller than a P2X2-GFP monomer, it could be assumed that the column has not been calibrated correctly. In addition, this peak is larger than the peaks observed for rPanx1-GFP, hP2X4-GFP and zfP2X4-GFP samples that were assumed to represent free GFP.

The localisation and glycosylation state of rPanx1-GFP corresponded closely to what has been observed previously. The majority of the protein is localised to the plasma membrane as other groups noted for mPanx1 (Penuela *et al*, 2009) and hPanx1 (Ma *et al*, 2009). rPanx1-GFP was sensitive to cleavage by Endo H, indicating that it endured high mannose glycosylation. In addition, further cleavage was observed following incubation with PNGase F suggesting the protein also underwent complex glycosylation in HEK cells, in agreement with work by Boassa *et al* where it was shown that complex glycosylation is important for membrane targeting (Boassa *et al*, 2007). Crosslinking experiments were also used to demonstrate that rPanx1 channels were capable of forming hexameric assemblies (Boassa *et al*, 2007). However when the rPanx1-GFP construct was purified from HEK-293 cells and analysed by gel filtration chromatography there was no evidence to suggest the formation of hexamers; the majority of the protein was present in two distinct peaks corresponding to molecular weights of 17 kDa and 156 kDa. These peaks are likely to account for free GFP and dimeric protein respectively. An additional 'shoulder' to the in-gel fluorescence trace was observed in the void volume that was likely to be aggregated protein. Therefore although the protein appeared to be glycosylated and localised correctly, it may not have formed hexameric channels in HEK-293 cells and consequently may not be functional. To determine whether or not the protein is functional, electrophysiology and biochemical experiments would have to be performed. However, these experiments were not undertaken due to time constraints.

The results from this chapter suggest that the rPanx1-GFP construct can be expressed and fully glycosylated in HEK-293 cells. In addition, confocal microscopy experiments showed that it was localised to the plasma membrane. However, when it was removed from the membrane and solubilised in detergent, it appeared to form predominantly dimers and free GFP indicating that either (i) the protein was not sufficiently solubilised by DDM, (ii) the protein was not forming hexamers in HEK cells or (iii) column calibration was incorrect and the observed peaks corresponded to different molecular weights. However, as the observed peak (156 kDa) was smaller than the peaks for zfP2X4-GFP and hP2X4-GFP (466 kDa), if zfP2X4-GFP and hP2X4-GFP

were forming trimers as expected, the rPanx1-GFP could not be forming hexamers. If, however, the P2X4 constructs were aggregating, it is possible that rPanx1-GFP was forming hexamers and rP2X2-GFP forming trimers. A much more detailed analysis of these protein constructs would be required to determine the correct molecular weight of these constructs.

rP2X2-GFP and hP2X4-GFP underwent core glycosylation but not complex glycosylation in HEK cells; this was in contrast to published data regarding P2X2 and P2X4 in the past whereby both undergo complex glycosylation in HEK cells. One explanation is that the lack of complex glycosylation was preventing the protein from reaching the cell surface efficiently and this may have resulted in the majority of the protein being expressed within the cell rather than at the surface. Additionally, incomplete glycosylation may have had an effect on the formation of functional oligomers. Alternatively, GFP tagging of the protein may have caused incorrect trafficking and glycosylation of P2X2 and P2X4. However there is little evidence to suggest that C-terminal GFP tagging of proteins has a negative effect on protein localisation (Palmer and Freeman, 2004; Lamping *et al,* 2007; Skube *et al*, 2010).

3.3.4 Conclusions

zfP2X4-GFP, rP2X2-GFP, rPanx1-GFP, hP2X4-GFP and hP2X4-int-CBD constructs were successfully expressed in HEK cells. hP2X4-GFP appeared to form a higher level of stable oligomers in detergent than zfP2X4-GFP but the exact oligomeric state of these proteins remains to be determined. In addition, the expression levels of hP2X4-GFP were significantly higher. However, rP2X2-GFP and rPanx1-GFP did not form stable trimers and hexamers respectively in detergent when purified from HEK cells. Although rPanx1-GFP expression was observed at the cell surface, both rP2X2-GFP and hP2X4-GFP were expressed predominantly intracellularly as expected for hP2X4-GFP due to localisation to lysosomes and endosomes. However rP2X2-GFP is usually localised mostly to the cell surface in HEK cells; one possible reason for this was that the GFP interfered with the correct glycosylation and trafficking of rP2X2-GFP.

Chapter 4 - Expression of rP2X2 and rPanx1 in the Drosophila eye

4.1 Chapter 4 introduction

4.1.1 The fruit fly, *Drosophila melanogaster*

The fruit fly, *Drosophila melanogaster*, has been used as a model organism for a great variety of biological and genetic research applications for many years due to their cheap maintenance costs, short life cycle and fully sequenced genome, allowing manipulation and analysis of many aspects of their genome and proteome (Adams *et al*, 2000). In addition, a system has been set up allowing a transgene to be expressed in any tissue of the fly under control of the *Gal4-UAS* system.

4.1.2 The *Gal4-UAS* system

The *Gal4-UAS* system, present in yeast, is used for specific and targeted gene expression (Laughon and Gesteland, 1984). Gal4 encodes a large regulatory protein (881 amino acids) of two galactose induced genes, *Gal1* and *Gal10* in yeast (*Saccharomyces cerevisae*). It was discovered by Guarente and colleagues that Gal4 binds to four specific 17 base pair sequences within DNA sequences, these sites are known as Upstream Activating Sequences (UAS) (Guarente *et al*, 1982). Using this knowledge, Fischer and colleagues went on to demonstrate that Gal4 could be used in *D. melanogaster* to direct expression of a reporter gene under the control of a UAS promoter (Fischer *et al*, 1988; Duffy, 2002; Brand and Perrimon, 1993). Vitally, the Gal4 protein itself appears to have no significant deleterious effects on the *Drosophila* phenotype (Duffy, 2002).

Applying this system to *Drosophila*, it is now possible to express a target gene in any specific tissue of the fly using a designated promoter cloned upstream of the Gal4 protein. A library of such fly stocks is readily available from Bloomingtons stock centre. Cloning a target gene downstream of a series of UAS sites (minimum of 3) will allow specific activation of that gene under the control of the Gal4 driver (Pfeiffer *et al*, 2010).

Initially a transgenic fly containing the target gene under the control of the UAS promoter is generated (see section 4.1.3). These flies are then crossed with flies carrying a Gal4 driver for controlled gene expression, this process is illustrated in Fig 4.1. In the absence of a Gal4 driver,

the target gene will remain silent, although a very low basal level of transcription can occur in some cases.

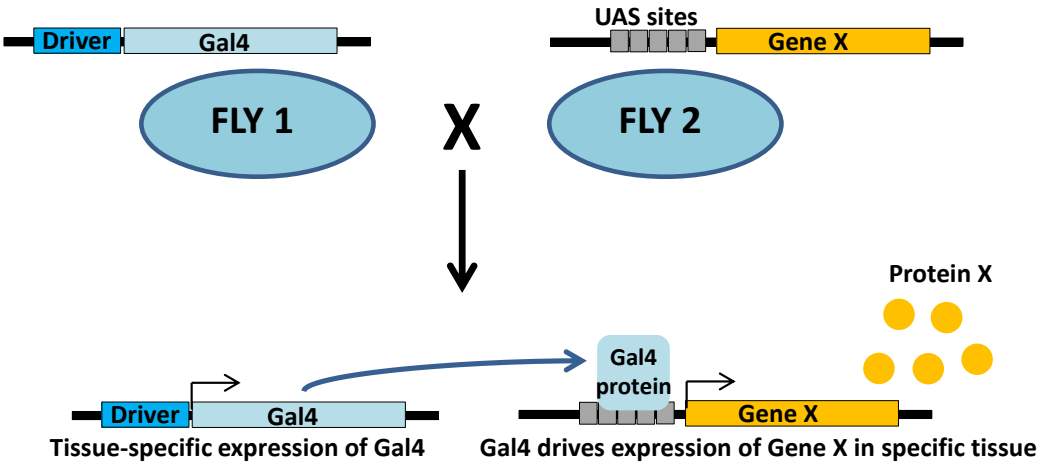

Figure 4.1– Schematic of the Gal4-UAS system, naturally present in yeast and transferred for use in fruit flies following evidence that GAL4 is able to induce transcription in *D. melanogaster* (Fischer *et al*, 1988). Upon production of GAL4 in a tissue of choice designated by the promoter, GAL4 binds to the UAS sites of a target gene, resulting in specific, targeted expression of a protein of interest.

For example, the glass multimer reporter (GMR)-Gal4 driver will promote expression of a protein under the control of the UAS promoter in the photoreceptor cells of the *Drosophila* eye, in all cells posterior to the morphogenetic furrow (Kramer and Staveley, 2003). This driver represents a pentameric repeat of the glass binding site, an enhancer region of the Rhodopsin 1 (Rh1) promoter. However it has been shown to drive a higher level of target protein expression when compared to the natural Rhodopsin-1 promoter, known as *ninaE* (Panneels *et al*, 2011).

4.1.3 Generating transgenic flies

To incorporate transgenes into the *Drosophila* genome, recombination at specific sites can be used. The site specific integrase from Phage ϕC31 mediates recombination between *attB* and *attP* recognition sites and can be used for the generation of transgenic flies (Thorpe *et al*, 1998; Groth *et al*, 2004). Two such transgenic *Drosophila* fly lines, *attP40* and *attP2,* contain an intergenic *attP* site on the third and second chromosome respectively. Endogenous sources of ϕC31 integrase were generated in the flies to circumvent the problems associated with co-injecting integrases, and thus raising the transformation efficiency (Bateman *et al*, 2006, Markstein *et al*, 2008). *pUAST-attB* is a vector containing an *attB* recognition site that allows it

to be recombined into the specific *attP* site in the fly genome, integrating the cloned transgene into *Drosophila* under control of 5 *UAS* sites. In addition, the vector contains a *white* gene which enables visual selection of flies with the specific, targeted transgene. This gene is responsible for restoring the orange eye colour in the white eyed *attP2* and *attP40* fly lines (Bischof *et al*, 2007) thus transgenic flies can be selected based on eye colour.

4.1.4 Expression of proteins in the *Drosophila* eye

The visual system of *Drosophila melanogaster* is incredibly complex; each photoreceptor cell contains a specialised membrane system that has evolved to hold millions of molecules of rhodopsin, the light-absorbing visual protein of the eye (Zuker *et al,* 1996). The compound eye is made up of approximately 800 unit eyes, termed ommatidia (Pichaud and Desplan, 2001), each of which holds 8 photoreceptor cells (R1-R8) (Fig 4.2 A).

Photoreceptor cells consist of a main cell body and a membranous structure, the rhabdomere, that is approximately 100 µM in length and is made up of a brush of roughly 60,000 tightly folded microvilli (Fig 4.2 B/C) (Kumar and Ready, 1995). Each microvillus is around 60 nm wide and 1-2 µM in length generating a huge surface area of approximately 3.6 – 7.2 m^2 membrane per cell (Hardie and Raghu, 2001).

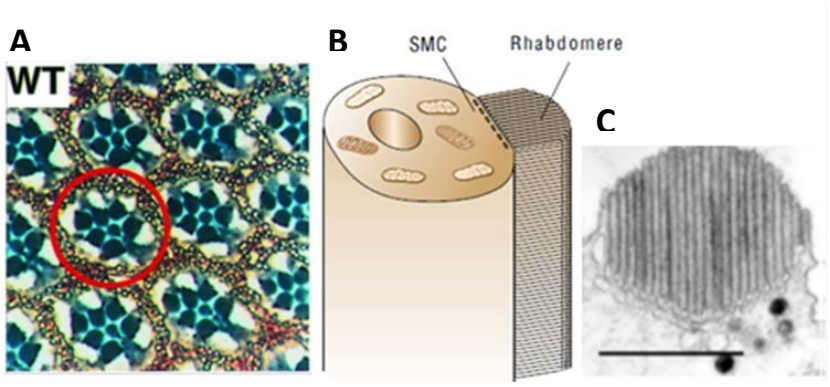

Figure 4.2 – The *Drosophila* visual system. (A) Section through adult eye. Individual photoreceptor cells (7 visible) within ommatidia in the eye can be distinguished from their dark circular rhabdomeres [Freeman, 2002– reprinted with permission from Wiley]. (B) Diagram of an individual photoreceptor cell showing the position of the rhabdomere. SMC = submicrovillar cistaernae [Hardie and Raghu, 2001]. (C) Scanning electron micrograph of a single rhabdomere organised into tightly packed tubular microvilli. Each microvillus is approximately 60 nm in diameter and 1-2 µm long. Fig 4.2B/C reprinted by permission from Macmillan Publishers Ltd: [Nature] (Hardie and Raghu), copyright (2001).

The photoreceptor cell subtypes (R1-R8) in *Drosophila* express different isoforms of rhodopsin. R1-R6 express only Rhodopsin 1 (Rh1), encoded by *ninaE*, the dominant form of rhodopsin that absorbs blue light. R7 cells express either Rh3 or Rh4 which are UV light absorbing molecules. R8 cells express either Rh5 or Rh6 which absorb blue and green light respectively (Earl and Britt, 2006). All rhodopsin isoforms are first expressed during pupal development relatively close together in time, with the onset of rhodopsin 1 expression occurring first, shortly followed by that of rhodopsin 3, 4 and 5 concurrently. Rhodopsin 6 is the last to be expressed, shortly after Rh3, Rh4 and Rh5 (Earl and Britt, 2006).

In *Drosophila melanogaster*, phototransduction involves a G-protein-coupled phosphoinositide pathway. Rhodopsin is converted to metarhodopsin upon photoisomerisation, activating heteromeric Gq protein and releasing the Gqα subunit by GTP-GDP exchange. The Gqα subunit subsequently activates phospholipase C resulting in the hydrolysis of PIP_2 to IP_3 and DAG. The increase in DAG or the reduction in PIP_2 levels has been hypothesised to lead to activation of the light sensitive channels, TRP and TRPL (Hardie, 2001).

The membranous structure of the fly compound eye, the rhabdomere, has been exploited to exogenously express a number of different membrane proteins, with the aim of overcoming some of the problems faced with low membrane protein yields using conventional expression systems. Panneels and colleagues trialled expression of ten different membrane proteins representing 3 important classes of membrane proteins (GPCRs, transporters and channels) in the compound eyes of *Drosophila* (see Table 4.1). Their results revealed the large capacity of the photoreceptor cells to express high levels of membrane protein, with expression levels of some targets nearing the natural levels of rhodopsin. The level of rhodopsin expressed in the membrane stacks was unaffected by the expression of other proteins. The resulting yield varied from 0.2 – 0.4 mg of purified membrane protein per 10,000 flies. Furthermore this system provided a more homogeneous population of protein when compared to insect cell expression, ideal for crystallisation and structural studies (Panneels *et al*, 2010; Panneels *et al*, 2011).

Table 4.1 – Expression levels of membrane proteins in the *Drosophila* eye. The specific protein and species are shown in column 1; the protein family each protein belongs to is shown in column 2. The expression level of each protein is shown in column 3. Rhodopsin 1 (endogenous) represents naturally expressed rhodopsin in the eye. Rhodopsin 1 (*Drosophila*) represent exogenously expressed recombinant GFP-fused rhodopsin-1. MP = membrane protein (Panneels and Sinning, 2010).

Membrane protein	Protein family	Expression level [pmol/mg total MP]
Rhodopsin-1 (Endogenous)	GPCR	272-544
Rhodopsin-1 (*Drosophila*)	GPCR	502
V2R (Human vasopressin receptor)	GPCR	>1000
CCR5 (Human chemokine receptor)	GPCR	555
DmGluRA (Drosophila glutamate receptor)	GPCR	226
mGluR5 (rat glutamate receptor)	GPCR	192
ChR2 (*Clamydomonas* channelrhodopsin)	Channel	206
SERT (*Drosophila* serotonin receptor)	Transporter	493
SERT (Human serotonin receptor)	Transporter	220
EAAT2 (Human glutamate transporter)	Transporter	173
EAAT1 (*Drosophila* glutamate receptor)	Transporter	716

4.1.5 Protein glycosylation in insects

Glycosylation of proteins in insects differs significantly from that in vertebrates. In vertebrates, there are three species of N-glycosylated proteins; (1) non-glycosylated proteins, (2) core, high mannose glycosylated proteins and (3) complex glycosylated proteins that have undergone further modifications in the Golgi (Freeman, 2000) (see introduction section 1.2.2 for more details). Correct glycosylation of membrane proteins is often essential for membrane targeting and function. However, in insects, complex glycosylation is a very rare event with the majority of N-glycosylated proteins existing as core glycosylated forms (Rendic *et al*, 2008). This may

affect the expression profile of membrane proteins expressed in *Drosophila melanogaster*. However, complex glycosylation of proteins can cause problems for crystallisation of proteins and structure determination due to the heterogeneity of the protein sample. Consequently if the protein is functional and targeted to the membrane in *Drosophila,* the lack of glycosylation may be advantageous for purification and structure determination (see section 1.2.2.4).

4.1.6 Aims of this chapter

In this chapter I aimed to express a number of membrane protein constructs in the *Drosophila* eye, to achieve a high yield of homogeneous, functional protein for purification and structural studies. rP2X2-GFP, hP2X4-GFP and rPanx1-GFP constructs were expressed in the *Drosophila* eye, which does not naturally express any P2X receptors or Panx channels, and proteins were purified using a number of different techniques including ion exchange chromatography, nickel affinity chromatography and immunoprecipitation. In addition the glycosylation and oligomeric state of these proteins was investigated using deglycosylation assays and size exclusion chromatography.

4.2 Chapter 4 results

4.2.1 Expression of membrane protein constructs in the fly eye

A fly line expressing *UAS*-eGFP (obtained from Bloomingtons stock centre) was crossed with a *GMR*-Gal4 driver fly line and a *Rh1*-Gal4 driver fly line to compare the ability of each driver to express high levels of GFP in the *Drosophila* eye. Visualisation of the fly eye under fluorescent conditions (using U-M401001 filter) showed that the *GMR-Gal4* driver promoted a higher level of expression of eGFP in the eye compared with the *Rh1-Gal4* driver (Fig 4.3) and hence *GMR-Gal4* was used for expression of all membrane protein constructs in the following experiments.

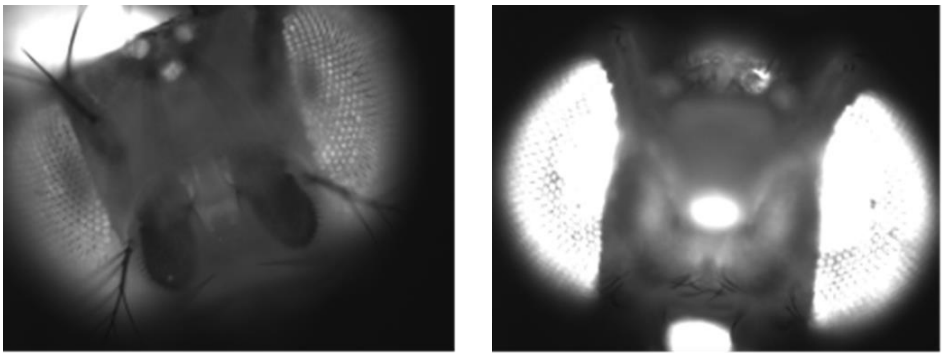

Figure 4.3 – *GMR-Gal4* drives a higher level of eGFP expression in the eye than *Rh1-Gal4*. (A) *UAS*-eGFP expressed under control of the *Rh1-Gal4* driver. (B) *UAS*-eGFP expressed under control of the *GMR-Gal4* driver. Fly heads visualised under fluorescent conditions.

To ensure that all the membrane protein was efficiently separated from the cytoplasmic protein during membrane protein extraction from flies, membrane and cytoplasmic protein fractions were blotted for rhodopsin (membrane protein) and β-actin (cytoplasmic protein). Membrane protein fractions were shown to contain rhodopsin but not β-actin. Additionally cytoplasmic fractions were shown to contain β-actin and not rhodopsin, indicating that the membrane protein extraction method is working correctly (Fig 4.4).

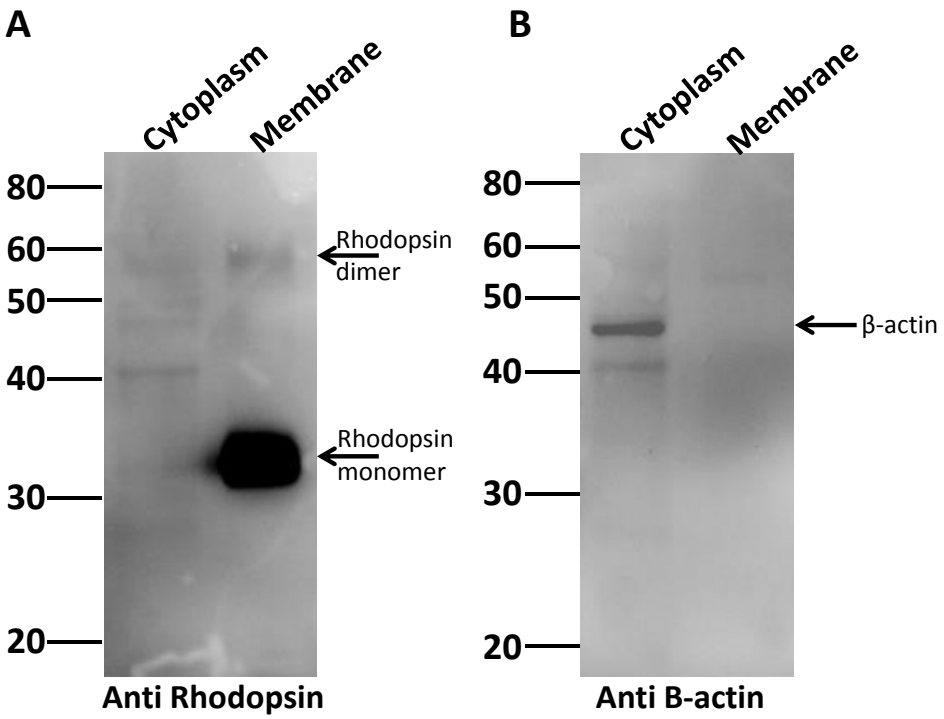

Figure 4.4 – Membrane and cytoplasmic protein fractions were efficiently separated after protein extraction from fly heads. Protein preps were made from 200 control fly heads and membranes were separated from cytoplasmic proteins by high-speed centrifugation. Western blots were performed using the cytoplasmic and membrane protein fractions with (A) anti-rhodopsin [DSHB] and (B) anti-β-actin [abcam].

Initially, transgenic flies expressing UAS-hP2X4::His (hP2X4-His) on the second chromosome (attP40 landing site) were generated and crossed with *GMR-Gal4* (BL8121) flies. However, very little or no protein expression was observed using either anti-His or anti-P2X4 antibodies (results not shown). It was then decided to couple constructs to eGFP for ease of detection, and to extend the study to other ion channels – flies expressing UAS-hP2X4::GFP (hP2X4-GFP), UAS-rP2X2::GFP (rP2X2-GFP) and UAS-rPanx1::GFP (rPanx1-GFP) transgenes on the second chromosome (attP40 landing site) were subsequently generated and crossed with *GMR-Gal4* (BL8121) flies. Membrane protein was extracted from approximately 200 progeny fly heads and western blotting was used to detect expression of the protein constructs in the fly. rP2X2-GFP (approx. 80 – 85 kDa) and rPanx1-GFP (approx. 65 – 70 kDa) were successfully expressed (Fig 4.5E). These GFP fusion proteins were also visualised in the eye using fluorescence microscopy (Fig 4.5 B/D). However, in confirmation of the previous negative result with hP2X4-His, hP2X4-GFP did not appear to be expressed in the fly under the control of *GMR*-Gal4 (Fig 4.5E). The effect of fly maintenance temperature and the number of copies of each transgene was also investigated. The data showed that a higher protein expression level was obtained

from rP2X2-GFP flies with 2 copies of both the rP2X2-GFP transgene and the GMR-Gal4 driver. In addition, the temperature at which the flies were maintained did not appear to have a large effect on protein expression levels (Fig 4.5F).

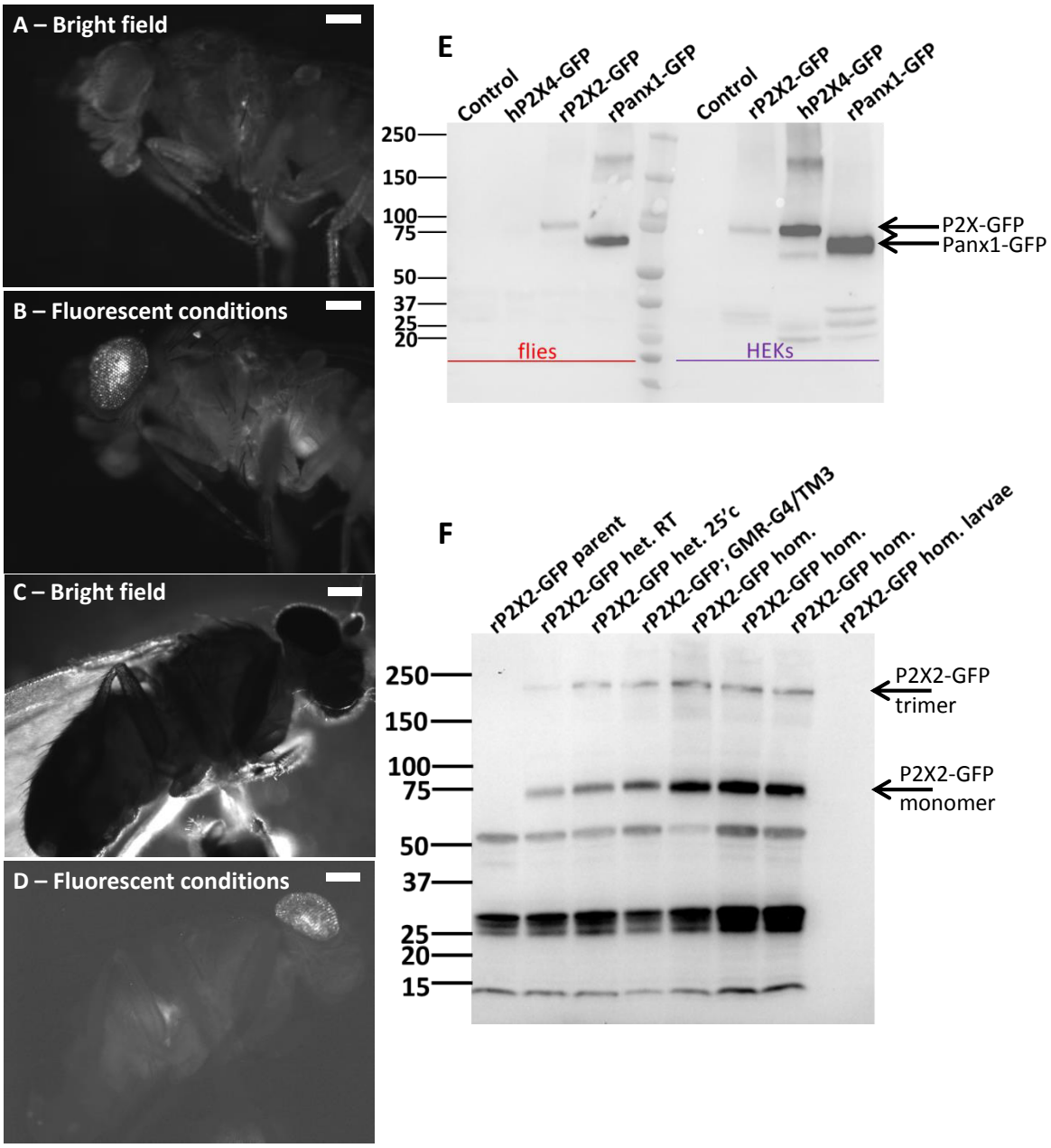

Figure 4.5 – rP2X2-GFP and rPanx1-GFP were successfully expressed in the *Drosophila* eye. rPanx1-GFP expressed in the fly eye under the control of the *GMR-Gal4* driver visualised under bright field conditions (A) and fluorescent conditions (B). rP2X2-GFP expressed in the fly eye under the control of the *GMR-Gal4 driver* visualised under bright field conditions (C) and fluorescent conditions (D). Scale bars = 200 µm. (E) Western blot of protein extracted from control flies and flies expressing hP2X4-GFP, rP2X2-GFP and rPanx1-GFP under control of the GMR-Gal4 driver (lanes 1 – 4) and transfected HEK cells appropriately (lanes 6 – 9) [anti GFP, Invitrogen]. 10 µg membrane protein loaded per lane. (F) Western blot of protein extracted from flies of various genotypes [anti P2X2, Alomone]; 'rP2X2-GFP parent' has copy of the rP2X2-GFP transgene but no driver to induce expression. 'rP2X2-GFP het.' has one copy of the rP2X2-GFP transgene and the driver. 'rP2X2-GFP; GMR-G4/TM3' flies are homozygous for the rP2X2-GFP transgene but only possess one copy of the Gal4 driver. 'rP2X2-GFP hom' flies are homozygous for both the rP2X2-GFP transgene and the Gal4 driver. RT (room temperature) or 25°c indicates the temperature at which the flies were raised. Lower molecular weight bands are assumed to be non-specific bands. 10 µg membrane protein loaded per lane.

To confirm the presence of the transcript and message for hP2X4-His and hP2X4-GFP in flies that did not appear to express protein, total DNA and RNA were extracted from *hP2X4* parent flies, w; *hP2X4; GMR-Gal4* flies, *hP2X4-GFP* parent flies and w; *hP2X4-GFP; GMR-Gal4* flies. Specific primers were used to amplify the *hP2X4* and *hP2X4-GFP* constructs from the DNA using PCR. In addition these primers were used on a cDNA prep made from the RNA extracts. The results showed that the *hP2X4* DNA was present in both parent flies and flies also carrying a *GMR*-Gal4 driver (although bands are faint in DNA preps made from *hP2X4-GFP* parent flies and *hP2X4-GFP; GMR-Gal4* flies due to poor quality DNA). In addition the *hP2X4* RNA was present in w;*hP2X4-his; GMR-Gal4* and w;*hP2X4-GFP; GMR-Gal4* flies. LUSH primers (responsible for amplifying a housekeeping gene, *LUSH*) were used as a control to ensure sufficient RNA extraction and cDNA preparation. *hP2X4* and *hP2X4-GFP* vector controls were also included to confirm that the PCR reaction took place and the primers were able to amplify the DNA (Fig 4.6). These results show that the DNA and mRNA are successfully made in the fly lines containing a Gal4 driver, therefore the problems underlying the low expression levels are downstream i.e. during or after protein synthesis.

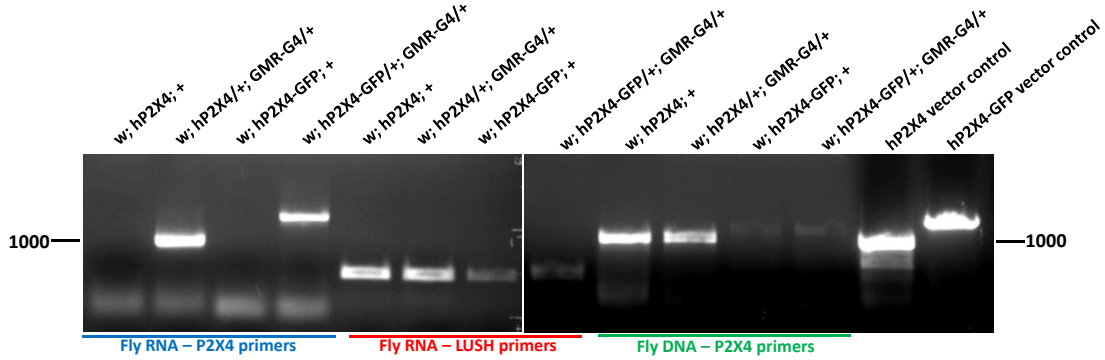

Figure 4.6 – *P2X4* RNA is made in *hP2X4-his; GMR-Gal4* and *hP2X4-GFP; GMR-Gal4* flies. PCR of *hP2X4-his* and *hP2X4-GFP* from cDNA preps made from parent flies (*w; hP2X4; +* and *w; hP2X4-GFP; +* respectively) which possess the *hP2X4* transgene but no driver to induce expression and flies expressing hP2X4 and hP2X4-GFP under control of the GMR-Gal4 driver (*w; hP2X4/+; GMR-G4/+* and *w; hP2X4-GFP/+; GMR-Gal4/+* respectively) (underlined in blue). PCR of housekeeping *LUSH* gene from cDNA prep of the same fly lines (underlined in red). PCR of *hP2X4-his and hP2X4-GFP f*rom the same fly line (underlined in green). Vector controls were also included to confirm working PCR conditions (Lane 13 and 14).

DDM has been shown to work well for the solubilisation of several P2X receptors (Sim *et* al, 2004; Mio *et al*, 2005; Mio *et al*, 2009; Kawate *et al*, 2009; Valente *et al*, 2011), thus this detergent was chosen for the solubilisation of rP2X2-GFP. To determine which was the most efficient detergent to use for solubilisation of rPanx1-GFP, a detergent screen was used to compare a number of different detergents; DDM, FC-12, NP40 (nonyl phenoxypolyethoxylethanol), N-OG (N-octyl glucosmine) and Triton (Triton-X-100), for protein extracted from both HEK-293 cells and flies. The screen showed that FC-12 and Triton were efficient at solubilising protein from both HEK-293 cells and *Drosophila,* whereas DDM and N-OG were less efficient at solubilising protein extracted from flies compared with HEK-293 cells. NP40 was inefficient at solubilising proteins from both flies and HEK-293 cells (Fig 4.7). FC-12 was used in all experiments for the solubilisation of rPanx1-GFP. Triton was not chosen for solubilisation due to its heterogeneous nature.

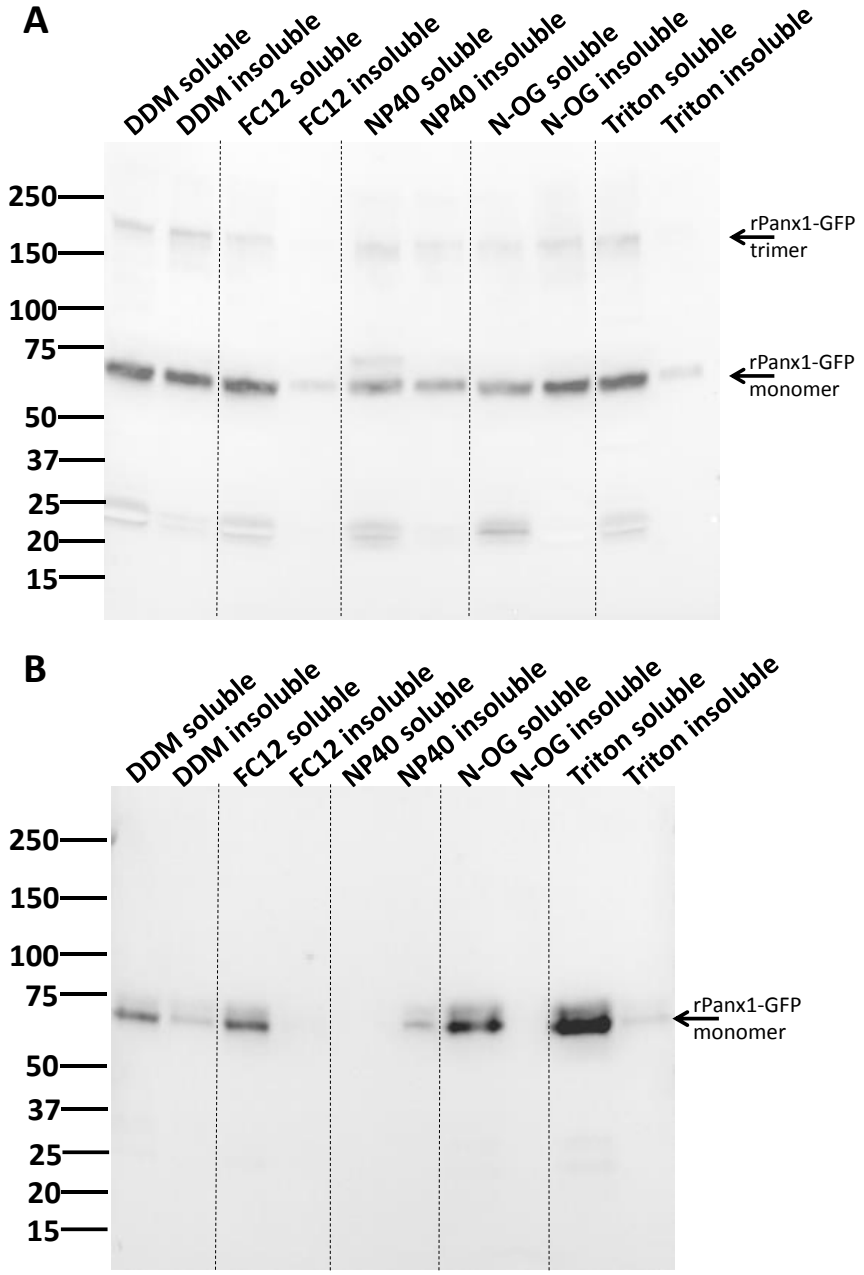

Figure 4.7 – Detergent screen for rPanx1-GFP. (A) Western blot of rPanx1-GFP extracted from HEK-293 cells and solubilised in various detergents [anti-GFP, Invitrogen]. For each detergent, protein was extracted from a 35 mm dish of cells and solubilised in RIPA buffer plus appropriate detergent. The insoluble pellet was resuspended RIPA buffer and the soluble supernatant fraction was collected. 10 µg protein was loaded in each lane. (B) Western blot of rPanx1-GFP extracted from *Drosophila* and solubilised in various detergents [anti GFP, Invitrogen]. For each detergent, membrane protein was extracted from 200 flies and solubilised in sucrose buffer. The insoluble pellet was resuspended in sucrose buffer and the soluble supernatant fraction was collected. Protein from the equivalent of ten flies was loaded in each lane. Detergent concentrations used – 1% DDM, 7.5mM FC12, 1% NP40, 1% N-OG, 1% Triton.

4.2.2 Glycosylation of rP2X2-GFP and rPanx1-GFP in *Drosophila*

The N-glycosylation state of rP2X2-GFP and rPanx1-GFP was investigated by incubating the proteins with Endo-H and PNGase F and investigating any changes in molecular weight. rPanx1-GFP did not undergo cleavage by either Endo-H or PNGase F suggesting it was not N-glycosylated in the fly. However, a reduction in the molecular weight of rP2X2-GFP following incubation with Endo H was observed suggesting it underwent high mannose glycosylation in the fly. However, as expected, neither protein underwent complex glycosylation in this system (Fig 4.8).

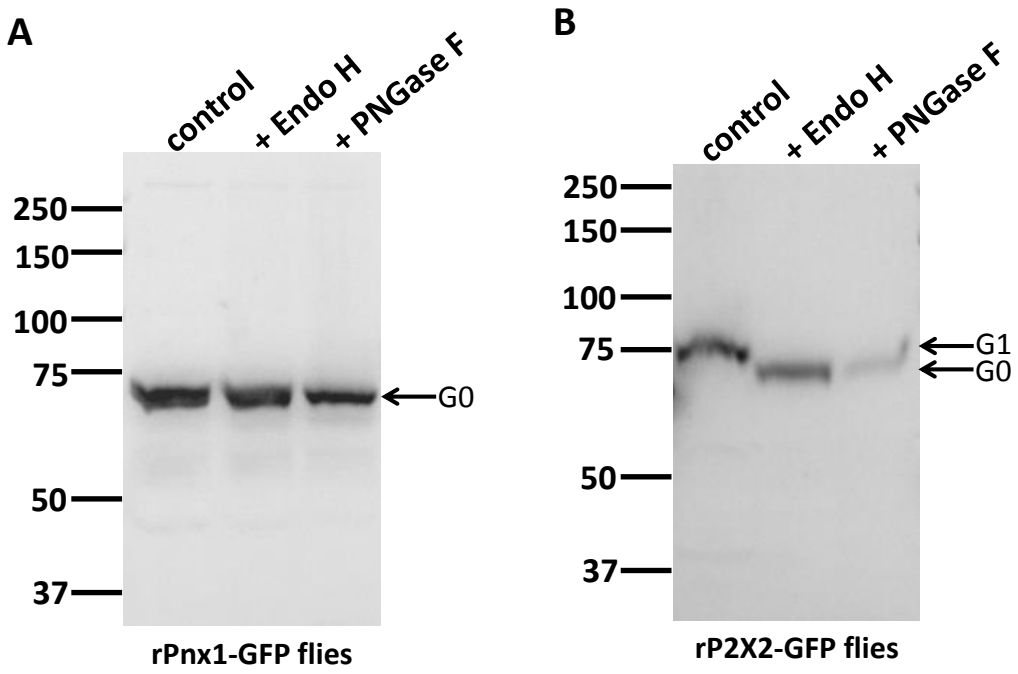

Figure 4.8 – N-linked glycosylation of rPanx1-GFP and rP2X2-GFP in *Drosophila*. (A) Western blot showing rPanx1-GFP extracted from *Drosophila* before (control) and after incubation with Endo H or PNGase F [anti-GFP, Invitrogen]. No decrease in molecular weight was observed indicating the protein is not glycosylated. Blot representative of 2 assays. (B) Western blot showing rP2X2-GFP extracted from *Drosophila* before (control) and after incubation with Endo H or PNGase F [anti-GFP, Invitrogen]. A reduction in the molecular weight of rP2X2-GFP following cleavage by Endo H is observed indicating high mannose glycosylation in *Drosophila.* Blot representative of 3 assays. G0 relates to the non-glycosylated protein, G1 relates to high-mannose glycosylated protein.

4.2.3 Purification of membrane proteins expressed in fly eyes

For small scale purification trials, membrane protein was extracted and purified from approximately 150 - 200 w; *rP2X2-GFP; GMR-Gal4* and w; *rPanx1-GFP; GMR-Gal4* flies using nickel affinity purification. Western blotting with an anti-GFP antibody demonstrated that both proteins successfully bound to nickel beads with no/very little protein remaining in the flowthrough/unbound fraction. Some of the rP2X2-GFP protein was successfully eluted with 500mM Imidazole; however a large proportion remained bound to the nickel beads (Fig 4.9A). The majority of rPanx1-GFP protein was successfully eluted with 500 mM Imidazole (Fig 4.9B).

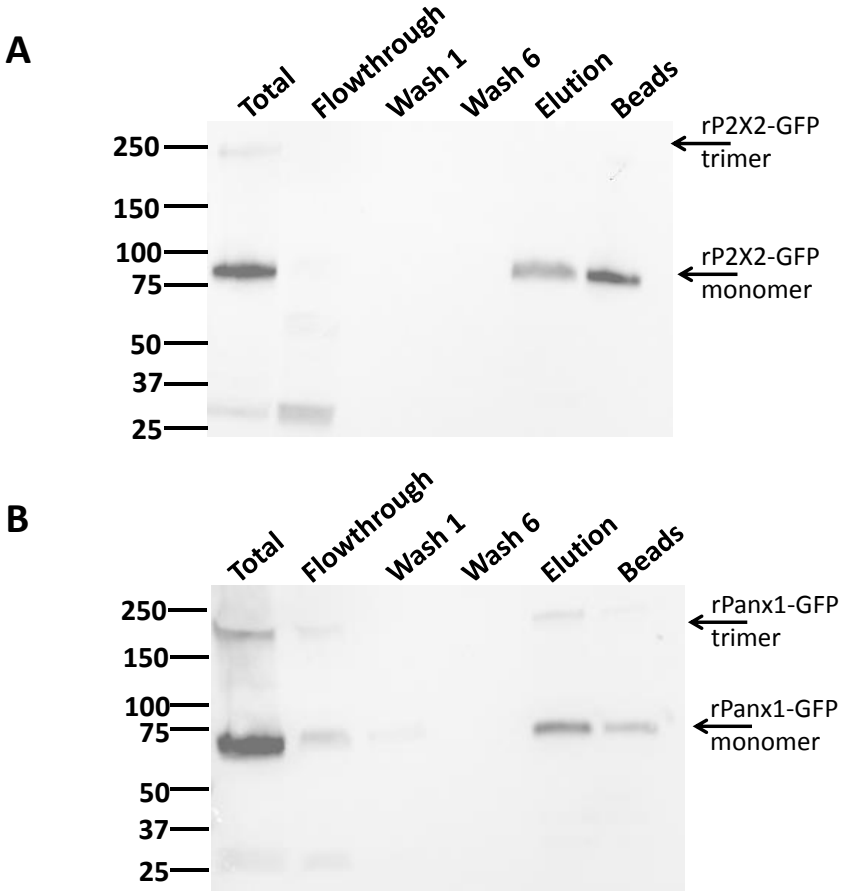

Figure 4.9 – Nickel affinity purification of rP2X2-GFP and rPanx1-GFP (200 flies). (A) Western blot showing nickel affinity purification of rP2X2-GFP from approx. 200 fly heads [anti-GFP, Invitrogen]. (B) Western blot showing nickel affinity purification of rPanx1-GFP from approx. 150 fly heads [anti-GFP, Invitrogen]. The equivalent of membrane protein from ten flies is loaded per lane. Total = Total protein from initial membrane protein extraction, Flowthrough = protein which didn't bind to nickel beads, Wash 1/6 = flowthrough after beads were washed with wash buffer, elution = protein eluted with 500 mM Imidazole, Beads = protein remaining stuck to beads after elution.

Purification of rPanx1-GFP was then performed on a larger scale; membrane protein was extracted from approximately 2,000 w; *rPanx1-GFP; GMR-Gal4* fly heads and purified using nickel affinity chromatography. As shown in Figure 4.10A, the majority of the protein successfully bound to nickel beads but a large amount was not eluted with 1M imidazole and remained bound to the nickel beads. In addition, a Coomassie-stained gel showed that large numbers of other proteins were also present in the elution, indicating that the purified protein fraction contained many contaminating proteins. In addition a band was not observed at 65 – 70 kDa, the molecular weight of pure rPanx1-GFP (Fig 4.10B).

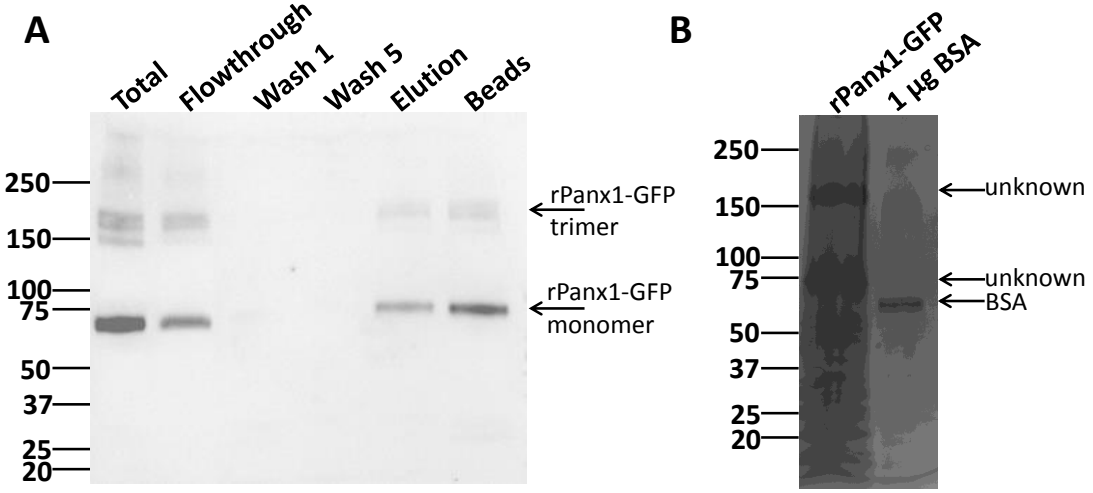

Figure 4.10 – Nickel affinity purification of rPanx1-GFP (2,000 flies) (A) Western blot showing nickel affinity purification of rPanx1-GFP extracted from approx. 2,000 fly heads [anti GFP, Invitrogen]. Protein from equivalent 10 heads loaded per lane. (B) Coomassie-stained gel of elution fraction following nickel affinity purification of rPanx1-GFP (approx. 500 fly heads loaded). 1 µg BSA control is shown for reference.

To try and improve the purity of the protein extracted from flies, alternative purification strategies were attempted. The next approach, in this case in an attempt to purify rP2X2-GFP from flies, was immunoprecipitation using a GFP antibody. Membrane protein was extracted from 1,800 w; *rP2X2-GFP; GMR-Gal4* fly heads and incubated with the GFP antibody [Invitrogen]. The protein-antibody complexes were then captured using protein A/G agarose resin. The purified protein was denatured and separated by SDS-PAGE, blotted with an anti-GFP antibody (Fig 4.11A) and stained with Coomassie (Fig 4.11B). A faint band was observed at approximately 80 kDa that was assumed to be purified rP2X2-GFP. Additional bands were observed at 25kDa and 50kDa representing the light and heavy chains of the immunoglobulin respectively (Fig 4.11). Although the protein elution following immunoprecipitation appeared relatively pure, the yield was low (1 µg BSA can be used for reference). The detection limit of the Coomassie stain used was approximately 100 ng and since the band was very faint, the

band appeared to be close to this limit, we estimated that 500 fly heads equated to approximately 100 ng pure protein (Fig 4.11). Immunoprecipitation experiments were performed by Hannah Garrard.

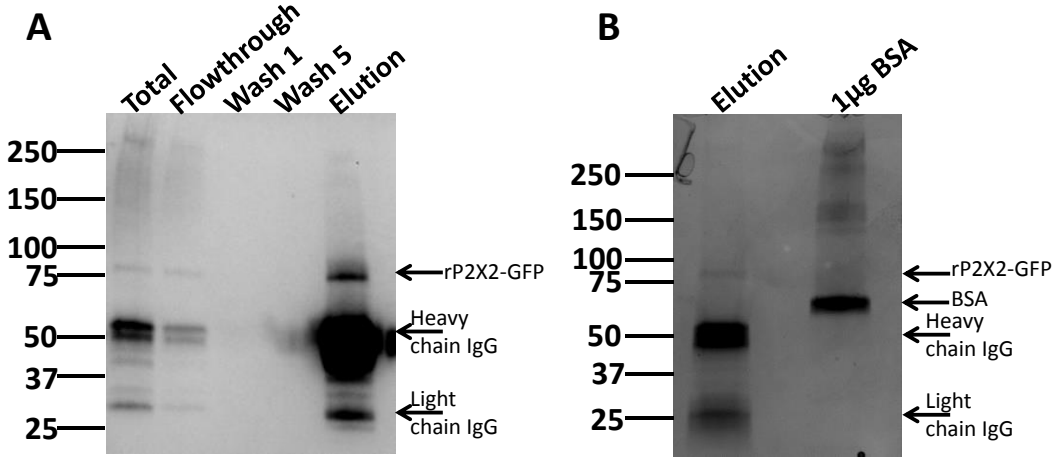

Figure 4.11 – Immunoprecipitation of rP2X2-GFP. Membrane protein was extracted from 1,800 *rP2X2- GFP; GMR-Gal4* fly heads and purified using immunoprecipitation with a P2X2 antibody [Alomone, 1:2000]. (A) Western blot of IP fractions [anti-GFP, Invitrogen]. Equivalent 10 fly heads loaded per lane, 50 fly heads loaded in elution (accounts for higher expression levels). (B) Coomassie-stained gel – purified protein from approximately 500 fly heads [Elution], 1 µg BSA is shown for reference (data - Hannah Garrard).

To distinguish between the possibilities that (1) the yield of protein expressed in the fly was low or (2) a large amount of the protein was lost during the immunoprecipitation procedure, further purification procedures were investigated. Membrane protein was extracted from 1,800 fly heads and purified using the GFP-TRAP system [Chromotek] for both rP2X2-GFP and rPanx1-GFP (Fig 4.12). However, the protein constructs did not bind to the GFP-TRAP beads (all protein was found in the flow-through fraction) and the purification was unsuccessful.

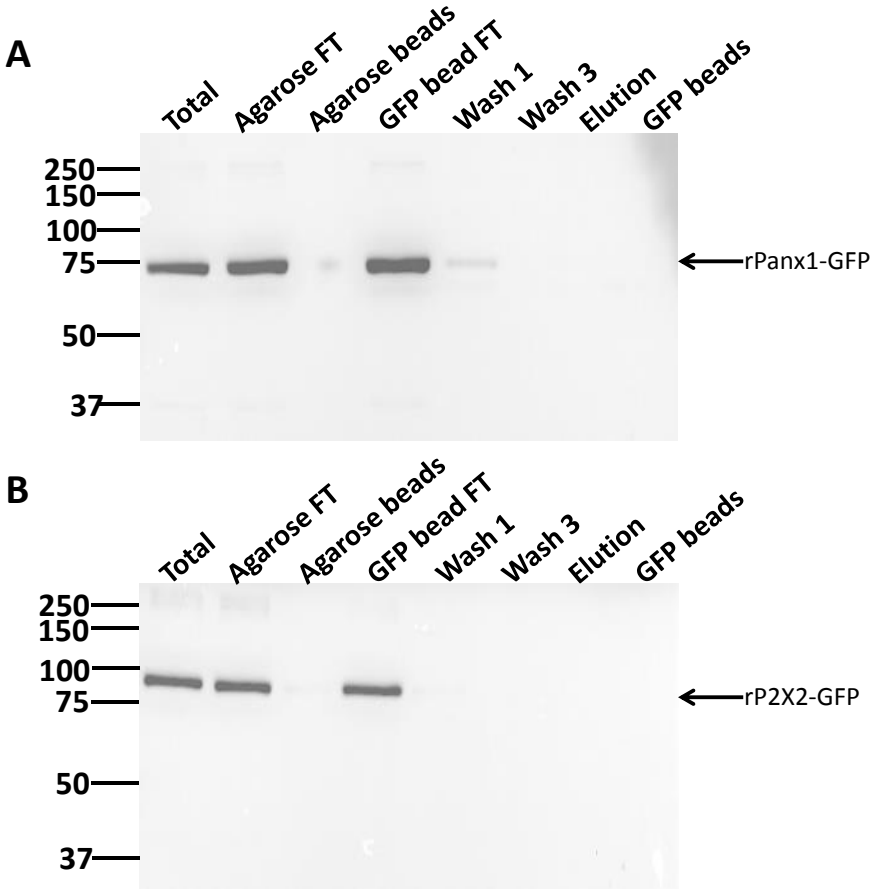

Figure 4.12 – GFP TRAP of rPanx1-GFP and rP2X2-GFP. Western blots of rPanx1-GFP (A) and rP2X2-GFP (B) protein fractions from *Drosophila* after GFP TRAP purification [Chromotek] [anti GFP, Invitrogen]. Membrane protein from w; *rPanx1-GFP; GMR-Gal4 flies* (A) and *w; rP2X2-GFP; GMR-Gal4* flies (B) was extracted from 1,800 fly heads and incubated with GFP-TRAP beads. Agarose FT = protein which didn't bind to control agarose beads. Agarose beads = protein bound to agarose beads. GFP beads FT = protein which didn't bind to GFP beads. Elution = protein eluted from GFP-TRAP beads GFP beads = protein remaining on beads after elution.

Reverting to the use of nickel affinity chromatography, membrane proteins were first bound to sepharose beads to eliminate any proteins binding non-specifically to the agarose bead itself (pre-clearance). Membrane protein was extracted from 500 w; *rP2X2-GFP; GMR-Gal4* fly heads and incubated with sepharose beads for 3 hours. The flowthrough from sepharose beads was used for nickel affinity chromatography. The majority of the protein successfully bound to nickel beads and was eluted upon addition of 1M imidazole (Fig 4.13A). However the purified fraction still contained high numbers of non-specific proteins (Fig 4.13B).

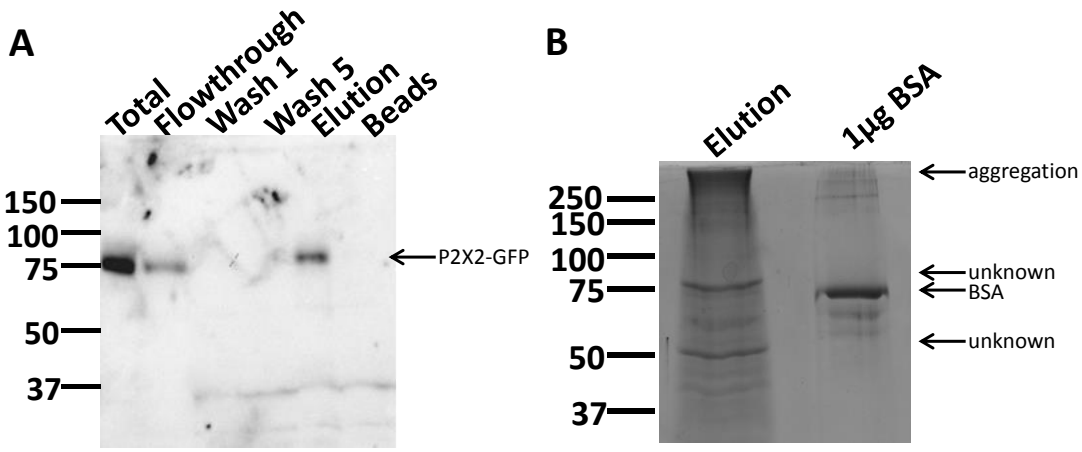

Figure 4.13 – Sepharose bead and nickel bead purification of rP2X2-GFP. (A) Western blot showing sepharose and nickel bead purification fractions from 500 w; *rP2X2-GFP; GMR-Gal4* flies (anti GFP, Invitrogen). 10 fly heads loaded per lane. (B) Coomassie-stained gel – 200 fly heads of purified protein loaded [elution], 1 µg BSA is shown for reference.

To further purify the protein, ion exchange chromatography was used as a pre-purification step before proceeding with sepharose bead and nickel bead purification. Membrane proteins were extracted from 5,000 w; *rPanx1-GFP; GMR-Gal4* fly heads and were separated using anion exchange chromatography. rPanx1-GFP was eluted from fraction 12 onwards and the majority was eluted in fractions 12 – 16. These fractions were collected and pooled (Fig 4.14A). The pooled protein was incubated with sepharose beads and the flowthrough was purified using nickel affinity chromatography. The protein successfully bound to the nickel beads and was eluted with 1M imidazole (Fig 4.14B). Protein from the equivalent of 500 fly heads and 1000 fly heads was run on a gel and stained with Coomassie. The protein was relatively pure with 2 bands at approximately 70 kDa and 160 – 200 kDa (Fig 4.14D). The purified protein was separated using fluorescence size exclusion chromatography to assess the oligomeric state of the protein. Two peaks were observed at approximately 17 kDa and 156 kDa (Fig 4.14E)

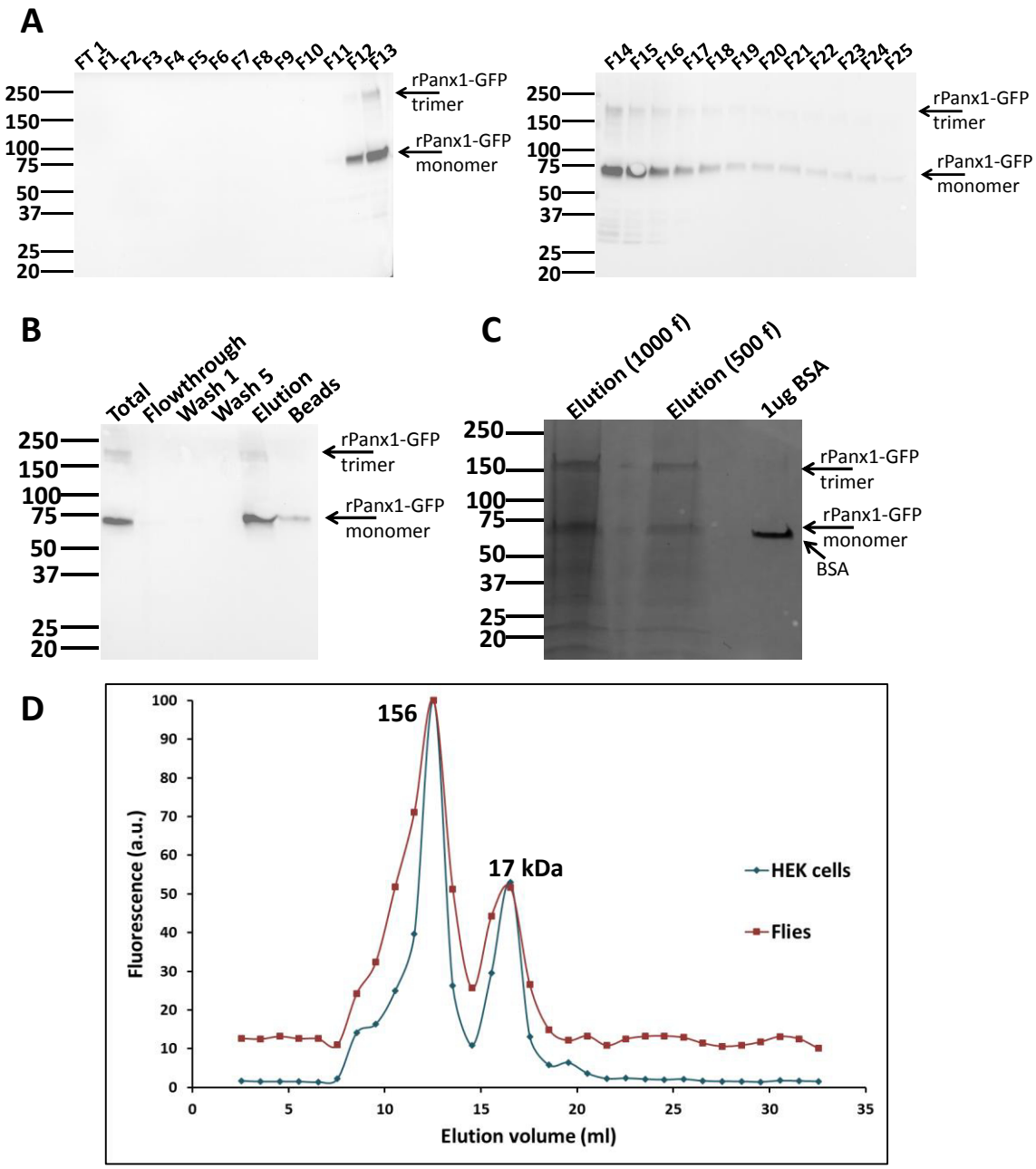

Figure 4.14 – Ion exchange chromatography, sepharose bead and nickel bead purification of rPanx1-GFP. (A) Western blot of rPanx1-GFP fractions which were separated using anion exchange chromatography [anti GFP, Invitrogen]. FT = flowthrough, F = fraction. 20 fly heads of protein loaded per lane. (B) Western blot showing sepharose bead and nickel affinity purification of fractions 12 – 16 [anti-GFP, Invitrogen]. 10 fly heads of protein loaded per lane. (C) Coomassie gel of purified rPanx1-GFP protein (Elution). The number of fly heads of protein loaded is shown above the lane. A 1 µg BSA sample is shown for reference. (D) FSEC elution profile of purified rPanx1-GFP from 5,000 flies (red). Two peaks are observed at fraction 11 and fraction 15 which correspond to molecular weights of approximately 156 kDa and 17 kDa respectively. The FSEC trace previously shown for purification of rPanx1-GFP from HEK-293 cells is shown in blue.

The expression levels of rP2X2-GFP were compared in protein extracts from w; *rP2X2-GFP; GMR-Gal4,* and *C155-Gal4; rP2X2-GFP* whole flies that express rP2X2 in the nervous system under control of *C155,* an enhancer trap line that expresses Gal4 under control of the *elav* promoter via the *P{w+=GawB}elav^{C155}* transgene (Lin and Goodman, 1994). The *elav* (*embryonic lethal abnormal visual system*) functions in nervous system development and maintenance. (Campos *et al* ,1985, 1987). The western blot shows that per fly, the amount of rP2X2-GFP protein is higher in flies when expressed under control of the pan-neural driver (Fig 4.15). Therefore for the final purification experiment of rP2X2-GFP, *C155; rP2X2-GFP* flies were used.

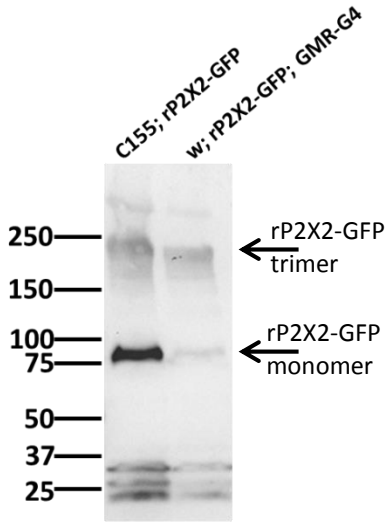

Figure 4.15 – *C155-Gal4* drives a higher level of rP2X2-GFP expression than *GMR*-Gal4. Western blot comparing expression of rP2X2-GFP under the control of the pan neural (C155-Gal4) driver and eye (GMR-Gal4) driver [anti GFP, Invitrogen]. 10 flies loaded per lane. Blot representative of 3 assays.

Membrane protein was extracted from 2,400 *C155; rP2X2-GFP* whole flies and purified using anion exchange chromatography, sepharose and nickel affinity purification as previously described for rPanx1-GFP. During ion exchange chromatography, the protein was eluted in fractions 12 to 21 with the majority in fractions 13 to 17 (Fig 4.16A). Thus fractions 13 – 17 were pooled and further purified. Although the protein successfully bound to nickel beads and was efficiently eluted with 1M imidazole, the Coomassie-stained gel (not shown) contained a very high number of impurities suggesting the purification was unsuccessful. As a result, purification experiments with *C155; rP2X2-GFP* flies were not continued.

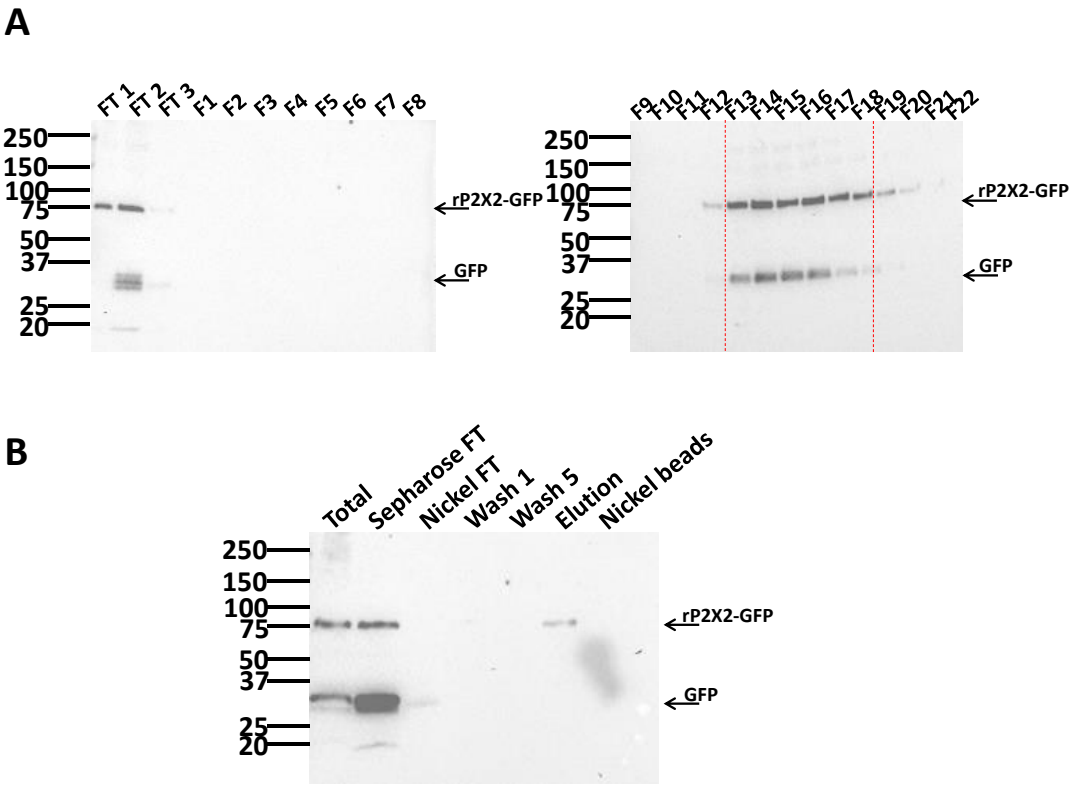

Figure 4.16 – Ion exchange chromatography, sepharose bead and nickel bead purification of rP2X2-GFP. (A) Western blot of rP2X2-GFP fractions which were separated using anion exchange chromatography [anti GFP, Invitrogen]. FT = flowthrough, F = fraction. Protein from equivalent of 20 flies loaded per lane. (B) Western blot showing further purification of rP2X2-GFP by sepharose bead and nickel affinity purification of fractions 13 – 17 [anti-GFP, Invitrogen]. 10 fly heads of protein loaded per lane.

4.2.4 Electron microscopy of rPanx1-GFP

The purified rPanx1-GFP was visualised using transmission electron microscopy. The yield of protein was low but the protein particles on the grid appeared to be relatively homogeneous (Fig 4.17). Due to time constraints, it was not possible to do extensive analysis of the particles and thus symmetry of the particles was not investigated. However by measuring the cross-sections of 100 particles and making a number of assumptions, the estimated mass of the particles was determined.

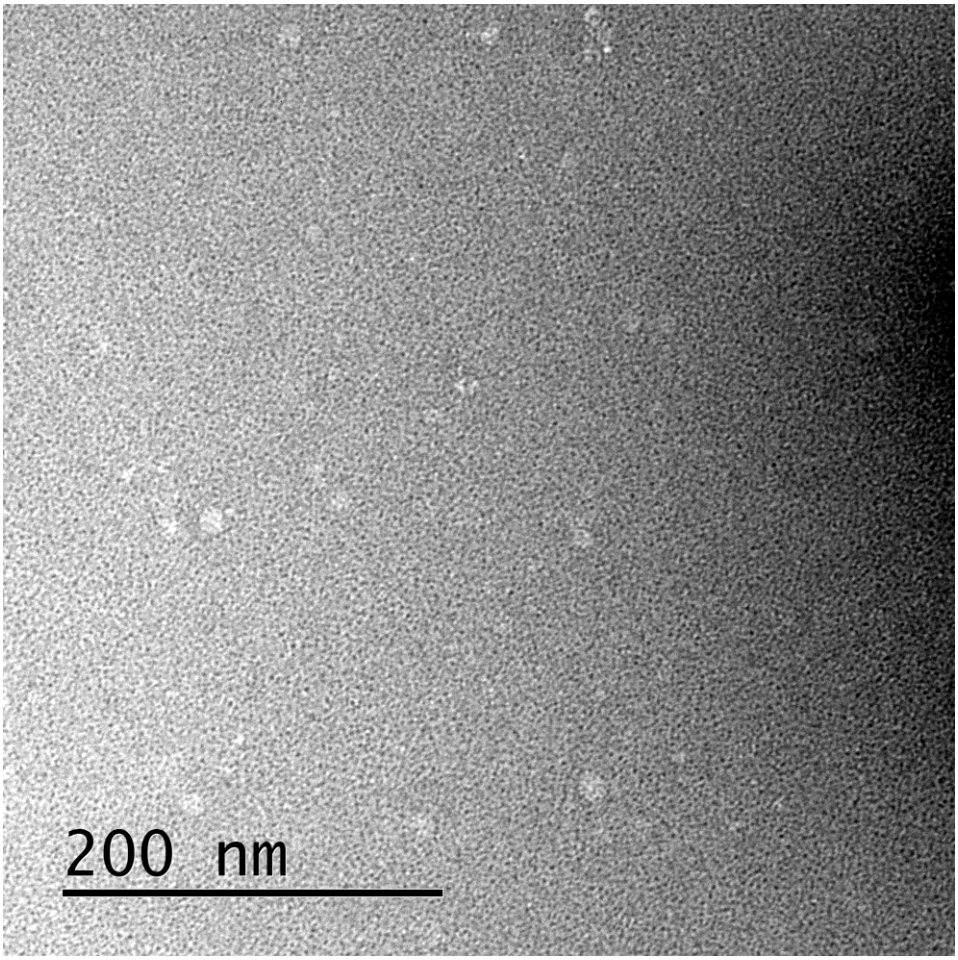

Figure 4.17 – Transmission electron microscope image of purified rPanx1-GFP. rPanx1-GFP was purified by IEC, IMAC and FSEC. The purified protein was concentrated and imaged in negative stained (2% uranyl acetate). TEM images were taken using a JEOL JEM 2100 LaB_6 microscope. Images were processed using EMAN Boxer software.

The first assumption made was that the channel is a cylindrical shape. The shortest (L1) and longest (L2) cross section of each of 100 particles was measured. The average L1 was 7.67 ± 1.82 nm and the average L2 was 11.15 ± 2.3 nm. L1 was assumed to be the diameter of the channel, L2 was assumed to be the length of the channel.

Using the equation: Volume of cylinder $(V) = \pi(L1^2 \div 4)L2$, the volume of the cylinder was estimated to be 515.18 nm^3. Assuming the average density of a protein is 1.35 g/cm^3 (Fischer *et al*, 2004) and the protein particles are solid blocks of protein with no water-filled cavities, the mass of each particle was calculated as 6.95 x 10^{-19} g. Each rPanx1-GFP monomer was estimated to have a mass of about 1.17 x 10^{-19} g based on a molecular weight of 70 kDa. Thus the mass of each particle equated to approximately 5.94 rPanx1 monomers. These results argue that, in contrast to the gel filtration results, rPanx1-GFP does form hexamers in

Drosophila. However, due to the number of assumptions made during these calculations, and the low number of particles measured, a much more detailed analysis on a larger scale is necessary to come to any definitive conclusions.

4.3 Chapter 4 – Discussion

4.3.1 Low-resolution structural studies of rP2X2 and rPanx1

Low resolution structures of both rP2X2 and rPanx1 have been published using EM (Mio *et al*, 2005; Mio *et al*, 2009; Ambrosi *et al*, 2010). For more details on these structures please see sections 1.5.2 and 1.4.2 respectively.

4.3.2 Expression of protein constructs in *Drosophila*

rP2X2-GFP and rPanx1-GFP protein constructs were successfully expressed in the *Drosophila* eye (Fig 4.5). However, hP2X4-GFP and hP2X4-his constructs did not appear to be expressed in this system. The underlying cause behind hP2X4 not being expressed is unclear. However the DNA and mRNA are present in the flies also carrying *the GMR*-Gal4 driver (Fig 4.6). This suggests that the DNA constructs were successfully integrated into the genome and were being transcribed in the presence of a Gal4 driver. One possibility is that the protein was being translated but immediately degraded by the cells, possibly due to misfolding, and thus the expression levels were very low and could not be observed by western blotting or fluorescence microscopy. Alternatively the mRNA may not have been translated efficiently, possibly due to the presence of rare *Drosophila* codons in the hP2X4 sequence.

Differences in codon usage between the construct to be expressed and the expression system can have a significant effect on protein expression as was demonstrated for the chemokine receptor, CCR5 in mammalian cells (Mirzabekov *et al,* 1999). The Graphical Codon Usage Analyser (GCAU) tool (accessed at http://gcua.schoedl.de/) was used to investigate codon usage of rP2X2-GFP, rPanx1-GFP and hP2X4-GFP to see if there were any significant differences between codon usage in the constructs and codon usage in *Drosophila* that might have affected protein expression. However the mean difference between the rPanx1-GFP sequence and *Drosophila melanogaster* codon usage was higher (21.27%) than for the *hP2X4-GFP* sequence (20.7%) and the *hP2X4-his* sequence (18.75%) (See appendix III). In addition there was little use of the codons that are rarely used in *Drosophila* such as TTA (Leu) and GGG (Gly) with relative adaptiveness values of 3% and 22% respectively (the relative adaptiveness values are based on the frequency of the codons used for each amino acid; the codon with the highest frequency is set at 100% relative adaptiveness and are all codons for that amino acid are scaled accordingly). This suggests that it is unlikely that any differences in codon usage were responsible for interfering with hP2X4 expression.

4.3.3 Purification of rP2X2-GFP and rPanx1-GFP

rP2X2-GFP and rPanx1-GFP were successfully expressed in *Drosophila* as shown by western blot analysis and fluorescence imaging (Fig 4.5). Purification of protein constructs from *Drosophila* eyes using nickel affinity purification alone was not successful as a large number of other proteins bound to the nickel beads and eluted upon the addition of imidazole (Fig 4.10). Work performed by Lichty *et al* compared the use of a number of affinity tags (including his-tag, Strep-tag, calmodulin-binding-peptide and FLAG-tag) to purify *E.coli* dihydrofolate reductase from *E. coli*, *Drosophila*, yeast and HeLa extracts. Whilst purification via the his-tag provided moderate purity from *E. coli* extracts, the purity was poor from *Drosophila*, yeast and HeLa extracts. Conversely, purification from *Drosophila* extracts using a strep-tag and streptactin resin or a FLAG tag and FLAG monoclonal antibody provided a much higher purity of eluted protein (Fig 4.18) (Lichty *et al*, 2005). Consequently, to improve protein purification using the *Drosophila* system, the His-tag should be replaced with either a strep-tag or a FLAG-tag for purification purposes.

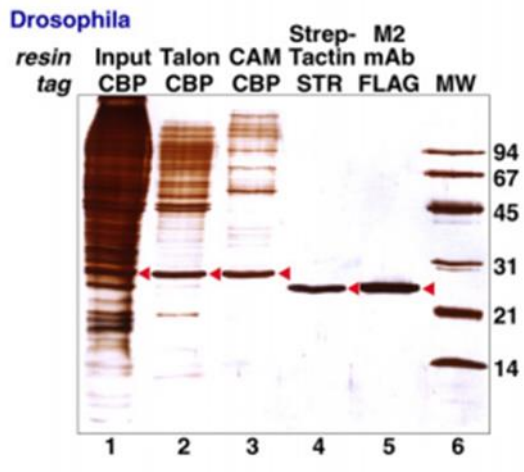

Figure 4.18 – Comparison of multiple resins for purification of tagged DHFR (E. coli dihydrofolate reductase) protein from *Drosophila* extracts. CBP = Calmodulin binding peptide. CAM = calmodulin. STR – Strep II tag. Lane 1 shows protein input. Lane 2 (Talon CBP) shows purification of DHFR via its His-tag using a Talon resin. Lane 3 (CAM CBP) shows purification via a CBP tag on a calmodulin resin. Lane 4 (Strep-tactin STR) shows purification via a Strep II tag on a Strep-tactin resin. Lane 5 (M2 mAb FLAG) shows purification via a FLAG tag using a FLAG monoclonal antibody. Reprinted from Protein Expression and Purification, 41(1), Lichty *et al*, Comparison of affinity tags for protein purification, p98-105., Copyright (2005), with permission from Elsevier.

The approximate yield of pure protein obtained from the *Drosophila* eye using ion exchange chromatography (IEC), sepharose and nickel affinity chromatography was 1 µg rPanx1-GFP per

500 fly heads (Fig 4.14). However previously published data showed purified proteins with yields of up to 0.2 – 0.4 mg protein per 1g of fly heads, this roughly equates to 10-20 µg protein per 500 flies (Panneels *et al*, 2011). Therefore the rPanx1-GFP yield is 10 – 20- fold lower than what has previously been obtained for other membrane proteins in this system which included 10 proteins from three major classes – GPCRs, transporters and channels (Table 4.1). It is unclear whether the starting yield of protein expressed in the *Drosophila* eye is much lower or if the lengthy purification process resulted in a large loss of protein. To help distinguish between these two possibilities, a non-denaturing gel and GFP antibody could be used to compare the yield from a whole protein extract to a known concentration of eGFP to see if this differs significantly from the yield of pure protein that was obtained.

However, when the protein (rP2X2-GFP) was purified using immunoprecipitation, a very low yield of protein was also obtained with an estimated concentration of 100 ng per 500 fly heads (Fig 4.11). This suggests that the protein expression levels are low in *Drosophila* as both purification methods give a low yield of purified protein. However the yield of rP2X2-GFP protein purified by immunoprecipitation was approximately 10-fold lower than the yield of rPanx1-GFP purified by IEC and nickel affinity chromatography. This difference could be as a result of the differing expression levels of rP2X2-GFP and rPanx1-GFP in the fly.

The use of the GFP-TRAP system was unsuccessful for the purification of both rP2X2-GFP and rPanx1-GFP from *Drosophila* as the proteins did not bind to the GFP-binding matrix (Fig 4.12). It is unclear why the proteins were unable to bind to the matrix; it is clear both proteins express the GFP fusion product in *Drosophila* from microscopy and western blotting with a GFP antibody (Fig 4.5). As the proteins are solubilised in detergent prior to purification, it is possible that the detergent molecules are blocking parts of the GFP and preventing it from binding to the GFP TRAP matrix.

4.3.4 Glycosylation of protein constructs in *Drosophila*

rPanx1-GFP does not appear to undergo high mannose or complex glycosylation in the *Drosophila* system, contrary to the complex glycosylation that occurs in HEK-293 cells (Fig 4.8). The high mannose form of rPanx1 is predominantly located at the endoplasmic reticulum whereas the complex glycosylated form is trafficked to the cell surface; thus glycosylation of pannexin 1 channels is important for membrane targeting. However glycosylation has no known effect on channel function or structure; the channels that reach the cell surface are fully functional (Penuela *et al,* 2009). This indicates that in this system, the channels may still

be successfully translated and folded but the majority may be unable to reach the cell surface and retained in the ER membranes. High resolution imaging techniques would be required to determine whether or not the protein is targeted to the cell surface in *Drosophila.*

FSEC of rPanx1-GFP showed that the protein does not form stable hexamers following purification from the fly eye. Two distinct peaks are observed at molecular weights equating to approximately 17 kDa and 156 kDa suggestive of the formation of free GFP and dimeric protein respectively (Fig 4.14). However the purified protein showed a very similar elution pattern when purified from HEK-293 cells, with peaks at the same molecular weights (Fig 3.8). This work suggested that rPanx1 does not form hexamers, contrary to evidence from previous cross linking experiments and the influence derived from their similarity to connexins (Boassa *et al*, 2007). In contrast, calculations performed using low resolution TEM images indicated that the protein was indeed hexameric (Section 4.2.44.2.4). However, to perform these calculations a number of assumptions were made. Firstly, it was assumed that the protein was the shape of a cylinder and secondly, it was assumed that the protein was a solid block of protein, with no water filled cavities. By making these assumptions, the size estimations made could be very inaccurate. In the future, a much larger number of particles will be used for the estimation of size and symmetry of the particles in order to build a model of structure. This will give much more insight into the state of the protein. The average cross sections of the particles were 7.67 nm and 11.18 nm for the short and long cross sections respectively. The estimated oligomer diameter for Panx1 calculated by Ambrosi and colleagues was 12 and 16 nm for two differing image averages. These averages are significantly higher than our estimated diameter of 7.67 nm. However, they did not provide an estimate of the length of the channel and thus this it is not possible to directly compare the results. To make any significant conclusions regarding the size and oligomeric state of the purified rPanx1-GFP, further analysis will need to be performed on the TEM images.

The deglycosylation assays demonstrated that rP2X2-GFP undergoes high mannose glycosylation but not complex glycosylation in the *Drosophila* system with a reduction in molecular weight observed following cleavage by Endo H (Fig 4.8) This result is in accordance with work that suggested insects including *Drosophila* only have the ability to perform high mannose glycosylation (Rendic *et al*, 2008), with very few examples of insect proteins that undergo complex glycosylation. In other systems such as HEK-293 cells, rP2X2 is shown to undergo complex glycosylation (Young *et al*, 2008). Glycosylation of P2X2 has been shown to be important for targeting to the cell membrane as well as protein function (Torres *et* al, 1998;

Newbolt *et al,* 1998). However distinguishing between the effects of high mannose glycosylation and complex glycosylation on protein targeting and function has not been determined. The oligomeric state of rP2X2-GFP was not determined because purification from whole flies (*C155; rP2X2-GFP*) was unsuccessful due to the larger number of contaminating proteins present in whole fly samples (Fig 4.16). This would need to be further investigated by either (i) using a purification procedure that further eliminates contaminating proteins or (ii) reverting back to the use of the GMR-Gal4 driver and purifying using IEC and nickel affinity chromatography. However generating flies expressing a new construct with a FLAG or Strep tag fused to rP2X2 may result in a more reliable and easier purification procedure.

4.3.5 Structure determination of membrane proteins

In order to crystallise a membrane protein, approximately 1 mg of pure protein is required for structure determination. Due to the low yield of both rPanx1-GFP and rP2X2-GFP obtained from *Drosophila*, crystallisation would require protein to be purified from 500,000 flies. However as recently published by Liao *et al*, high resolution protein structures can be obtained without crystallisation. Liao and colleagues solved the structure of TRPV1 to a resolution of 3.4 Å using electron cryo-microscopy in the native and ligand-bound state (the modified 'minimal functional construct' used was a tetramer of approximately 270 kDa in mass) (Liao *et al*, 2013; Liao *et al*, 2014). This required the use of a newly developed direct electron detector and new image processing algorithims in order to improve signal and contrast of cryo-EM images. Although the construct required significant mutagenesis to achieve a homogenous population for structure determination, the final protein concentration that was required was only 0.7 mg/ml. This significant advance in membrane protein structure determination may be able to be extended in the future for even smaller molecules such as P2X receptors. Despite the low yield of protein obtained from the *Drosophila* system, if the protein is of sufficient quality and homogeneity, it may be possible to solve the structure of a P2X receptor or Panx channel using this technique.

4.3.6 Conclusions

rP2X2-GFP and rPanx1-GFP were successfully expressed in the eye of the fruit fly, *Drosophila melanogaster.* However, purification of these proteins proved difficult and lengthy, partially due to the choice of purification tag (His-tag) which was previously shown to be inefficient for purification from *Drosophila* (Lichty *et al*, 2005). The yield of rPanx1-GFP purified by IEC and IMAC was low equating to approximately 1 µg of protein per 500 flies. The yield of rP2X2-GFP

purified by immunoprecipitation with a GFP antibody was even lower, equating to approximately 100 ng of protein per 500 flies. These results indicate that either there is a large loss of protein during extraction and purification or the starting yield of both proteins is very low. The answer to this question will hold relevance to the future of using this system for expression of P2X receptors and pannexin channels for structural studies.

In *Drosophila*, rP2X2-GFP was demonstrated to undergo high mannose, core glycosylation, which is important for protein trafficking and function. We also prove that rP2X2-GFP is functional in *Drosophila* (see chapter 5) indicating that at least a proportion of the protein is indeed correctly targeted to the cell surface and folded. The rPanx1-GFP results are more inconclusive as the protein did not appear to undergo N-glycosylation, which is important for Panx trafficking. In addition, following purification and FSEC, the majority of the protein appeared to form dimers in contrast to analysis of TEM images that indicated the formation of hexamers.

Chapter 5 - Expression of rP2X2-GFP in the *Drosophila* taste system

5.1 Chapter 5 – Introduction

5.1.1 The *Drosophila* taste system

Taste reception in *Drosophila melanogaster* is mediated by sensory neurons that are contained in hair-like cuticular structures called sensilla. These sensilla are distributed widely over the body surface but are particularly concentrated in the mouthparts, legs, anterior wing margins, and in the ovipositor in females (Montell, 2009) (Fig 5.1). The distal part of the proboscis is formed by two labella, each of which holds approximately 31 external taste sensilla (Wang *et al*, 2004), in addition to the smaller taste pegs that are present in the pseudotrachea (the ridges on the labellum) and internal proboscis, leading to the oesophagous. The taste sensilla function in the decision to accept or reject food, but may also participate in pre-copulatory behaviour by the male (Greenspan and Ferveur, 2000; Thorne *et al*, 2004). Like the sensilla on the mouthparts, the leg sensilla are also involved in the detection of attractive and aversive compounds in food, whereby contact can induce proboscis extension and retraction respectively (Wang, 2004). In addition, they are involved in the detection of pheromones during courtship in males (Bray and Amrein, 2003; Montell, 2009). The sensilla located around the ovipositor of female flies possibly play a different role allowing the assessment of food quality for larvae before laying eggs (Yang *et al*, 2008).

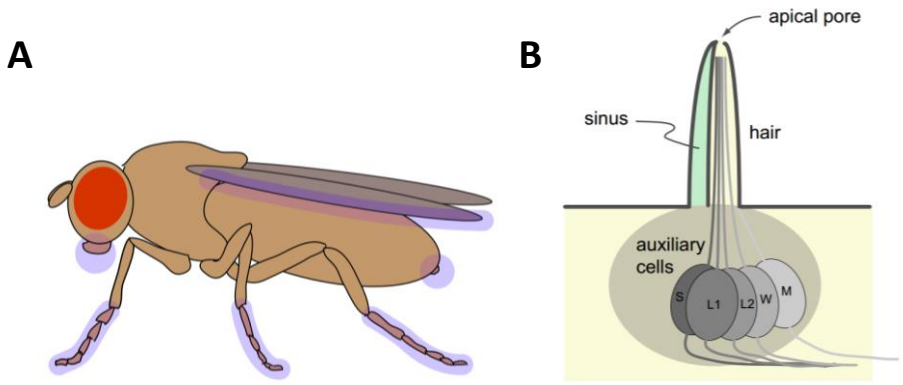

Figure 5.1 – The taste system of *Drosophila melanogaster.* (A) Cartoon showing the position of taste sensilla on *Drosophila melanogaster* (highlighted in purple). (Anterior wing margins, Ovipositor [females], legs and labellum). (B) Cartoon showing the structure of a typical taste sensillum. Each sensillum contains 4 GRNs (S, W, L1 and L2) and a mechanosensory neuron (M) with dendrites extending to the tip of the sensillum and cell bodies located beneath the cuticle. The apical pore is also shown at the tip of the sensillum. The auxillary cells are the trichogen, tormogen and thecogen cells. The sinus is produced from the trichogen and tormogen cells (Schweisguth and Posakony, 1994). The thecogen cell is responsible for envleloping the neurons (Isono and Morita, 2010). Cartoons drawn by Dr Wynand Van der Goes van Naters. Cardiff Universitv

The labellar taste sensilla can be divided into three morphological types –the small 'S', intermediate 'I' and long 'L' type sensilla. The location of each sensillum on the labellum is similar between different labella, and all have been named according to their morphological type and position (see Fig 5.2). 'S' and 'L'-type sensilla contain one mechanosensory neuron and 4 gustatory receptor neurons (GRNs). The GRNs are the "water" cell (W), the "sugar" cell (S), the "salt" cell (L1) and the "bitter" cell (L2). The GRNs are bipolar neurons with a cell body located beneath the cuticle in the sensillum, a dendrite that extends to the tip of the taste sensillum and an axon that projects to taste centres in the CNS. The major taste centre for the labellum is in the suboesophageal ganglion (SOG) whereas the leg GRNs project to the thoracic-abdominal ganglion or the SOG (Dunipace *et al*, 2001; Stocker, 2004). The four GRNs are sensitive to aqueous solutions of low osmolarity (i.e. water), various sugars, salts (such as monovalent alkali halides) and compounds that humans perceive as bitter, respectively (Dunipace *et al*, 2001; Stocker, 2004; Weiss *et al*, 2011). 'I' sensilla contain only 2 GRNs, one responds to both sugar compounds and low salt concentrations (10 - 50mM NaCl), the other responds to bitter compounds and high salt concentrations (over 400mM NaCl) (Hiroi *et al,* 2004; Montell 2009). Among and within the morphological types of sensilla there is functional heterogeneity. For example, the bitter neurons within 'S' and within 'I' type sensilla can be divided into several classes with different but overlapping ligand specificities. Denatonium

benzoate, berberine chloride and sparteine sulphate were best ligands for class Ia neurons while caffeine, umbelliferone and theophylline elicited strongest responses from class Ib neurons among the chemicals tested. Bitter compounds that activate GRNs in 'L' type sensilla have not yet been identified (Weiss *et* al, 2011).

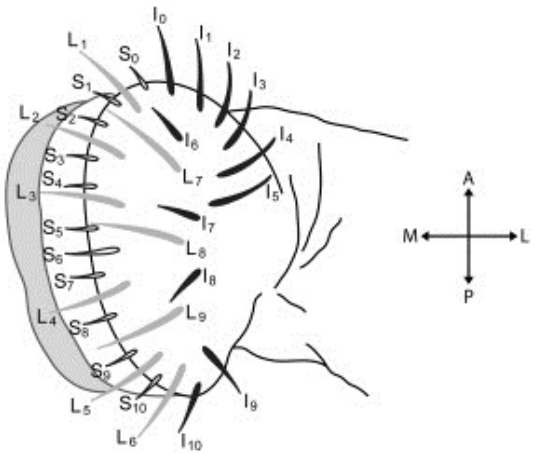

Figure 5.2 – The location of each taste sensillum on the fly labellum. Schematic of a typical *Drosophila* labellum showing the position of each of the 31 taste sensilla. Each sensillum is labelled according to its morphology and position on the labellum, although there is some variation between different labella. A – anterior, P – posterior, M – medial, L – lateral. Image – Weiss *et al*, 2011. Reprinted from Neuron, 69(2), Weiss *et al*, The Molecular and Cellular Basis of Bitter Taste in Drosophila, 258-272., Copyright (2011), with permission from Elsevier.

Sensilla have an apical pore through which chemicals from the substrate diffuse upon contact (Mitchell *et al*, 1999). Tastants then interact with receptors in the dendrites of the taste neurons. The *Gr* gene family (Clyne *et al*, 2000; Dunipace *et al*, 2001; Scott *et al*, 2001) underlies sugar and bitter taste. As is the case for signalling in olfactory receptors encoded by the *Or* gene family (Sato et al 2008; Wicher et al 2008), it is not yet clear whether Gr receptors function as ionotropic or metabotropic receptors, or both. In heterologous expression systems (HEK cells and *Xenopus* oocytes) a Gr from the silkworm, *Bombyx mori*, was able to respond selectively to D-fructose in a G-protein independent manner (Sato et al 2011), while several other studies have shown that sugar reception in *Drosophila* is reduced in mutants of G-proteins (Ishimoto *et al*, 2005; Ueno *et al*, 2006; Kain *et al*, 2010). There are 60 *Gr* genes in *Drosophila*, some of which undergo alternative splicing so that the family encodes a total of 68 gustatory receptors. Each sugar GRN in adults expresses a defined set of at least 3-5 *Gr* genes, whereas bitter GRNs co-express 6-29 gustatory receptors (Weiss *et al*, 2011). The expression of some *Gr* genes is restricted to a small number of neurons, and others are widely expressed (Stocker, 2004). The Gr5a receptor mediates responses to trehalose, m-α-glucoside, glucose

and melezitose (Dahanukar *et al*, 2001, 2007) and is expressed in the sugar neuron in all labellar sensilla (Thorne *et al*, 2004; Weiss *et al*. 2011). Different subsets of the *Gr64* gene cluster (Gr64*a-f*) are co-expressed with Gr5a and mediate responses to a complementary set of attractive compounds including sucrose, maltose, several other sugars and glycerol (Dahanukar *et al*, 2007; Jiao et al, 2007; Wisotsky *et al*, 2011)

5.1.2 Taste recordings in *Drosophila*

A taste sensillum has an apical pore that allows entry of tastants into the hair where they interact with receptors in the dendrites of the GRNs (Sellier, 2010). Extracellular recordings of the action potentials generated by GRNs can be attained by placing the tip of an electrode over the tip of a taste sensillum and thus into contact with the pore. In the technique described by Hodgson *et al* (1955), the recording electrode is also used to deliver the stimulus: a chemical is dissolved with an electrolyte in a solution that is taken up in a glass pipette placed over an Ag/AgCl wire electrode. To record responses to stimuli, the glass pipette is positioned over the tip of the hair (Fig 5.3).

The taste system can be manipulated by expressing a protein of interest in the GRNs using the *Gal4-UAS* system (see section 4.1.2). This can be achieved using a pan-neural driver such as *C155-Gal4*, an enhancer trap line that expresses Gal4 under control of the *elav* promoter. *C155-Gal4* drives expression of the protein in all of the GRNs (Lin and Goodman, 1994). Alternatively a more specific driver such as *Gr5a-Gal4* can be used to induce expression specifically in sugar neurons (Stocker, 2004).

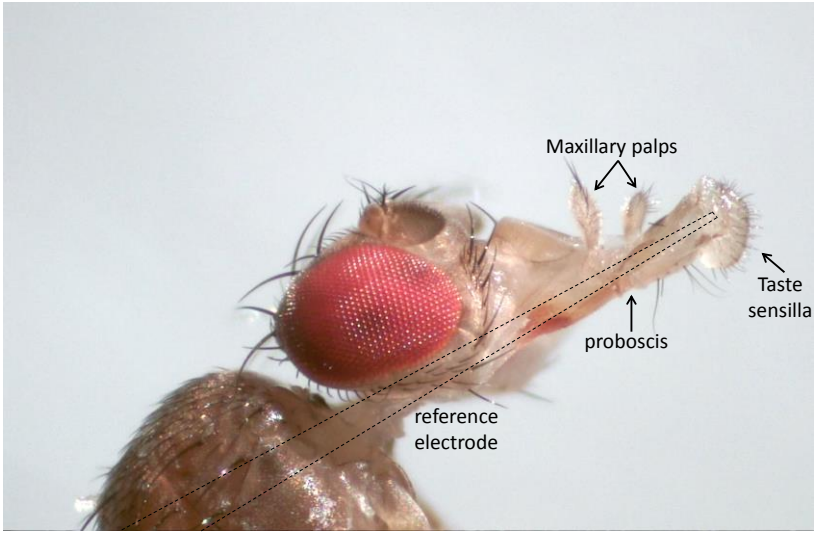

Figure 5.3 – Taste recordings in *Drosophila*. Image showing how the reference electrode containing salt solution is inserted into the back of the fly and extended through the neck and proboscis until movement of the proboscis is ceased. A second electrode containing the stimulus dissolved in water with 30 mM tricholine citrate (TCC) added as electrolyte is placed over the tip of the taste sensillum to record action potential responses to the stimulus.

5.2 Aims and objectives

In this chapter, I aimed to investigate the function of the rP2X2-GFP channel expressed in GRNs of *Drosophila melanogaster*. In addition I sought to use the *Drosophila* taste system as a novel, medium throughput drug screening system for rP2X2 receptors using an adenosine nucleotide library consisting of 80 compounds.

5.3 Chapter 5 – Results

5.3.1 Expression of rP2X2-GFP in the nervous system

To determine whether rP2X2 is produced as a functional protein in *Drosophila*, taste neurons expressing rP2X2 were tested for sensitivity to ATP. Using the pan-neural driver *C155*, rP2X2-GFP was expressed in the taste hairs of the fly. In flies expressing P2X2-GFP under control of the pan-neural driver, fluorescence microscopy shows expression in both taste cell bodies and their processes (Fig 5.4). Under low magnification in these flies, the body is fluorescent where large densities of neurons are present, such as the brain and other parts of the CNS.

Electrophysiological recordings of action potentials from taste neurons were performed according to the technique of Hodgson et al (1955). In this technique, a pipette containing the stimulus solution is placed over the hair tip; the pipette also acts as the recording electrode (see section 5.1.2). A solvent control (30 mM tricholine citrate, TCC), 100 µM ADP and 100 µM ATP were tested on up to three taste sensilla per fly. Each stimulus was also tested on control flies that carry the *UAS-rP2X2::GFP::his* transgene but not a driver to induce expression.

In these control flies the stimuli elicited a low level of action potential activity (3.9±0.8 impulses in 5s; mean±SEM) and no significant difference between the responses to the solvent control and ATP were observed (Mann Whitney, p=0.8817).

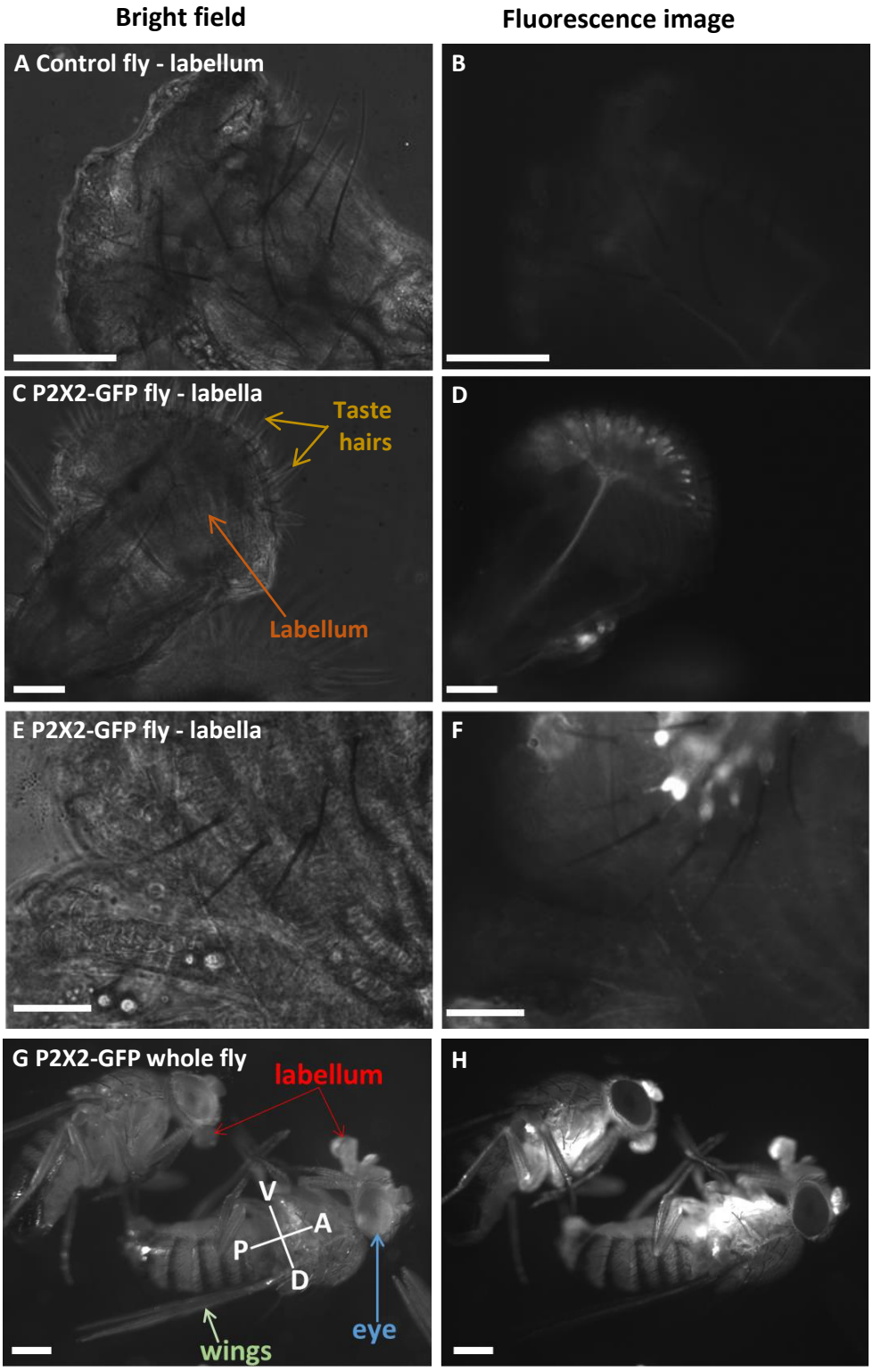

Figure 5.4 – Expression of P2X2-GFP in the *Drosophila* nervous system. (A) Bright field image of a labellum in a fly not expressing P2X2-GFP. (B) Fluorescence image of the same labellum. In C-H, P2X2-GFP was expressed under control of the *C155-Gal4* pan-neural driver and flies were imaged in bright field illumination (C,E,G) and in fluorescent conditions (D,F,H). A- F scale bars = 50 µm. G-H scale bars = 200 µm.

In flies with the *C155* transgene driving expression of rP2X2-GFP, the non-stimulated impulse activity, measured by applying a solvent control, was significantly higher than in flies not expressing rP2X2-GFP (Mann Whitney, p=0.0002). Again the response to ADP did not differ from the response elicited by the solvent control. However, ATP did elicit a strong response (Fig 5.6; 189±43 impulses per 5 s, mean±SEM). This shows that expression of rP2X2-GFP provides the *Drosophila* taste neurons with sensitivity to ATP, but not to ADP, as expected from a functional P2X receptor.

However, the onset-kinetics of P2X mediated responses in *Drosophila* taste neurons were much slower than those mediated by endogenous gustatory receptors. When sucrose, a tastant to which *Drosophila* responds behaviourally, was applied to the tip of a taste sensillum, a phasic tonic train of action potentials was elicited (Fig 5.5). The peak impulse rate, as defined by the shortest two consecutive interspike intervals in the spike train between three spikes of similar amplitude, in response to sucrose was attained within 40 ms of application (30±2 ms, mean±SEM, N=10). However, when ATP was applied to the tip of a taste sensillum in a rP2X2-GFP expressing fly, on-kinetics were much slower; the impulse rate increasing gradually over 20 s of recording (Fig 5.5). For this reason, response magnitude was determined by counting the number of action potentials between 10 and 15 s following compound application in all experiments with nucleotides in sections 5.2.1 and 5.2.2. It was not possible to reliably distinguish the activities of the four chemosensory neurons in a sensillum during responses to ATP, and so the total number of action potentials generated by the neurons have been summed.

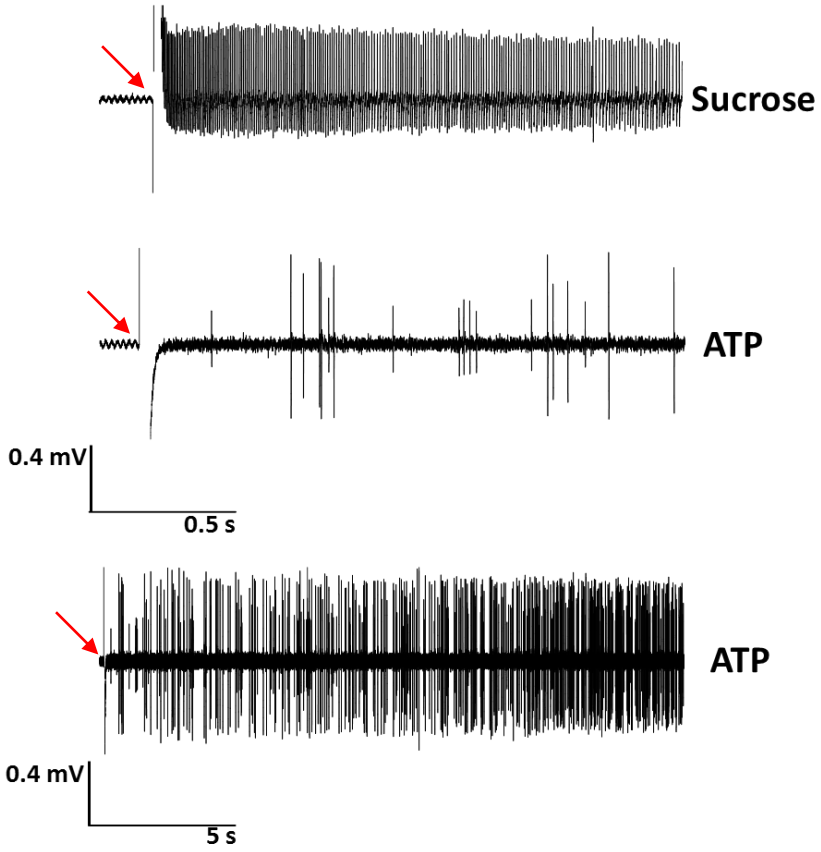

Figure 5.5 – The on-kinetics of the response to ATP is much slower than to sucrose. Top trace: 2 s response to sucrose applied to a taste sensillum. Middle trace: 2 s response to ATP applied to a taste sensillum of a P2X2-GFP fly. Bottom trace: 20 s response to ATP applied to a taste sensillum of a P2X2-GFP fly. Arrowheads indicate onset of stimulus application.

To obtain responses to ATP from only one of the neurons in the sensilla, expression of rP2X2-GFP under control of a driver specific to the neuron that responds to sucrose and other sugars, referred to as the "sugar" neuron, was investigated. The labellar sugar neuron expresses receptors from an 8 member subfamily of the 60 member *Gr* gene family. One of these is *Gr5a*, which is required for the reception of trehalose, melezitose, glucose and m-α-glucoside (Dahanukar et al., 2001, 2007). The promoter of *Gr5a* fused to *GAL4* was tested as a driver for the expression of rP2X2-GFP. In these flies (genotype *w*; *UAS-rP2X2::GFP::His*; *Gr5a-GAL4*), rP2X2-GFP should only be expressed in the sugar neuron in each sensillum. As was the case with the pan-neural driver, non-stimulated activity was higher in flies expressing rP2X2-GFP under control of the *Gr5a* promoter than in control flies (9.8±2.6, mean±SEM, N=10, Mann Whitney, p=0.0134). ATP elicited a higher level of excitatory responses (Fig 5.6). However, contrary to expectation, responses were elicited by ATP in more than one neuron in each sensillum suggesting that *Gr5a-GAL4* drove expression in multiple neurons.

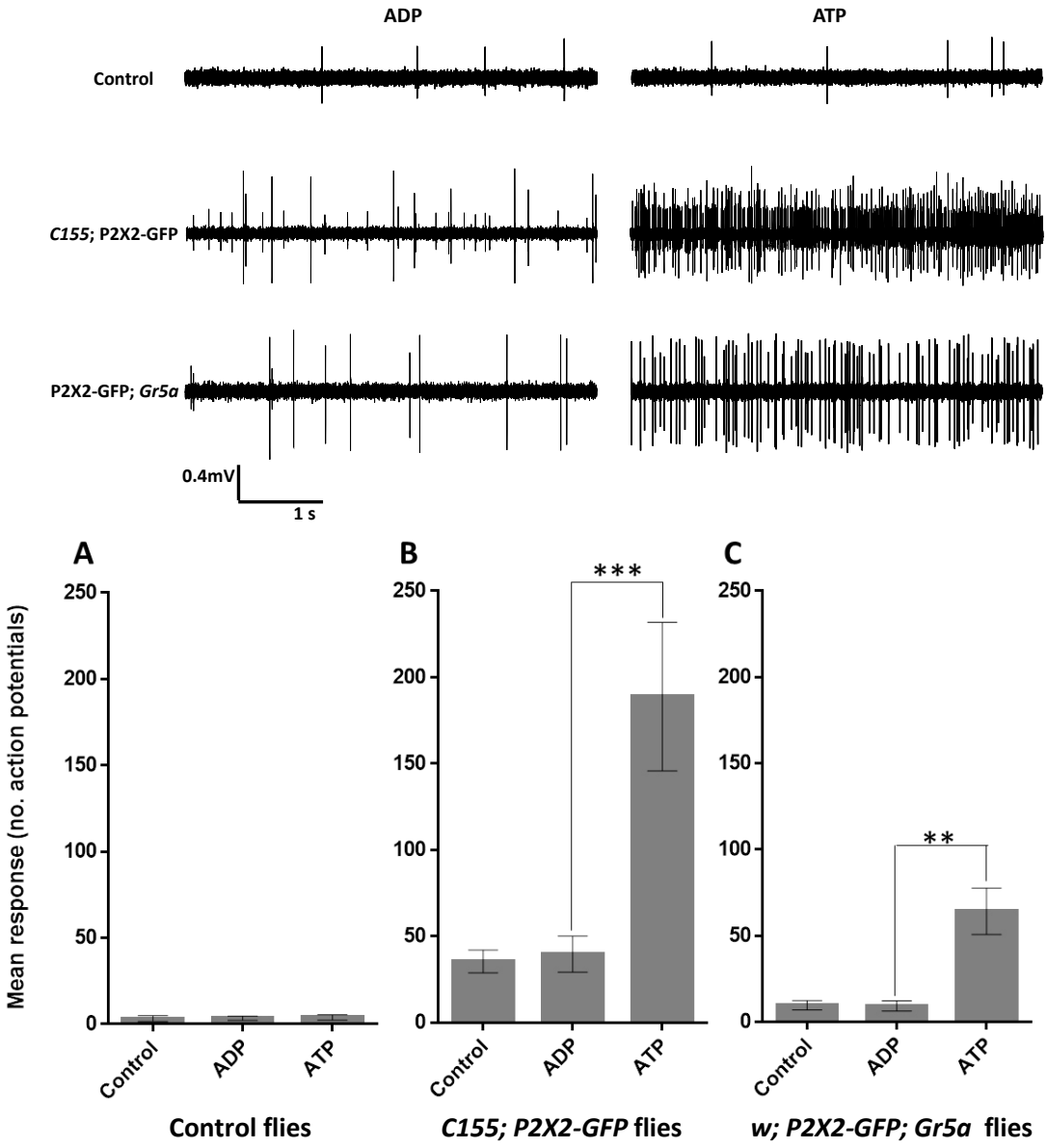

Figure 5.6 – ATP elicits responses in flies expressing rP2X2-GFP. (Top) Representative traces of responses elicited by ADP and ATP in control, P2X2-GFP; *Gr5a* and *C155*; P2X2-GFP flies. Traces show responses elicited between 10 and 15 s after compound application. (Bottom) Graph showing mean response to solvent control (30mM TCC), 100 µM ADP and 100 µM ATP from taste neurons in control flies (a) and in flies expressing P2X2-GFP using a pan-neural driver (b) or *Gr5a-Gal4* (c). N = 10 – 12. Error bars represent SEM. (*** p<0.0001; ** p= 0.0002, pKruskal-Wallis one-way ANOVA; Dunn's post test). No significant difference between responses was observed for control flies (p=0.978).

A range of ATP concentrations were tested on *C155*; *rP2X2-GFP* and *w*; *rP2X2-GFP*; *Gr5a* flies to construct a dose response curve. The concentrations tested ranged from 1 µM to 1000 µM both sets of flies (Fig 5.7). The ATP responses in both sets of flies were dose dependent with a threshold of approximately 10^{-5} M, the calculated EC_{50} for ATP in *C155; P2X2-GFP* flies was 147 µM and the hill slope was 1.938. The EC_{50} of ATP in *P2X2-GFP; Gr5a* flies was 206 µM with a hill slope of 2.049 (Fig 5.7).

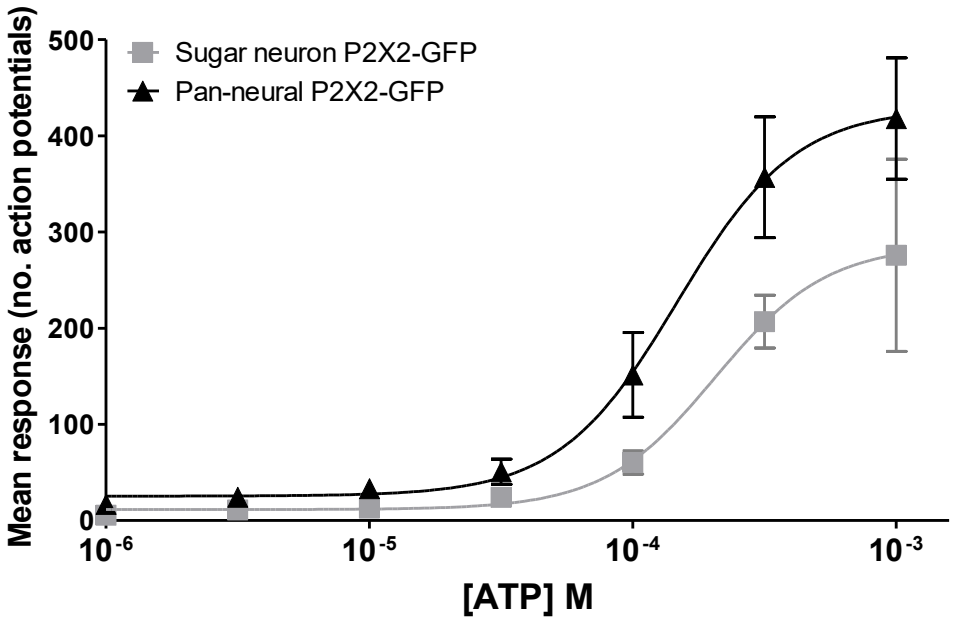

Figure 5.7 – The ATP response is dose-dependent in P2X2-GFP flies. ATP dose response curve for *P2X2-GFP*; *Gr5a* flies (grey) and *C155; P2X2-GFP* flies (black). N = 6-12 sensilla per concentration. Error bars represent SEM. Each ATP concentration was tested on a minimum of 2 different flies.

5.3.2 Testing an adenosine nucleotide library as rP2X2-GFP agonists

Having determined that rP2X2 acts as a functional ligand-gated ion channel in *Drosophila* taste neurons, we considered whether the taste system of *Drosophila* could be developed as an assay system to screen for agonists of P2X receptors. Although the pharmacology of P2X2 has been studied more thoroughly than that of any other P2X receptor, a limited number of chemicals have been tested as agonists of P2X2. We obtained an 80 compound adenosine nucleotide library (Jena Biosciences), which comprises ATP and a great variety of modifications both in the adenine and ribose moieties as well as in the number and bonding of the phosphate groups (see Appendix IV for a full list of structures). All 80 compounds from the adenosine nucleotide library were tested as potential agonists of rP2X2-GFP using the *Drosophila* taste system. 2MeSATP has been reported to be a P2X2 agonist (Evans *et al*, 1999) and was also tested. To verify that the neurons in a sensillum were still functional after preparing the fly for recordings, sucrose, a solvent control and 100 μM ATP were applied before testing each adenosine nucleotide. Only sensilla with a robust response to sucrose and an ATP response more than three times that of the solvent control were used for experiments. ATP responses among different sensilla were variable and ranged from 13 to 712 impulses. The nucleotide responses have therefore been normalised to ATP. The average TCC control response corresponded to approximately 10% of the ATP response. Some of the nucleotides elicited a similar or higher response than ATP which was significantly different from the TCC response; these were ATPγS, ATPαS, and 2F-ATP with responses corresponding to 102%, 114% and 142% of the average ATP response, respectively (Fig 5.8). These highly effective agonists were retested on an additional three sensilla (Fig 5.9). Most nucleotides elicited responses intermediate between the solvent control TCC and ATP; the four strongest partial agonists were mant-n6-methyl-ATP, AP_4, dATP, and *ara*ATP with responses corresponding to 33%, 31%, 44% and 43% of the average ATP response respectively (Fig 5.8). However statistical analysis suggested that the responses did not differ significantly to that of TCC. However due to the low number of repeats for each compound and thus the large error, it would be useful to repeat each compound an additional 3 times to get more reliable results and statistical analysis.

Other nucleotides elicited a response that was lower than the average solvent control response (10%). These included 8-[(4-Amino)butyl]-amino-ATP, N6-(6-Amino)hexyl-dATP, N6-(6-Amino)hexyl-ATP and AP5A with normalised responses corresponding to 2.7%, 4.0%, 4.5% and 5% respectively (Fig 5.8). Expression of rP2X2-GFP in neurons appears to endow the

neurons with a non-stimulated action potential activity, as measured by responses to the solvent control, which may result from spontaneous channel openings. One interpretation of a suppression of the solvent control response by these four compounds is that they interact with the P2X2 receptor to stabilise a closed conformation of the channel. However statistical analysis suggested that the responses did not differ significantly from TCC and thus this would need to be investigated further to see if these compounds have an effect on the receptor.

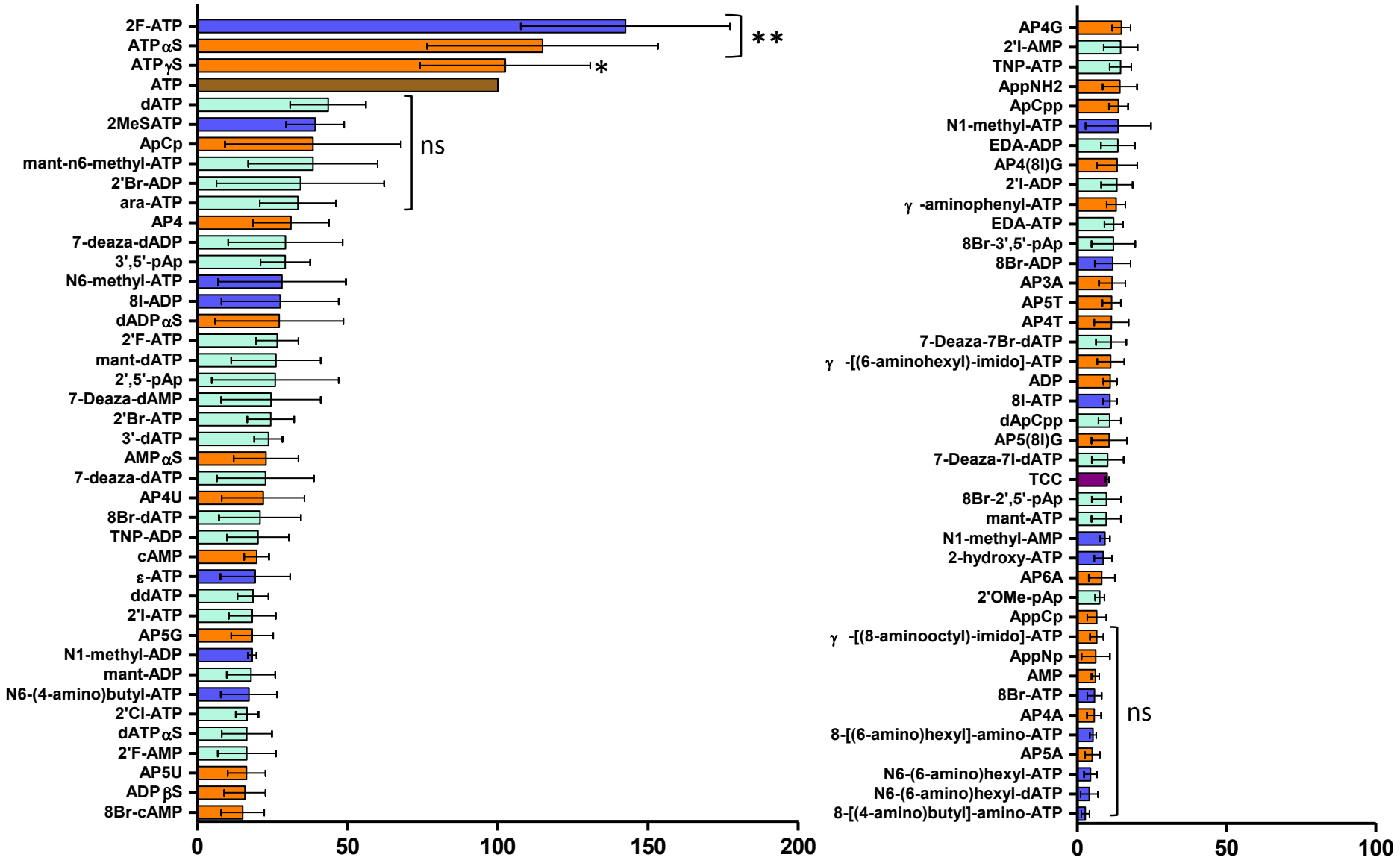
2F-ATP
ATPαS
ATPγS
ATP
dATP
2MeSATP
ApCp
mant-n6-methyl-ATP
2'Br-ADP
ara-ATP
AP4
7-deaza-dADP
3',5'-pAp
N6-methyl-ATP
8I-ADP
dADPαS
2'F-ATP
mant-dATP
2',5'-pAp
7-Deaza-dAMP
2'Br-ATP
3'-dATP
AMPαS
7-deaza-dATP
AP4U
8Br-dATP
TNP-ADP
cAMP
ε-ATP
ddATP
2'I-ATP
AP5G
N1-methyl-ADP
mant-ADP
N6-(4-amino)butyl-ATP
2'Cl-ATP
dATPαS
2'F-AMP
AP5U
ADPβS
8Br-cAMP
**
*
ns
0
50
100
150
200
AP4G
2'I-AMP
TNP-ATP
AppNH2
ApCpp
N1-methyl-ATP
EDA-ADP
AP4(8I)G
2'I-ADP
γ -aminophenyl-ATP
EDA-ATP
8Br-3',5'-pAp
8Br-ADP
AP3A
AP5T
AP4T
7-Deaza-7Br-dATP
γ -[(6-aminohexyl)-imido]-ATP
ADP
8I-ATP
dApCpp
AP5(8I)G
7-Deaza-7I-dATP
TCC
8Br-2',5'-pAp
mant-ATP
N1-methyl-AMP
2-hydroxy-ATP
AP6A
2'OMe-pAp
AppCp
γ -[(8-aminooctyl)-imido]-ATP
AppNp
AMP
8Br-ATP
AP4A
8-[(6-amino)hexyl]-amino-ATP
AP5A
N6-(6-amino)hexyl-ATP
N6-(6-amino)hexyl-dATP
8-[(4-amino)butyl]-amino-ATP
ns
0
50
100

Figure 5.8 – Mean responses of P2X2-GFP to 80 adenosine nucleotides. 80 adenosine nucleotides were applied to the tip of taste sensilla of flies expressing P2X2-GFP under the control of the pan-neural driver *C155-Gal4*. Bars show the mean compound response 10 – 15 s after application to the taste sensillum, normalised to the number of action potentials elicited by ATP. Error bars are SEM, N=3. ATP is shown in brown and the solvent control (TCC) is shown in purple. Blue bars represent AMP/ADP/ATP derivatives with altered adenine moieties, orange represents altered phosphate groups and cyan represents altered ribose moieties. See Appendix IV for structures. One way ANOVA was used to determine if the ten compounds with the highest and lowest responses were significantly different from the control TCC response and thus represent agonists and antagonists respectively. Significant responses are represented by ** ($P<0.01$) and * ($P<0.05$). ns = not significant.

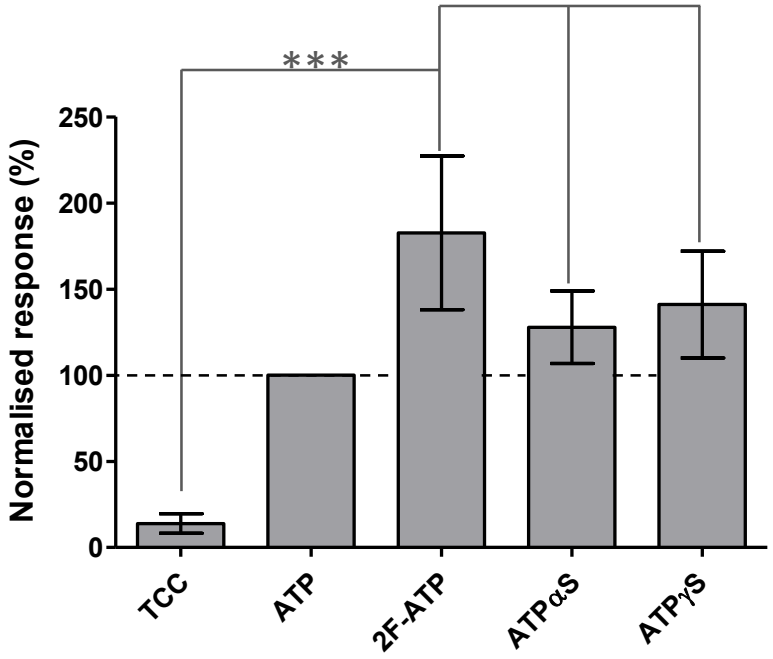

Figure 5.9 – 2F-ATP, ATPαS and ATPγS elicit responses significantly different from TCC. Each compound was tested on 6 sensilla, each on a different fly. Graph shows the mean response for each compound normalised to ATP. Statistical analysis: (*** p<0.0001; Kruskal-Wallis one-way ANOVA; Dunn's post test, N=6). 2F-ATP (P=0.1233), ATPαS (p=0.2422) and ATPγS (p=0.2425) responses do not differ significantly from that of ATP (one sample t-test, N=6).

To ensure that the effects of the nucleotides that gave a higher response than TCC were as a result of rP2X2 activation and not activation of endogenous *Drosophila* receptors, they were also tested on control flies. None of the compounds induced a higher response than TCC in control flies demonstrating that they act on rP2X2 (Fig 5.10).

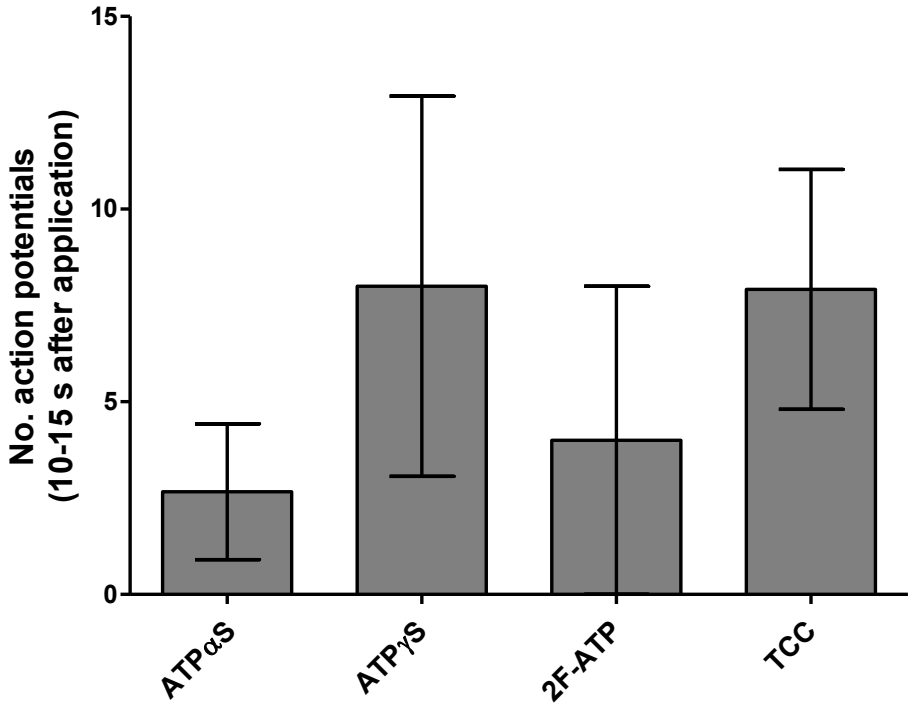

Figure 5.10 – None of the P2X2 agonists elicit responses in control flies. The compounds which initiated a response of more than 50% of the ATP response in *rP2X2-GFP* flies were tested on control flies (*rP2X2-GFP* parent flies) and action potentials were recorded. None of the compounds tested (ATPαS, ATPγS or 2F-ATP) induced a response largely different from the TCC response in control flies demonstrating that they act specifically on rP2X2-GFP.

Separating out the compound library into ATP, ADP and AMP derivatives allows comparison among agonists within these groups. As noted before 2-fluoro-ATP, which has a substitution in the purine base, is the best ligand among the ATP derivatives (Fig 5.11A). While some modifications in the phosphate groups are tolerated, modifications of the ribose sugar all cause loss of effectiveness. Among the ADP derivatives, ADP itself elicited the lowest response; any derivative tested appears to give a higher response (Fig. 5.11B). Likewise, among the AMP derivatives AMP itself was least effective (Fig. 5.11C). As the modifications available in the library for ADP and AMP corresponded only partly, it is not possible to compare the profiles between agonists in these two groups.

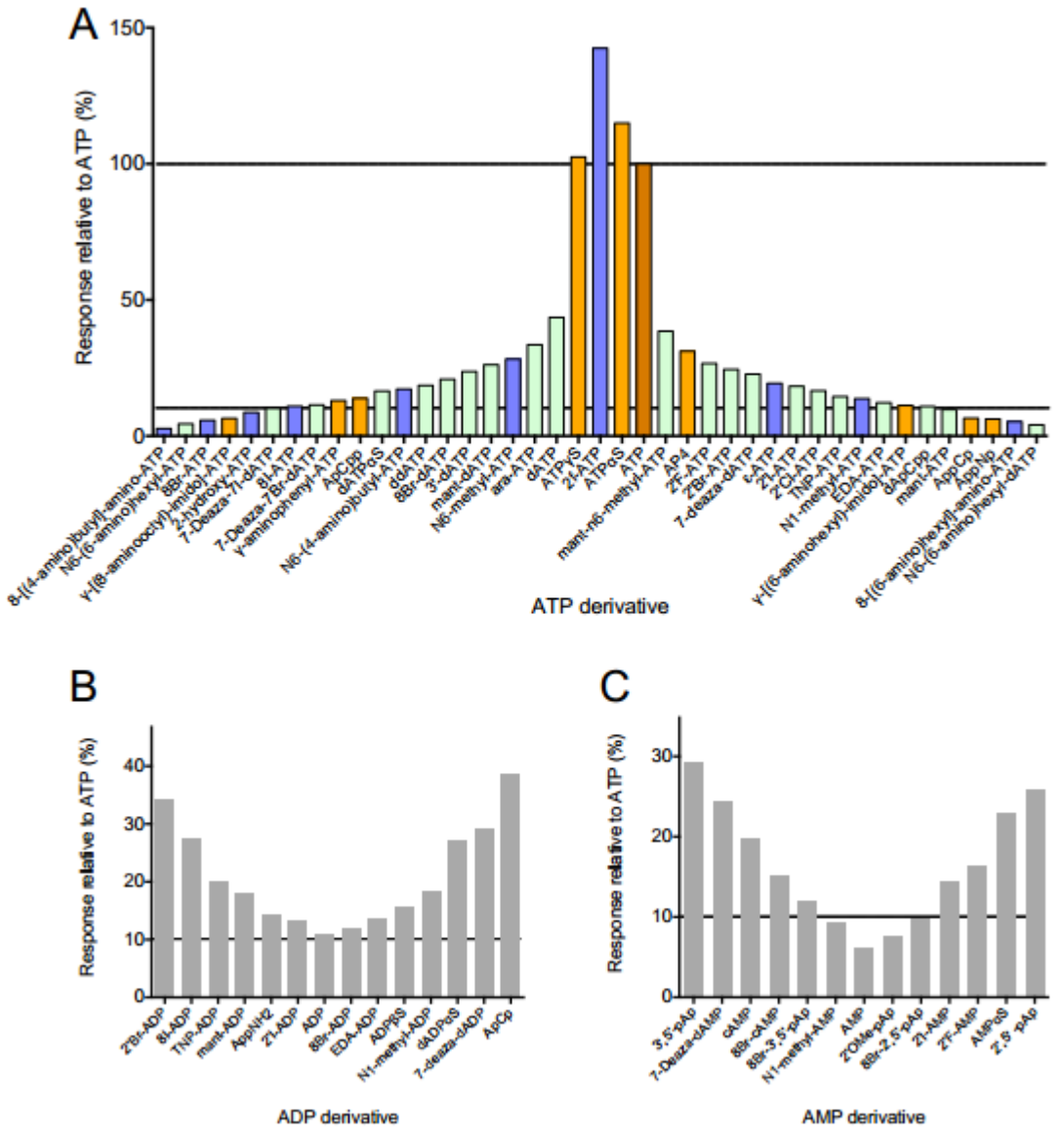

Figure 5.11 – Comparison of responses to ATP, ADP and AMP derivatives. Compounds were grouped according to the number of phosphate groups they have. (A) ATP derivatives with ATP shown in brown, compounds with ribose modifications are shown in cyan, phosphate modifications are shown in orange and adenine modifications are shown in blue. (B) ADP derivatives and (C) AMP derivatives. The bars shown represent the average response relative to ATP (%). The line at approx. 10% shows the average solvent control TCC response. The line at 100% represents the ATP response.

5.3.3 Localising rP2X2-GFP to the tip of the taste sensillum

Work by Dr Wynand van Der Goes van Naters showed that removing the tip of the *Drosophila* taste sensillum caused a loss of response to sucrose. This suggests that the gustatory receptors are localised to the tip of the taste sensillum. However, the sensilla in rP2X2-GFP flies were still responsive to ATP following tip removal suggesting the rP2X2 receptors are not being targeted

to the tip of the hair (data not shown). This may explain why sucrose responses are observed immediately after agonist application whereas the ATP response has much slower on-kinetics.

The gustatory receptor protein is likely to contain a subcellular targeting motif because a transgene carrying only the coding region of a gustatory receptor gene can fully rescue responses in a deletion mutant for the receptor (Dahanukar *et al*, 2007). We surmised a targeting motif may be conserved among Gr proteins. Amino acid sequences of five gustatory receptors were aligned (Gr64a, Gr64e, Gr5a, Gr32a and Gr43a) to identify conserved candidate regions that could be involved in localisation of the receptors to the apical tip of the GRN dendrite (Fig 5.12). The C-terminal domain of the receptors appeared to be the most highly conserved. A putative Short Targeting Sequence (STS, from residue 430 onwards) and a Long Targeting Sequence (LTS, from residue 332 onwards) were selected. Regions encoding the STS and LTS of Gr64a were amplified by PCR from cDNA from *w1118* flies, using forward primers that also encode a Thrombin cleavage site and a Myc-tag, and these were ligated onto the 3' end of rat *P2X2* to generate *rP2X2-Thr-Myc-STS* and *rP2X2-Thr-Myc-LTS* fusion constructs.

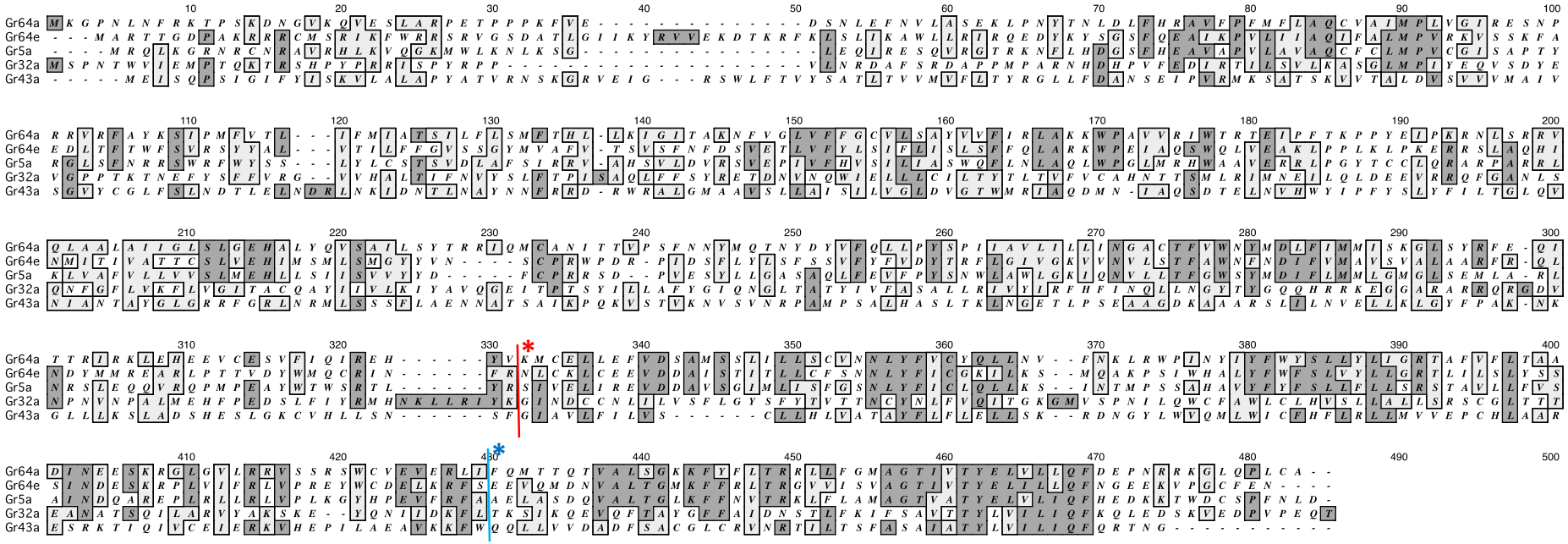

Figure 5.12 – Sequence alignment of gustatory receptors. The amino acid sequences of five diverse gustatory receptors (Gr64a, Gr64e, Gr5a, Gr32a and Gr43a) were aligned. Conserved residues are shaded in dark grey and amino acids which display similar properties are shaded in light grey. The start of the long targeting sequence (LTS) begins at residue 332 and is indicated by the red asterisk. The start of the short targeting sequence (STS) begins at residue 430 and is indicated by the blue asterisk.

The *rP2X2-myc-LTS* and *rP2X2-myc-STS* constructs were injected into *Drosophila* embryos to generate phiC31 mediated integration of transgenes on the third chromosome (attP2 site) (Markstein *et al*, 2008). Fly lines expressing the constructs under control of the *C155* driver were obtained. However due to time constraints, it has not yet been possible to test the activity of rP2X2 in these fly lines.

5.4 Chapter 5 - Discussion

5.4.1 P2X receptors form functional LGICs in *Drosophila* taste neurons

rP2X2-GFP was shown to be functional in *Drosophila* under control of both the pan-neural *C155-Gal4* and sugar neuron *Gr5a-Gal4* drivers (Fig 5.6). Robust responses were elicited to ATP but not to ADP or the solvent TCC in rP2X2-GFP flies while GRNs in control flies did not respond to ATP (Fig 5.6).

The basal number of action potentials elicited in response to TCC or ADP was higher in rP2X2-GFP expressing flies compared to control flies. There are two possible reasons for this result. Firstly, there may be spontaneous ATP release in *Drosophila* causing activation of the receptors in the absence of exogenously applied ATP. Alternatively, the receptors may be undergoing a basal level of activation in the absence of ATP. To distinguish between these two possibilities, an enzyme such as apyrase (catalyses the hydrolysis of ATP to ADP and Pi (Smith *et al*, 2002)) could be co-applied to the sensillum with TCC to see if this reduces the basal level of responses. Additionally, a rP2X2 antagonist (such as suramin or PPADS) could be co-applied to the taste hair to ensure the increase in TCC response is as a result of the rP2X2-GFP activation.

The response curve to ATP mediated by rP2X2-GFP under control of both the pan neural (*C155-Gal4*) and sugar neuron (*Gr5a-Gal4*) drivers showed a dose dependent increase. However, a higher concentration of ATP was required to activate the channel and a right-hand shift in the dose response curve was observed when compared to rP2X2 expressed in other systems (Fig 5.7). For example in HEK-293 cells the EC_{50} of rP2X2-GFP is 4.4 µM (Bobanovik *et al*, 2002) and in Xenopus oocytes the EC_{50} is approximately 15 µM (Khakh *et al*, 2001a). However the EC_{50} of rP2X2-GFP expressed in the *Drosophila* system was 147-206 µM. This rightward shift in ATP response could be as a result of the receptor not folding and functioning correctly in *Drosophila*. However, the P2X receptor is not exclusively localised to the tip of the dendrite where the stimulus enters the pore. One possible reason for the difference in ATP potency is that the taste sensillum pore is so small that the response is affected by the time required for the diffusion of ATP into the sensillum. In the time taken for the ATP to diffuse in to the sensillum, the neuron is adapting causing a shift in the dose response curve to the right. This could be investigated by removing the tip of the sensillum to make the access hole larger and seeing what effect this has on the ATP response.

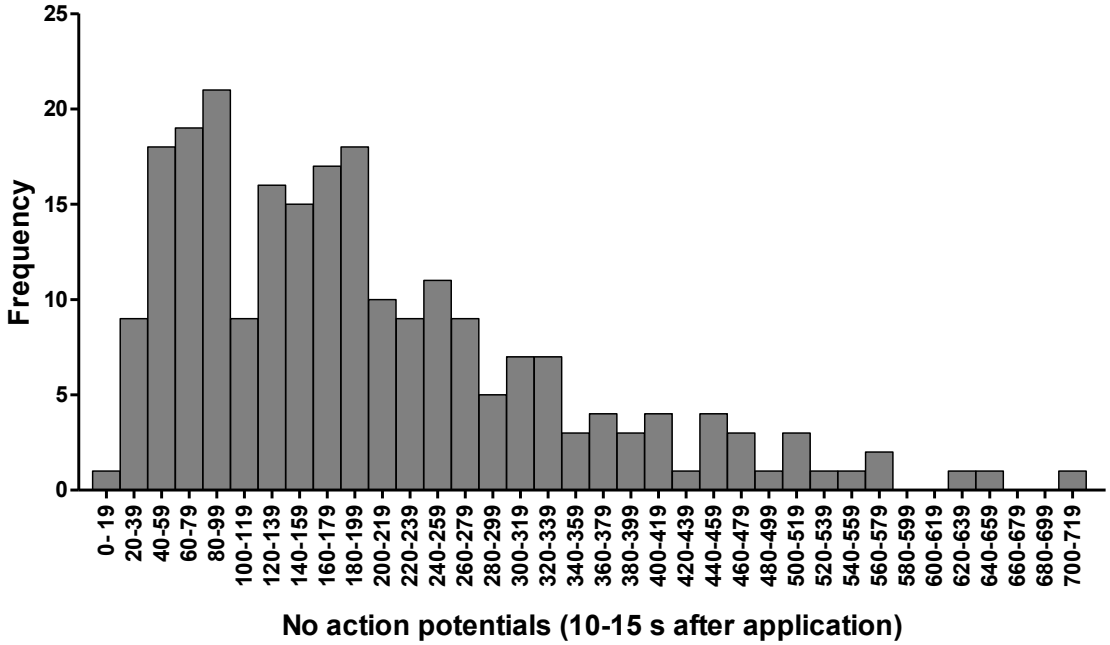

Figure 5.13 – Variation of ATP responses in P2X2-GFP flies. ATP responses were measured from each sensillum between 10 and 15 s after ATP application. The frequency of each block of action potential numbers is shown in this histogram. Two main peaks are observed at 50 – 99 and 150 -199 action potentials.

The ATP response varies between different flies and sensilla. A histogram was generated that represents the frequency distribution of the ATP response in the sample of sensilla tested (Fig 5.13). The frequency distribution appears to be multimodal. Two main peaks were observed between 40–99 and 120-199 action potentials. This indicates there may be at least two classes of sensilla responding to ATP at differing rates; one is less responsive to ATP with a peak of 40–99 action potentials whereas the other is more responsive with a peak of 120–199 action potentials. This could be due to certain sensilla types acting as better hosts of the receptors.

5.4.2 Using the taste system as a compound screening technique for rP2X2 receptors

P2X2 receptors are major drug targets with roles in pain sensation, inflammation and hearing loss (Cockayne *et* al, 2005; Hunskaar and Hole, 1987; Xu and Huang, 2002; Yan *et al*, 2013). Selective, potent P2X2 agonists and antagonists could provide new therapies for a range of conditions. The taste system of *Drosophila* provides a novel medium throughput screening system for P2X2 agonists and holds the advantage of having the receptor expressed in a neural system.

In this thesis, an adenosine nucleotide library consisting of 80 compounds was tested on flies expressing rP2X2-GFP. Although nucleotides are not considered to have great therapeutic potential because of their central importance in many processes in the body, testing this library provides a proof of concept that the screen is feasible and a range of responses to the nucleotides were observed. In addition it allows us to speculate why certain adenosine nucleotides are able to activate P2X2 while others have no effect, giving insight into which parts of the ATP molecule are necessary for receptor activation. This information will help in the design of new and selective agonists and/or antagonists of P2X2. I chose to test the nucleotide library on flies expressing rP2X2-GFP under control of the *C155-Gal4* driver rather than the *Gr5a-Gal4* driver because responses to ATP were elicited in more than one neuron in *Gr5a* flies, suggesting that the driver is expressing rP2X2-GFP in other neurons as well as the sugar neurons. This is possibly due to leaky expression of the Gal4 driver rather than expression that is faithful to the endogenous localisation of Gr5a.

5.4.3 Testing the adenosine nucleotide library

The taste system of *Drosophila* has provided us with a novel platform for drug screening in search for new P2X2 agonists and antagonists. So far 80 adenosine nucleotides have successfully been tested using this system which elicited a large range of responses. Some of the nucleotides that displayed a response similar to ATP include 2F-ATP, ATPαS and ATPγS. Initially, only the compounds with 3 or more phosphate residues have been analysed due to the previously documented importance of the gamma phosphate in receptor activation (Hattori and Gouaux, 2012). A schematic of ATP is shown in Appendix IV noting the nomenclature of the various parts of the molecule used below.

5.4.4 Changes to the phosphate groups

Fig 5.11A shows that some modifications to the phosphate groups (shown in blue) of ATP can be tolerated by P2X2. ATPαS and ATPγS are ATP derivatives that contain a sulphide group in place of a hydroxyl group on either the α or γ phosphate respectively. Both ATPαS and ATPγS elicited responses similar to ATP in rP2X2-GFP flies with responses of 103% and 115% respectively. In the rP2X2 structural model based on the zfP2X4.1 crystal structure, the hydroxyl groups form hydrogen bonds with residues in the ligand binding site (see Fig 5.14B). This indicates that when these hydroxyl groups are replaced with sulphide groups, interactions can still be formed with the receptor and thus can still fully activate rP2X2. ATPαS and ATPγS have also been shown to activate P2X2 in other systems such as *Xenopus* oocytes using patch

clamping where ATPαS and ATPγS gave responses equivalent to 80% and 85% of the ATP response respectively (King *et al*, 1997).

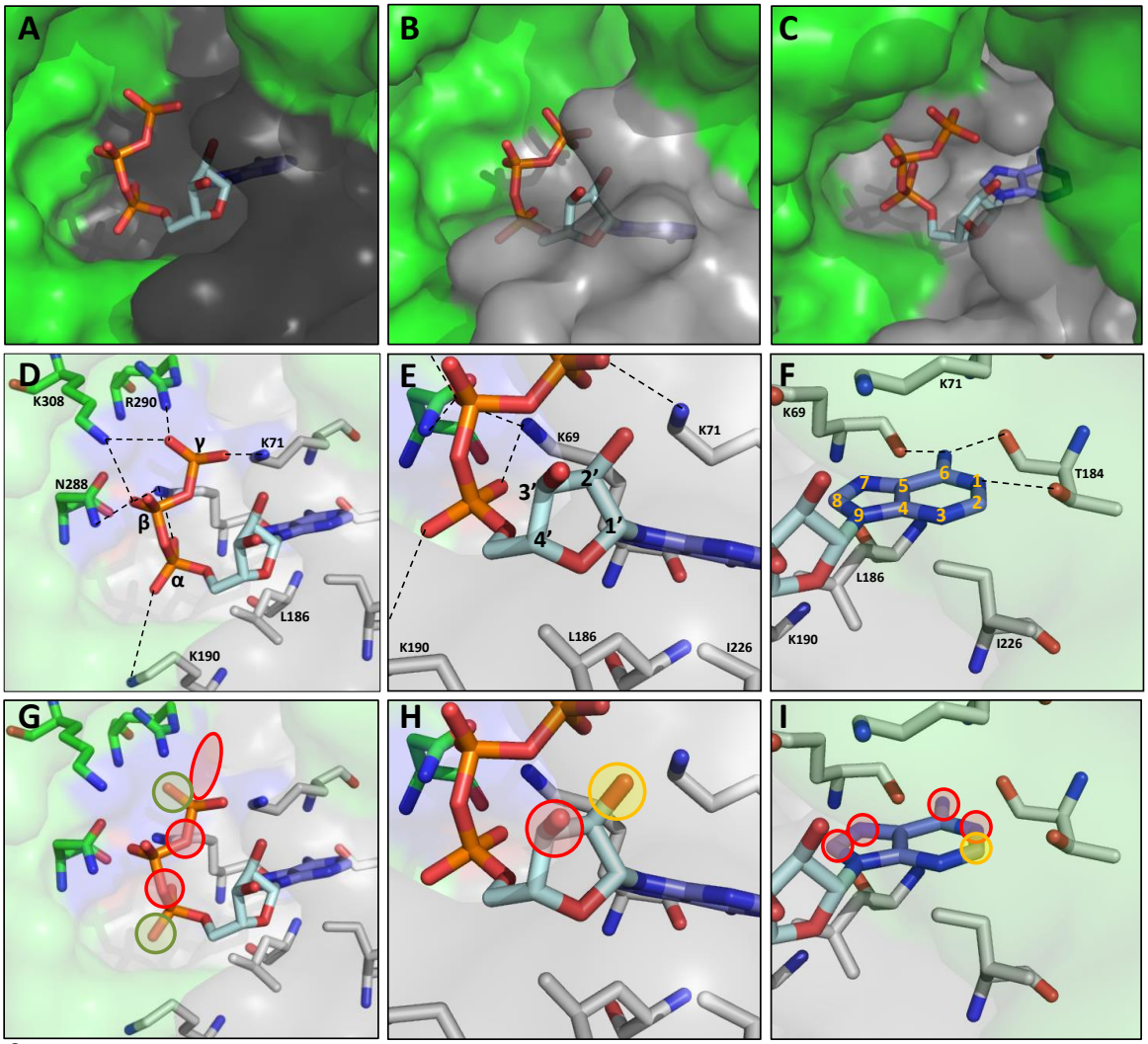

Summary:

- **Substitutions to α and γ OH groups (ATPαS and ATPγS) tolerated and act as full agonists**
- **Substitutions to either oxygen adjoining phosphate groups not tolerated and nucleotides do not activate P2X2.**
- **Groups added to the end of the γ phosphate interfere with ATP binding and/or agonist activity.**

Summary:

- **2' OH group does not undergo critical interactions with binding pocket.**
- **3' OH more important in making P2X2 activation.**
- **Bulky substitutions cannot be tolerated at either position.**

Summary:

- **One substitution (fluorine) at position 2 gave rise to a full agonist but hydroxyl substitution or bulky additions at position 2 affected activation.**
- **Additions to position 1, 6, 7 or 8 interfere with ATP binding and/or agonist activity.**

Figure 5.14 – Model of rP2X2 ATP binding pocket. (A-C) Schematics showing position of ATP buried within the rP2X2 binding pocket, from angles which match schematics below. (D) The phosphate groups, shown in orange, are predicted to interact with residues from both adjacent subunits. (E) The ribose sugar, shown in cyan, is not predicted to interact with any rP2X2 residues. (F) The adenine ring, shown in blue, is predicted to interact with residues from one of the adjacent subunits. Dotted lines represent hydrogen bonds. (G-I) Testing the adenosine compound library on rP2X2 expressed in *D. melanogaster*, we summarised which residues appear to be important in channel activation. Positions where all ATP substitutions tested could be tolerated and gave full functional responses are circled in green. Positions where some, but not all, ATP substitutions tested could be tolerated and gave some functional responses are circled in yellow. At positions where any substitution gave rise to a molecule which could not activate P2X2 are circled in red. Nitrogen atoms are shown in blue, oxygen atoms are shown in red.

dAppCp and AppCp (also called β,γ-methylene-ATP) have an oxygen to methyl substitution joining the β and γ phosphate groups. dAppCp also lacks the ribose 2' hydroxyl group. The oxygen substitution has a significant effect on channel function with responses for dAppCp and AppCp of 10.8% and 6.6% respectively. AppCp has been shown to be a partial agonist of rP2X2 receptors before but with an EC_{50} >300 μM, it has a low potency (Liu *et al*, 2001). Therefore at a concentration of 100 μM it would be unlikely to activate the receptor in this system due to the rightward shift of the dose response curve. Similarly AppNp, where the same oxygen is substituted for an imido group, elicited a response of 6.2%. ApCpp (also called α,β-methylene-ATP) has an oxygen to methyl substitution joining the α and β phosphates. This substitution also prevents receptor activation giving a response of 13.8%. This is in agreement with previous findings that suggested it is inactive at P2X2 receptors (Liu *et* al, 2001). This suggests that the oxygen atoms linking the phosphate groups together are vital for receptor activation. These oxygen atoms do not appear to be involved in the formation of interactions with the binding pocket in the rP2X2 structural model (Fig 5.14D). However alterations of these residues may lead to changes in the conformation of the phosphate groups, preventing critical interactions with the subunits.

This agonist screen showed that the compounds AP3A, AP4A, AP5A and AP6A did not activate rP2X2 receptors with responses of 12%, 5.7%, 5% and 8.2% respectively. This is in contrast to previously published data that suggested AP4A is an agonist at rP2X2 expressed in Xenopus oocytes with an EC_{50} of 15.2 μM (Pintor *et al*, 1996; Wildman *et al*, 2002). However it is possible that the AP4A nucleotide was unstable and degraded to AMP and ATP and thus the effects seen in the past were due to activation by ATP. As the activity of AP4A has only been investigated in *Xenopus* oocytes, it would be useful to study its activity in other systems such as HEK-293 cells. The addition of another adenosine molecule and additional phosphate group to the ATP nucleotide increases the size of the agonist substantially and it seems unlikely the P2X receptor would be able to accommodate this but this would need to be further investigated. Other dinucleotide polyphosphates (AP5(8I)G, AP4T, AP5T, AP4(8I)G, AP4G, AP5U, AP5G, AP4U) did not activate rP2X2 with responses ranging from 10.7% to 22%. However, AP4, which has the addition of an extra phosphate group but no additional nucleoside, elicited partial activation of rP2X2-GFP with an average response of 31%. The rP2X2 homology model shows the gamma-phosphate group located at the edge of the binding pocket. As rP2X2 can still undergo partial activation by AP4, it is likely that the extra phosphate group lies outside the binding pocket (Fig 5.14A).

γ-[(6-aminohexyl)-imido]-ATP and γ-[(8-aminooctyl)-imido]-ATP have an aminohexyl-imido or aminooctyl-imido group attached the gamma phosphate of ATP. These nucleotides are inactive at rP2X2-GFP with responses of 11.2% and 6.5% of the ATP response respectively suggesting that, as with the diadenosine polyphosphates, the receptor cannot accommodate bulky additions to the end of the phosphate groups. Likewise, γ-aminophenyl-ATP has a 4-aminophenyl group attached to the gamma phosphate and doesn't activate the receptor with an average response of 13%.

This data indicates that the addition of bulky groups to the end of the gamma phosphate of ATP prevent activation of the receptor despite the fact the gamma phosphate is located at the outside edge of the binding pocket (Fig 5.13G).

5.4.5 Changes to the adenine ring

Fig 5.11A shows that few alterations of the adenine ring of ATP (shown in red) can be tolerated by P2X2. N1-methyl-ATP contains a methyl group attached to the N1 position of the adenine ring of ATP. The addition of this group to ATP prevented the nucleotide from activating rP2X2 in this system (17% of the ATP response). One possible explanation is that the methyl group is preventing the compound from accessing the binding pocket. Alternatively the compound may be accessing the binding pocket but the presence of the methyl group is preventing it from forming the hydrogen bond that is predicted to be formed between the N1 position of the adenine ring and the T184 residue of the adjacent subunit in the rP2X2 model (Fig 5.14F).

2F-ATP is an ATP derivative with a fluorine to hydrogen substitution at position 2 of the adenine ring. 2F-ATP fully activated rP2X2 with an average response of 142%. In the rP2X2 model, the hydrogen atom does not interact with the binding pocket (Fig 5.14F) suggesting that this substitution is unlikely to affect ATP forming interactions with the binding pocket and so 2F-ATP is still able to activate P2X2. 2F-ATP has not previously been tested on P2X2 receptors making this nucleotide a novel agonist. However, 2-hydroxy-ATP, which has the addition of a hydroxyl group at position 2 of the adenine ring, does not activate rP2X2; it elicited an average response of 8.7% showing that it is not just the addition of the group that may affect binding but also the specific properties of the group are important for interactions with the binding pocket. The extra hydroxyl group in 2-hydroxyATP might be involved in the formation of hydrogen bonds with residues in the binding pocket with which ATP does not interact; this may in turn prevent activation.

N^6-(6-amino)hexyl-dATP and N^6-(6-amino)hexyl-ATP display a lower response than the TCC controls with average responses of 4% and 4.5% of the ATP response. A (6-amino)hexyl side group is added to the amino group at the 6th position of the adenine ring of ATP in these compounds. Additionally, N^6-(6-amino)hexyl-dATP is lacking the 2' hydroxyl group on the ribose sugar. The amino group at the 6th position of the adenine ring is predicted to form 2 interactions with the T184 side chain of the adjacent P2X subunit in the rP2X2 homology model (Fig 5.14F). Consequently the addition of this bulky side chain may interfere with the formation of these hydrogen bonds and prevent channel opening or they may completely prevent the nucleotide from accessing the binding site as the adenine ring is buried deep in the binding pocket (Fig 5.14C). N6-(4-amino)butyl-ATP has an additional (4-amino)butyl group linked to the amino group at position 6 of the adenine ring. Similarly, the response to this compound does not differ largely from TCC (17%). Ɛ-ATP has an etheno group attached to the 1st and 6th position of the adenine ring. This group prevents the nucleotide from activating the receptor with a response of 19.4%. N6-methyl-ATP holds a less bulky, methyl group attached to the amino group at position 6 of the adenine ring. This nucleotide gives a partial response of 28.2% of the ATP response but with a large error of 21.3%, this makes it difficult to determine whether or not this compound is having an effect without further investigation. Mant-6-methyl-ATP is the same as N6-methyl-ATP but with an additional mant group attached to the 2' or 3' hydroxyl groups of the ribose sugar. This nucleotide gave an average response of 38.5% but with a large error of 21.5%, this also makes it difficult to determine what effect it has without further investigation. However, as both N6-methyl-ATP and mant-ATP give lower responses, mant-n6-methyl-ATP is unlikely to partially activate rP2X2. All these data indicate that additional groups at position 6 of the adenine ring cannot be accommodated and disrupt receptor activation (Fig 5.14I).

7-Deaza-7I-dATP and 7-Deaza-7Br-dATP lack the 2' hydroxyl group and have an iodine residue or bromine residues attached at position 7 of the adenine ring. These nucleotides gave responses of 10.2% and 11.4% respectively which are lower than the response of dATP (43.6%) indicating that the addition of iodine or bromine to position 7 of the adenine ring has a significant effect on agonist activity. However, the nitrogen atom at position 7 of the adenine ring in ATP is not predicted to form interactions with rP2X2 (Fig 5.14F).

The nucleotide that gave the smallest response was 8-[(4-amino)butyl]-amino-ATP. This nucleotide has an additional amino group at position 8 of the adenine ring. The amino group is further attached to a butyl group and another amino group. 8-[(4-amino)butyl]-amino-ATP

gave a response of 2.7% of the ATP response which is 7.3% less than the control TCC response in rP2X2-GFP flies. This lower response is approximately equivalent to the basal response observed in control flies. I speculate that this compound might act as a rP2X2 antagonist and thus prevents basal channel opening either spontaneously or by competing with ATP released in the *Drosophila* taste sensillum. However, if 8-[(4-amino)butyl]-amino-ATP is acting as a competitive antagonist, the binding pocket must be able to accommodate the addition of the large side group to the 8 position of the adenine ring (Fig 5.14C). Further investigation would be required to determine whether or not this nucleotide is acting as an antagonist.

8Br-dATP, 8Br-ATP and 8I-ATP have an additional bromine or iodine group attached to the 8th position of the adenine ring respectively. These nucleotides are inactive at rP2X2-GFP with responses of 20.9%, 5.8% and 11% of the ATP response for 8Br-dATP, 8Br-ATP and 8I-ATP respectively. The differences between responses for 8Br-dATP and 8Br-ATP are likely to be as a result of the large variation between flies with a great error of 13.6% for 8Br-dATP. In the rP2X2 model, the 8th position of the adenine ring does not appear to be involved in interacting with the binding pocket (Fig 5.14F). However these results suggest that even small additions at this position can have an effect on P2X2 activity suggesting that it may indeed interact with the receptor (Fig 5.14I).

5.4.6 Changes to the ribose sugar

Interestingly, the data from the nucleotide library indicates that any alteration to the ribose moiety of ATP has a significant effect on the ability of the nucleotide to activate P2X receptors (Fig 5.11A). Interestingly, no part of the ribose sugar is predicted to interact with the P2X2 binding pocket in the rP2X2 structural model. This data indicates that conversely, most of the residues of the ribose sugar play a large role in receptor activation. DeoxyATP (dATP) lacks the 2’ hydroxyl group on the ribose sugar moiety of ATP. dATP appears to retain some agonistic effects at rP2X2-GFP (43% of the ATP response) indicating that this hydroxyl group does not undergo significant interactions with the ATP binding pocket; this is in agreement with what is predicted in our rP2X2 homology model (Fig 5.14E). However when the 3’ hydroxyl group is removed from the ribose sugar (3’ dATP), there is a larger reduction in agonist potency with an average response of 23% of the ATP response. In addition upon removal of both the 2’ and 3’ hydroxyl groups (ddATP) the response is reduced further to approximately 16% of the ATP response. These results suggest the 3’ hydroxyl group is playing a role in ATP binding. However the homology model of the binding pocket does not show this residue interacting with any portion of the binding pocket (Fig 5.14E). The 2’ hydroxyl group is set in a different orientation

in *ara*-ATP; this nucleotide still partially activates the receptor with an average response of 42.6%. Thus this suggests that changes to the 2' hydroxyl group of ATP does not completely abolish receptor activation, but there is a decrease in agonist potency (Fig 5.14H).

Mant dATP and Mant-ATP have a large O-(N-methyl-anthraniloyl) group attached to either the 2' or 3' hydroxyl group of ATP. These nucleotides are inactive at rP2X2 with responses of 26% and 9.7% (differences are likely due to large error – 14.9% for Mant dATP). Similarly EDA-ATP has the addition of an O-(2-Aminoethyl-carbamoyl) group to either the 2' or 3' hydroxyl group of ATP and this addition prevents receptor activation with a response of 12.2%. TNP-ATP has the addition of a O-Trinitrophenyl-adenosine group to the 2',3' hydroxyl groups of ATP. TNP-ATP does not activate rP2X2 with a response of 14.5%. However it has previously been shown to act as an antagonist at rP2X2 receptors (Virginio *et al,* 1998). Therefore bulky additions at the 2' and 3' positions of the ribose sugar cannot be tolerated and prevent activation. This is likely due to the nucleotides being unable to access the binding pocket, with the ribose sugar buried between the subunits (Fig 5.14B/H).

5.4.7 P2X2 response to AMP and ADP derived nucleotides

The compounds were separated into those with one (AMP derivatives), two (ADP derivatives) and three (ATP derivatives) phosphate groups to allow comparisons between individual groups to be made (Fig 5.11). Among the AMP derivatives, AMP was shown to elicit the lowest response (Fig 5.11C). Similarly, among the ADP derivatives, ADP was shown to elicit the lowest response (Fig 5.11B). This data indicates that any modification made to AMP or ADP enabled the nucleotide to elicit a higher P2X2 response. Thus this suggests that the P2X receptor has not only evolved specificity for ATP, but also evolved not to respond to the co-occurring species AMP and ADP. Whether the principle that receptors show these two modes of specificity –for the ligand and against co-occurring similar reaction products- holds true for other systems besides rat P2X2, remains to be investigated.

5.4.8 Adenosine nucleotide library: Summary

A range of responses were observed after testing the adenosine nucleotide library as potential agonists of rP2X2.

Fig 5.15A shows a hypothetical response graph where none of the compounds, other than ATP, elicited a P2X2 response significantly different to the TCC control. In this situation, it could be concluded that every feature of the ATP molecule is critical for activation and thus plays a part in receptor activation. Fig 5.15C shows another hypothetical response graph

where the responses vary largely for the adenosine derivatives and many of them are able to partially or fully activate P2X2. In this situation, it could be concluded that there are many features of the ATP molecule that are not necessary for P2X2 activation and can be compromised without loss of agonist activity. The actual data (Fig 5.15B) shows an intermediate effect, but it is closer to what is observed in Fig 5.15A. This suggests that the majority of the changes to ATP could not be tolerated and are necessary for P2X2 activation.

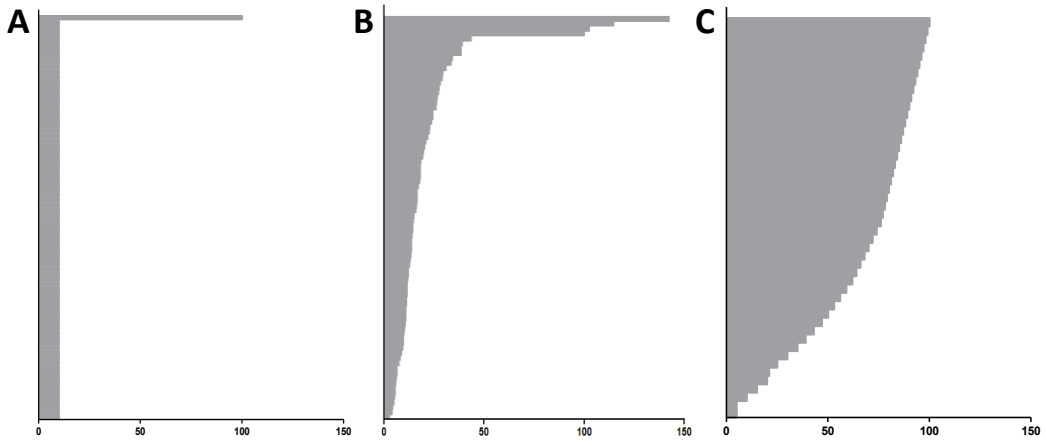

Figure 5.15 – Theoretical compound response profiles of P2X2. (A) Theoretical response profile for ATP; no other derivatives activated P2X2. (B) Actual response profile for adenosine nucleotide compound library tested. (C) Theoretical response profile for ATP if many factors were not critical for ATP activation.

The nucleotide library screen has given a detailed insight into what is required for ATP to bind to and activate rP2X2 receptors. It is clear that the addition of large side groups to any part of the nucleotide has a significant effect on agonist activity. Altering the connecting residues between phosphate groups appears to have a notable effect on activation of rP2X2, in agreement with previous findings. This is in contrast to activity at other P2X receptors such as P2X1 and P2X5 (Wildman *et al*, 2002) indicating that the outer part of the binding pocket may differ in the different receptors. Substitutions of the phosphate hydroxyl groups to sulphide groups can be tolerated (ATPαS and ATPγS) indicating that the interactions made by the hydroxyl groups predicted in the rP2X2 model can either still be formed, or are not essential for receptor activation (Fig 5.14G). Further investigation is required to see what other substitutions can be tolerated.

The ribose sugar possesses a 2’ and a 3’ hydroxyl group. Removal or alteration of the 2’ hydroxyl group does not completely prevent agonistic activity whereas the 3’ hydroxyl group seems to be of more importance for receptor activation. This suggests that, in contrast to what

is predicted in the rP2X2 model, the 2' and 3' hydroxyl groups interact with the receptor. Addition of larger groups to the 2' or 3' position of the ribose sugar also disrupts agonist activity at P2X2. As the ribose sugar is buried within the binding pocket of the rP2X2 model (Fig 5.14B), the additional groups may prevent the nucleotide from fitting in the binding pocket.

Addition of large side groups to any part of the adenine ring prevents the nucleotide from activating the receptor. This part of the molecule is expected to be buried deep in the binding pocket in the homology model (Fig 5.14C) and so it is likely that with bulky side chains, the nucleotides cannot fit in the binding pocket. Interestingly, 2F-ATP acts as a potent agonist at rP2X2 whereas 2hydroxy-ATP has no agonistic activity. Additionally, 2MeSATP had a partial agonistic effect at rat P2X2 (39%). This compound has a methylthio group attached at position 2 of the adenine ring. Therefore although hydrogen substitutions can be tolerated at this position, the properties of the group play a role in interacting with the binding pocket. This could be as a result of 2-hydroxyATP forming interactions with P2X2 that are not formed by ATP. This would suggest that, in agreement with the rP2X2 model, position 2 of the adenine ring does not play a role in receptor activation (Fig 5.14F).

5.4.9 Problems faced with using the taste system as a compound-screening system

There are a number of problems faced when analysing this data, largely because of the large variation in responses observed between flies. For example, the TCC response in some flies can be as high as 50% of the ATP response where others may be 0% of the ATP response. Although we only used flies where the TCC response was 33% or less than the ATP response, this still allowed a large variation of responses for nucleotides which had no effect. As only 3 repeats were performed for each nucleotide, the error was large if one sensillum gave a high background response. In addition, some sensilla retained activity following ATP application in the absence of an agonist giving a high response even when the nucleotide had no activity. These problems account for the large errors observed with a number of nucleotides. To overcome these problems there are 2 main solutions; firstly with more time it would be necessary to test each nucleotide a minimum of 6 times to give more accurate results with less error. In addition, to account for the sensilla that retain activity after ATP application, TCC would be re-applied after ATP to ensure the neuron has returned to its basal state before testing the nucleotide of interest.

5.4.10 P2X2 expressed in other systems

A number of other systems have been used for the expression of P2X2 receptors and the testing of compounds as potential agonists or antagonists of the receptor. In 1999, Grubb and Evans tested the effect of 2MeSATP, α,β-meATP, β,γ-meATP, UTP, TNP-ATP, suramin and PPADS on P2X2 receptors expressed in cultured adult rat dorsal root ganglion cells. They used whole-cell and outside-out patch clamp recordings to test the response of P2X2. In this system, reproducible responses to 10 μM ATP could only be obtained if a time gap of 4-5 minutes was given between agonist applications. To test the action of antagonistic compounds, they had to be presuperfused over the neuron and added to the superfusate that is applied to the cell. After application of suramin to a neuron, a time interval of 40 minutes was required before the baseline returned to control levels. During these experiments, the effects of 9 compounds were tested on P2X2 receptors over a lengthy time period due to the time intervals necessary between applications for levels to return to baseline. They concluded that 2MeSATP and α,β-meATP were agonists and β,γ-meATP and UTP were ineffective at P2X2Rs. TNP-ATP, PPADS and suramin all had antagonistic effects (Grubb and Evans, 1999).

Another expression system that has been used for P2X receptors is the *Xenopus* oocyte. Liu and colleagues, 2001, expressed P2X2 in *Xenopus* oocytes and tested the agonist activity of ATP, 2MeSATP, ATPγS, α,β-meATP, β,γ-meATP, AP_5A and UTP using voltage clamp procedures. Using this method, the application of agonists were separated by a time gap of 20 minutes. They also tested PPADS, RB-2, Suramin, TNP-ATP and IP_5I as antagonists at P2X2 which required a 1 minute pre-application, and were applied during agonist application. Their results showed that ATP, 2MeSATP and ATPγS acted as P2X2 agonists (EC_{50} values of 4.3, 6.9 and 8.4 respectively). However in contrast to Grubb and Evans, 1999, (and in agreement with my results) they concluded that α,β-meATP was inactive at P2X2Rs. They also found that β,γ-meATP, AP_5A and UTP were ineffective at P2X2 receptors (Liu *et al*, 2001).

The effect of adenine dinucleotides were also tested on P2X2 expressed in *Xenopus* oocytes. In this study by Pintor *et al*, the effects of AP_2A, AP_3A, AP_4A, AP_5A and AP_6A were studied on P2X2. They concluded that AP_4A had an EC_{50} of 15.2 μM, which was close to that of ATP (EC_{50} = 3.7 μM). In addition, AP_5A potentiated P2X2 responses to ATP, lowering the EC_{50} to 2.95 μM when co-applied (Pintor *et al*, 1996).

King and colleagues (1997) investigated the effect of extracellular pH on the agonistic effects of various P2X2 agonists. Eighteen compounds were tested using voltage-clamp

electrophysiology on P2X2 expressed in *Xenopus* oocytes with results concluding that ATP, 2-MeSATP, ATPγS and ATPαS acted as potent P2X2 agonists and CTP, BzATP, ADP, 2-MeSADP, ADPβS, AMP, α,β-meATP, β,γ-meATP, UTP, ITP, GTP, 2'-dATP, 3'-dATP and adenosine elicited little or no response. Under acidic conditions (pH 6.5 compared to pH 7.4), they noted that there was a 5-fold increase in ATP-affinity for all four agonists but no change in the order of potency (King *et al*, 1997).

Baqi *et al* (2011) identified 2 selective P2X2 antagonists (PSB-1011 [IC50 – 79 nM] and PSB-12011 [IC50 – 86 nM]) which blocked ATP mediated currents in *Xenopus* oocytes expressing P2X2 receptors. In this study, a library of 59 anthraquinone derivatives of RB-2 were tested as antagonists using 2 electrode voltage-clamp electrophysiology (Baqi *et al*, 2011).

Although *Xenopus* oocytes have proved effective in the past for testing compounds as potential agonists or antagonists of P2X2, there are some limitations to using this model; one of these is the recovery time required between repeated agonist applications. For these reasons, it would be difficult and time-consuming to use *Xenopus* oocytes to screen large compound libraries as potential agonists or antagonists of P2XRs and may explain why the above studies (Liu *et al*, 2001; Pintor *et al*, 1996; King *et al*, 1997) investigated only a small number of compounds (6 – 18 compounds), with the exception of Baqi *et al* (2011). The use of the *Drosophila* taste system as a novel drug screening system of P2XRs provides a much faster way of screening larger numbers of compounds with access to many sensilla per fly, meaning many compounds can be tested on each fly without significant time intervals between compounds. With 80 compounds having already been tested (Fig 5.5), this system can now be extended for the testing of other large compound libraries to help discover novel P2X2 drugs.

In addition, if P2X2 receptors can be successfully localised to the tip of the taste sensilla, the responses can be recorded over a 2-3 second time period, as opposed to a 20-second time period, which will result in many more compounds being tested in a shorter length of time, improving the through-put of this system. In addition, it may reduce the response variations between flies, thus reducing the error.

5.4.11 Conclusions

rP2X2 is functional in the *Drosophila* taste system where responses are elicited in response to ATP in rP2X2-GFP expressing flies but not in control flies. However, the concentration of ATP required to activate the receptor is significantly higher than the concentration required to

activate P2X2 receptors in other systems. This could be as a result of the receptors position within the neuronal dendrites in the sensillum resulting in a time delay for activation.

This system can also be used as a novel, medium through-put compound screening technique for drug discovery. By screening an adenosine nucleotide library consisting of 80 compounds, a P2X2 agonist was identified, 2F-ATP, which elicited higher responses that ATP at rP2X2 receptors. This screen was also used to identify components of the ATP molecule that contribute to activation of rP2X2. It was shown that very few alterations to the ATP molecule were tolerated by P2X2 and the majority of the nucleotides did not activate the receptor. In particular, very few alterations to ribose gave nucleotides with activity at P2X2. However a few problems were faced using this system due to a large variation in response between flies. This made it difficult, in some cases, to establish if a partial response was real or as a result of this variation.

Chapter 6 – Final Discussion

In this thesis, a protein expression system has been presented which covers two distinct aspects of biological research; protein expression for (i) purification and subsequent structural studies and (ii) a novel, medium-throughput drug-screening technique. Due to their relevance in many human diseases and conditions, P2X receptors and pannexin channels represent key drug targets (Tsuda *et al*, 2003; Le Feuvre *et al*, 2002; White *et al*, 2005; Greig *et al,* 2003; Wicki-Stordeur and Swayne, 2014; Penuela *et al,* 2013). Our successful expression of P2X2 and Panx channels in the eyes of *Drosophila* provides a method for the generation of material that may be suitable for future structure determination using TEM and single particle analysis, a technique that does not require a high yield of protein, and has the potential (as demonstrated for the LGIC TRPV1) to produce data of sufficient resolution to 'solve' the 3D-structure (Liao *et al*, 2013; Liao *et al*, 2014). However, the gel filtration data so far indicates that Panx1 may not be forming stable hexamers in *Drosophila.* This is in contrast to small-scale analysis of TEM images, whereby the approximate volume of each particle was calculated. Based on a number of assumptions, this analysis estimated the channel to be hexameric. More rigorous analysis is necessary to come to any definitive conclusions regarding the state of the pannexin channels. In addition, using the *Drosophila* taste system electrophysiology assay, we can ensure that the P2X receptor proteins that we are using for structural studies are correctly folded and functional, thus although the oligomeric state of P2X2 has not yet been studied in *Drosophila,* it is known that at least a portion is forming stable trimers due to its functional role in the taste system.

During this project, the work in chapter 3 was undertaken prior to chapter 4 and 5. However the work in chapters 4 and 5 was performed concurrently. As a result, time constraints affected the final experiments and analysis for the final stages of both chapters; this included full analysis of rPanx1-GFP EM data and structural model building. In addition, testing the compound library in chapter 5 was performed at the very end of time course and thus each compound was only tested 3 times. Therefore although statistical analysis has been included for the adenosine library, this may explain why most differences among the responses were not statistically significant. The production of flies expressing P2X2-targeting sequence constructs was also hampered by time constraints at the end of the project.

6.1 Evaluation of *Drosophila* eyes as a membrane protein expression system

There are many systems readily available to use for the heterologous expression of membrane proteins. However, each system displays a series of advantages and disadvantages with no solitary system providing an efficient universal expression system.

6.1.1 *Escherichia coli*

The most commonly used expression system for recombinant proteins is *E. coli.* However upon over-expression of membrane proteins in *E. coli*, they are often not folded correctly and form large aggregates in the form of inclusion bodies (Palmer and Wingfield, 2004). Although the formation of inclusion bodies allows for a high level of protein expression without causing host toxicity, the protein is often mis-folded and so is not useful for structural studies. Nevertheless, there have been a number of progressions that were designed to improve the use of *E. coli* as an expression system for membrane proteins. For example, mutant strains of *E. coli* were developed by selection from the BL21(DE3) strain, e.g. C41 and C43, that are more resistant to the toxicity caused by membrane protein over-expression. Although these strains allow expression of higher levels of membrane protein without toxic effects, the proteins are still aggregated into inclusion bodies (Miroux and Walker, 1996). Another mutant strain, Lemo21, was also developed from the BL21(DE3) strain. Lemo21 was engineered so that the activity of T7 RNA polymerase could be accurately controlled by T7 lysozyme which allows optimization of overexpression of any membrane protein (Wagner *et al*, 2008). The use of Mistic, a *Bacillus subtilis* protein that spontaneously associates with the inner membrane, bypassing the cellular translocon machinery, has also been investigated. Mistic has been used as an N-terminal fusion tag to membrane proteins in *E. coli* to facilitate targeting of the protein to the membrane, resulting in an increase in the protein yield (Roosild *et* al, 2005; Kefala *et al*, 2007; Dvir and Choe, 2009).

6.1.2 Insect cells

Insect cells provide an alternative system for membrane protein over-expression that is better designed for the expression of eukaryotic proteins for a number of reasons including their ability to perform post-translational modifications such as glycosylation and the formation of disulphide bridges which are important for protein trafficking and structure respectively. Although the process of glycosylation in insect cells does not directly replicate that which is

noted in mammalian cells (i.e. No/little complex glycosylation), it is much closer to the natural modifications that occur in mammalian cells compared with bacterial or yeast systems (Rendic *et* al, 2008). In addition, the lack of complex glycosylation may prove to be an advantage in terms of protein structure determination as reducing complex glycosylation reduces protein heterogeneity and improves the formation of ordered crystals (Chang *et al*, 1993). However the respective yield of membrane protein produced in insect cells compared to *E. coli* is sufficiently lower, with many membrane proteins being produced at < 0.1% of the total membrane protein compared to 1 - 10 % in *E. coli*. This is increased even further in Mistic *E. coli* strains (3-20%) (Bernaudat *et al*, 2011).

6.1.3 Mammalian cells

Mammalian cells represent the most appropriate host for heterologous expression of mammalian membrane proteins as they possess all the machinery necessary to modify and traffic the proteins to the cell surface. However the addition of complex glycans to membrane proteins can often be deleterious for crystal formation and thus structure determination (Chang *et al*, 1993). In light of this, the GnTI- cell line was developed which lacks the tools to perform complex glycosylation and thus proteins only undergo core glycosylation (Reeves *et al,* 2002). A disadvantage of using mammalian cells is their higher cost to maintain than *E. coli,* yeast and insect cells. In addition they often produce low yields of heterologous membrane proteins (Gan *et al*, 2006; Allen *et al*, 2009).

6.1.4 Cell free systems

A relatively new system that is being developed for the rapid, efficient production of membrane proteins is a cell-free expression system. A cell-free expression system is an *in vitro* tool that consists of all the components required for the production and expression of proteins without the involvement of a live cell. Cell-free systems are useful for studying biological reactions because they minimize the other interactions that are found in a cell (Jackson *et al*, 2004). The use of a cell-free system eliminates problems with cell toxicity and reduces problems with proteolytic degradation. In addition it is possible to supply high levels of cofactors, ligands etc into the reaction. One of the largest advantages of a cell free system is the ability to directly express membrane proteins into hydrophobic or membrane-mimetic environments such as detergents which may facilitate functional folding of the protein (Reckel *et al*, 2010). One example of the use of an *E. coli* cell-free system was for structural determination of the TM domains of three classes of *E. coli* histidine kinase receptors using

NMR analysis – ArcB, QSeC and KdpD at a resolution of 2.7 – 3.2 Å (Maslennikov *et al*, 2010). Recently, the crystal structure of diacylglycerol kinase, an integral membrane enzyme, was solved at a resolution of 2.28 Å using cell-free expression and crystallisation in lipid mesophases (Boland *et al*, 2014). Other structures solved using cell-free expression systems include Acetabularia rhodopsin II from marine alga at 3.2 Å (Wada *et* al, 2011), the *E. coli* EmrE multidrug transporter at a resolution of 4.5 Å (Chen *et al*, 2007) and an integral membrane enzyme diacylglycerol kinase at 2.28 Å (Boland *et al,* 2014). However, the number of membrane protein structures that have been solved using these systems remains extremely low.

6.1.5 *Drosophila melanogaster*

The main problems that are faced regarding heterologous expression of membrane proteins for structural studies are host toxicity, incorrect protein folding, protein heterogeneity and low expression yields and thus high costs to obtain high yields of protein. The use of *Drosophila melanogaster* as a membrane protein expression system overcomes many of these problems. It has been shown that expression of a number of membrane proteins can be tolerated by the *Drosophila* photoreceptor cells without any noteable effects on the fly itself. In addition, the expression levels of endogeneous rhodopsin do not seem to be affected (Panneels *et al*, 2011) which is important for the structural integrity of the rhabdomere (Kumar and Ready, 1995). Panneels and colleagues demonstrated that high yields of a number of different membrane proteins (a mixture of GPCRs, transporters and channels) could be obtained by expression in the fly eye under control of a *GMR-Gal4* driver (0.2 – 0.4 mg per 10,000 flies) (see Table 4.1). In combination with the cheap cost of fly maintenance, this makes it viable to obtain enough protein for crystallization and structural studies. However, the data presented in this thesis show that the yield of purified rP2X2 and rPanx1 channels was much lower than that shown by Panneels *et al* for other membrane proteins. The low yields of rP2X2 and rPanx1 obtained (approx. 1 µg per 500 flies - Chapter 4) significantly hinders the use of this system for the production of enough protein for 3D-crystallization trials. However, it is possible that if the membrane protein extraction and purification procedures are fully optimized, the yield could be significantly improved. For example, protein may be lost during detergent solubilisation of the membranes (see section 6.2). Alternatively there are stages where some protein may be lost during purification including protein that doesn't bind efficiently to the anion resin during ion exchange chromatography and protein that doesn't bind to the nickel beads during IMAC. To improve binding of protein to the anion resin, the buffers need to be optimised to maximise

binding but in addition, a column with a larger binding capacity would ensure that all the protein is able to bind. Buffers and conditions such as temperature would also need to be optimised to ensure maximum binding of His-tagged protein to nickel beads. However, for more efficient protein purification, using an alternative tag for purification purposes such as the Strep-tag may provide a means of a one-step purification procedure and this would significantly reduce the amount of protein lost at various stages of the lengthy purification procedure.

rP2X2 appeared to undergo high mannose glycosylation but no complex glycosylation in *Drosophila*; consequently, expression in this system overcomes the obstacle of the heterogeneous populations of protein that are often obtained with mammalian expression systems. Another significant advantage of using *Drosophila* as a host system of P2X receptors is the capacity to ensure that the protein is functional using electrophysiological recordings (chapter 5). As the protein is known to be functional, and responsive to its ligand, ATP, at least a proportion is correctly folded and targeted to the cell surface. Providing that the yield of protein can be significantly improved (see above), the fruit fly provides a promising new system for membrane protein expression.

6.2 Detergent solubilisation of membrane proteins

For the majority of structural studies of membrane proteins, it is vital that they are successfully reconstituted in a suitable detergent. Finding a detergent that can efficiently extract the protein from the membrane while maintaining it in a fully folded, functional state is a significant challenge. There are a large number of different types of detergents available; broadly classified into ionic detergents, non-ionic detergents and zwitterionic detergents. Ionic detergents, e.g. SDS, contain a charged head group and a hydrophobic hydrocarbon chain. Although ionic detergents tend to be very effective at removing and solubilising membrane proteins from the lipid bilayer, they are generally denaturing and are thus rarely useful for structural studies. Non-ionic detergents, e.g. DDM, consist of an uncharged head group and a hydrophobic hydrocarbon chain. Non-ionic detergents are often chosen to reconstitute membrane proteins for structural studies as they generally break protein-lipid interactions with little effect on protein-protein interactions, therefore they are usually non-denaturing. Zwitterionic detergents, e.g. CHAPS, have a net zero charge arising from both positive and negatively charged groups. Zwitterionic detergents are often used for structural studies but are can be more deactivating than non-ionic detergents (Seddon *et al*, 2004).

Generally, detergents with shorter alkyl chains are more disruptive to the membrane (Privé, 2007). In addition, detergents that form small micelles (e.g. n-octyl-β-D-glucoside or n-octyl-β-D-maltoside) may not completely cover the hydrophobic regions of the membrane protein, thus causing protein aggregation. However, the small micelle size allows for more of the protein to be exposed to form protein-protein interactions which makes them more desirable for the formation of crystal-lattices (Gutmann *et al*, 2007). In light of this, a relatively large number of membrane protein structures have been solved using small micelle detergents. For example, 161 structures have been solved using n-octyl-β-D-glucoside (Membrane protein databank, accessed 27/09/14) (Raman *et al*, 2006).

DDM, a non-ionic detergent with a 12-carbon hydrocarbon chain, is a particularly popular choice of detergent used for membrane protein solubilisation due to its ability to reconstitute many membrane proteins in their functional state; 150 structures have been published in the membrane protein databank using DDM for solubilsation (accessed 27/09/14). However, DDM forms large micelles which means less of the protein is exposed and able to form protein-protein interactions, this can interfere with crystallisation; nevertheless it has been used successfully in a number of cases (Gutmann *et al,* 2007; Huang *et al*, 2003, Hattori and Gouaux, 2012). Concentrations much higher than the CMC of DDM are required for protein solubilisation (i.e. DDM CMC = 0.009% but proteins are often solubilised in 1 – 4% DDM). This is often the case for long-chain detergents (Privé, 2007). DDM has been used for the solubilisation of a number of different P2X receptors (Sim *et* al, 2004; Mio *et al*, 2005; Mio *et* al, 2009; Kawate *et al*, 2009; Valente *et al*, 2011). The data in this thesis has also demonstrated its ability to solubilise hP2X4-GFP and zfP2X4-GFP from the membrane and potentially maintain their oligomeric structures (chapter 3).

FC-12 is an zwitterionic detergent with a 12 carbon hydrocarbon tail and although efficient at membrane protein solubilisation, it is often denaturing. To date, only 3 crystal structures have determined in the presence of FC-12; the OmpF porin (3.8 Å) (Kefala *et al*, 2010), the zinc transporter YiiP (DDM was also present in the crystallisation sample) (Lu and Fu, 2007) and rat monoamine oxidase A (Ma *et al*, 2004). However, FC-12 has been commonly used in NMR studies (Raman *et al*, 2007).

A study by Newstead and colleagues analysed the expression of 43 eukaryotic membrane proteins in *S. cerevisae* and showed that 70% of the well-expressed proteins were stable, correctly targeted and monodisperse in either DDM or FC-12 (Newstead *et al*, 2007).

Triton-X-100 is a non-ionic detergent that is often used in combination with a mild, non-denaturing zwitterionic detergent such as 3-[(3-cholamidopropyl)dimethylammonio]-1-propanesulfonate (CHAPS). 27 protein structures have been successfully solved in the presence of Triton (Membrane protein databank – accessed 27/09/14) (Kalipatnapu and Chattopadhyay, 2005). However, as Triton is not a homogeneous solution i.e. the length of the hydrophobic tail varies between molecules, it is not an ideal choice for crystallisation of membrane proteins.

The choice of detergent for solubilisation of a membrane protein is extremely important and often complex screening is required to find a suitable detergent. As each protein is very different, each case is specific and there is no detergent that is suitable for the solubilisation of all membrane proteins. To improve the use of the *Drosophila* system for purification of membrane proteins, it would be useful to do a large detergent screen for both rPanx1 and rP2X2 to ensure they are being efficiently solubilised and importantly, not denatured. This will be important for maximising protein yield and maintaining structure for crystallisation. For the purification of rPanx1 for low resolution structural studies by Ambrosi *et al*, 2010, two detergents were used; Sarkosyl (N-Lauryl Sarkosine), an anionic detergent and Brij 58, a non-ionic detergent (Ambrosi *et al*, 2010). DDM was used for the successful solubilisation of zfP2X4 (Kawate *et al,* 2009) and DdP2XA (Valente *et al,* 2011) and thus was a logical choice for the solubilisation of rP2X2.

However, the results in this thesis show that in the presence of DDM, purified rP2X2-GFP from HEK-293 cells does not appear to form stable trimers, though it is possible that the protein is forming trimers but with the dissociated GFP, they cannot be identified using FSEC. It is not known whether this is also the case in *Drosophila* as the protein has not yet been purified to a sufficient level to enable FSEC analysis of the protein. However it is unclear whether (i) P2X2 is not forming trimers in HEK-293 cells, (ii) DDM is not efficient for its solubilisation or (iii) the degradation of GFP makes it impossible to determine the oligomeric state of P2X2 using FSEC. To distinguish between these possibilities, it would be advantageous to perform a large-scale detergent screen to enable the identification of a detergent that can maintain the trimeric structure of P2X2. In addition, if DDM is not efficient at solubilising P2X2 from the membrane, it may be causing a reduction in the yield of P2X2. To decipher whether the peak observed is indeed that of free GFP, the purified protein could be separated by SDS PAGE and detected with a P2X2 antibody and a GFP antibody to see if the expected bands are observed. A small-scale detergent screen was performed on rPanx1-GFP purified from both HEK-293 cells and

from *Drosophila*. This screen showed that the detergents FC-12 and Triton were efficient at extracting Panx1 channels from the membrane. FC-12 was chosen for solubilisation of Panx1 due to the heterogeneous nature of Triton. However, FSEC results show that the majority of Panx1 protein formed dimeric units in the presence of DDM (HEK-293 cells) and FC-12 (*Drosophila*). Although neither system appeared to assemble Panx1-GFP hexamers, it is also possible that both DDM and FC-12 disrupt the channel structure and cause dissociation of the subunits. As with P2X2, to further investigate this, it would be useful to perform a large-scale detergent screen to identify a detergent that maintains the native protein structure.

6.3 Evaluation of the *Drosophila* taste system as a compound-screening system

Many systems have been developed that enable a library of compounds to be tested as novel agonists or antagonists of membrane proteins. Many of these systems use heterologous expression of membrane proteins in cell lines or *Xenopus* oocytes to test the compounds. The *Drosophila* taste system provides a novel, medium throughput drug screening method using electrophysiology that has the advantage of expressing the receptors *in vivo*. In addition, the fruit fly does not naturally express any known P2X receptors, P2Y receptors or Panx channels making it a useful system to study the exogenously expressed receptors in isolation.

6.3.1 Calcium imaging techniques

Calcium imaging techniques are commonly used as drug screening systems for P2X receptors. For example the selective P2X4 antagonists, PSB-12054 and PSB-12062, were discovered using calcium imaging techniques in 1321-N1 astrocytoma cells stably expressing the hP2X4 receptor (Hernandez-Olmos *et al*, 2012). Hernandez-Olmos and colleagues tested the activity of a number of phenoxazine and related acridone and bezoxazine derivatives on P2X4 receptors. This technique involves loading cells with a labelled calcium indicator (in this case, Fluo-4-AM) that exhibits an increase in fluorescence when bound to Ca^{2+}. Upon activation of P2X4, calcium influx causes an increase in cell fluorescence and the activity of the receptor can be monitored. The calcium imaging technique can be performed in a number of different ways, one of which involves plating cells onto a 96 well plate; this technique allows relatively medium throughput compound screening as multiple compounds can be tested with each plate. However, although this technique is higher-throughput than other electrophysiology techniques (see section 6.3.2), it is much less sensitive (Wood *et al*, 2004). In addition, when testing the activity of P2X receptors using calcium imaging, it is essential that the cell does not express any endogenous P2X or P2Y receptors as they would cause an increase in intracellular calcium in response to

ATP, making it difficult to study the effects of the exogenously expressed protein. Commonly used cells such as HEK-293 cells cannot be used without first blocking the activity of the endogenous P2Y receptors. This can be done using an IP_3 blocker such as 2-APB which prevents the release of calcium from intracellular stores (Maruyama *et al*, 1997).

6.3.2 *In vitro* electrophysiology techniques

Patch-clamp electrophysiology techniques have been commonly used to test the function and to characterize P2X receptors in cell culture e.g. in HEK cells (Li *et al*, 2008). Patch clamp recordings involve placing an electrode, with an open tip of about 1 µm, at the edge of the cell membrane using a micro-manipulator, creating a high-resistance seal with the cell. The electrode is filled with a solution with a similar composition to the cytoplasm and a silver wire responsible for recording the electric current is placed in contact with this solution. Compounds can then be added to the solution to investigate the activity of ion channels. Electrophysiology techniques can be used to test the activity of multiple compounds as potential P2X agonists or antagonists. For example Grubb and Evans tested the effect of various P2X agonists on P2X2 receptors using electrophysiological experiments in cultured adult rat dorsal root ganglion cells (Grubb and Evans, 1999). However the technique is technically challenging and relatively low throughput; to test multiple agonists/antagonists, lengthy time intervals were necessary between applications (see Section 5.4.10 for more details). In addition, run-down is a common problem faced when using the patch clamp technique on P2X receptors; the current amplitude decreases upon successive agonist applications (Lewis and Evans, 2000). These factors contribute to the relatively low throughput of this system; it is better used to fully characterise 'hit' compounds after they have been discovered using other screening protocols.

Automated patch-clamp electrophysiology techniques have been developed that allow a more high-throughput approach for screening compounds (for example the PatchXpress 7000A is estimated to obtain 2,000 data points per day – Wood *et al*, 2004). The first step in the development of automated methods for patch-clamp of mammalian cells was the discovery that a planar substrate could replace a glass micropipette and thus a seal could be formed by bringing the cell to the substrate; this removed many of the difficult technical requirements and time consuming components associated with patch-clamp electrophysiology. Many of the devices that take advantage of this use multiwell plates so that multiple compounds can be screened simultaneously. However, there are problems associated with these systems. For example, a seal may not be formed in every single well, resulting in a success rate of <100%

and so data needs to be analysed carefully. In addition the machinery required to perform automated patch clamp electrophysiology is costly (Wood *et al*, 2004).

6.3.3 Electrophysiology on *Xenopus oocytes*

Xenopus oocytes represent a popular system used for the screening of compounds on the activity of P2X receptors with many of the key agonists and antagonists identified using this system (Pintor *et* al, 1996; King *et* al, 1997; Liu *et* al, 2001; Wildman *et al*, 2002; Baqi *et al*, 2011). In addition, the recently identified P2X2 specific antagonists, PSB-12011 and PSB-1011 were identified following a screen of anthraquinone derivatives on P2X2 expressed in *Xenopus* oocytes (Baqi *et al*, 2011). However the use of this system for compound screening is relatively low throughput. The advantages and disadvantages of using this system has been summarized in more detail in Section 5.4.10.

6.3.4 The *Drosophila* taste system

This thesis aims to highlight the potential use of the *Drosophila* taste system as a useful and novel method to screen the activity of compound libraries on P2X receptors. The data shows that the system can be used in this way as 80 compounds from an adenosine nucleotide library were tested on P2X2 expressed in the nervous system of *Drosophila* (chapter 5). Using this system, approximately 12 compounds were tested per day (with an n=3 for each compound). However, this number is likely to rise upon increased experience using the system. There was a large variation in response from the 80 compounds tested; specifically three compounds were highlighted that appear to be agonists of rP2X2 (2F-ATP, ATPαS and ATPγS). Although the latter two have already been characterized as P2X2 agonists (King *et al*, 1997; Liu *et al*, 2001), it was the first time 2F-ATP was demonstrated to be a rP2X2 agonist. The basal response to the solvent control, TCC, was significantly higher in flies expressing P2X2 compared with control flies. Possible reasons for this were that (i) P2X2 undergoes some activation in the absence of an agonist or (ii) there is some spontaneous ATP release in the fly resulting in channel activation (see section 5.3.1). A number of compounds (8-[(4-Amino)butyl]-amino-ATP, N6-(6-Amino)hexyl-dATP, N6-(6-Amino)hexyl-ATP and AP5A) elicited a response substantially lower than that of TCC. Thus one possibility, as previously mentioned, is that these compounds are acting as antagonists - blocking the activity of P2X2 and preventing any spontaneous channel opening. Although this needs to be further investigated to determine whether or not this is the case, it may represent the first system whereby compounds can be tested as agonists or antagonists in the same screening protocol.

However, there are still a number of problems to overcome for this system to be used as a medium throughput screening technique, including the large variation of responses observed between different flies which could result in false-positive results. The variation between sensilla may be as a result of the expression pattern of the receptors within the sensillum; thus if they can be localized to the tip of the sensillum, this may decrease the variation (see section 5.3.3). In addition, once localized to the tip, each compound will only need to be applied for 2 - 3 seconds largely speeding up the process of compound screening and allowing the testing of an estimated 20-30 compounds per day (with an n=3 for each compound), making the system more viable for testing large numbers of compounds. These localization experiments are vitally important for the future of this system.

6.4 Conclusions and future directions

In this thesis, it has been shown that rP2X2-GFP and rPanx1-GFP can be expressed in both the *Drosophila* eye and nervous system under control of the *Gal4-UAS* system. rP2X2-GFP underwent high-mannose glycosylation in the fly (Fig 4.8) and was shown to be functional (Fig 5.6) indicating that despite having no endogenous P2X receptors, the fly is capable of expressing, folding and trafficking functional P2X2 receptors. However, the conclusions regarding the state of rPanx1-GFP in the fly were less easily ascertained, as it did not appear to undergo N-linked glycosylation in the fly (Fig 4.8) and the function has not been tested. In addition, our gel filtration data indicated that rPanx1-GFP did not form stable hexamers in either HEK-293 cells or *Drosophila* eyes (Fig 4.14) suggesting either that hexamers are not the biologically functional unit of this protein, it may not be correctly folded or detergent solubilisation is inefficient. In contrast, TEM analysis indicated that the protein formed hexameric units in the *Drosophila* eye (Fig 4.17). However due to the assumptions made regarding the shape and density of the protein, this needs to be investigated in more details for any conclusive details on the state of rPanx1-GFP. Despite the low rP2X2 and rPanx1 protein yields obtained following purification, if the protein is of sufficient quality, it may still be useful for low-resolution structural studies. In the future, it would be useful to add an alternative tag such as a Strep-tag to the receptors before expressing them in *Drosophila*, allowing purification via Streptactin, which may prove to be a more efficient purification technique in *Drosophila* and therefore provide a higher protein yield.

The expression of rP2X2 in the nervous system of *Drosophila* also enabled its function to be tested. The data showed that flies expressing rP2X2 respond to ATP whereas control flies do not respond indicating that the channel is trafficked to the cell surface and folded in the

Drosophila taste system (Fig 5.6). An ATP dose response curve was generated for the response of flies expressing rP2X2 in both the nervous system (*C155-Gal4*) and the sugar neurons (*Gr5a-Gal4*) (Fig 5.7). There was a dose-dependent increase in response to ATP, however, the ATP concentration required to activate rP2X2 was higher than what has been recorded in other systems, possibly due to the distribution of P2X2 in the sensillum. The function of rP2X2 in *Drosophila* led to the use of the *Drosophila* taste system as a new, medium-throughput system for screening of compound libraries, in a search for novel P2X2 agonists. The data in this thesis shows that large compound screens can be performed by expressing rP2X2 in the taste system. The response of rP2X2 to 80 adenosine nucleotides was investigated using the taste system. Three nucleotides were shown to activate P2X2 at similar levels to ATP; these were ATPγS, ATPαS and 2F-ATP. In addition to uncovering an unknown P2X2 agonist, 2F-ATP, it provided information on many of the molecular aspects of the ATP molecule that appear to be important for binding to rP2X2 (see section 5.4.3). For example, it appeared that any alteration to the ribose moiety caused a significant reduction in agonist potency, whereas some phosphate or adenine alterations could be tolerated. It was also noted that the receptor has not only evolved to respond to specifically to ATP, but has evolved to not respond to the commonly co-occurring molecules ADP and AMP (Fig 5.11). In the future this system could also be adapted to speed up the process of testing compounds by localizing the P2X2 receptors to the tip of the taste hair. In addition, other P2X receptors such as P2X1 and P2X3 could be expressed in this system in a search for novel agonists at these receptors.

Appendix I – Standard curves

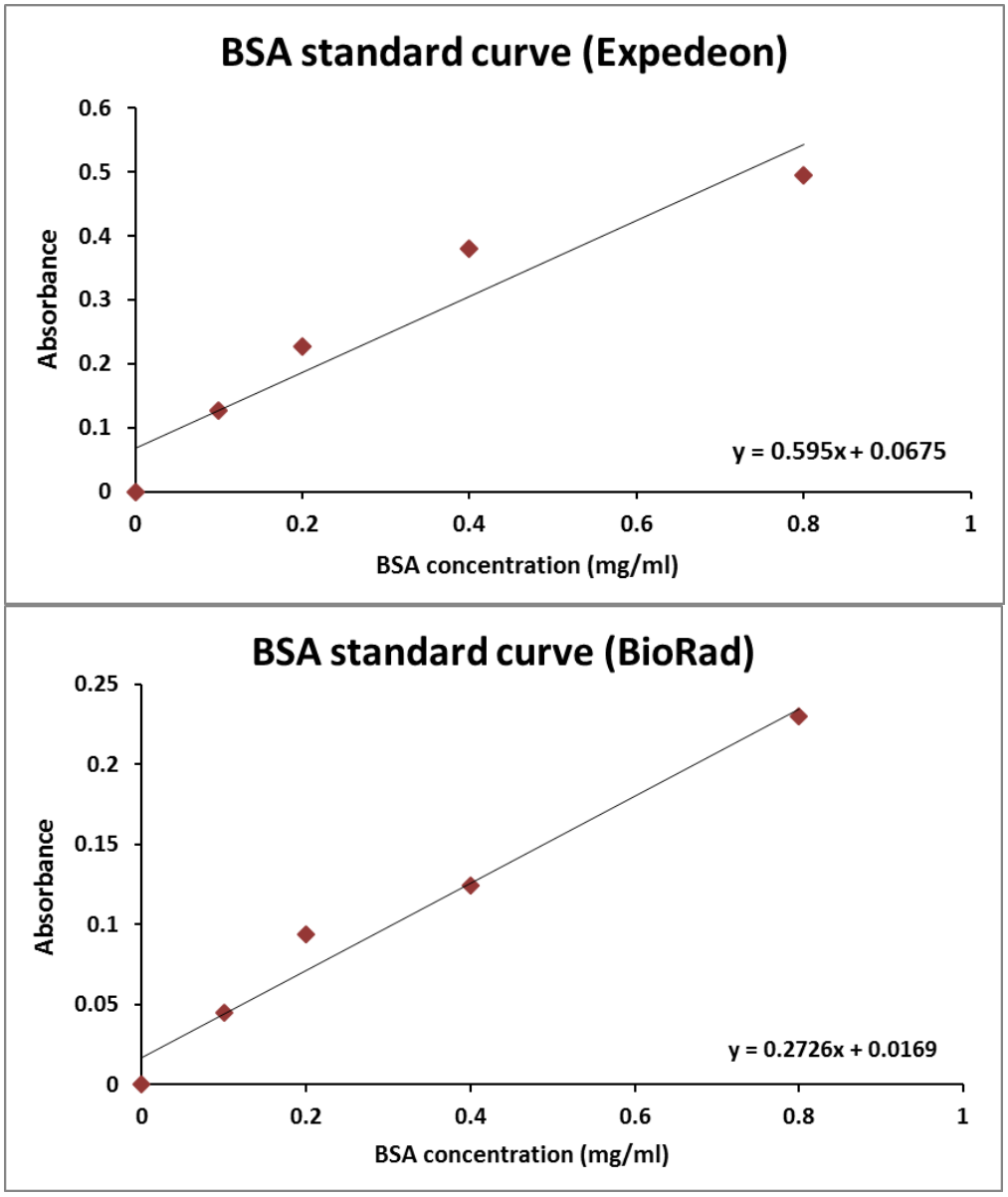

Figure App. 1 – BSA standard curves - BSA standard curves (BSA concentration vs. absorbance at 595 nm) shown for Expedeon Bradford Ultra (top) and BioRad protein assay reagent (bottom).

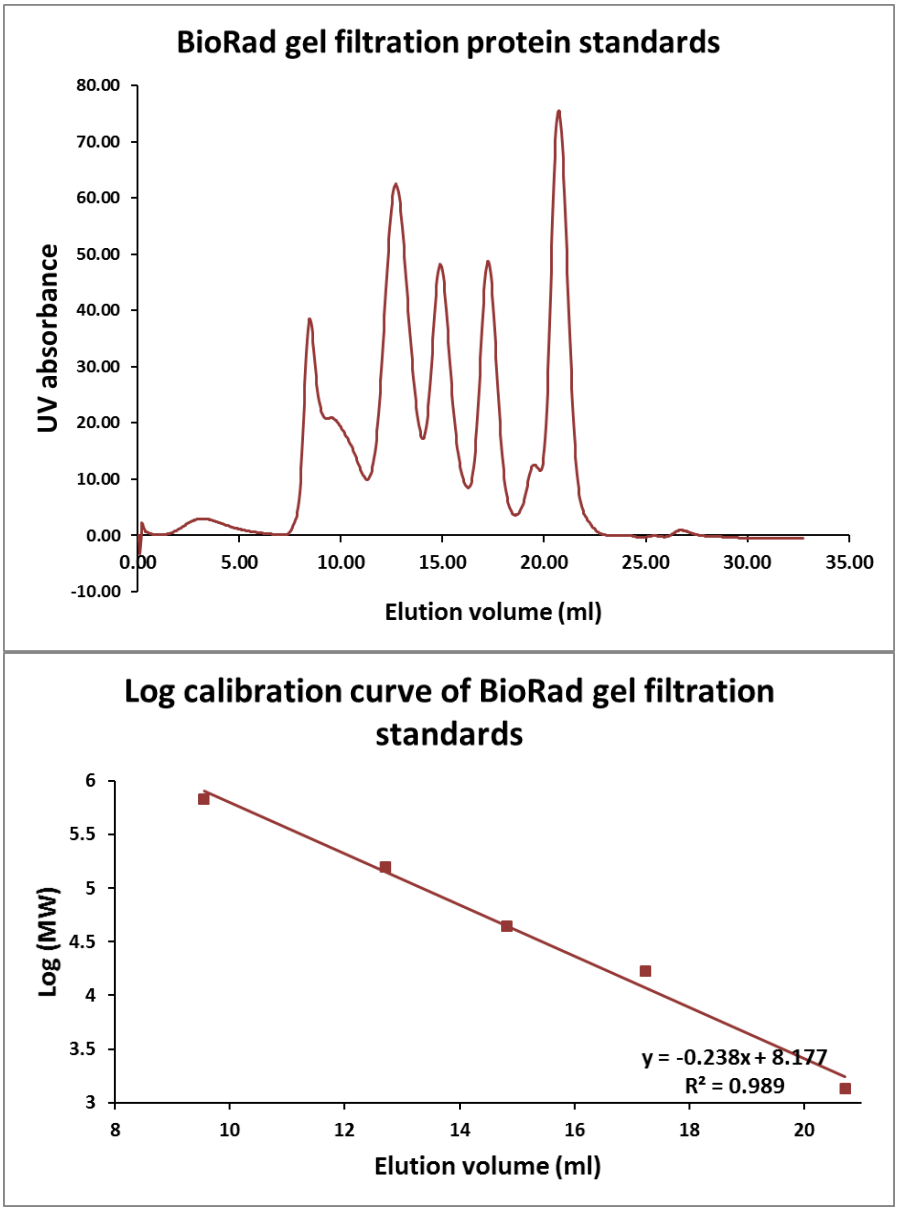

Figure App. 2 – Gel filtration protein standards (A) Elution of BioRad gel filtration standards on Superdex200 columns. Peaks correspond to thyroglobulin, bovine γ-globulin, chicken ovalbumin, equine myoglobin and vit B12 from left to right respectively. (B) Standard curve plotting LogMW of standard against elution volume.

Appendix II – Construct maps

pL118

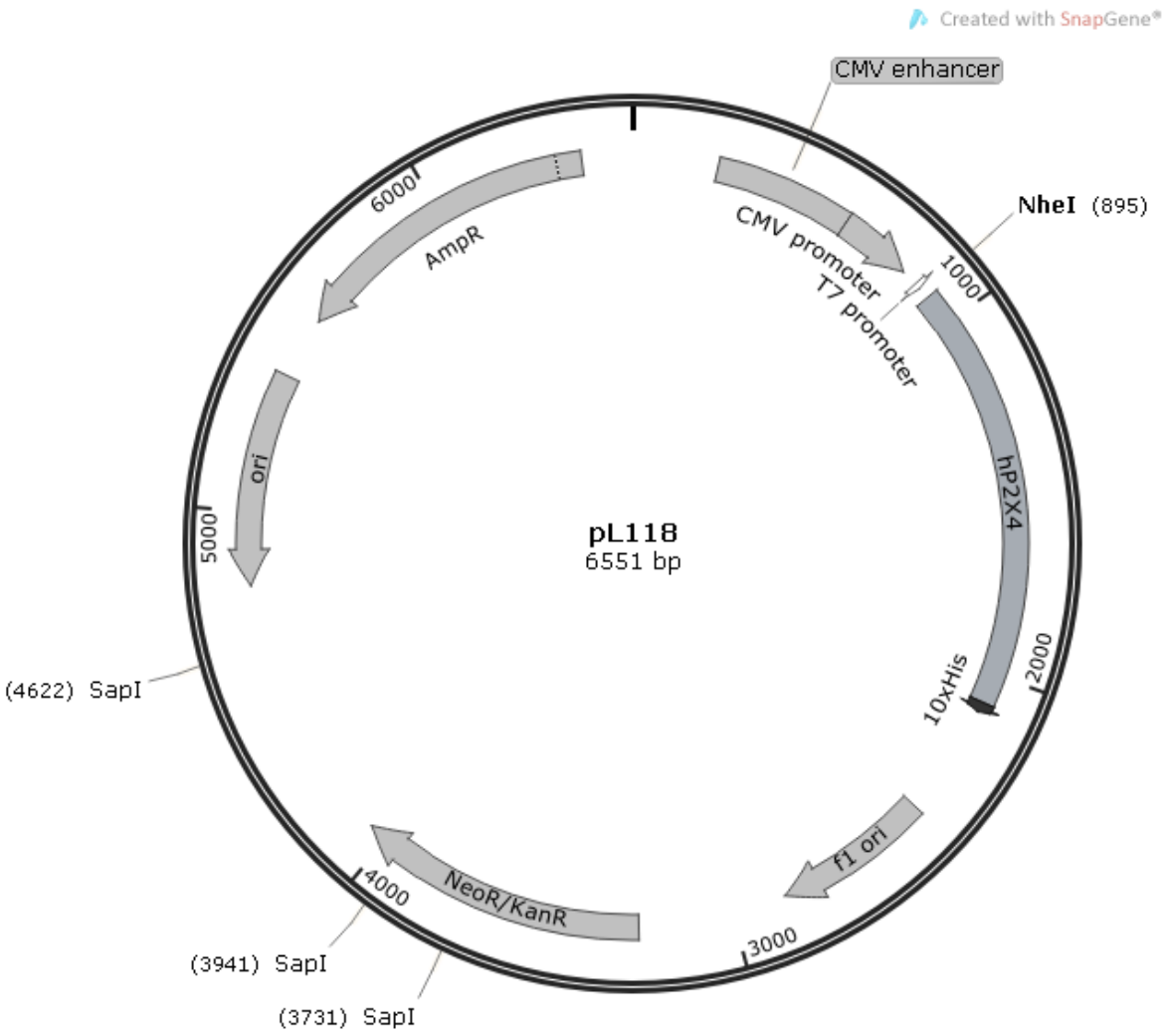

hP2X4-int-CBD

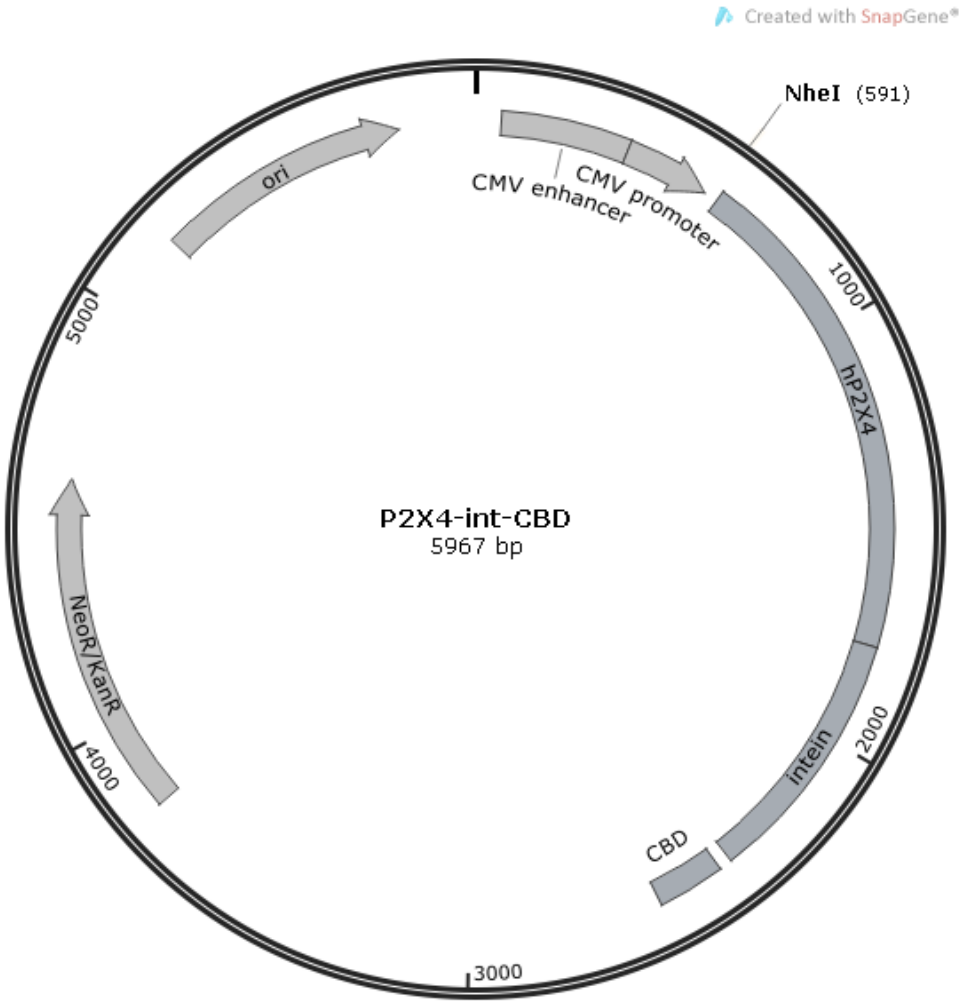

p927

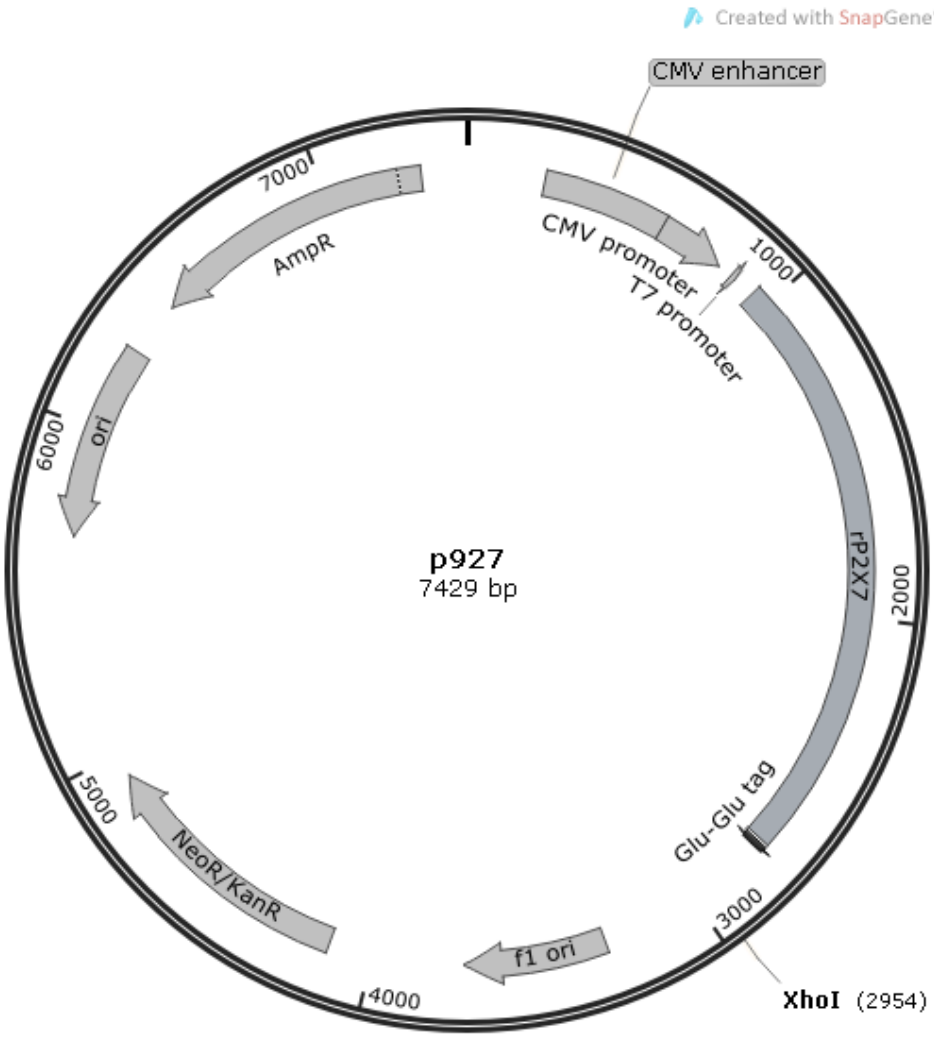
Created with SnapGene®
CMV enhancer
CMV promoter
T7 promoter
1000
rP2X7
2000
Glu-Glu tag
3000
XhoI (2954)
f1 ori
4000
NeoR/KanR
5000
ori
6000
AmpR
7000
p927
7429 bp

hP2X4-GFP

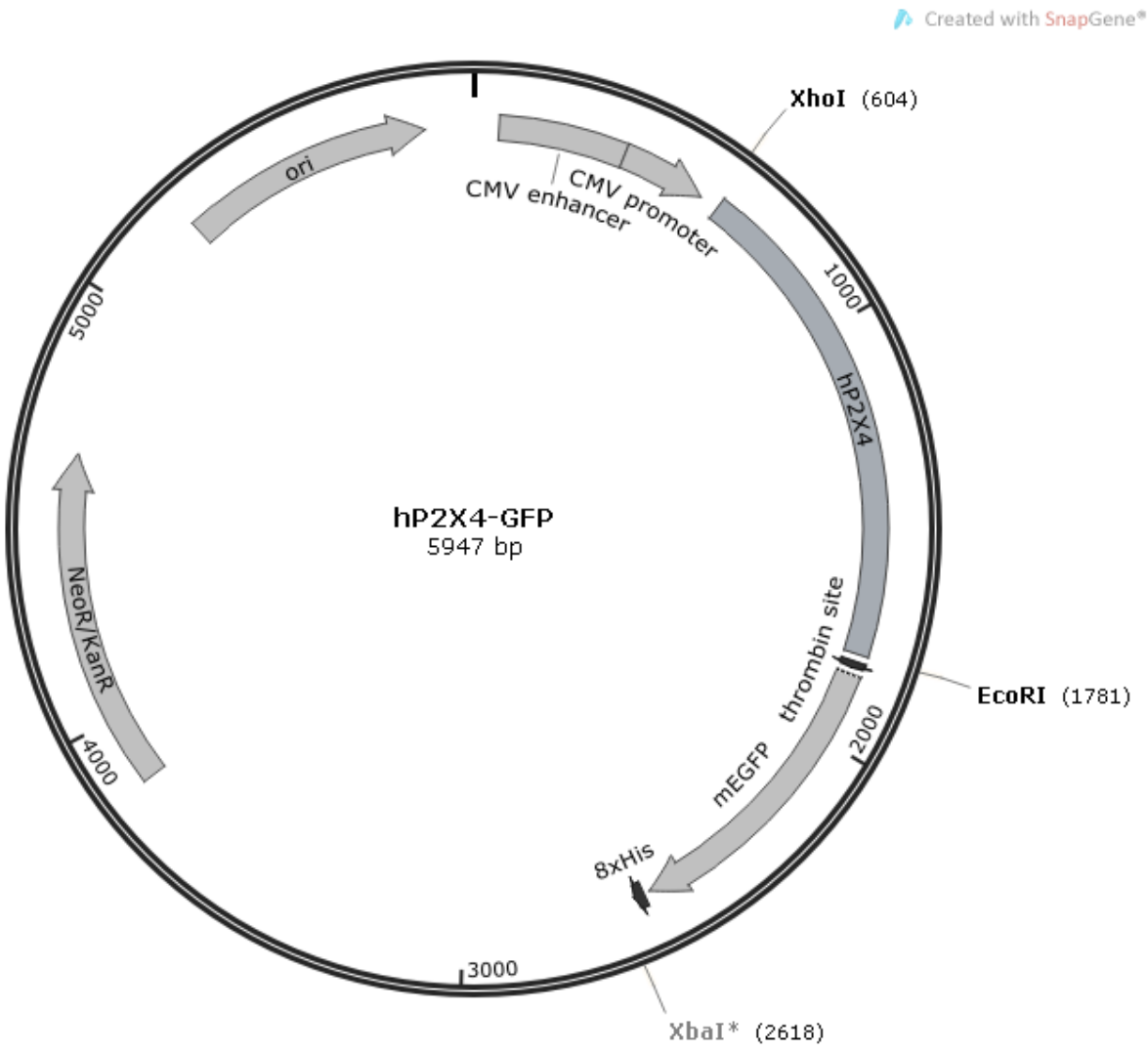
Created with SnapGene®
XhoI (604)
ori
CMV enhancer
CMV promoter
1000
hP2X4
thrombin site
EcoRI (1781)
2000
mEGFP
8xHis
3000
XbaI* (2618)
4000
NeoR/KanR
5000
hP2X4-GFP
5947 bp

rPanx1-GFP

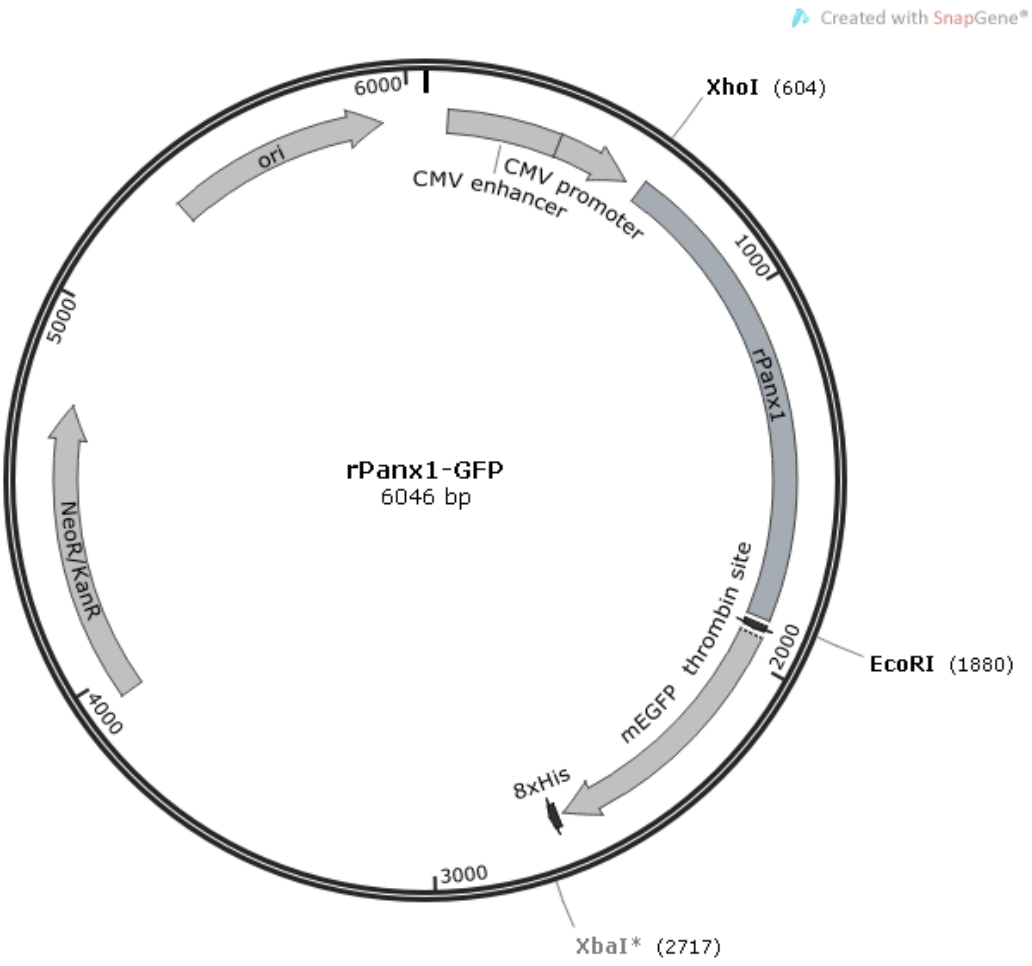
Created with SnapGene®
6000
XhoI (604)
ori
CMV enhancer
CMV promoter
1000
5000
rPanx1
rPanx1-GFP
6046 bp
NeoR/KanR
thrombin site
mEGFP
2000
EcoRI (1880)
4000
8xHis
3000
XbaI* (2717)

rP2X2-GFP

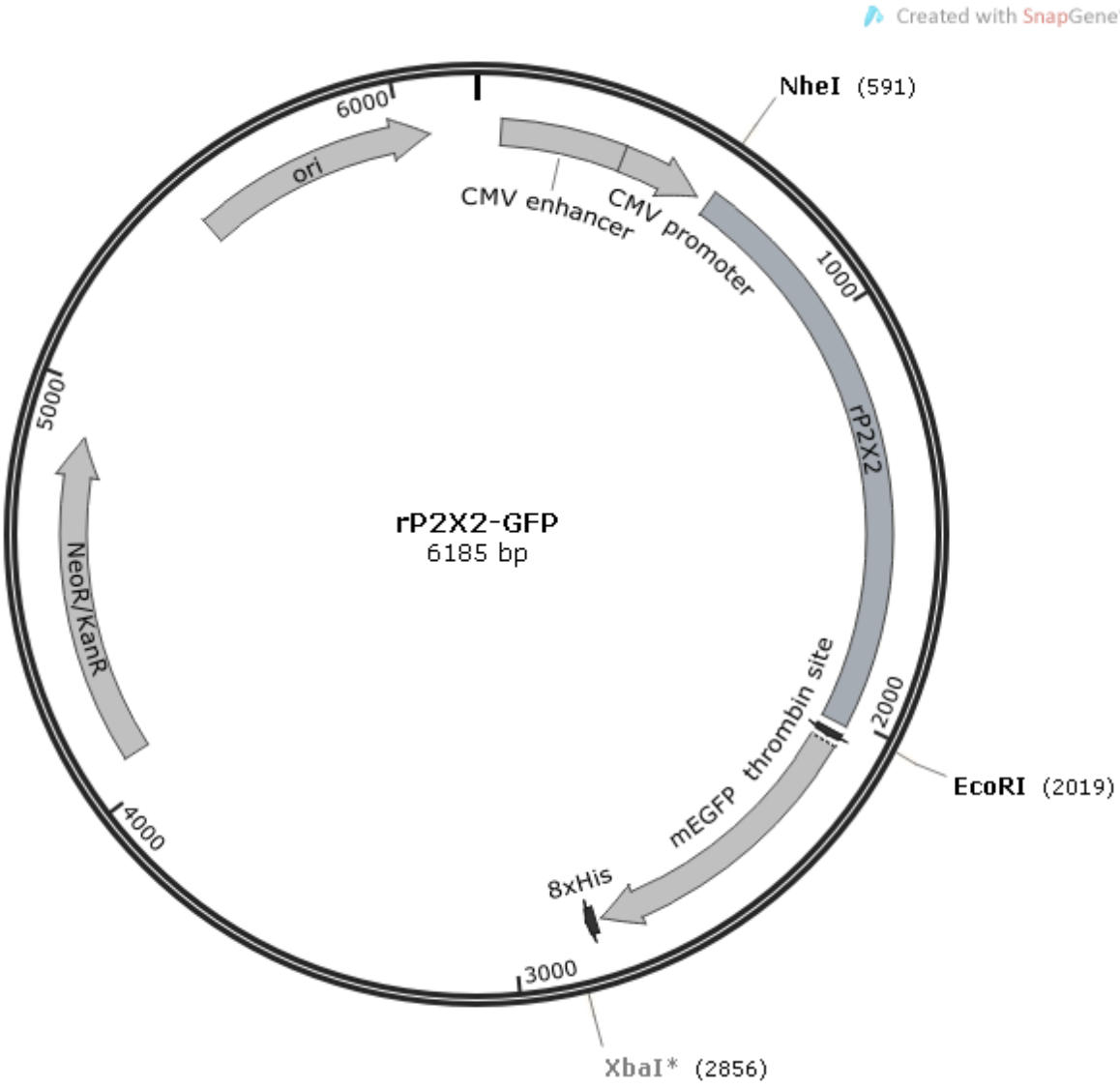
Created with SnapGene®
NheI (591)
6000
ori
CMV enhancer
CMV promoter
1000
rP2X2
5000
rP2X2-GFP
6185 bp
NeoR/KanR
mEGFP
thrombin site
2000
EcoRI (2019)
4000
8xHis
3000
XbaI* (2856)

rP2X7-GFP

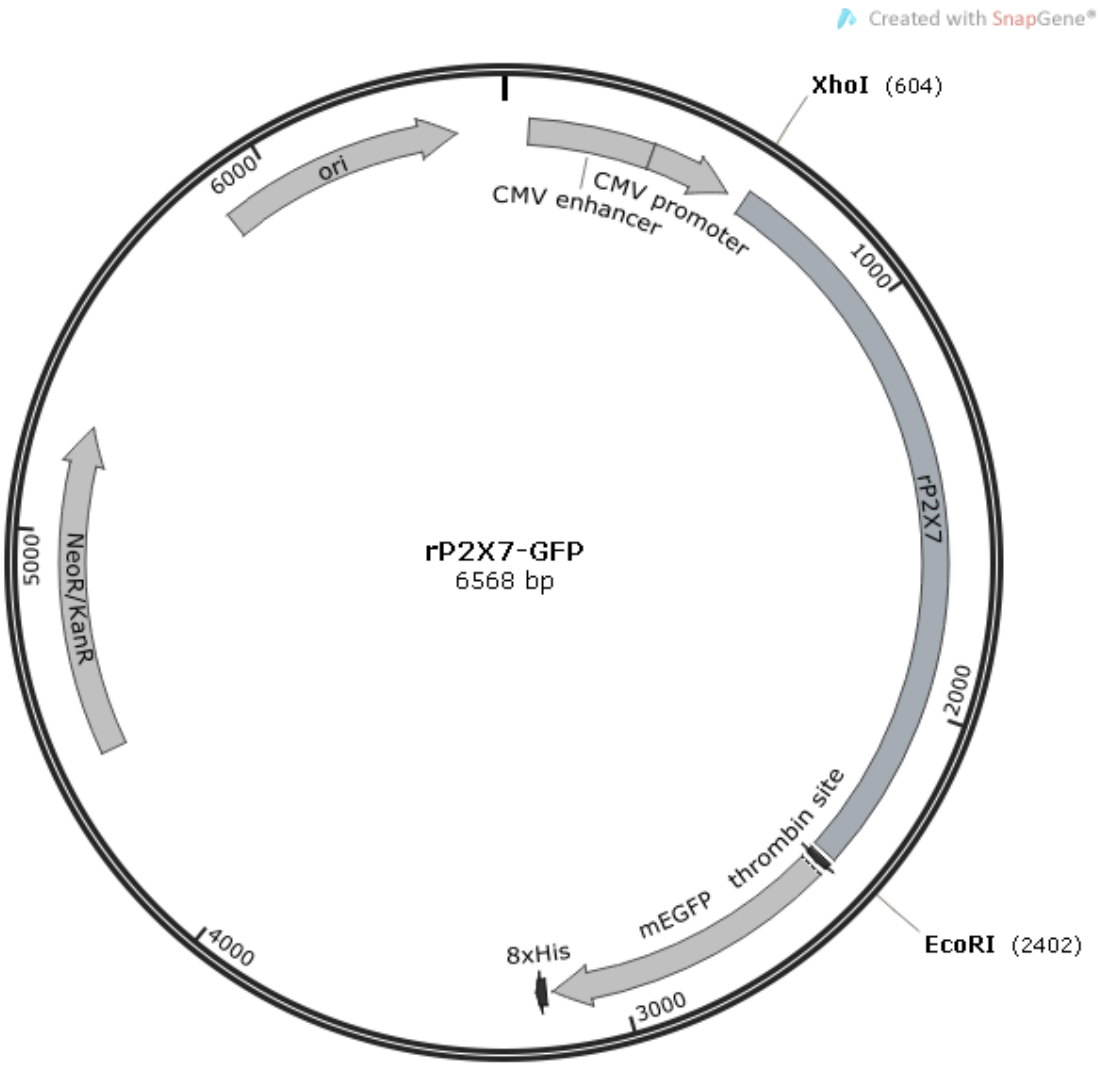
Created with SnapGene®
XhoI (604)
6000
ori
CMV enhancer
CMV promoter
1000
rP2X7
2000
EcoRI (2402)
3000
8xHis
mEGFP
thrombin site
4000
5000
NeoR/KanR
rP2X7-GFP
6568 bp

UAS-hP2X4-his

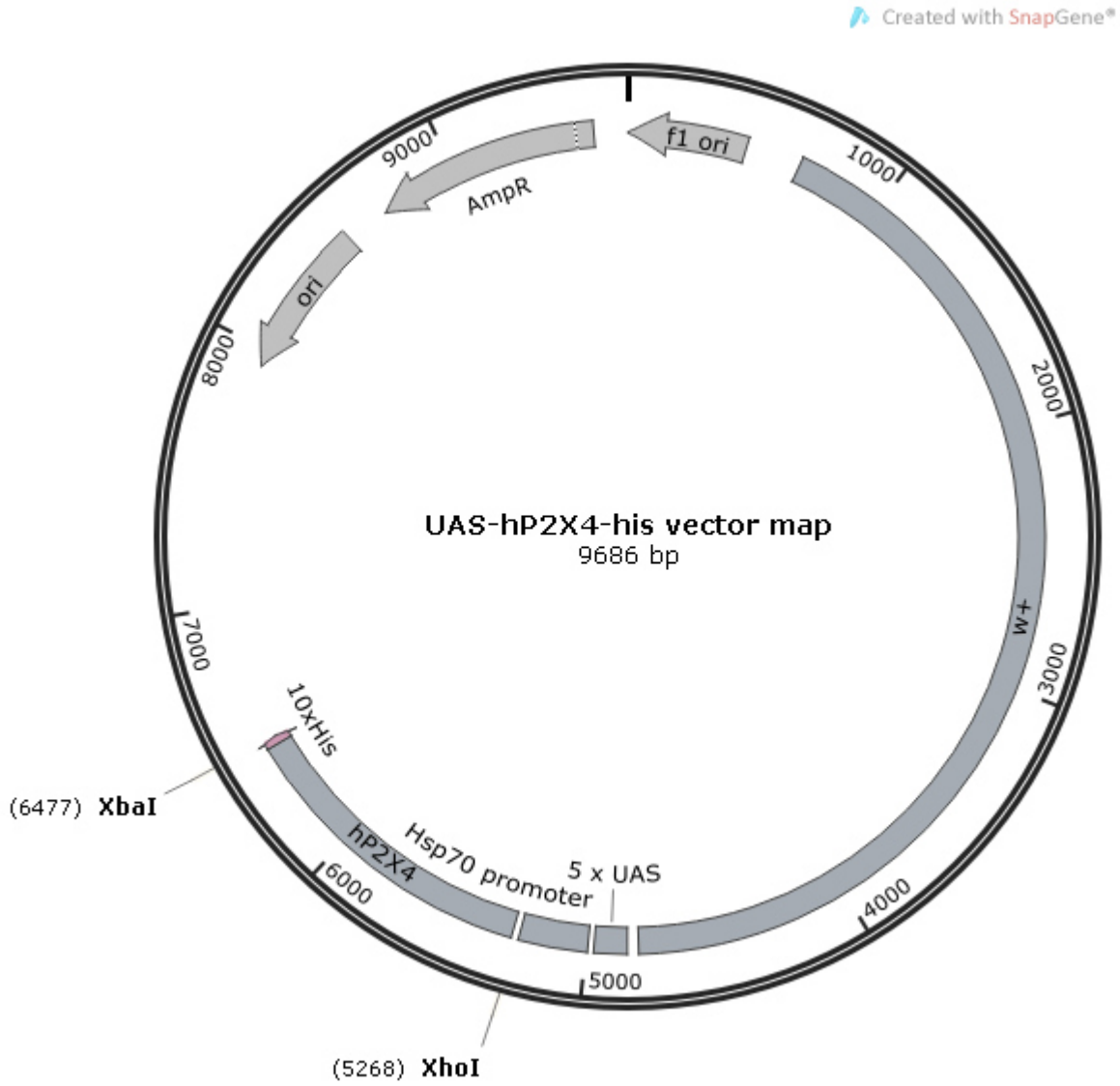

UAS-hP2X4-GFP

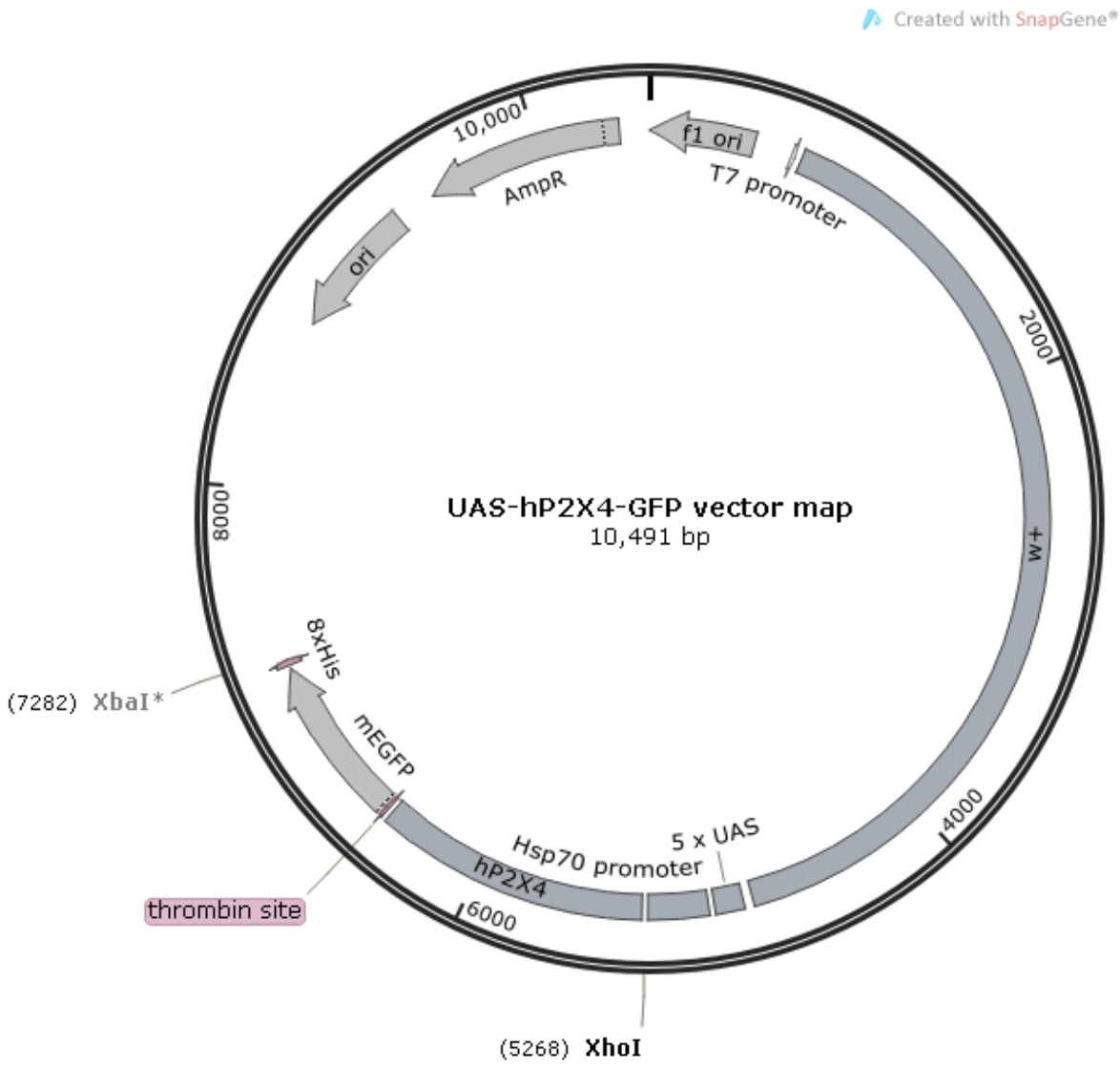

UAS-rP2X2-GFP

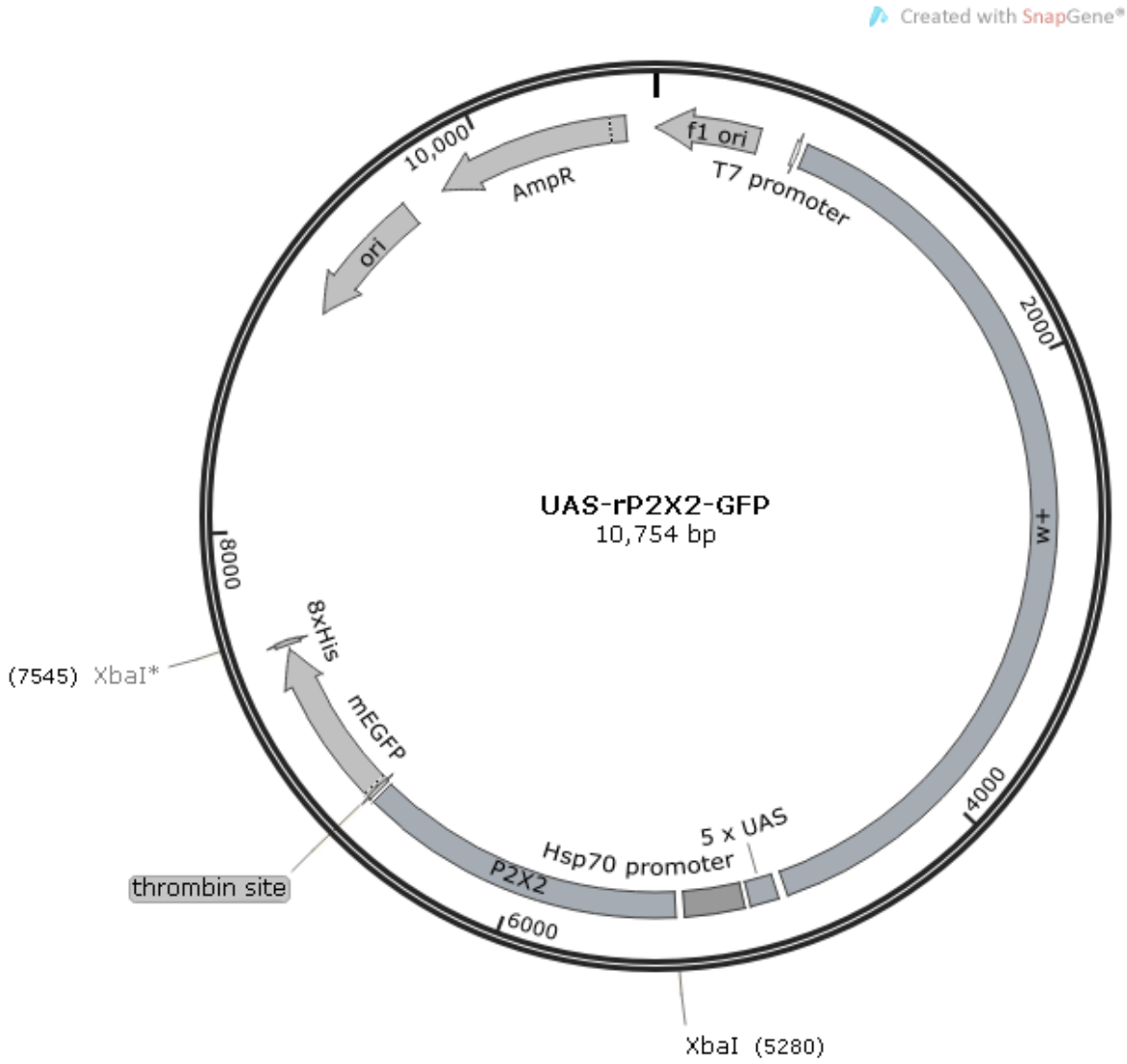

UAS-rPanx1-GFP

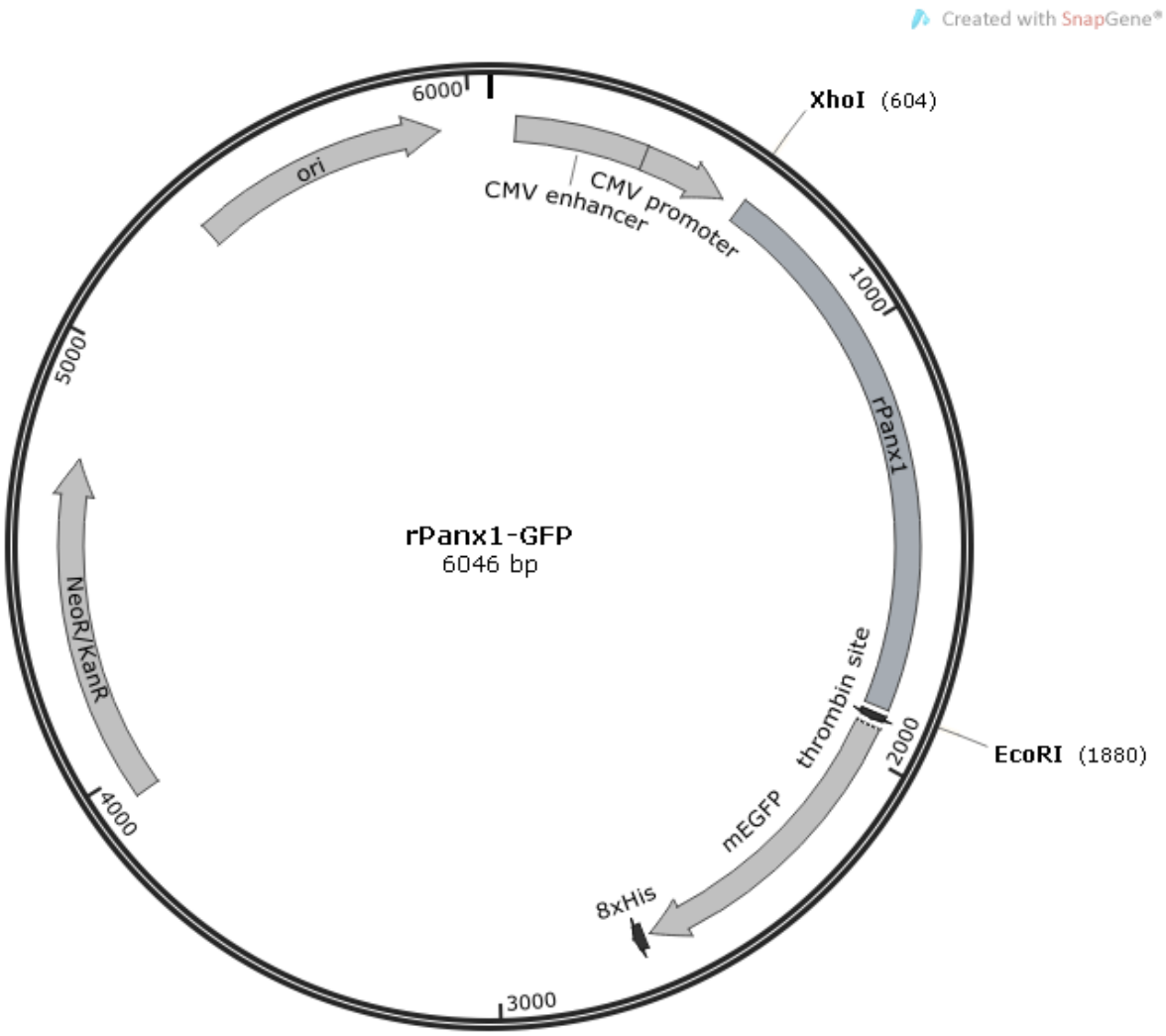

UAS19-rP2X2-GFP

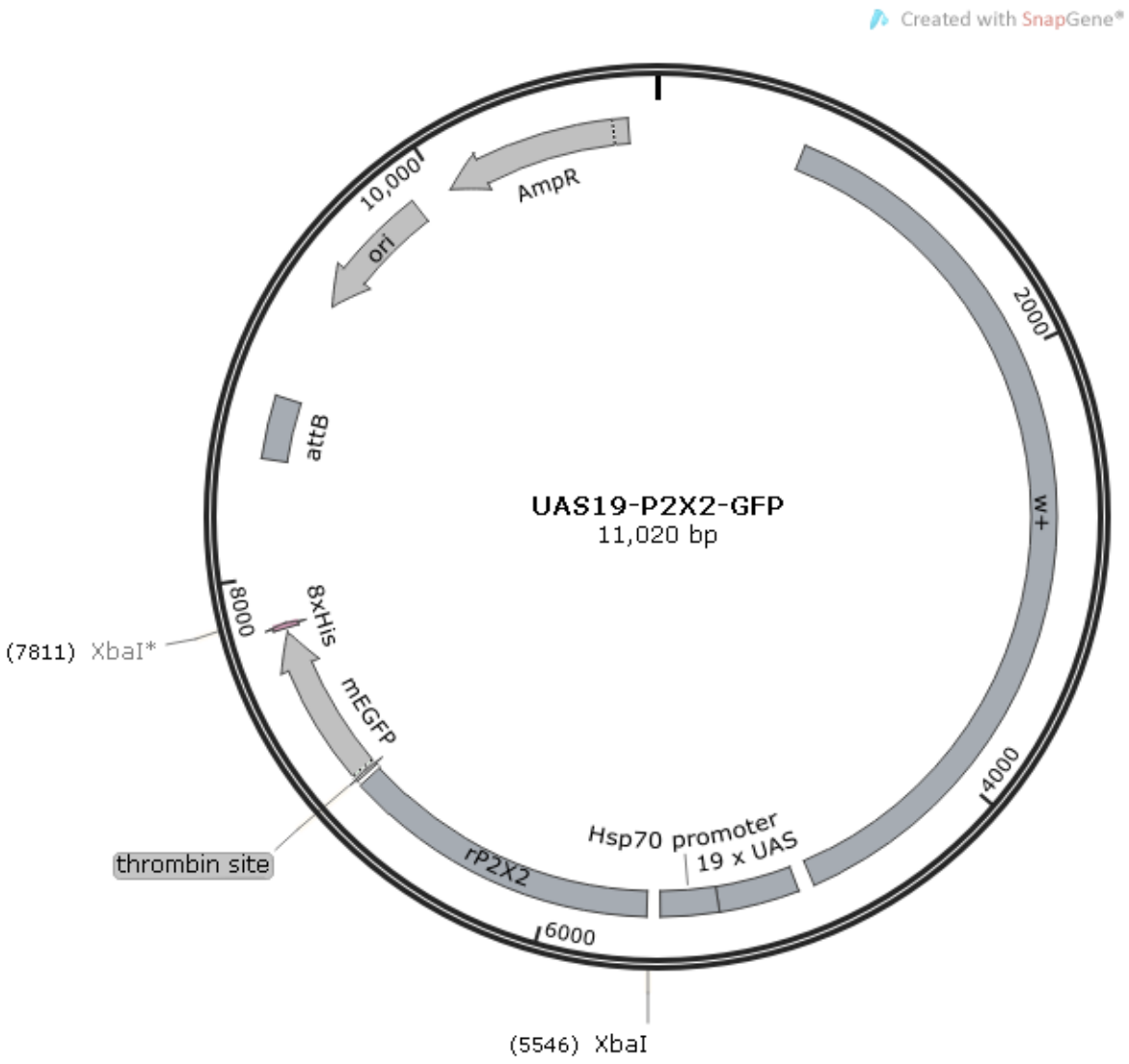

UAS19-rPanx1-GFP

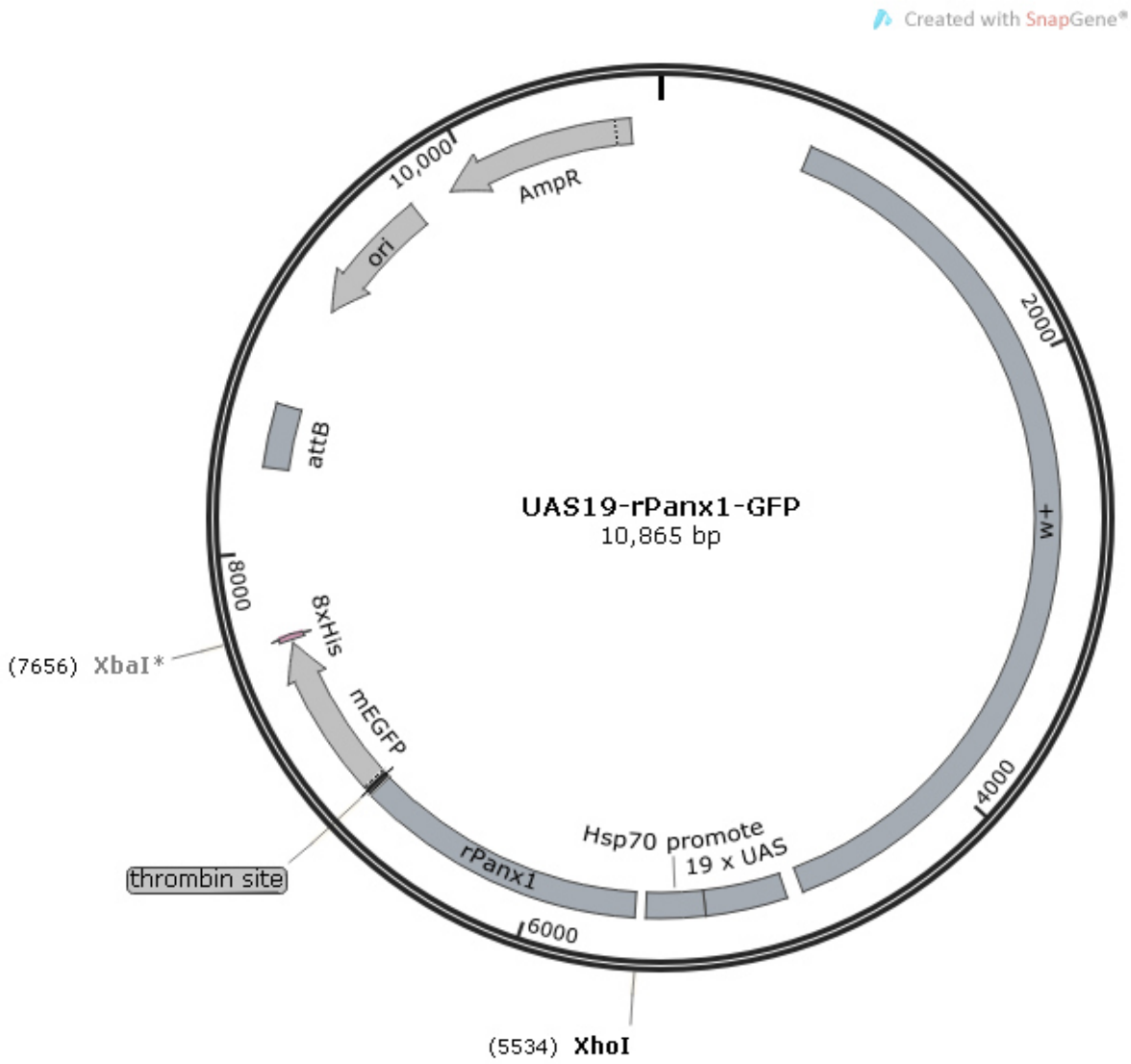

UAS19-rP2X2-myc-STS

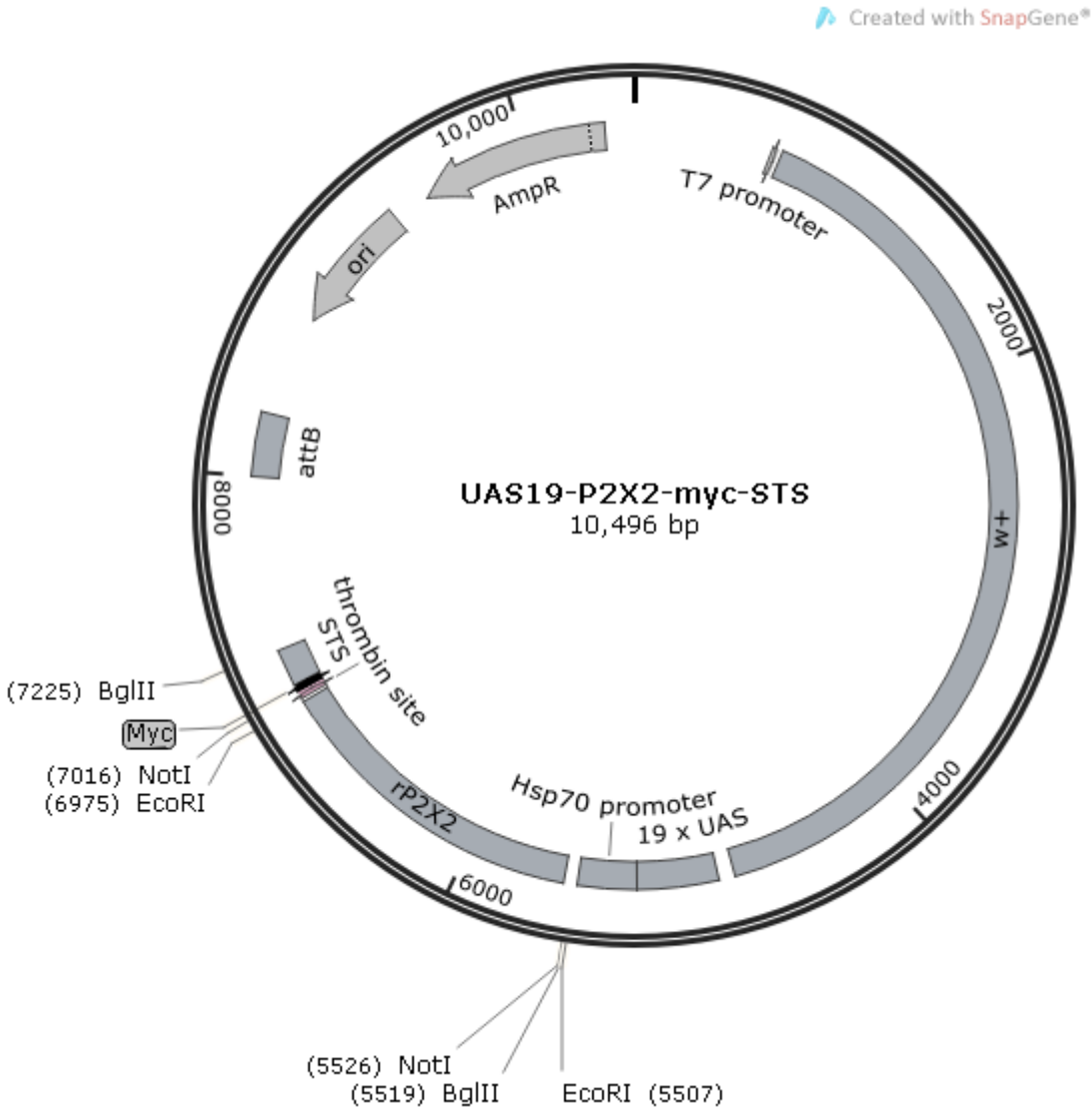

UAS19-rP2X2-myc-LTS

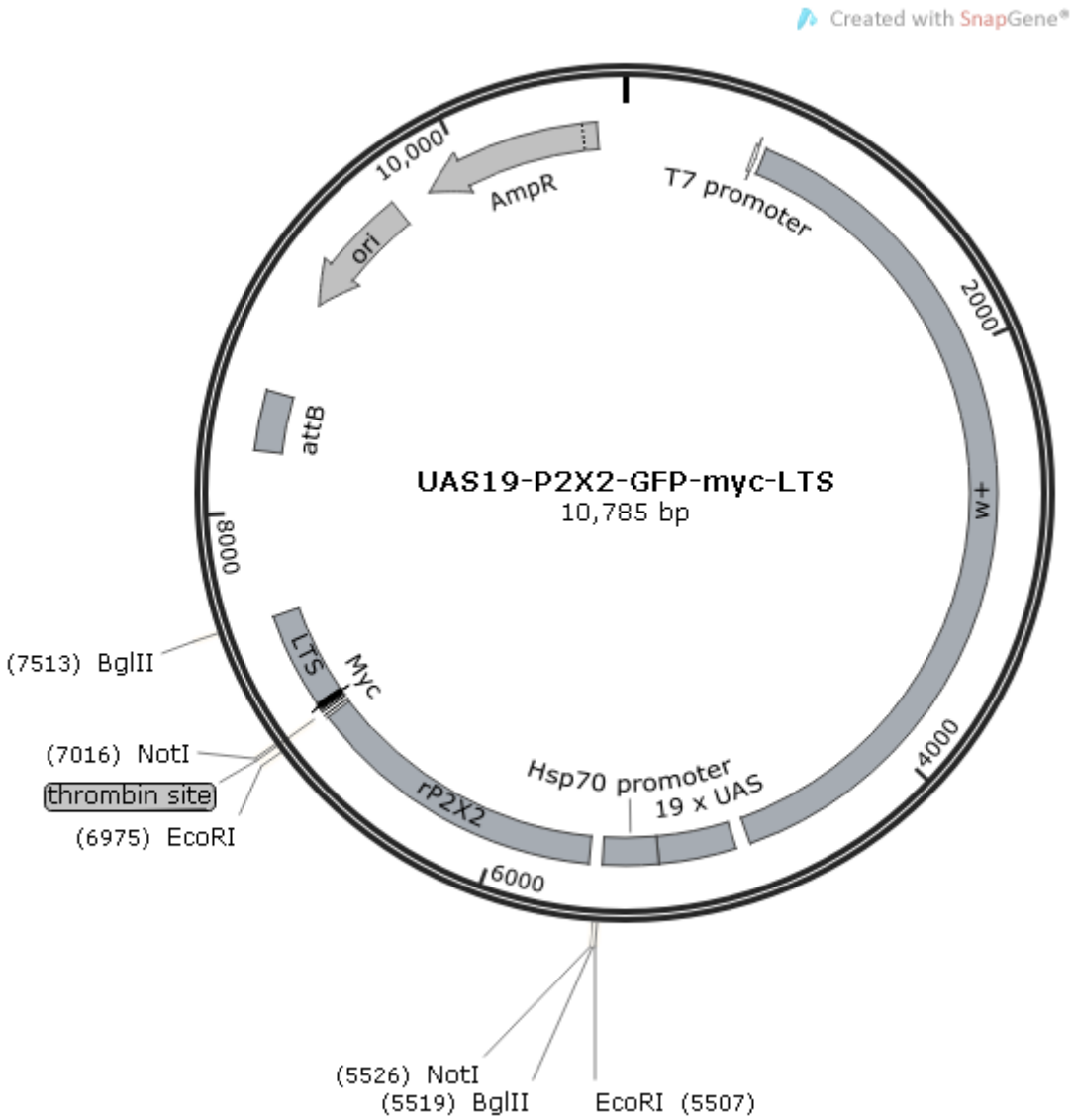

Appendix III – Codon usage charts

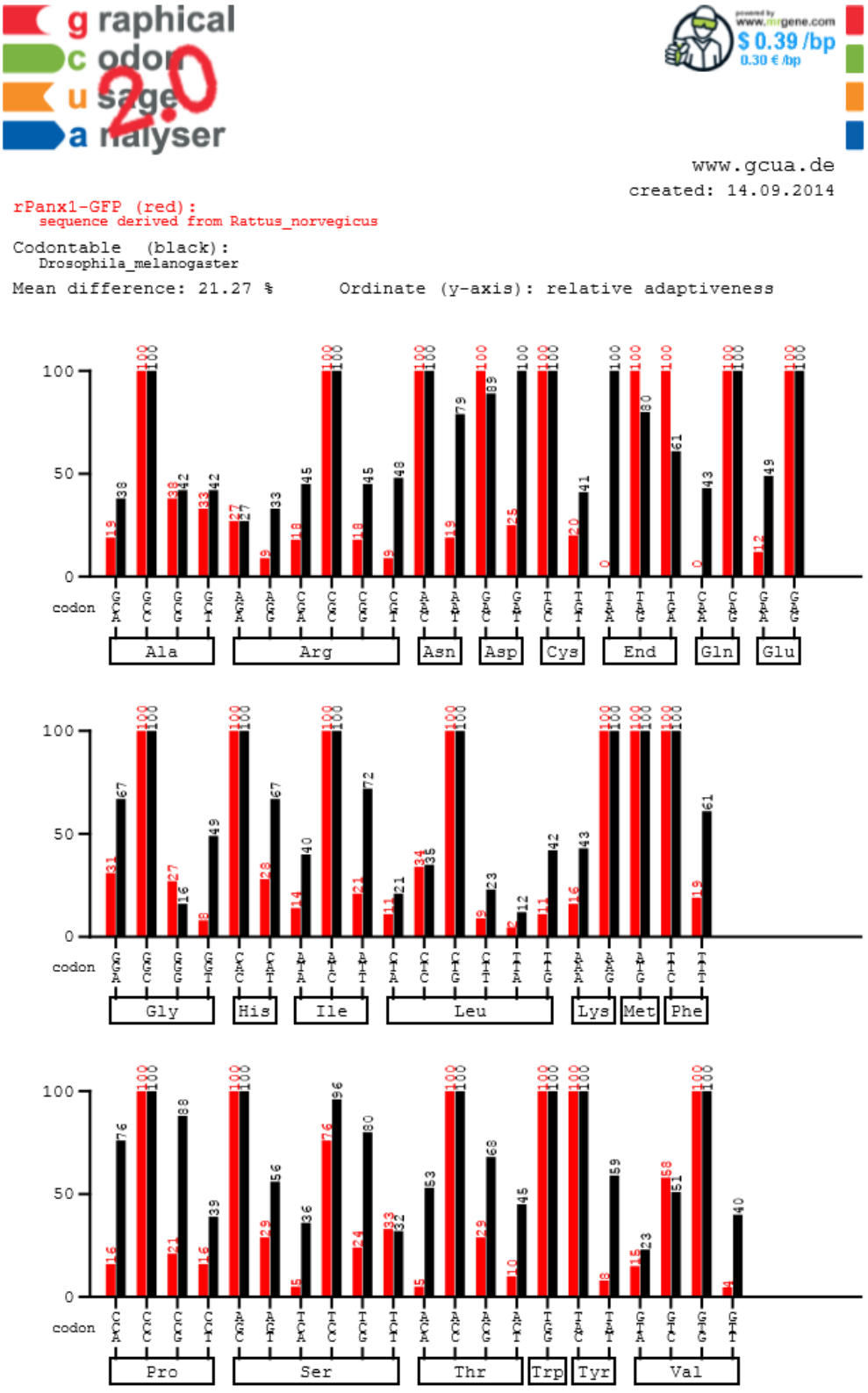

www.gcua.de
created: 14.09.2014

hP2X4-GFP (red):
sequence derived from Homo_sapiens

Codontable (black):
Drosophila_melanogaster

Mean difference: 20.7 % Ordinate (y-axis): relative adaptiveness

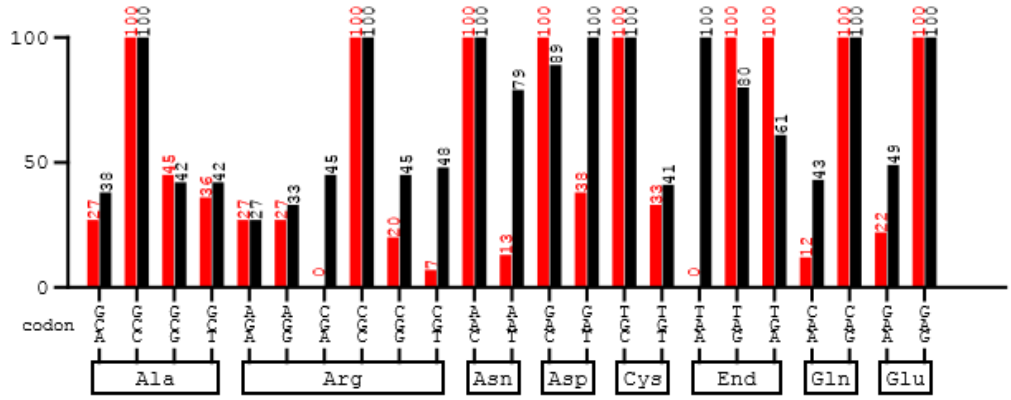

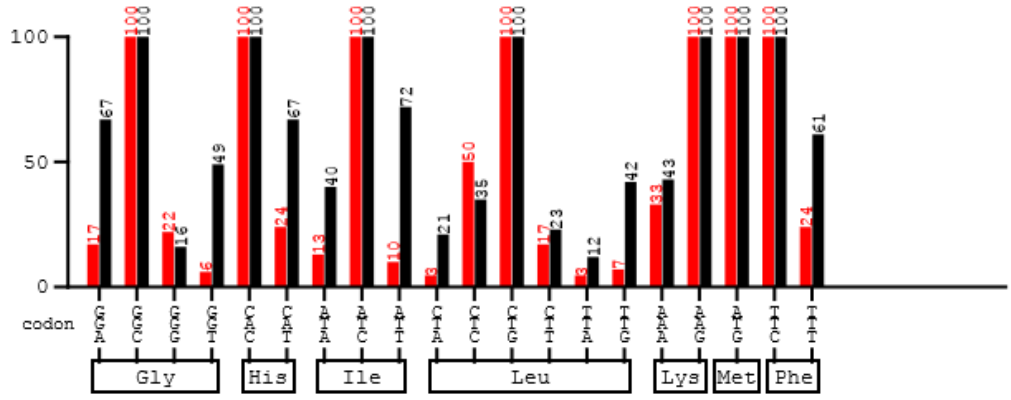

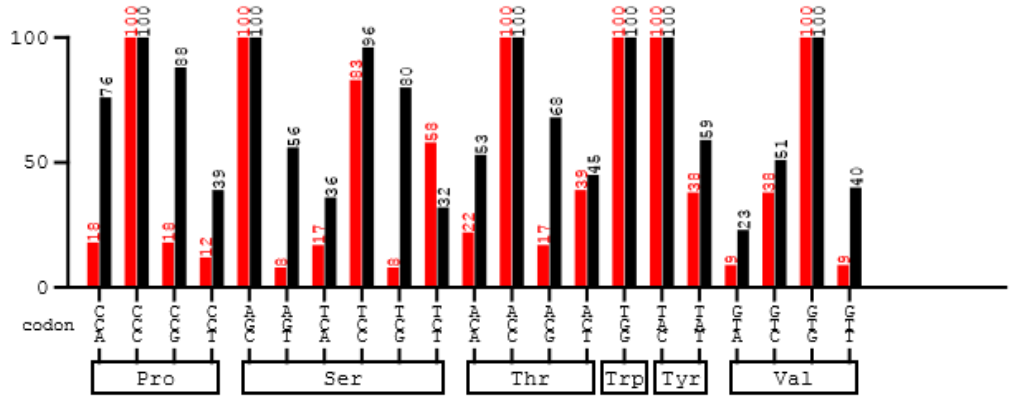

www.gcua.de
created: 14.09.2014

rP2X2-GFP (red):
sequence derived from Rattus_norvegicus

Codontable (black):
Drosophila_melanogaster

Mean difference: 18.55 % Ordinate (y-axis): relative adaptiveness

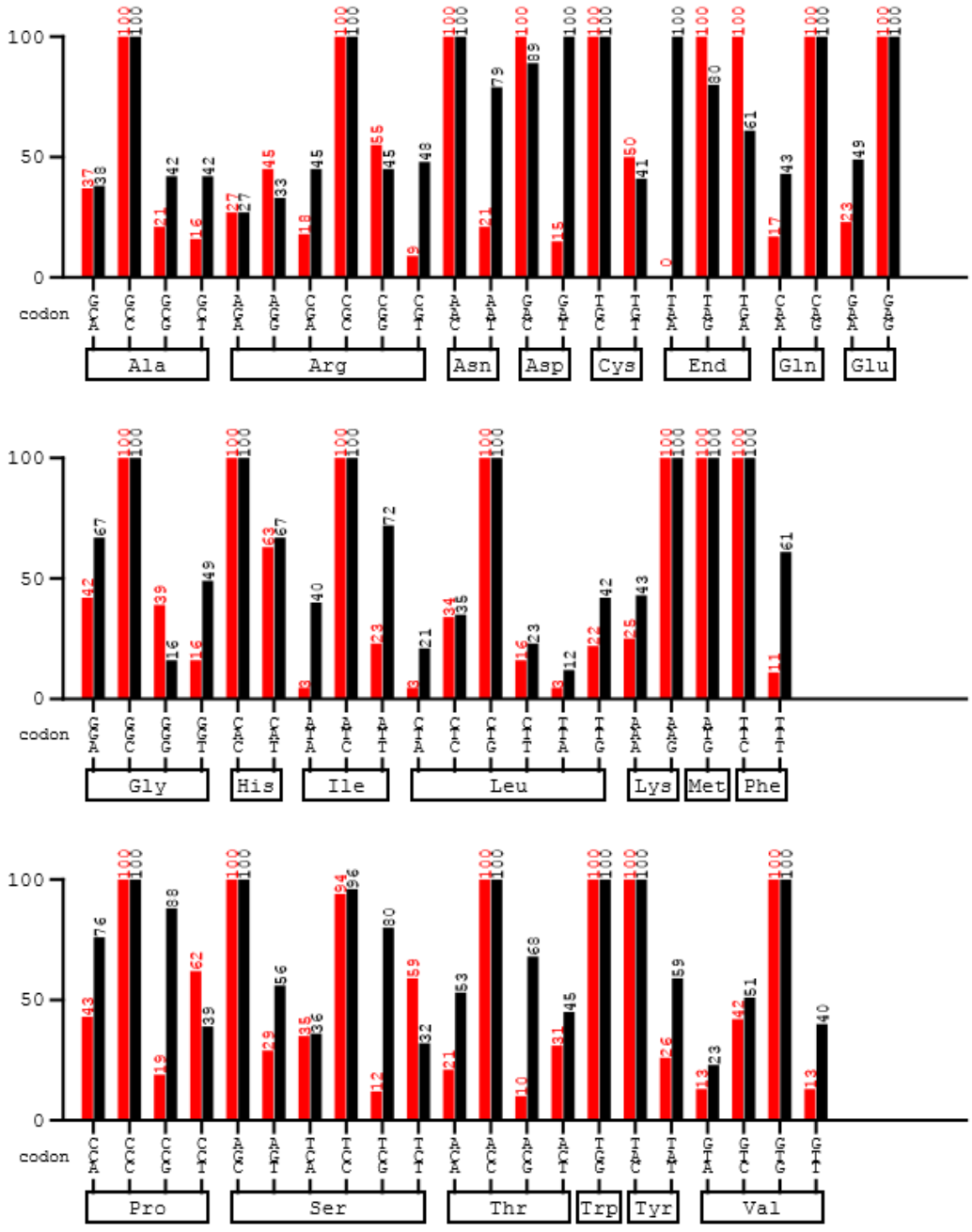

Appendix IV – Adenosine nucleotide library

This appendix lists the adenosine nucleotides that were tested for their effect on rat P2X2 expressed *Drosophila* taste neurons. Eighty chemicals were obtained as a library (Cat. No. LIB-101) from Jena Biosciences (Jena, Germany). Chemicals were >95% pure (HPLC) and racemic, if the derivative of ATP has additional chiral centers.

The appendix is divided into derivatives of ATP (subdivided modifications of the ribose, adenine group, phosphate group moieties), derivatives of ADP and AMP, and a set of dinucleotides. Within divisions structures are organized by rank order of effectiveness on rat P2X2 as in Figure 5.8.

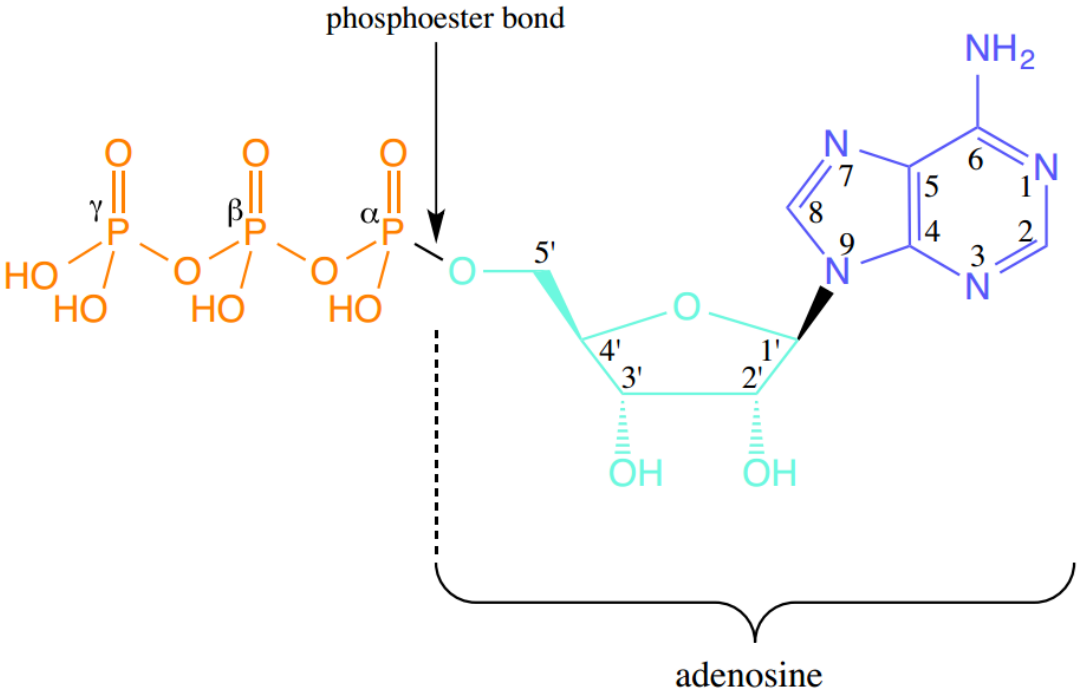

The colour of bars in Figure 5.8 correspond to the modifications of ATP. I.e. ribose modifications are cyan, phosphate modifications are orange and adenine modifications are blue.

Appendix content:
Ribose modifications of ATP (Figure App. 3A-D)
Adenine modifications of ATP (Figure App. 4A, B)
Phosphate group modifications of ATP (Figure App. 5A, B)
ADP derivatives (Figure App. 6A, B)
AMP derivatives (Figure App. 7A, B)
Dinucleotides (Figure App. 8A, B)

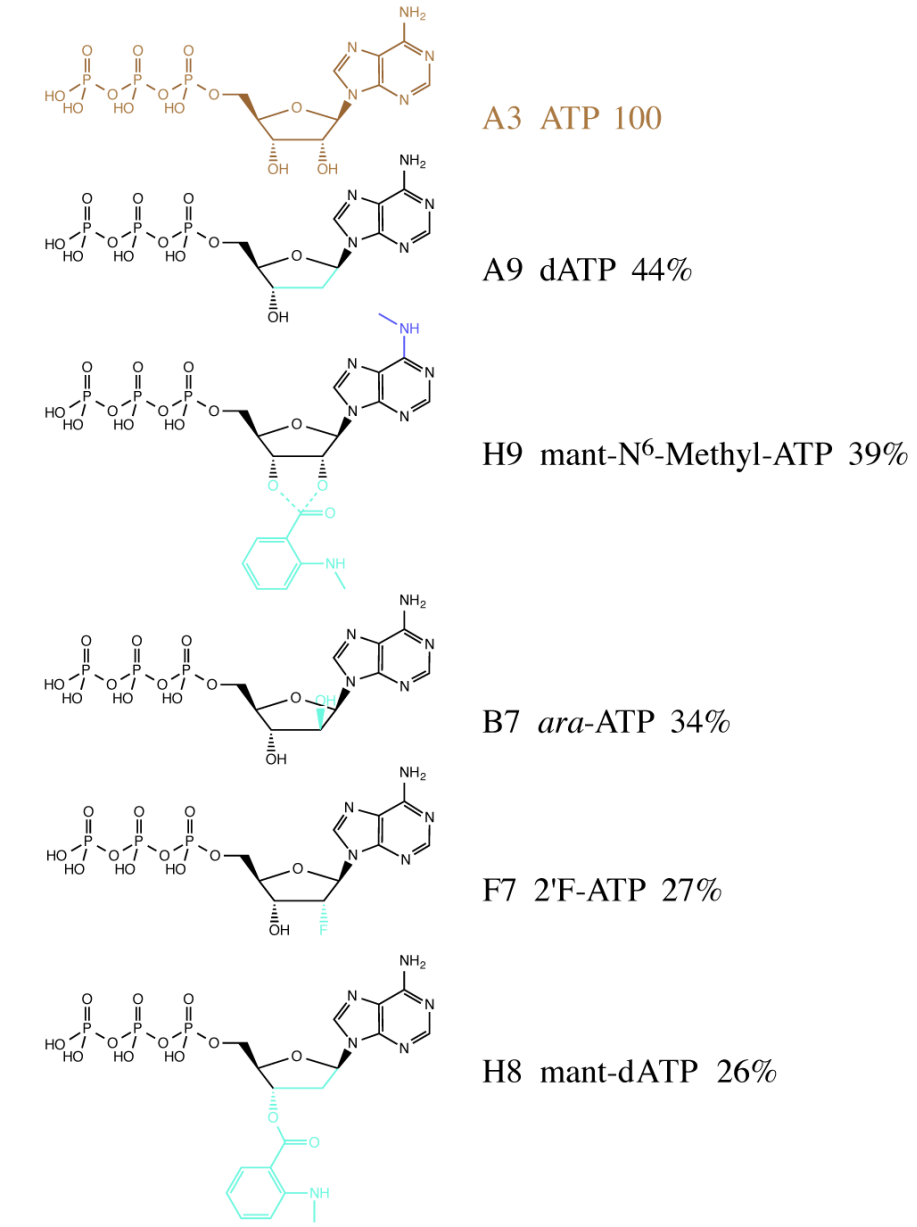

Figure App. 3A – Chemical structures of ATP derivatives with altered ribose moieties. ATP is shown in brown. Altered ribose groups are shown in cyan, altered adenine groups are shown in blue and altered phosphate groups are shown in orange. The response of each compound relative to ATP is shown (%) and are ordered respectively.

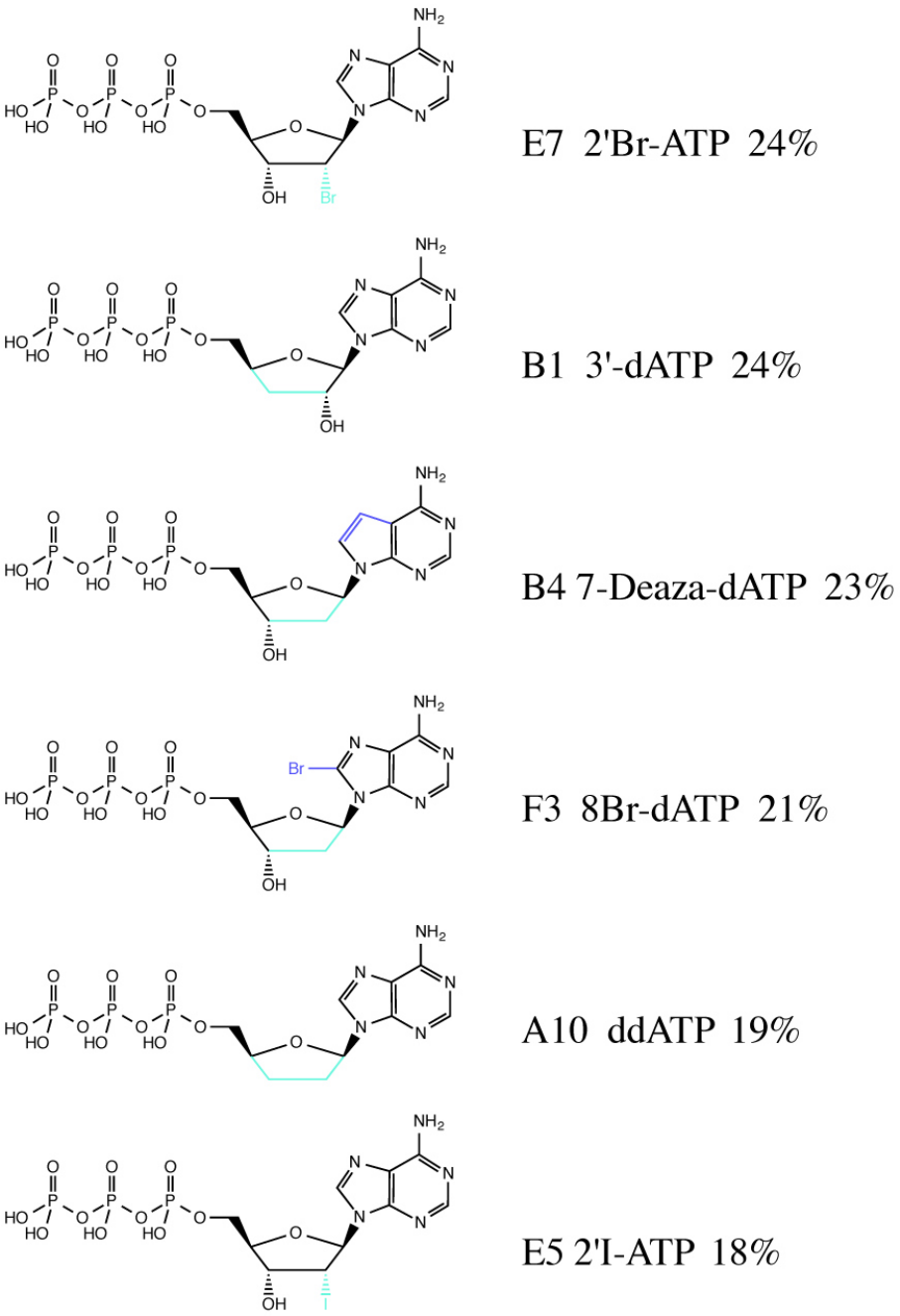

Figure App. 3B – Chemical structures of ATP derivatives with altered ribose moieties. Altered ribose groups are shown in cyan, altered adenine groups are shown in blue and altered phosphate groups are shown in orange. The response of each compound relative to ATP is shown (%) and are ordered respectively.

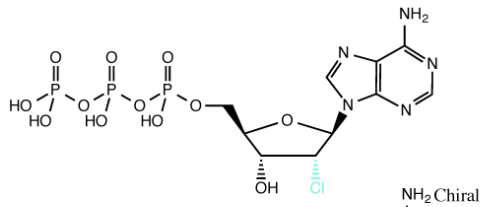

F8 2'Cl-ATP 17%

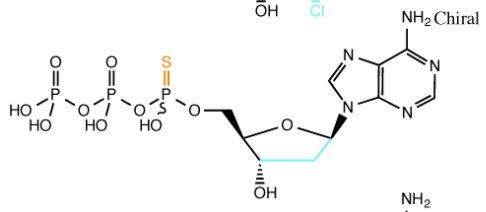

C1 dATPαS 17%

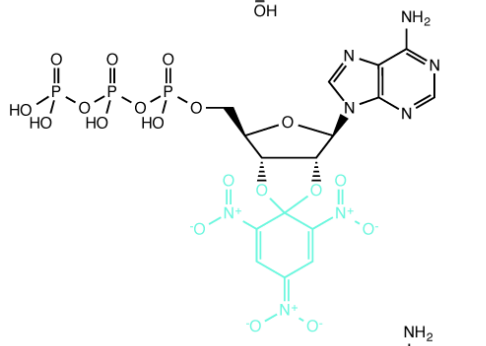

H5 TNP-ATP 15%

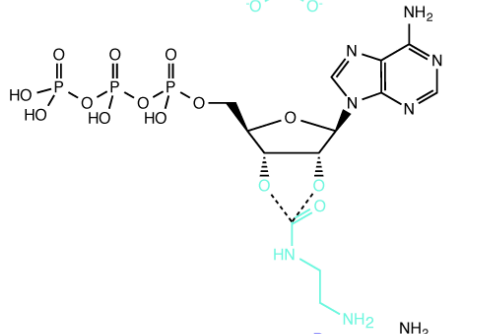

H1 EDA-ATP 12%

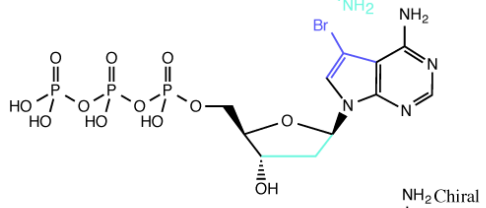

G1 7-Deaza-7Br-dATP 11%

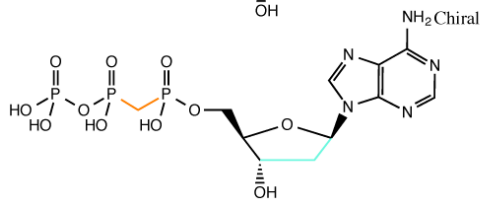

C8 dApCpp 11%

Figure App. 3C – Chemical structures of ATP derivatives with altered ribose moieties. Altered ribose groups are shown in cyan, altered adenine groups are shown in blue and altered phosphate groups are shown in orange. The response of each compound relative to ATP is shown (%) and are ordered respectively.

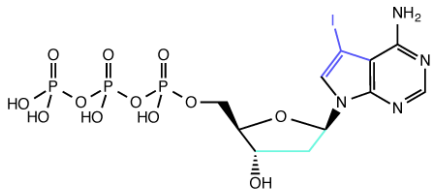

F10 7-Deaza-7I-dATP 10%

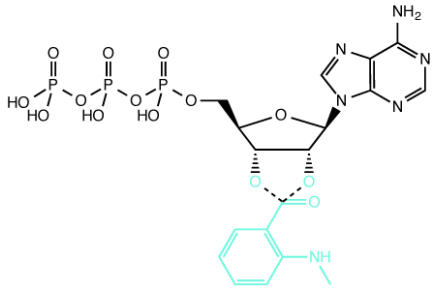

H7 mant-ATP 10%

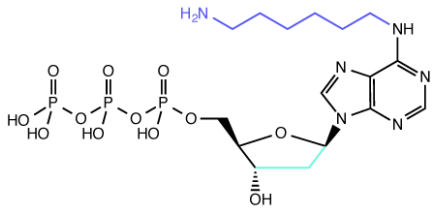

G7 N^6-(6-Amino)hexyl-dATP 4%

Figure App. 3D – Chemical structures of ATP derivatives with altered ribose moieties. Altered ribose groups are shown in cyan, altered adenine groups are shown in blue and altered phosphate groups are shown in orange. The response of each compound relative to ATP is shown (%) and are ordered respectively.

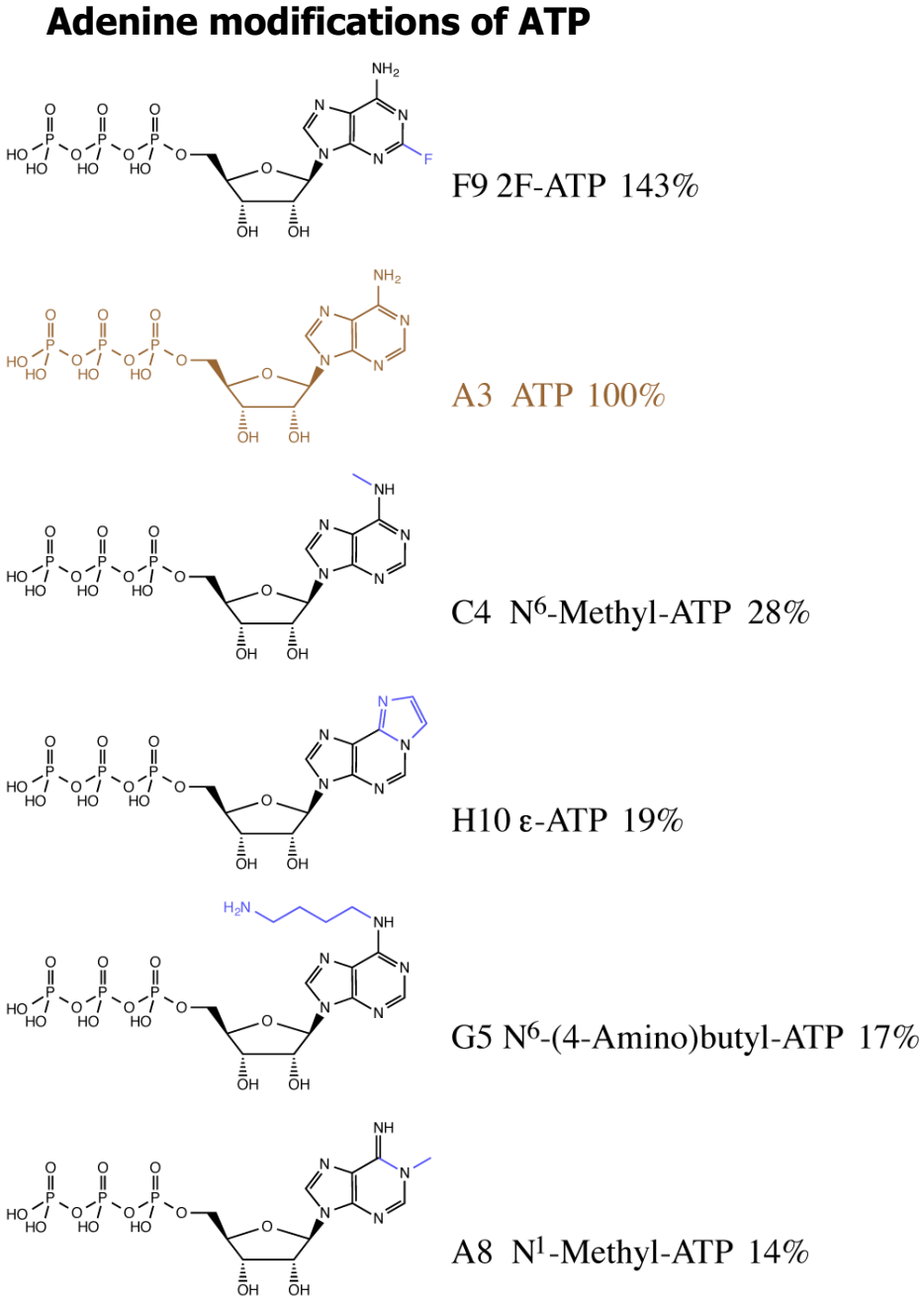

Figure App. 4A – ATP is shown in brown. Chemical structures of ATP derivatives with altered adenine moieties. Altered adenine groups are shown in blue. The response of each compound relative to ATP is shown (%) and are ordered respectively.

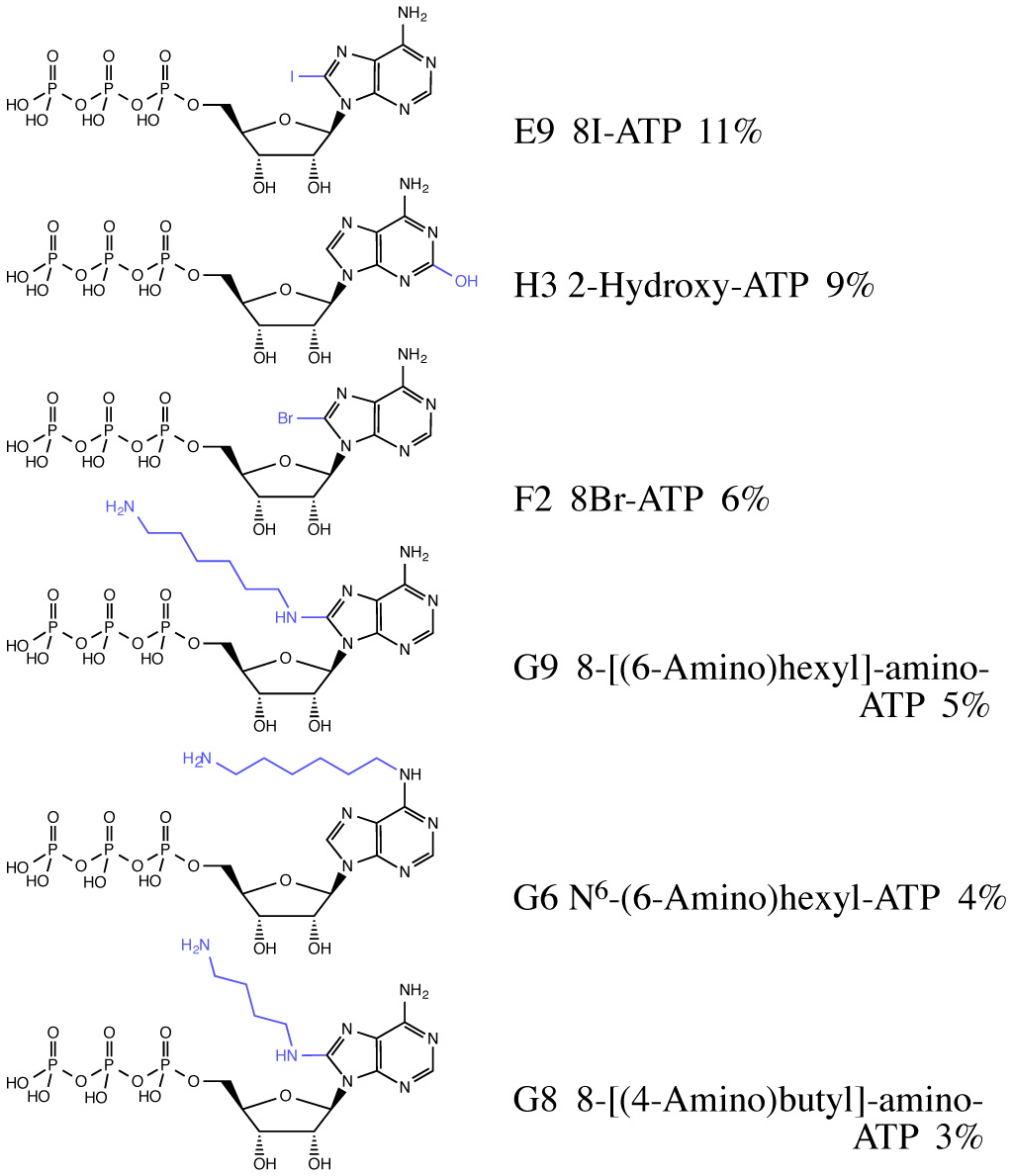

Figure App.4B – Chemical structures of ATP derivatives with altered adenine moieties. Altered adenine groups are shown in blue. The response of each compound relative to ATP is shown (%) and are ordered respectively.

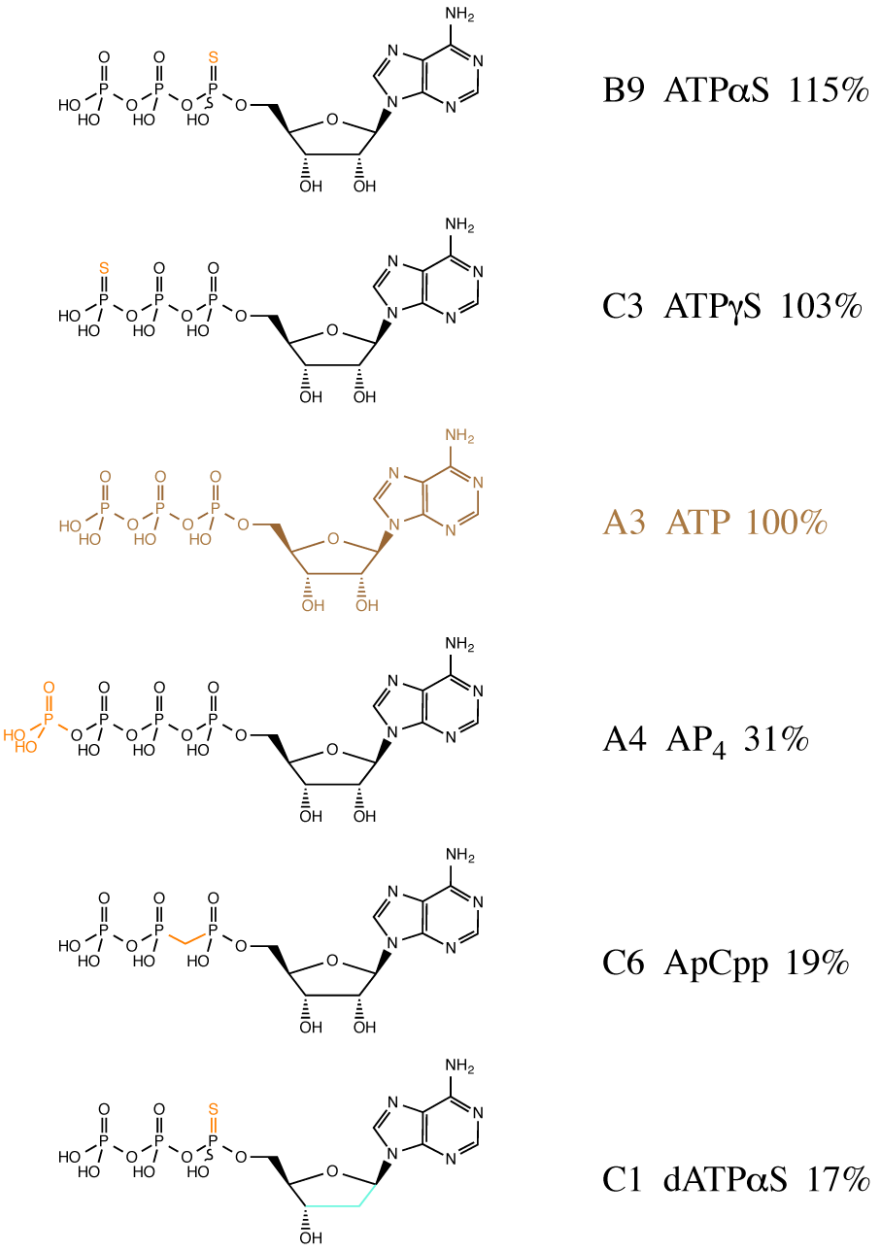

Figure App. 5A – ATP is shown in brown. Chemical structures of ATP derivatives with altered phosphate groups. Altered phosphate groups are shown in orange, ribose alterations are shown in cyan. The response of each compound relative to ATP is shown (%) and are ordered respectively.

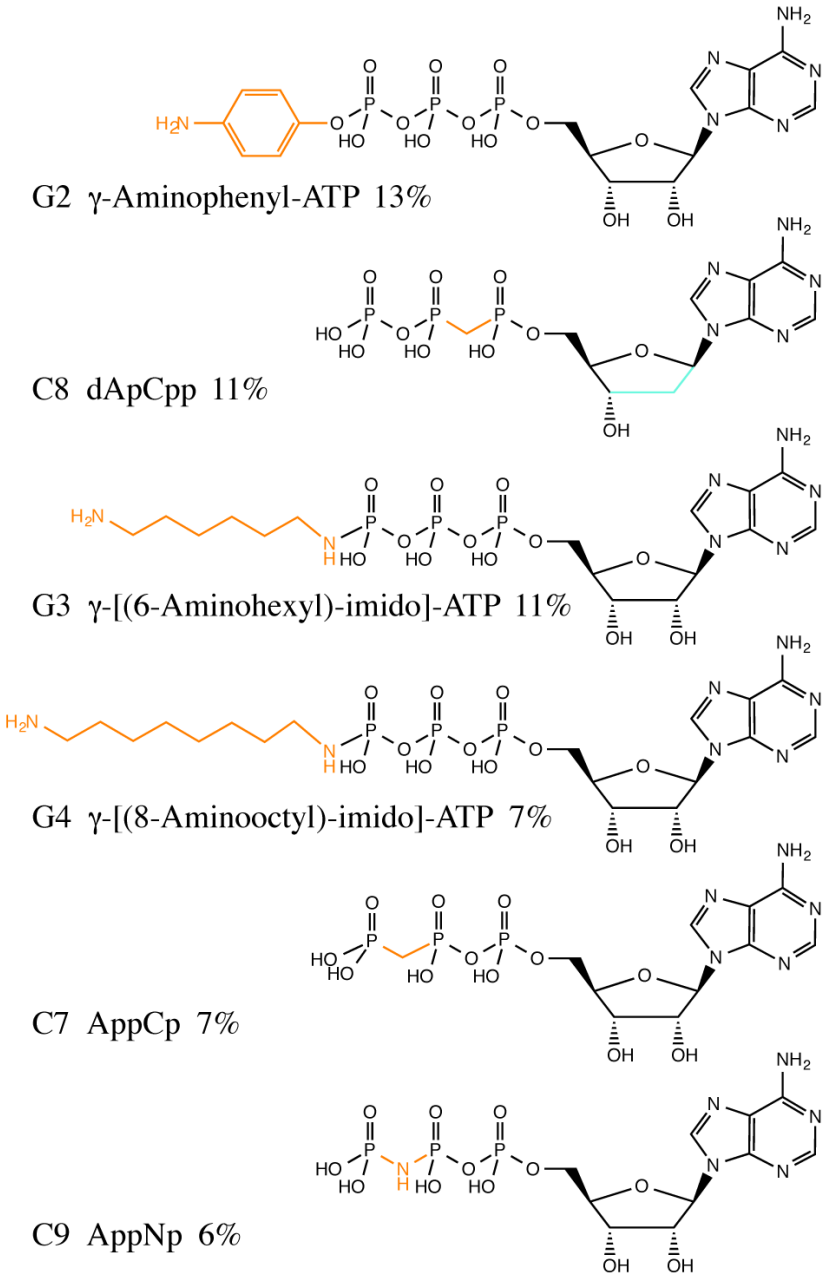

Figure App. 5B – Chemical structures of ATP derivatives with altered phosphate groups. Altered phosphate groups are shown in orange, ribose alterations are shown in cyan. The response of each compound relative to ATP is shown (%) and are ordered respectively.

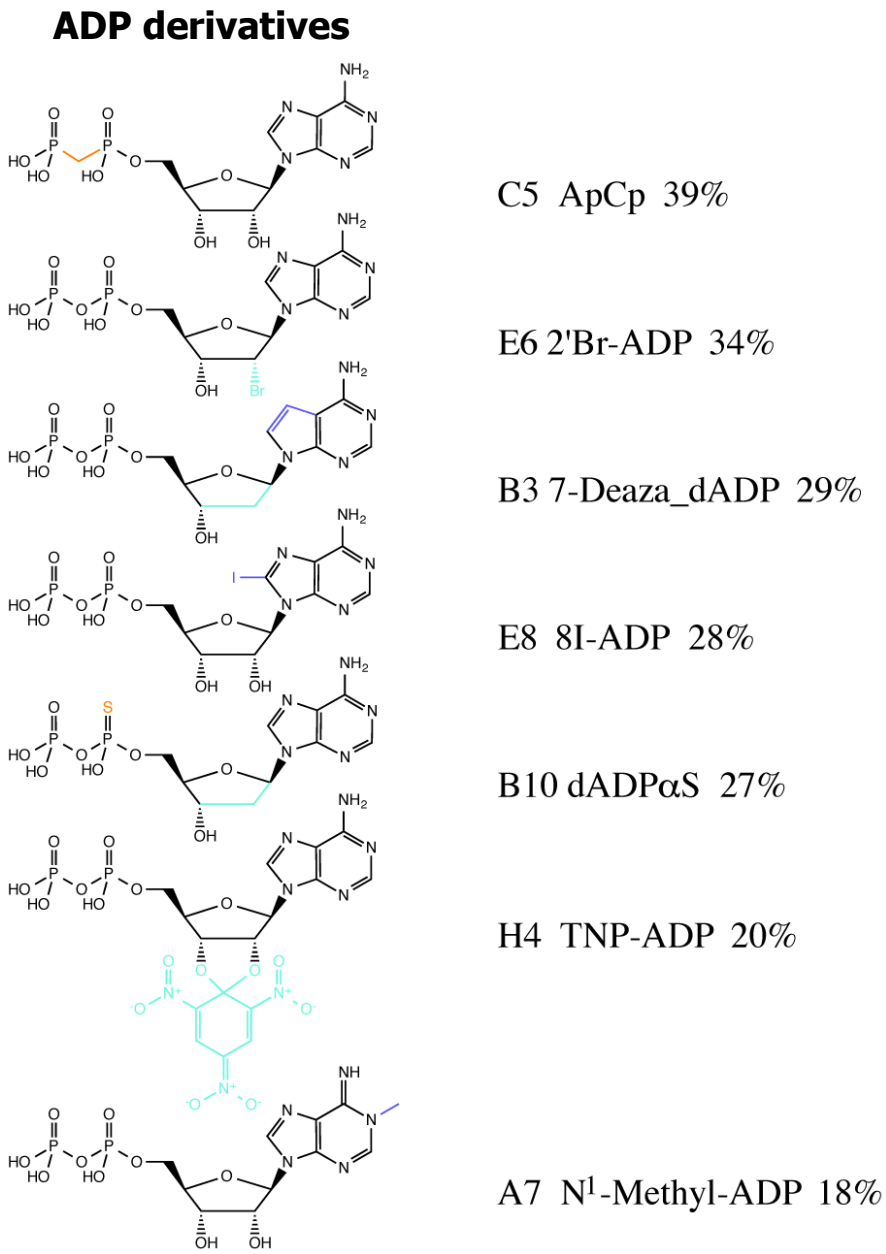

Figure App. 6A – ADP derivatives. Alterations to ribose are shown in cyan, altered adenine groups are shown in blue and altered phosphate groups are shown in orange. The response of each compound relative to ATP is shown (%) and are ordered respectively.

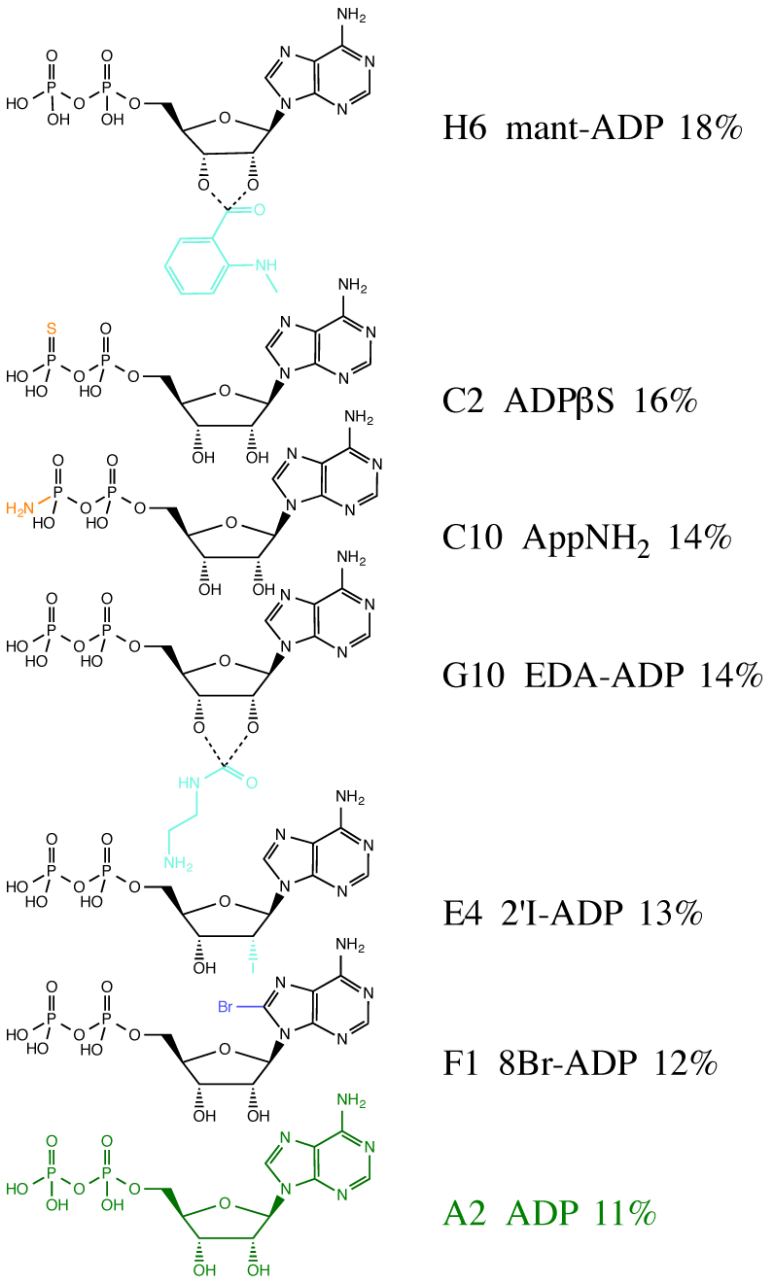

Figure App. 6B – ADP derivatives. Alterations to ribose are shown in cyan, altered adenine groups are shown in blue and altered phosphate groups are shown in orange. The response of each compound relative to ATP is shown (%) and are ordered respectively.

AMP derivatives

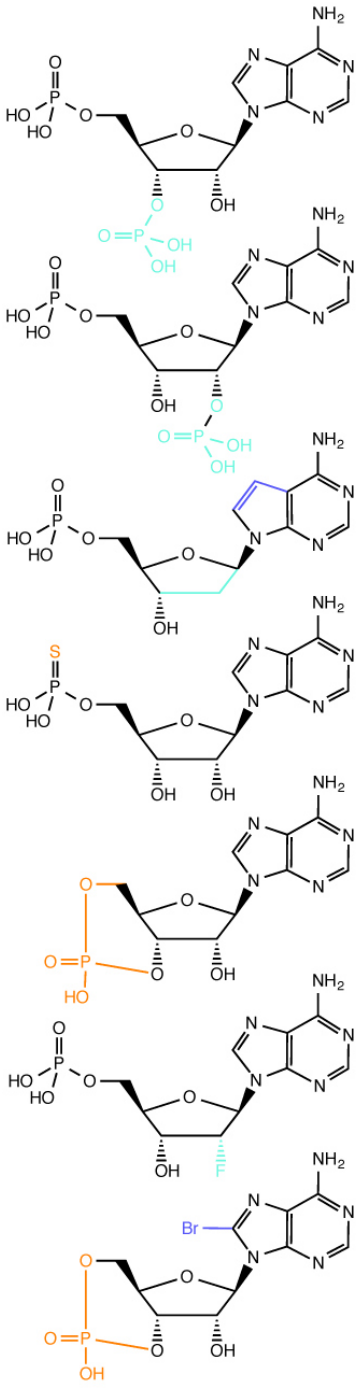

B5 3'-5'-pAp 29%

B6 2',5'-pAP 26%

B2 7-Deaza-dAMP 25%

B8 AMPαS 23%

A5 cAMP 20%

F6 2'F-AMP 17%

E10 8Br-cAMP 15%

Figure App. 7A – AMP derivatives. Alterations to ribose are shown in cyan, altered adenine groups are shown in blue and altered phosphate groups are shown in orange. The response of each compound relative to ATP is shown (%) and are ordered respectively.

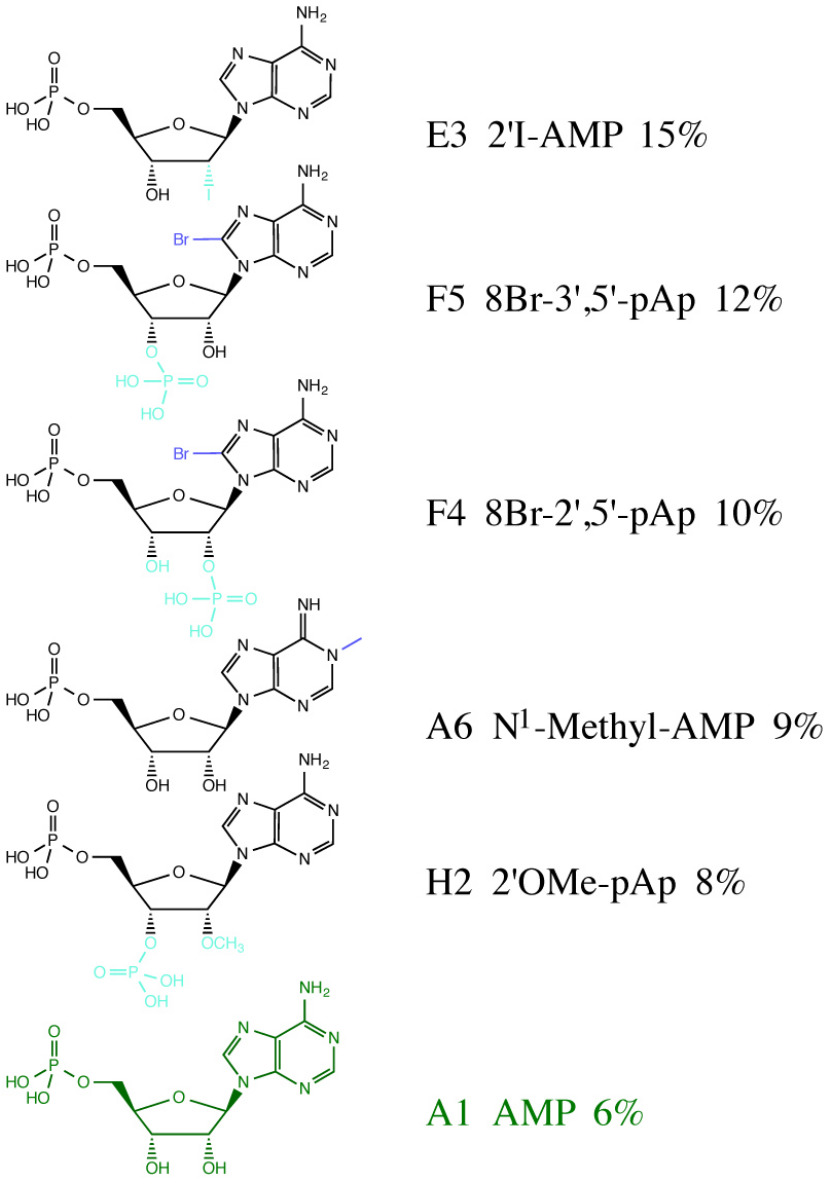

Figure App. 7B – AMP derivatives. Alterations to ribose are shown in cyan, altered adenine groups are shown in blue and altered phosphate groups are shown in orange. The response of each compound relative to ATP is shown (%) and are ordered respectively.

Dinucleotides

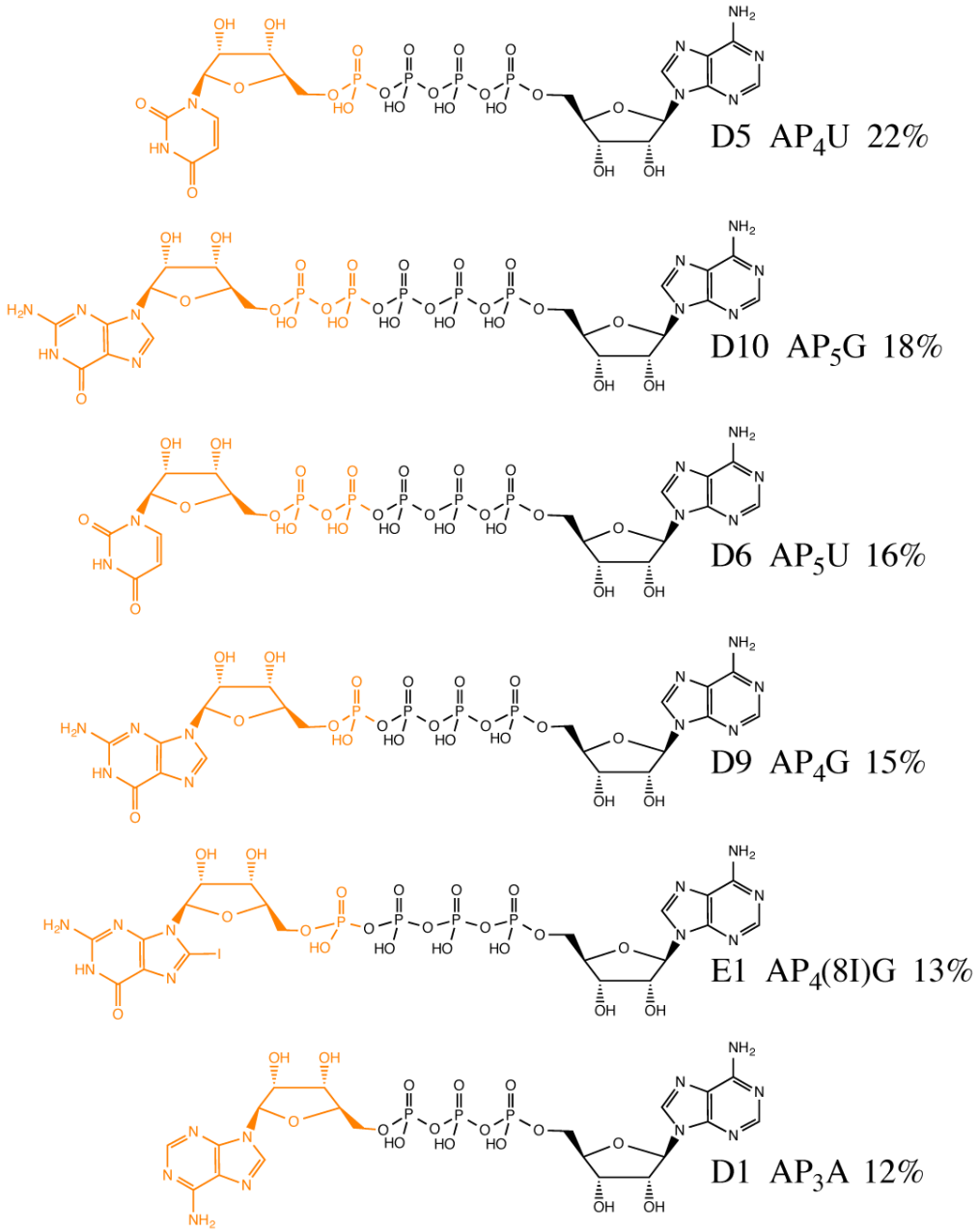

Figure App. 8A – Dinucleotides. Altered phosphate groups are shown in orange. The response of each compound relative to ATP is shown (%) and compounds are ordered respectively.

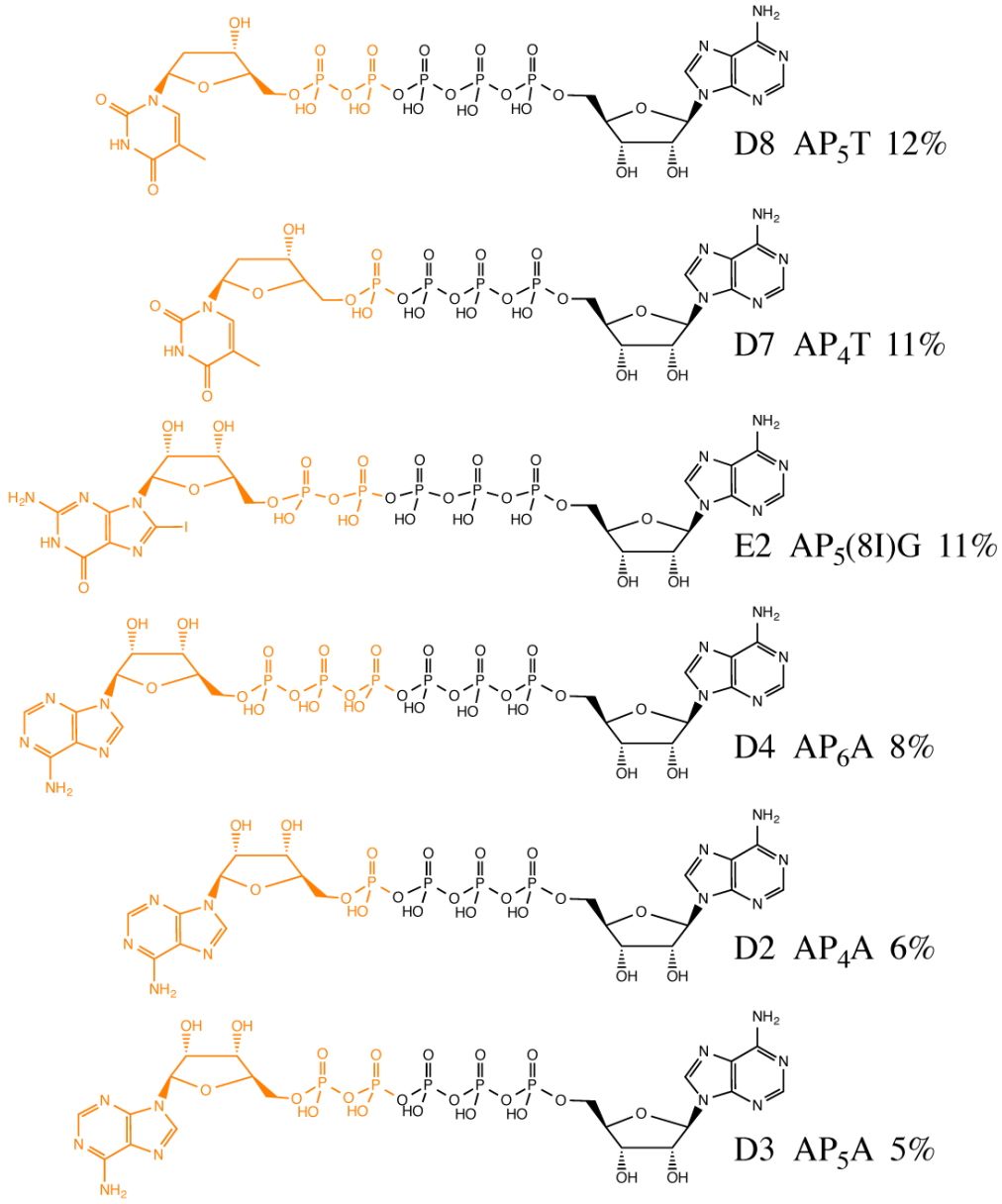

Figure App. 8B – Dinucleotides. Altered phosphate groups are shown in orange. The response of each compound relative to ATP is shown (%) and compounds are ordered respectively.

References

ABBRACCHIO M. P., BURNSTOCK G., 1994 Purinoceptors: Are there families of P2X and P2Y purinoceptors? Pharmacol. Ther. **64**: 445–475.

ABRAMOWSKI P., OGRODOWCZYK C., MARTIN R., PONGS O., 2014 A Truncation Variant of the Cation Channel P2RX5 Is Upregulated during T Cell Activation. PLoS One **9**: e104692.

ABU-QARN M., EICHLER J., SHARON N., 2008 Not just for Eukarya anymore: protein glycosylation in Bacteria and Archaea. Curr. Opin. Struct. Biol. **18**: 544–50.

ADAMS M. D., CELNIKER S. E., HOLT R. A., EVANS C. A., GOCAYNE J. D., AMANATIDES P. G., SCHERER S. E., LI P. W., HOSKINS R. A., GALLE R. F., GEORGE R. A., LEWIS S. E., RICHARDS S., ASHBURNER M., HENDERSON S. N., SUTTON G. G., WORTMAN J. R., YANDELL M. D., ZHANG Q., CHEN L. X., BRANDON R. C., ROGERS Y. H., BLAZEJ R. G., CHAMPE M., PFEIFFER B. D., WAN K. H., DOYLE C., BAXTER E. G., HELT G., NELSON C. R., GABOR G. L., ABRIL J. F., AGBAYANI A., AN H. J., ANDREWS-PFANNKOCH C., BALDWIN D., BALLEW R. M., BASU A., BAXENDALE J., BAYRAKTAROGLU L., BEASLEY E. M., BEESON K. Y., BENOS P. V, BERMAN B. P., BHANDARI D., BOLSHAKOV S., BORKOVA D., BOTCHAN M. R., BOUCK J., BROKSTEIN P., BROTTIER P., BURTIS K. C., BUSAM D. A., BUTLER H., CADIEU E., CENTER A., CHANDRA I., CHERRY J. M., CAWLEY S., DAHLKE C., DAVENPORT L. B., DAVIES P., PABLOS B. DE, DELCHER A., DENG Z., MAYS A. D., DEW I., DIETZ S. M., DODSON K., DOUP L. E., DOWNES M., DUGAN-ROCHA S., DUNKOV B. C., DUNN P., DURBIN K. J., EVANGELISTA C. C., FERRAZ C., FERRIERA S., FLEISCHMANN W., FOSLER C., GABRIELIAN A. E., GARG N. S., GELBART W. M., GLASSER K., GLODEK A., GONG F., GORRELL J. H., GU Z., GUAN P., HARRIS M., HARRIS N. L., HARVEY D., HEIMAN T. J., HERNANDEZ J. R., HOUCK J., HOSTIN D., HOUSTON K. A., HOWLAND T. J., WEI M. H., IBEGWAM C., JALALI M., KALUSH F., KARPEN G. H., KE Z., KENNISON J. A., KETCHUM K. A., KIMMEL B. E., KODIRA C. D., KRAFT C., KRAVITZ S., KULP D., LAI Z., LASKO P., LEI Y., LEVITSKY A. A., LI J., LI Z., LIANG Y., LIN X., LIU X., MATTEI B., MCINTOSH T. C., MCLEOD M. P., MCPHERSON D., MERKULOV G., MILSHINA N. V, MOBARRY C., MORRIS J., MOSHREFI A., MOUNT S. M., MOY M., MURPHY B., MURPHY L., MUZNY D. M., NELSON D. L., NELSON D. R., NELSON K. A., NIXON K., NUSSKERN D. R., PACLEB J. M., PALAZZOLO M., PITTMAN G. S., PAN S., POLLARD J., PURI V., REESE M. G., REINERT K., REMINGTON K., SAUNDERS R. D., SCHEELER F., SHEN H., SHUE B. C., SIDÉN-KIAMOS I., SIMPSON M., SKUPSKI M. P., SMITH T., SPIER E., SPRADLING A. C., STAPLETON M., STRONG R., SUN E., SVIRSKAS R., TECTOR C., TURNER R., VENTER E., WANG A. H., WANG X., WANG Z. Y., WASSARMAN D. A., WEINSTOCK G. M., WEISSENBACH J., WILLIAMS S. M., WOODAGET, WORLEY K. C., WU D., YANG S., YAO Q. A., YE J., YEH R. F., ZAVERI J. S., ZHAN M., ZHANG G., ZHAO Q., ZHENG L., ZHENG X. H., ZHONG F. N., ZHONG W., ZHOU X., ZHU S., ZHU X., SMITH H. O., GIBBS R. A., MYERS E. W., RUBIN G. M., VENTER J. C., 2000 The genome sequence of Drosophila melanogaster. Science **287**: 2185–95.

ALBERTS B., JOHNSON A., LEWIS J., RAFF M., ROBERTS K., WALTER P., 2002 Ion Channels and the Electrical Properties of Membranes.

ALLEN S. J., RIBEIRO S., HORUK R., HANDEL T. M., 2009 Expression, purification and in vitro functional reconstitution of the chemokine receptor CCR1. Protein Expr. Purif. **66**: 73–81.

ALLSOPP R. C., EVANS R. J., 2011 The intracellular amino terminus plays a dominant role in desensitization of ATP-gated P2X receptor ion channels. J. Biol. Chem. **286**: 44691–701.

ALLSOPP R. C., FARMER L. K., FRYATT A. G., EVANS R. J., 2013 P2X receptor chimeras highlight roles of the amino terminus to partial agonist efficacy, the carboxyl terminus to recovery from desensitization, and independent regulation of channel transitions. J. Biol. Chem. **288**: 21412–21.

AMBROSI C., GASSMANN O., PRANSKEVICH J. N., BOASSA D., SMOCK A., WANG J., DAHL G., STEINEM C., SOSINSKY G. E., 2010 Pannexin1 and Pannexin2 channels show quaternary similarities to connexons and different oligomerization numbers from each other. J Biol Chem **285**: 24420–24431.

AN H. J., GIP P., KIM J., WU S., PARK K. W., MCVAUGH C. T., SCHAFFER D. V, BERTOZZI C. R., LEBRILLA C. B., 2012 Extensive determination of glycan heterogeneity reveals an unusual abundance of high mannose glycans in enriched plasma membranes of human embryonic stem cells. Mol. Cell. Proteomics **11**: M111.010660.

ANDREWS S. P., MASON J. S., HURRELL E., CONGREVE M., 2014 Structure-based drug design of chromone antagonists of the adenosine A2A receptor. Medchemcomm **5**: 571.

ANTONIO L. S., STEWART A. P., VARANDA W. A., EDWARDSON J. M., 2014 Identification of P2X2/P2X4/P2X6 heterotrimeric receptors using atomic force microscopy (AFM) imaging. FEBS Lett. **588**: 2125–8.

ARDISSONE V., RADAELLI E., ZARATIN P., ARDIZZONE M., LADEL C., GATTORNO M., MARTINI A., GRASSI F., TRAGGIAI E., 2011 Pharmacologic P2X purinergic receptor antagonism in the treatment of collagen-induced arthritis. Arthritis Rheum. **63**: 3323–32.

ARINAMINPATHY Y., KHURANA E., ENGELMAN D. M., GERSTEIN M. B., 2009 Computational analysis of membrane proteins: the largest class of drug targets. Drug Discov. Today **14**: 1130–5.

BAO L., LOCOVEI S., DAHL G., 2004 Pannexin membrane channels are mechanosensitive conduits for ATP. FEBS Lett. **572**: 65–8.

BAQI Y., HAUSMANN R., ROSEFORT C., RETTINGER J., SCHMALZING G., MÜLLER C. E., 2011 Discovery of potent competitive antagonists and positive modulators of the P2X2 receptor. J. Med. Chem. **54**: 817–30.

BARANOVA A., IVANOV D., PETRASH N., PESTOVA A., SKOBLOV M., KELMANSON I., SHAGIN D., NAZARENKO S., GERAYMOVYCH E., LITVIN O., TIUNOVA A., BORN T. L., USMAN N., STAROVEROV D., LUKYANOV S., PANCHIN Y., 2004 The mammalian pannexin family is homologous to the invertebrate innexin gap junction proteins. Genomics **83**: 706–716.

BARDEN N., HARVEY M., GAGNÉ B., SHINK E., TREMBLAY M., RAYMOND C., LABBÉ M., VILLENEUVE A., ROCHETTE D., BORDELEAU L., STADLER H., HOLSBOER F., MÜLLER-MYHSOK B., 2006 Analysis of single nucleotide polymorphisms in genes in the chromosome 12Q24.31 region points to P2RX7 as a susceptibility gene to bipolar affective disorder. Am. J. Med. Genet. B. Neuropsychiatr. Genet. **141B**: 374–82.

BARRERA N. P., ORMOND S. J., HENDERSON R. M., MURRELL-LAGNADO R. D., EDWARDSON J. M., 2005 Atomic force microscopy imaging demonstrates that P2X2 receptors are trimers but that P2X6 receptor subunits do not oligomerize. J. Biol. Chem. **280**: 10759–65.

BARRERA N. P., HENDERSON R. M., MURRELL-LAGNADO R. D., EDWARDSON J. M., 2007 The stoichiometry of P2X2/6 receptor heteromers depends on relative subunit expression levels. Biophys. J. **93**: 505–12.

BATEMAN J. R., LEE A. M., WU C., 2006 Site-specific transformation of Drosophila via phiC31 integrase-mediated cassette exchange. Genetics **173**: 769–77.

BAUMANN K., ADELANTADO N., LANG C., MATTANOVICH D., FERRER P., 2011 Protein trafficking, ergosterol biosynthesis and membrane physics impact recombinant protein secretion in Pichia pastoris. Microb. Cell Fact. **10**: 93.

BENHAM C. D., TSIEN R. W., A novel receptor-operated Ca2+-permeable channel activated by ATP in smooth muscle. Nature **328**: 275–8.

BENTON R., DAHANUKAR A., 2011 Electrophysiological recording from Drosophila taste sensilla. Cold Spring Harb Protoc **2011**: 839–850.

BERNAUDAT F., FRELET-BARRAND A., POCHON N., DEMENTIN S., HIVIN P., BOUTIGNY S., RIOUX J.-B., SALVI D., SEIGNEURIN-BERNY D., RICHAUD P., JOYARD J., PIGNOL D., SABATY M., DESNOS T., PEBAY-PEYROULA E., DARROUZET E., VERNET T., ROLLAND N., 2011 Heterologous expression of membrane proteins: choosing the appropriate host. PLoS One **6**: e29191.

BINDA C., NEWTON-VINSON P., HUBÁLEK F., EDMONDSON D. E., MATTEVI A., 2002 Structure of human monoamine oxidase B, a drug target for the treatment of neurological disorders. Nat. Struct. Biol. **9**: 22–6.

BINDA C., LI M., HUBALEK F., RESTELLI N., EDMONDSON D. E., MATTEVI A., 2003 Insights into the mode of inhibition of human mitochondrial monoamine oxidase B from high-resolution crystal structures. Proc. Natl. Acad. Sci. U. S. A. **100**: 9750–5.

BISCHOF J., MAEDA R. K., HEDIGER M., KARCH F., BASLER K., 2007 An optimized transgenesis system for Drosophila using germ-line-specific phiC31 integrases. Proc. Natl. Acad. Sci. U. S. A. **104**: 3312–7.

BO X., JIANG L.-H., WILSON H. L., KIM M., BURNSTOCK G., SURPRENANT A., NORTH R. A., 2003 Pharmacological and biophysical properties of the human P2X5 receptor. Mol. Pharmacol. **63**: 1407–16.

BOASSA D., AMBROSI C., QIU F., DAHL G., GAIETTA G., SOSINSKY G., 2007 Pannexin1 channels contain a glycosylation site that targets the hexamer to the plasma membrane. J. Biol. Chem. **282**: 31733–43.

BOASSA D., QIU F., DAHL G., SOSINSKY G., 2008 Trafficking dynamics of glycosylated pannexin 1 proteins. Cell Commun. Adhes. **15**: 119–32.

BOBANOVIC L. K., ROYLE S. J., MURRELL-LAGNADO R. D., 2002 P2X receptor trafficking in neurons is subunit specific. J. Neurosci. **22**: 4814–24.

BODIN P., BURNSTOCK G., 2001 Evidence that release of adenosine triphosphate from endothelial cells during increased shear stress is vesicular. J. Cardiovasc. Pharmacol. **38**: 900–8.

BODNAR M., WANG H., RIEDEL T., HINTZE S., KATO E., FALLAH G., GRÖGER-ARNDT H., GINIATULLIN R., GROHMANN M., HAUSMANN R., SCHMALZING G., ILLES P., RUBINI P., 2011 Amino acid residues constituting the agonist binding site of the human P2X3 receptor. J. Biol. Chem. **286**: 2739–49.

BOLAND C., LI D., SHAH S. T. A., HABERSTOCK S., DÖTSCH V., BERNHARD F., CAFFREY M., 2014 Cell-free expression and in meso crystallisation of an integral membrane kinase for structure determination. Cell. Mol. Life Sci.

BONIFACINO J. S., DELL'ANGELICA E. C., SPRINGER T. A., 2001 Immunoprecipitation. Curr. Protoc. Protein Sci. **Chapter 9**: Unit 9.8.

BORNHORST J. A., FALKE J. J., 2000 Purification of proteins using polyhistidine affinity tags. Methods Enzymol. **326**: 245–54.

BOUÉ-GRABOT E., ARCHAMBAULT V., SÉGUÉLA P., 2000 A protein kinase C site highly conserved in P2X subunits controls the desensitization kinetics of P2X(2) ATP-gated channels. J. Biol. Chem. **275**: 10190–5.

BRACEY M. H., HANSON M. A., MASUDA K. R., STEVENS R. C., CRAVATT B. F., 2002 Structural adaptations in a membrane enzyme that terminates endocannabinoid signaling. Science **298**: 1793–6.

BRAND A. H., PERRIMON N., 1993 Targeted gene expression as a means of altering cell fates and generating dominant phenotypes. Development **118**: 401–15.

BRAUN K., RETTINGER J., GANSO M., KASSACK M., HILDEBRANDT C., ULLMANN H., NICKEL P., SCHMALZING G., LAMBRECHT G., 2001 NF449: a subnanomolar potency antagonist at recombinant rat P2X1 receptors. Naunyn. Schmiedebergs. Arch. Pharmacol. **364**: 285–90.

BRAY S., AMREIN H., 2003 A putative Drosophila pheromone receptor expressed in male-specific taste neurons is required for efficient courtship. Neuron **39**: 1019–29.

BRETSCHER M. S., 1972 Asymmetrical lipid bilayer structure for biological membranes. Nat. New Biol. **236**: 11–2.

BROTHERTON-PLEISS C. E., DILLON M. P., FORD A. P. D. W., GEVER J. R., CARTER D. S., GLEASON S. K., LIN C. J., MOORE A. G., THOMPSON A. W., VILLA M., ZHAI Y., 2010 Discovery and optimization of RO-85, a novel drug-like, potent, and selective P2X3 receptor antagonist. Bioorg. Med. Chem. Lett. **20**: 1031–6.

BUELL G., LEWIS C., COLLO G., NORTH R. A., SURPRENANT A., 1996 An antagonist-insensitive P2X receptor expressed in epithelia and brain. EMBO J. **15**: 55–62.

BURDA P., AEBI M., 1999 The dolichol pathway of N-linked glycosylation. Biochim. Biophys. Acta **1426**: 239–57.

BURNSTOCK G., CAMPBELL G., SATCHELL D., SMYTHE A., 1970 Evidence that adenosine triphosphate or a related nucleotide is the transmitter substance released by non-adrenergic inhibitory nerves in the gut. Br. J. Pharmacol. **40**: 668–88.

BURNSTOCK G., KENNEDY C., 1985 Is there a basis for distinguishing two types of P2-purinoceptor? Gen. Pharmacol. **16**: 433–40.

BURNSTOCK G., 2006 Purinergic signalling--an overview. Novartis Found. Symp. **276**: 26–48; discussion 48–57, 275–81.

BURNSTOCK G., 2007 Purine and pyrimidine receptors. Cell. Mol. Life Sci. **64**: 1471–83.

BURNSTOCK G., VERKHRATSKY A., 2010 Long-term (trophic) purinergic signalling: purinoceptors control cell proliferation, differentiation and death. Cell Death Dis. **1**: e9.

BURROUGHS A. M., IYER L. M., ARAVIND L., 2012 The natural history of ubiquitin and ubiquitin-related domains. Front. Biosci. (Landmark Ed. **17**: 1433–60.

CAMPOS A. R., GROSSMAN D., WHITE K., 1985 Mutant alleles at the locus elav in Drosophila melanogaster lead to nervous system defects. A developmental-genetic analysis. J. Neurogenet. **2**: 197–218.

CAMPOS A. R., ROSEN D. R., ROBINOW S. N., WHITE K., 1987 Molecular analysis of the locus elav in Drosophila melanogaster: a gene whose embryonic expression is neural specific. EMBO J. **6**: 425–31.

CAO L., YOUNG M. T., BROOMHEAD H. E., FOUNTAIN S. J., NORTH R. A., 2007 Thr339-to-serine substitution in rat P2X2 receptor second transmembrane domain causes constitutive opening and indicates a gating role for Lys308. J. Neurosci. **27**: 12916–23.

CARPENTER E. P., BEIS K., CAMERON A. D., IWATA S., 2008 Overcoming the challenges of membrane protein crystallography. Curr. Opin. Struct. Biol. **18**: 581–6.

CHANG V. T., CRISPIN M., ARICESCU A. R., HARVEY D. J., NETTLESHIP J. E., FENNELLY J. A., YU C., BOLES K. S., EVANS E. J., STUART D. I., DWEK R. A., JONES E. Y., OWENS R. J., DAVIS S. J., 2007 Glycoprotein structural genomics: solving the glycosylation problem. Structure **15**: 267–73.

CHATAIGNEAU T., LEMOINE D., GRUTTER T., 2013 Exploring the ATP-binding site of P2X receptors. Front. Cell. Neurosci. **7**: 273.

CHAUDHARY S., PAK J. E., GRUSWITZ F., SHARMA V., STROUD R. M., 2012 Overexpressing human membrane proteins in stably transfected and clonal human embryonic kidney 293S cells. Nat. Protoc. **7**: 453–66.

CHAUMONT S., JIANG L.-H., PENNA A., NORTH R. A., RASSENDREN F., 2004 Identification of a trafficking motif involved in the stabilization and polarization of P2X receptors. J. Biol. Chem. **279**: 29628–38.

CHEKENI F. B., ELLIOTT M. R., SANDILOS J. K., WALK S. F., KINCHEN J. M., LAZAROWSKI E. R., ARMSTRONG A. J., PENUELA S., LAIRD D. W., SALVESEN G. S., ISAKSON B. E., BAYLISS D. A., RAVICHANDRAN K. S., 2010 Pannexin 1 channels mediate "find-me" signal release and membrane permeability during apoptosis. Nature **467**: 863–867.

CHEN C. C., AKOPIAN A. N., SIVILOTTI L., COLQUHOUN D., BURNSTOCK G., WOOD J. N., 1995 A P2X purinoceptor expressed by a subset of sensory neurons. Nature **377**: 428–31.

CHEN Y.-J., PORNILLOS O., LIEU S., MA C., CHEN A. P., CHANG G., 2007 X-ray structure of EmrE supports dual topology model. Proc. Natl. Acad. Sci. U. S. A. **104**: 18999–9004.

CHESSELL I. P., MICHEL A. D., HUMPHREY P. P., 1998 Effects of antagonists at the human recombinant P2X7 receptor. Br. J. Pharmacol. **124**: 1314–20.

CHONG S., MONTELLO G. E., ZHANG A., CANTOR E. J., LIAO W., XU M. Q., BENNER J., 1998 Utilizing the C-terminal cleavage activity of a protein splicing element to purify recombinant proteins in a single chromatographic step. Nucleic Acids Res. **26**: 5109–15.

CIEŚLA J., FRĄCZYK T., RODE W., 2011 Phosphorylation of basic amino acid residues in proteins: important but easily missed. Acta Biochim. Pol. **58**: 137–48.

CLARK A. G., EISEN M. B., SMITH D. R., BERGMAN C. M., OLIVER B., MARKOW T. A., KAUFMAN T. C., KELLIS M., GELBART W., IYER V. N., POLLARD D. A., SACKTON T. B., LARRACUENTE A. M., SINGH N. D., ABAD J. P., ABT D. N., ADRYAN B., AGUADE M., AKASHI H., ANDERSON W. W., AQUADRO C. F., ARDELL D. H., ARGUELLO R., ARTIERI C. G., BARBASH D. A., BARKER D., BARSANTI P., BATTERHAM P., BATZOGLOU S., BEGUN D., BHUTKAR A., BLANCO E., BOSAK S. A., BRADLEY R. K., BRAND A. D., BRENT M. R., BROOKS A. N., BROWN R. H., BUTLIN R. K., CAGGESE C., CALVI B. R., BERNARDO DE CARVALHO A., CASPI A., CASTREZANA S., CELNIKER S. E., CHANG J. L., CHAPPLE C., CHATTERJI S., CHINWALLA A., CIVETTA A., CLIFTON S. W., COMERON J. M., COSTELLO J. C., COYNE J. A., DAUB J., DAVID R. G., DELCHER A. L., DELEHAUNTY K., DO C. B., EBLING H., EDWARDS K., EICKBUSH T., EVANS J. D., FILIPSKI A., FINDEISS S., FREYHULT E., FULTON L., FULTON R., GARCIA A. C. L., GARDINER A., GARFIELD D. A., GARVIN B. E., GIBSON G., GILBERT D., GNERRE S., GODFREY J., GOOD R., GOTEA V., GRAVELY B., GREENBERG A. J., GRIFFITHS-JONES S., GROSS S., GUIGO R., GUSTAFSON E. A., HAERTY W., HAHN M. W., HALLIGAN D. L., HALPERN A. L., HALTER G. M., HAN M. V, HEGER A., HILLIER L., HINRICHS A. S., HOLMES I., HOSKINS R. A., HUBISZ M. J., HULTMARK D., HUNTLEY M. A., JAFFE D. B., JAGADEESHAN S., JECK W. R., JOHNSON J., JONES C. D., JORDAN W. C., KARPEN G. H., KATAOKA E., KEIGHTLEY P. D., KHERADPOUR P., KIRKNESS E. F., KOERICH L. B., KRISTIANSEN K., KUDRNA D., KULATHINAL R. J., KUMAR S., KWOK R., LANDER E., LANGLEY C. H., LAPOINT R., LAZZARO B. P., LEE S.-J., LEVESQUE L., LI R., LIN C.-F., LIN M. F., LINDBLAD-TOH K., LLOPART A., LONG M., LOW L., LOZOVSKY E., LU J., LUO M., MACHADO C. A., MAKALOWSKI W., MARZO M., MATSUDA M., MATZKIN L., MCALLISTER B., MCBRIDE C. S., MCKERNAN B., MCKERNAN K., MENDEZ-LAGO M., MINX P., MOLLENHAUER M. U., MONTOOTH K., MOUNT S. M., MU X., MYERS E., NEGRE B., NEWFELD S., NIELSEN R., NOOR M. A. F., O'GRADY P., PACHTER L., PAPACEIT M., PARISI M. J., PARISI M., PARTS L., PEDERSEN J. S., PESOLE G., PHILLIPPY A. M., PONTING C. P., POP M., PORCELLI D., POWELL J. R., PROHASKA S., PRUITT K., PUIG M., QUESNEVILLE H., RAM K. R., RAND D., RASMUSSEN M. D., REED L. K., REENAN R., REILY A., REMINGTON K. A., RIEGER T. T.,

RITCHIE M. G., ROBIN C., ROGERS Y.-H., ROHDE C., ROZAS J., RUBENFIELD M. J., RUIZ A., RUSSO S., SALZBERG S. L., SANCHEZ-GRACIA A., SARANGA D. J., SATO H., SCHAEFFER S. W., SCHATZ M. C., SCHLENKE T., SCHWARTZ R., SEGARRA C., SINGH R. S., SIROT L., SIROTA M., SISNEROS N. B., SMITH C. D., SMITH T. F., SPIETH J., STAGE D. E., STARK A., STEPHAN W., STRAUSBERG R. L., STREMPEL S., STURGILL D., SUTTON G., SUTTON G. G., TAO W., TEICHMANN S., TOBARI Y. N., TOMIMURA Y., TSOLAS J. M., VALENTE V. L. S., VENTER E., VENTER J. C., VICARIO S., VIEIRA F. G., VILELLA A. J., VILLASANTE A., WALENZ B., WANG J., WASSERMAN M., WATTS T., WILSON D., WILSON R. K., WING R. A., WOLFNER M. F., WONG A., WONG G. K.-S., WU C.-I., WU G., YAMAMOTO D., YANG H.-P., YANG S.-P., YORKE J. A., YOSHIDA K., ZDOBNOV E., ZHANG P., ZHANG Y., ZIMIN A. V, BALDWIN J., ABDOUELLEIL A., ABDULKADIR J., ABEBE A., ABERA B., ABREU J., ACER S. C., AFTUCK L., ALEXANDER A., AN P., ANDERSON E., ANDERSON S., ARACHI H., AZER M., BACHANTSANG P., BARRY A., BAYUL T., BERLIN A., BESSETTE D., BLOOM T., BLYE J., BOGUSLAVSKIY L., BONNET C., BOUKHGALTER B., BOURZGUI I., BROWN A., CAHILL P., CHANNER S., CHESHATSANG Y., CHUDA L., CITROEN M., COLLYMORE A., COOKE P., COSTELLO M., D'ACO K., DAZA R., HAAN G. DE, DEGRAY S., DEMASO C., DHARGAY N., DOOLEY K., DOOLEY E., DORICENT M., DORJE P., DORJEE K., DUPES A., ELONG R., FALK J., FARINA A., FARO S., FERGUSON D., FISHER S., FOLEY C. D., FRANKE A., FRIEDRICH D., GADBOIS L., GEARIN G., GEARIN C. R., GIANNOUKOS G., GOODE T., GRAHAM J., GRANDBOIS E., GREWAL S., GYALTSEN K., HAFEZ N., HAGOS B., HALL J., HENSON C., HOLLINGER A., HONAN T., HUARD M. D., HUGHES L., HURHULA B., HUSBY M. E., KAMAT A., KANGA B., KASHIN S., KHAZANOVICH D., KISNER P., LANCE K., LARA M., LEE W., LENNON N., LETENDRE F., LEVINE R., LIPOVSKY A., LIU X., LIU J., LIU S., LOKYITSANG T., LOKYITSANG Y., LUBONJA R., LUI A., MACDONALD P., MAGNISALIS V., MARU K., MATTHEWS C., MCCUSKER W., MCDONOUGH S., MEHTA T., MELDRIM J., MENEUS L., MIHAI O., MIHALEV A., MIHOVA T., MITTELMAN R., MLENGA V., MONTMAYEUR A., MULRAIN L., NAVIDI A., NAYLOR J., NEGASH T., NGUYEN T., NGUYEN N., NICOL R., NORBU C., NORBU N., NOVOD N., O'NEILL B., OSMAN S., MARKIEWICZ E., OYONO O. L., PATTI C., PHUNKHANG P., PIERRE F., PRIEST M., RAGHURAMAN S., REGE F., REYES R., RISE C., ROGOV P., ROSS K., RYAN E., SETTIPALLI S., SHEA T., SHERPA N., SHI L., SHIH D., SPARROW T., SPAULDING J., STALKER J., STANGE-THOMANN N., STAVROPOULOS S., STONE C., STRADER C., TESFAYE S., THOMSON T., THOULUTSANG Y., THOULUTSANG D., TOPHAM K., TOPPING I., TSAMLA T., VASSILIEV H., VO A., WANGCHUK T., WANGDI T., WEIAND M., WILKINSON J., WILSON A., YADAV S., YOUNG G., YU Q., ZEMBEK L., ZHONG D., ZIMMER A., ZWIRKO Z., ALVAREZ P., BROCKMAN W., BUTLER J., CHIN C., GRABHERR M., KLEBER M., MAUCELI E., MACCALLUM I., 2007 Evolution of genes and genomes on the Drosophila phylogeny. Nature **450**: 203–18.

CLARKE S., 1993 Protein methylation. Curr. Opin. Cell Biol. **5**: 977–83.

CLYNE P. J., WARR C. G., CARLSON J. R., 2000 Candidate taste receptors in Drosophila. Science **287**: 1830–4.

COCKAYNE D. A., DUNN P. M., ZHONG Y., RONG W., HAMILTON S. G., KNIGHT G. E., RUAN H.-Z., MA B., YIP P., NUNN P., MCMAHON S. B., BURNSTOCK G., FORD A. P. D. W., 2005 P2X2 knockout mice and P2X2/P2X3 double knockout mice reveal a role for the P2X2 receptor subunit in mediating multiple sensory effects of ATP. J. Physiol. **567**: 621–39.

CODDOU C., YAN Z., OBSIL T., HUIDOBRO-TORO J. P., STOJILKOVIC S. S., 2011 Activation and regulation of purinergic P2X receptor channels. Pharmacol. Rev. **63**: 641–83.

COMPAN V., ULMANN L., STELMASHENKO O., CHEMIN J., CHAUMONT S., RASSENDREN F., 2012 P2X2 and P2X5 subunits define a new heteromeric receptor with P2X7-like properties. J. Neurosci. **32**: 4284–96.

CONGREVE M., ANDREWS S. P., DORÉ A. S., HOLLENSTEIN K., HURRELL E., LANGMEAD C. J., MASON J. S., NG I. W., TEHAN B., ZHUKOV A., WEIR M., MARSHALL F. H., 2012 Discovery of 1,2,4-triazine derivatives as adenosine A(2A) antagonists using structure based drug design. J. Med. Chem. **55**: 1898–903.

CROSS B. C. S., HIGH S., 2009 Dissecting the physiological role of selective transmembrane-segment retention at the ER translocon. J. Cell Sci. **122**: 1768–77.

DAHANUKAR A., FOSTER K., GOES VAN NATERS W. M. VAN DER, CARLSON J. R., 2001 A Gr receptor is required for response to the sugar trehalose in taste neurons of Drosophila. Nat. Neurosci. **4**: 1182–6.

DAHANUKAR A., LEI Y.-T., KWON J. Y., CARLSON J. R., 2007 Two Gr genes underlie sugar reception in Drosophila. Neuron **56**: 503–16.

DAMER S., NIEBEL B., CZECHE S., NICKEL P., ARDANUY U., SCHMALZING G., RETTINGER J., MUTSCHLER E., LAMBRECHT G., 1998 NF279: a novel potent and selective antagonist of P2X receptor-mediated responses. Eur. J. Pharmacol. **350**: R5–6.

DANDO R., ROPER S. D., 2009 Cell-to-cell communication in intact taste buds through ATP signalling from pannexin 1 gap junction hemichannels. J. Physiol. **587**: 5899–906.

DAVIES M. G., BERKOWITZ D. E., HAGEN P. O., 1995 Constitutive nitric oxide synthase is expressed and nitric oxide-mediated relaxation is preserved in retrieved human aortocoronary vein grafts. J. Surg. Res. **58**: 732–8.

DEISENHOFER J., EPP O., MIKI K., HUBER R., MICHEL H., 1985 Structure of the protein subunits in the photosynthetic reaction centre of Rhodopseudomonas viridis at 3Å resolution. Nature **318**: 618–24.

DEVASAHAYAM M., 2007 Factors affecting the expression of recombinant glycoproteins. Indian J. Med. Res. **126**: 22–7.

DIAZ-HERNANDEZ M., COX J. A., MIGITA K., HAINES W., EGAN T. M., VOIGT M. M., 2002 Cloning and characterization of two novel zebrafish P2X receptor subunits. Biochem. Biophys. Res. Commun. **295**: 849–53.

DIAZ-HERNANDEZ J. I., GOMEZ-VILLAFUERTES R., LEÓN-OTEGUI M., HONTECILLAS-PRIETO L., PUERTO A. DEL, TREJO J. L., LUCAS J. J., GARRIDO J. J., GUALIX J., MIRAS-PORTUGAL M. T., DIAZ-HERNANDEZ M., 2012 In vivo P2X7 inhibition reduces amyloid plaques in Alzheimer's disease through GSK3β and secretases. Neurobiol. Aging **33**: 1816–28.

DING S., SACHS F., 1999 Ion permeation and block of P2X(2) purinoceptors: single channel recordings. J. Membr. Biol. **172**: 215–23.

DONNELLY-ROBERTS D. L., NAMOVIC M. T., HAN P., JARVIS M. F., 2009 Mammalian P2X7 receptor pharmacology: comparison of recombinant mouse, rat and human P2X7 receptors. Br. J. Pharmacol. **157**: 1203–14.

DOROGHAZI J. R., JU K.-S., BROWN D. W., LABEDA D. P., DENG Z., METCALF W. W., CHEN W., PRICE N. P. J., 2011 Genome sequences of three tunicamycin-producing Streptomyces Strains, S. chartreusis NRRL 12338, S. chartreusis NRRL 3882, and S. lysosuperificus ATCC 31396. J. Bacteriol. **193**: 7021–2.

DUCKWITZ W., HAUSMANN R., ASCHRAFI A., SCHMALZING G., 2006 P2X5 subunit assembly requires scaffolding by the second transmembrane domain and a conserved aspartate. J. Biol. Chem. **281**: 39561–72.

DUFFY J. B., 2000 GAL4 system in Drosophila: a fly geneticist's Swiss army knife. Genesis **34**: 1–15.

DUNIPACE L., MEISTER S., MCNEALY C., AMREIN H., 2001 Spatially restricted expression of candidate taste receptors in the Drosophila gustatory system. Curr. Biol. **11**: 822–835.

DUTZLER R., CAMPBELL E. B., CADENE M., CHAIT B. T., MACKINNON R., 2002 X-ray structure of a ClC chloride channel at 3.0 A reveals the molecular basis of anion selectivity. Nature **415**: 287–94.

DUTZLER R., CAMPBELL E. B., MACKINNON R., 2003 Gating the selectivity filter in ClC chloride channels. Science **300**: 108–12.

DVIR H., CHOE S., 2009 Bacterial expression of a eukaryotic membrane protein in fusion to various Mistic orthologs. Protein Expr. Purif. **68**: 28–33.

DYKE M. W. VAN, SIRITO M., SAWADOGO M., 1992 Single-step purification of bacterially expressed polypeptides containing an oligo-histidine domain. Gene **111**: 99–104.

EARL J. B., BRITT S. G., 2006 Expression of Drosophila rhodopsins during photoreceptor cell differentiation: insights into R7 and R8 cell subtype commitment. Gene Expr. Patterns **6**: 687–94.

ECCLES J. C., 1964 *The Physiology of Synapses*. Elsevier Science.

EGAN T. M., HAINES W. R., VOIGT M. M., 1998 A domain contributing to the ion channel of ATP-gated P2X2 receptors identified by the substituted cysteine accessibility method. J. Neurosci. **18**: 2350–9.

ENNION S., HAGAN S., EVANS R. J., 2000 The role of positively charged amino acids in ATP recognition by human P2X(1) receptors. J. Biol. Chem. **275**: 29361–7.

ENNION S. J., EVANS R. J., 2002 Conserved cysteine residues in the extracellular loop of the human P2X(1) receptor form disulfide bonds and are involved in receptor trafficking to the cell surface. Mol. Pharmacol. **61**: 303–11.

ERHARDT J. A., PILLARISETTI K., TOOMEY J. R., 2003 Potentiation of platelet activation through the stimulation of P2X1 receptors. J. Thromb. Haemost. **1**: 2626–35.

ERHARDT A., LUCAE S., UNSCHULD P. G., ISING M., KERN N., SALYAKINA D., LIEB R., UHR M., BINDER E. B., KECK M. E., MÜLLER-MYHSOK B., HOLSBOER F., 2007 Association of polymorphisms in P2RX7 and CaMKKb with anxiety disorders. J. Affect. Disord. **101**: 159–68.

ERICKSON J., NEIDHART D. J., VANDRIE J., KEMPF D. J., WANG X. C., NORBECK D. W., PLATTNER J. J., RITTENHOUSE J. W., TURON M., WIDEBURG N., 1990 Design, activity, and 2.8 A crystal structure of a C2 symmetric inhibitor complexed to HIV-1 protease. Science **249**: 527–33.

EVANS R. J., LEWIS C., BUELL G., VALERA S., NORTH R. A., SURPRENANT A., 1995 Pharmacological characterization of heterologously expressed ATP-gated cation channels (P2x purinoceptors). Mol. Pharmacol. **48**: 178–83.

FERGUSON A. D., MCKEEVER B. M., XU S., WISNIEWSKI D., MILLER D. K., YAMIN T.-T., SPENCER R. H., CHU L., UJJAINWALLA F., CUNNINGHAM B. R., EVANS J. F., BECKER J. W., 2007 Crystal structure of inhibitor-bound human 5-lipoxygenase-activating protein. Science **317**: 510–2.

FERRARI D., PIZZIRANI C., GULINELLI S., CALLEGARI G., CHIOZZI P., IDZKO M., PANTHER E., VIRGILIO F. DI, 2007 Modulation of P2X7 receptor functions by polymyxin B: crucial role of the hydrophobic tail of the antibiotic molecule. Br. J. Pharmacol. **150**: 445–54.

FEUVRE R. A. LE, BROUGH D., IWAKURA Y., TAKEDA K., ROTHWELL N. J., 2002 Priming of macrophages with lipopolysaccharide potentiates P2X7-mediated cell death via a caspase-1-dependent mechanism, independently of cytokine production. J. Biol. Chem. **277**: 3210–8.

FINGER T. E., DANILOVA V., BARROWS J., BARTEL D. L., VIGERS A. J., STONE L., HELLEKANT G., KINNAMON S. C., 2005 ATP signaling is crucial for communication from taste buds to gustatory nerves. Science **310**: 1495–9.

FISCHER J. A., GINIGER E., MANIATIS T., PTASHNE M., 1988 GAL4 activates transcription in Drosophila. Nature **332**: 853–6.

FISCHER H., POLIKARPOV I., CRAIEVICH A. F., 2004 Average protein density is a molecular-weight-dependent function. Protein Sci. **13**: 2825–8.

FISCHER W., ZADORI Z., KULLNICK Y., GRÖGER-ARNDT H., FRANKE H., WIRKNER K., ILLES P., MAGER P. P., 2007 Conserved lysin and arginin residues in the extracellular loop of P2X(3) receptors are involved in agonist binding. Eur. J. Pharmacol. **576**: 7–17.

FOUNTAIN S. J., BURNSTOCK G., 2009 An evolutionary history of P2X receptors. Purinergic Signal. **5**: 269–72.

FREEMAN M., 2002 A fly's eye view of EGF receptor signalling. EMBO J. **21**: 6635–42.

FREEMAN WH, 2000 Protein Glycosylation in the ER and Golgi Complex.

FRICK A., ERIKSSON U. K., MATTIA F. DE, OBERG F., HEDFALK K., NEUTZE R., GRIP W. J. DE, DEEN P. M. T., TÖRNROTH-HORSEFIELD S., 2014 X-ray structure of human aquaporin 2 and its implications for nephrogenic diabetes insipidus and trafficking. Proc. Natl. Acad. Sci. U. S. A. **111**: 6305–10.

GADSBY D. C., 2009 Ion channels versus ion pumps: the principal difference, in principle. Nat. Rev. Mol. Cell Biol. **10**: 344–52.

GAN L., ALEXANDER J. M., WITTELSBERGER A., THOMAS B., ROSENBLATT M., 2006 Large-scale purification and characterization of human parathyroid hormone-1 receptor stably expressed in HEK293S GnTI- cells. Protein Expr. Purif. **47**: 296–302.

GARAVITO R. M., FERGUSON-MILLER S., 2001 Detergents as tools in membrane biochemistry. J. Biol. Chem. **276**: 32403–6.

GARCIA-GUZMAN M., STÜHMER W., SOTO F., 1997 Molecular characterization and pharmacological properties of the human P2X3 purinoceptor. Brain Res. Mol. Brain Res. **47**: 59–66.

GARGETT C. E., WILEY J. S., 1997 The isoquinoline derivative KN-62 a potent antagonist of the P2Z-receptor of human lymphocytes. Br. J. Pharmacol. **120**: 1483–90.

GEEST M. VAN, LOLKEMA J. S., 2000 Membrane topology and insertion of membrane proteins: search for topogenic signals. Microbiol. Mol. Biol. Rev. **64**: 13–33.

GEHI R., SHAO Q., LAIRD D. W., 2011 Pathways regulating the trafficking and turnover of pannexin1 protein and the role of the C-terminal domain. J. Biol. Chem. **286**: 27639–53.

GORDON J. L., 1986 Extracellular ATP: effects, sources and fate. Biochem. J. **233**: 309–19.

GREENSPAN R. J., FERVEUR J. F., 2000 Courtship in Drosophila. Annu. Rev. Genet. **34**: 205–232.

GREIG A. V. H., LINGE C., HEALY V., LIM P., CLAYTON E., RUSTIN M. H. A., MCGROUTHER D. A., BURNSTOCK G., 2003 Expression of purinergic receptors in non-melanoma skin cancers and their functional roles in A431 cells. J. Invest. Dermatol. **121**: 315–27.

GROTH A. C., FISH M., NUSSE R., CALOS M. P., 2004 Construction of transgenic Drosophila by using the site-specific integrase from phage phiC31. Genetics **166**: 1775–82.

GRUBB B. D., EVANS R. J., 1999 Characterization of cultured dorsal root ganglion neuron P2X receptors. Eur. J. Neurosci. **11**: 149–154.

GRUENINGER-LEITCH F., D'ARCY A., D'ARCY B., CHÈNE C., 1996 Deglycosylation of proteins for crystallization using recombinant fusion protein glycosidases. Protein Sci. **5**: 2617–22.

GRUSWITZ F., CHAUDHARY S., HO J. D., SCHLESSINGER A., PEZESHKI B., HO C.-M., SALI A., WESTHOFF C. M., STROUD R. M., 2010 Function of human Rh based on structure of RhCG at 2.1 A. Proc. Natl. Acad. Sci. U. S. A. **107**: 9638–43.

GU J. G., MACDERMOTT A. B., 1997 Activation of ATP P2X receptors elicits glutamate release from sensory neuron synapses. Nature **389**: 749–53.

GU B. J., ZHANG W. Y., BENDALL L. J., CHESSELL I. P., BUELL G. N., WILEY J. S., 2000 Expression of P2X(7) purinoceptors on human lymphocytes and monocytes: evidence for nonfunctional P2X(7) receptors. Am J Physiol Cell Physiol **279**: C1189–97.

GUARENTE L., YOCUM R. R., GIFFORD P., 1982 A GAL10-CYC1 hybrid yeast promoter identifies the GAL4 regulatory region as an upstream site. Proc. Natl. Acad. Sci. U. S. A. **79**: 7410–4.

GUDIPATY L., HUMPHREYS B. D., BUELL G., DUBYAK G. R., 2001 Regulation of P2X(7) nucleotide receptor function in human monocytes by extracellular ions and receptor density. Am J Physiol Cell Physiol **280**: C943–53.

GUTMANN D. A. P., MIZOHATA E., NEWSTEAD S., FERRANDON S., POSTIS V., XIA X., HENDERSON P. J. F., VEEN H. W. VAN, BYRNE B., 2007 A high-throughput method for membrane protein solubility screening: the ultracentrifugation dispersity sedimentation assay. Protein Sci. **16**: 1422–8.

HAGEL L., 2001 Gel-filtration chromatography. Curr. Protoc. Mol. Biol. **Chapter 10**: Unit 10.9.

HARDIE R. C., RAGHU P., 2001 Visual transduction in Drosophila. Nature **413**: 186–93.

HARDIE R. C., 2001 Phototransduction in Drosophila melanogaster. J. Exp. Biol. **204**: 3403–9.

HASSAINE G., DELUZ C., GRASSO L., WYSS R., TOL M. B., HOVIUS R., GRAFF A., STAHLBERG H., TOMIZAKI T., DESMYTER A., MOREAU C., LI X.-D., POITEVIN F., VOGEL H., NURY H., 2014 X-ray structure of the mouse serotonin 5-HT3 receptor. Nature **512**: 276–281.

HATTORI M., GOUAUX E., 2012 Molecular mechanism of ATP binding and ion channel activation in P2X receptors. Nature **485**: 207–12.

HAYDEN J. D., BROWN L. R., GUNAWARDENA H. P., PERKOWSKI E. F., CHEN X., BRAUNSTEIN M., 2013 Reversible acetylation regulates acetate and propionate metabolism in Mycobacterium smegmatis. Microbiology **159**: 1986–99.

HECHLER B., LENAIN N., MARCHESE P., VIAL C., HEIM V., FREUND M., CAZENAVE J.-P., CATTANEO M., RUGGERI Z. M., EVANS R., GACHET C., 2003 A role of the fast ATP-gated P2X1 cation channel in thrombosis of small arteries in vivo. J. Exp. Med. **198**: 661–7.

HEFTI M. H., VUGT-VAN DER TOORN C. J. VAN, DIXON R., VERVOORT J., 2001 A novel purification method for histidine-tagged proteins containing a thrombin cleavage site. Anal. Biochem. **295**: 180–5.

HEJJAS K., SZEKELY A., DOMOTOR E., HALMAI Z., BALOGH G., SCHILLING B., SAROSI A., FALUDI G., SASVARI-SZEKELY M., NEMODA Z., 2009 Association between depression and the Gln460Arg polymorphism of P2RX7 gene: a dimensional approach. Am. J. Med. Genet. B. Neuropsychiatr. Genet. **150B**: 295–9.

HELENIUS A., AEBI M., 2004 Roles of N-linked glycans in the endoplasmic reticulum. Annu. Rev. Biochem. **73**: 1019–49.

HERNANDEZ-OLMOS V., ABDELRAHMAN A., EL-TAYEB A., FREUDENDAHL D., WEINHAUSEN S., MÜLLER C. E., 2012 N-substituted phenoxazine and acridone derivatives: structure-activity relationships of potent P2X4 receptor antagonists. J. Med. Chem. **55**: 9576–88.

HIROI M., MEUNIER N., MARION-POLL F., TANIMURA T., 2004 Two antagonistic gustatory receptor neurons responding to sweet-salty and bitter taste in Drosophila. J Neurobiol **61**: 333–342.

HODGSON E. S., LETTVIN J. Y., ROEDER K. D., 1955 Physiology of a primary chemoreceptor unit. Science **122**: 417–8.

HOLTON F. A., HOLTON P., 1954 The capillary dilator substances in dry powders of spinal roots; a possible role of adenosine triphosphate in chemical transmission from nerve endings. J. Physiol. **126**: 124–140.

HOLTON P., 1959 The liberation of adenosine triphosphate on antidromic stimulation of sensory nerves. J. Physiol. **145**: 494–504.

HONORE P., DONNELLY-ROBERTS D., NAMOVIC M. T., HSIEH G., ZHU C. Z., MIKUSA J. P., HERNANDEZ G., ZHONG C., GAUVIN D. M., CHANDRAN P., HARRIS R., MEDRANO A. P., CARROLL W., MARSH K., SULLIVAN J. P., FALTYNEK C. R., JARVIS M. F., 2006 A-740003 [N-(1-{[(cyanoimino)(5-quinolinylamino) methyl]amino}-2,2-dimethylpropyl)-2-(3,4-dimethoxyphenyl)acetamide], a novel and selective P2X7 receptor antagonist, dose-dependently reduces neuropathic pain in the rat. J. Pharmacol. Exp. Ther. **319**: 1376–85.

HU B., SENKLER C., YANG A., SOTO F., LIANG B. T., 2002 P2X4 receptor is a glycosylated cardiac receptor mediating a positive inotropic response to ATP. J. Biol. Chem. **277**: 15752–7.

HU A., ZHANG W., WANG Z., 2010 Functional feedback from mushroom bodies to antennal lobes in the Drosophila olfactory pathway. Proc. Natl. Acad. Sci. U. S. A. **107**: 10262–7.

HUANG Y., LEMIEUX M. J., SONG J., AUER M., WANG D.-N., 2003 Structure and mechanism of the glycerol-3-phosphate transporter from Escherichia coli. Science **301**: 616–20.

HUANG Y. A., STONE L. M., PEREIRA E., YANG R., KINNAMON J. C., DVORYANCHIKOV G., CHAUDHARI N., FINGER T. E., KINNAMON S. C., ROPER S. D., 2011 Knocking out P2X receptors reduces transmitter secretion in taste buds. J. Neurosci. **31**: 13654–61.

HUDLICKA O., BROWN M., EGGINTON S., 1992 Angiogenesis in skeletal and cardiac muscle. Physiol. Rev. **72**: 369–417.

HÜLSMANN M., NICKEL P., KASSACK M., SCHMALZING G., LAMBRECHT G., MARKWARDT F., 2003 NF449, a novel picomolar potency antagonist at human P2X1 receptors. Eur. J. Pharmacol. **470**: 1–7.

HUNSKAAR S., HOLE K., 1987 The formalin test in mice: dissociation between inflammatory and non-inflammatory pain. Pain **30**: 103–14.

ICHIMIYA T., MANYA H., OHMAE Y., YOSHIDA H., TAKAHASHI K., UEDA R., ENDO T., NISHIHARA S., 2004 The twisted abdomen phenotype of Drosophila POMT1 and POMT2 mutants coincides with their heterophilic protein O-mannosyltransferase activity. J. Biol. Chem. **279**: 42638–47.

INOUE M., TERADA T., OKUDA M., INUI K.-I., 2005 Regulation of human peptide transporter 1 (PEPT1) in gastric cancer cells by anticancer drugs. Cancer Lett. **230**: 72–80.

ISHIMOTO H., TAKAHASHI K., UEDA R., TANIMURA T., 2005 G-protein gamma subunit 1 is required for sugar reception in Drosophila. EMBO J. **24**: 3259–65.

ISONO K., MORITA H., 2010 Molecular and cellular designs of insect taste receptor system. Front. Cell. Neurosci. **4**: 20.

ITZSTEIN M. VON, WU W. Y., KOK G. B., PEGG M. S., DYASON J. C., JIN B., PHAN T. VAN, SMYTHE M. L., WHITE H. F., OLIVER S. W., 1993 Rational design of potent sialidase-based inhibitors of influenza virus replication. Nature **363**: 418–23.

JAAKOLA V.-P., GRIFFITH M. T., HANSON M. A., CHEREZOV V., CHIEN E. Y. T., LANE J. R., IJZERMAN A. P., STEVENS R. C., 2008 The 2.6 angstrom crystal structure of a human A2A adenosine receptor bound to an antagonist. Science **322**: 1211–7.

JACKSON A. M., BOUTELL J., COOLEY N., HE M., 2004 Cell-free protein synthesis for proteomics. Brief. Funct. Genomic. Proteomic. **2**: 308–19.

JANKNECHT R., MARTYNOFF G. DE, LOU J., HIPSKIND R. A., NORDHEIM A., STUNNENBERG H. G., 1991 Rapid and efficient purification of native histidine-tagged protein expressed by recombinant vaccinia virus. Proc. Natl. Acad. Sci. U. S. A. **88**: 8972–6.

JANKNECHT R., NORDHEIM A., 1992 Affinity purification of histidine-tagged proteins transiently produced in HeLa cells. Gene **121**: 321–4.

JARVIS M. F., BIANCHI B., UCHIC J. T., CARTMELL J., LEE C.-H., WILLIAMS M., FALTYNEK C., 2004 [3H]A-317491, a novel high-affinity non-nucleotide antagonist that specifically labels human P2X2/3 and P2X3 receptors. J. Pharmacol. Exp. Ther. **310**: 407–16.

JENNINGS B. H., 2011 Drosophila – a versatile model in biology & medicine. Mater. Today **14**: 190–195.

JENTSCH T. J., HÜBNER C. A., FUHRMANN J. C., 2004 Ion channels: function unravelled by dysfunction. Nat. Cell Biol. **6**: 1039–47.

JIANG L. H., MACKENZIE A. B., NORTH R. A., SURPRENANT A., 2000a Brilliant blue G selectively blocks ATP-gated rat P2X(7) receptors. Mol. Pharmacol. **58**: 82–8.

JIANG L. H., RASSENDREN F., SURPRENANT A., NORTH R. A., 2000b Identification of amino acid residues contributing to the ATP-binding site of a purinergic P2X receptor. J. Biol. Chem. **275**: 34190–6.

JIANG R., LEMOINE D., MARTZ A., TALY A., GONIN S., PRADO DE CARVALHO L., SPECHT A., GRUTTER T., 2011 Agonist trapped in ATP-binding sites of the P2X2 receptor. Proc. Natl. Acad. Sci. U. S. A. **108**: 9066–71.

JIAO Y., MOON S. J., MONTELL C., 2007 A Drosophila gustatory receptor required for the responses to sucrose, glucose, and maltose identified by mRNA tagging. Proc. Natl. Acad. Sci. U. S. A. **104**: 14110–5.

JIMENEZ-PACHECO A., MESURET G., SANZ-RODRIGUEZ A., TANAKA K., MOONEY C., CONROY R., MIRAS-PORTUGAL M. T., DIAZ-HERNANDEZ M., HENSHALL D. C., ENGEL T., 2013 Increased neocortical expression of the P2X7 receptor after status epilepticus and anticonvulsant effect of P2X7 receptor antagonist A-438079. Epilepsia **54**: 1551–61.

JOHNSON E. C., PAK W. L., 1986 Electrophysiological study of Drosophila rhodopsin mutants. J. Gen. Physiol. **88**: 651–73.

JONES C. A., CHESSELL I. P., SIMON J., BARNARD E. A., MILLER K. J., MICHEL A. D., HUMPHREY P. P., 2000 Functional characterization of the P2X(4) receptor orthologues. Br. J. Pharmacol. **129**: 388–94.

JONES C. A., VIAL C., SELLERS L. A., HUMPHREY P. P. A., EVANS R. J., CHESSELL I. P., 2004 Functional regulation of P2X6 receptors by N-linked glycosylation: identification of a novel alpha beta-methylene ATP-sensitive phenotype. Mol. Pharmacol. **65**: 979–85.

JONES S., EVANS R. J., MAHAUT-SMITH M. P., 2014 Ca2+ influx through P2X1 receptors amplifies P2Y1 receptor-evoked Ca2+ signaling and ADP-evoked platelet aggregation. Mol. Pharmacol. **86**: 243–51.

JUNG K.-Y., MOON H. D., LEE G. E., LIM H.-H., PARK C.-S., KIM Y.-C., 2007 Structure-activity relationship studies of spinorphin as a potent and selective human P2X(3) receptor antagonist. J. Med. Chem. **50**: 4543–7.

KACZMAREK-HÁJEK K., LÖRINCZI E., HAUSMANN R., NICKE A., 2012 Molecular and functional properties of P2X receptors--recent progress and persisting challenges. Purinergic Signal. **8**: 375–417.

KAIN P., BADSHA F., HUSSAIN S. M., NAIR A., HASAN G., RODRIGUES V., 2010 Mutants in phospholipid signaling attenuate the behavioral response of adult Drosophila to trehalose. Chem. Senses **35**: 663–73.

KALIPATNAPU S., CHATTOPADHYAY A., 2005 Membrane protein solubilization: recent advances and challenges in solubilization of serotonin1A receptors. IUBMB Life **57**: 505–12.

KARAKAS E., FURUKAWA H., 2014 Crystal structure of a heterotetrameric NMDA receptor ion channel. Science **344**: 992–7.

KASLOW D. C., SHILOACH J., 1994 Production, purification and immunogenicity of a malaria transmission-blocking vaccine candidate: TBV25H expressed in yeast and purified using nickel-NTA agarose. Biotechnology. (N. Y). **12**: 494–9.

KATOH T., TIEMEYER M., 2013 The N's and O's of Drosophila glycoprotein glycobiology. Glycoconj. J. **30**: 57–66.

KAWATE T., MICHEL J. C., BIRDSONG W. T., GOUAUX E., 2009 Crystal structure of the ATP-gated P2X(4) ion channel in the closed state. Nature **460**: 592–8.

KEFALA G., KWIATKOWSKI W., ESQUIVIES L., MASLENNIKOV I., CHOE S., 2007 Application of Mistic to improving the expression and membrane integration of histidine kinase receptors from Escherichia coli. J. Struct. Funct. Genomics **8**: 167–72.

KEW J., DAVIES C., 2010 *Ion Channels: From Structure to Function*. Oxford University Press.

KHAKH B. S., BURNSTOCK G., KENNEDY C., KING B. F., NORTH R. A., SÉGUÉLA P., VOIGT M., HUMPHREY P. P., 2001a International union of pharmacology. XXIV. Current status of the nomenclature and properties of P2X receptors and their subunits. Pharmacol. Rev. **53**: 107–18.

KHAKH B. S., SMITH W. B., CHIU C. S., JU D., DAVIDSON N., LESTER H. A., 2001b Activation-dependent changes in receptor distribution and dendritic morphology in hippocampal neurons expressing P2X2-green fluorescent protein receptors. Proc. Natl. Acad. Sci. U. S. A. **98**: 5288–93.

KHAKH B. S., NORTH R. A., 2006 P2X receptors as cell-surface ATP sensors in health and disease. Nature **442**: 527–32.

KING B. F., WILDMAN S. S., ZIGANSHINA L. E., PINTOR J., BURNSTOCK G., 1997 Effects of extracellular pH on agonism and antagonism at a recombinant P2X2 receptor. Br. J. Pharmacol. **121**: 1445–53.

KING B. F., LIU M., PINTOR J., GUALIX J., MIRAS-PORTUGAL M. T., BURNSTOCK G., 1999 Diinosine pentaphosphate (IP5I) is a potent antagonist at recombinant rat P2X1 receptors. Br. J. Pharmacol. **128**: 981–8.

KLAPPERSTÜCK M., BÜTTNER C., NICKEL P., SCHMALZING G., LAMBRECHT G., MARKWARDT F., 2000 Antagonism by the suramin analogue NF279 on human P2X(1) and P2X(7) receptors. Eur. J. Pharmacol. **387**: 245–52.

KOTNIS S., BINGHAM B., VASILYEV D. V, MILLER S. W., BAI Y., YEOLA S., CHANDA P. K., BOWLBY M. R., KAFTAN E. J., SAMAD T. A., WHITESIDE G. T., 2010 Genetic and functional analysis of human P2X5 reveals a distinct pattern of exon 10 polymorphism with predominant expression of the nonfunctional receptor isoform. Mol. Pharmacol. **77**: 953–60.

KOTO M., TANOUYE M. A., FERRUS A., THOMAS J. B., WYMAN R. J., 1981 The morphology of the cervical giant fiber neuron of Drosophila. Brain Res. **221**: 213–7.

KRACUN S., CHAPTAL V., ABRAMSON J., KHAKH B. S., 2010 Gated access to the pore of a P2X receptor: structural implications for closed-open transitions. J. Biol. Chem. **285**: 10110–21.

KRAMER J. M., STAVELEY B. E., 2003 GAL4 causes developmental defects and apoptosis when expressed in the developing eye of Drosophila melanogaster. Genet. Mol. Res. **2**: 43–7.

KUCENAS S., LI Z., COX J. A., EGAN T. M., VOIGT M. M., 2003 Molecular characterization of the zebrafish P2X receptor subunit gene family. Neuroscience **121**: 935–45.

KUMAR J. P., READY D. F., 1995 Rhodopsin plays an essential structural role in Drosophila photoreceptor development. Development **121**: 4359–70.

KUUSINEN A., ARVOLA M., OKER-BLOM C., KEINÄNEN K., 1995 Purification of recombinant GluR-D glutamate receptor produced in Sf21 insect cells. Eur. J. Biochem. **233**: 720–6.

LABASI J. M., PETRUSHOVA N., DONOVAN C., MCCURDY S., LIRA P., PAYETTE M. M., BRISSETTE W., WICKS J. R., AUDOLY L., GABEL C. A., 2002 Absence of the P2X7 receptor alters leukocyte function and attenuates an inflammatory response. J. Immunol. **168**: 6436–45.

LAMBRECHT G., FRIEBE T., GRIMM U., WINDSCHEIF U., BUNGARDT E., HILDEBRANDT C., BÄUMERT H. G., SPATZ-KÜMBEL G., MUTSCHLER E., 1992 PPADS, a novel functionally selective antagonist of P2 purinoceptor-mediated responses. Eur. J. Pharmacol. **217**: 217–9.

LAMPING E., MONK B. C., NIIMI K., HOLMES A. R., TSAO S., TANABE K., NIIMI M., UEHARA Y., CANNON R. D., 2007 Characterization of three classes of membrane proteins involved in fungal azole resistance by functional hyperexpression in Saccharomyces cerevisiae. Eukaryot. Cell **6**: 1150–65.

LAUGHON A., GESTELAND R. F., 1984 Primary structure of the Saccharomyces cerevisiae GAL4 gene. Mol. Cell. Biol. **4**: 260–7.

LÊ K. T., PAQUET M., NOUEL D., BABINSKI K., SÉGUÉLA P., 1997 Primary structure and expression of a naturally truncated human P2X ATP receptor subunit from brain and immune system. FEBS Lett. **418**: 195–9.

LEBON G., WARNE T., EDWARDS P. C., BENNETT K., LANGMEAD C. J., LESLIE A. G. W., TATE C. G., 2011 Agonist-bound adenosine A2A receptor structures reveal common features of GPCR activation. Nature **474**: 521–5.

LECKER S. H., GOLDBERG A. L., MITCH W. E., 2006 Protein degradation by the ubiquitin-proteasome pathway in normal and disease states. J. Am. Soc. Nephrol. **17**: 1807–19.

LEDERKREMER G. Z., 2009 Glycoprotein folding, quality control and ER-associated degradation. Curr. Opin. Struct. Biol. **19**: 515–23.

LEE Y., MOON S. J., MONTELL C., 2009 Multiple gustatory receptors required for the caffeine response in Drosophila. Proc. Natl. Acad. Sci. U. S. A. **106**: 4495–500.

LEE C.-H., LÜ W., MICHEL J. C., GOEHRING A., DU J., SONG X., GOUAUX E., 2014 NMDA receptor structures reveal subunit arrangement and pore architecture. Nature **511**: 191–197.

LEMMON M. A., SCHLESSINGER J., 2010 Cell signaling by receptor tyrosine kinases. Cell **141**: 1117–34.

LENERTZ L. Y., WANG Z., GUADARRAMA A., HILL L. M., GAVALA M. L., BERTICS P. J., 2010 Mutation of putative N-linked glycosylation sites on the human nucleotide receptor P2X7 reveals a key residue important for receptor function. Biochemistry **49**: 4611–9.

LEWIS C., NEIDHART S., HOLY C., NORTH R. A., BUELL G., SURPRENANT A., 1995 Coexpression of P2X2 and P2X3 receptor subunits can account for ATP-gated currents in sensory neurons. Nature **377**: 432–5.

LEWIS C. J., EVANS R. J., 2000 Lack of run-down of smooth muscle P2X receptor currents recorded with the amphotericin permeabilized patch technique, physiological and pharmacological characterization of the properties of mesenteric artery P2X receptor ion channels. Br. J. Pharmacol. **131**: 1659–66.

LI F., GUO N., MA Y., NING B., WANG Y., KOU L., 2014 Inhibition of P2X4 suppresses joint inflammation and damage in collagen-induced arthritis. Inflammation **37**: 146–53.

LIAO M., CAO E., JULIUS D., CHENG Y., 2013 Structure of the TRPV1 ion channel determined by electron cryo-microscopy. Nature **504**: 107–12.

LIAO M., CAO E., JULIUS D., CHENG Y., 2014 Single particle electron cryo-microscopy of a mammalian ion channel. Curr. Opin. Struct. Biol. **27C**: 1–7.

LICHTY J. J., MALECKI J. L., AGNEW H. D., MICHELSON-HOROWITZ D. J., TAN S., 2005 Comparison of affinity tags for protein purification. Protein Expr. Purif. **41**: 98–105.

LIMA S. Q., MIESENBÖCK G., 2005 Remote control of behavior through genetically targeted photostimulation of neurons. Cell **121**: 141–52.

LIN D. M., GOODMAN C. S., 1994 Ectopic and increased expression of Fasciclin II alters motoneuron growth cone guidance. Neuron **13**: 507–23.

LIU M., KING B. F., DUNN P. M., RONG W., TOWNSEND-NICHOLSON A., BURNSTOCK G., 2001 Coexpression of P2X(3) and P2X(2) receptor subunits in varying amounts generates heterogeneous populations of P2X receptors that evoke a spectrum of agonist responses comparable to that seen in sensory neurons. J. Pharmacol. Exp. Ther. **296**: 1043–50.

LODISH H., BERK A., ZIPURSKY S. L., MATSUDAIRA P., BALTIMORE D., DARNELL J., 2000 Membrane Proteins.

LOHMAN A. W., WEAVER J. L., BILLAUD M., SANDILOS J. K., GRIFFITHS R., STRAUB A. C., PENUELA S., LEITINGER N., LAIRD D. W., BAYLISS D. A., ISAKSON B. E., 2012 S-nitrosylation inhibits pannexin 1 channel function. J. Biol. Chem. **287**: 39602–12.

LU M., FU D., 2007 Structure of the zinc transporter YiiP. Science **317**: 1746–8.

LUCAE S., SALYAKINA D., BARDEN N., HARVEY M., GAGNÉ B., LABBÉ M., BINDER E. B., UHR M., PAEZ-PEREDA M., SILLABER I., ISING M., BRÜCKL T., LIEB R., HOLSBOER F., MÜLLER-MYHSOK B., 2006 P2RX7, a gene coding for a purinergic ligand-gated ion channel, is associated with major depressive disorder. Hum. Mol. Genet. **15**: 2438–45.

LYNCH K. J., TOUMA E., NIFORATOS W., KAGE K. L., BURGARD E. C., BIESEN T. VAN, KOWALUK E. A., JARVIS M. F., 1999 Molecular and functional characterization of human P2X(2) receptors. Mol. Pharmacol. **56**: 1171–81.

MA J., YOSHIMURA M., YAMASHITA E., NAKAGAWA A., ITO A., TSUKIHARA T., 2004 Structure of rat monoamine oxidase A and its specific recognitions for substrates and inhibitors. J. Mol. Biol. **338**: 103–14.

MA W., HUI H., PELEGRIN P., SURPRENANT A., 2009 Pharmacological characterization of pannexin-1 currents expressed in mammalian cells. J. Pharmacol. Exp. Ther. **328**: 409–18.

MACAULEY-PATRICK S., FAZENDA M. L., MCNEIL B., HARVEY L. M., 2005 Heterologous protein production using the Pichia pastoris expression system. Yeast **22**: 249–70.

MAEDA S., NAKAGAWA S., SUGA M., YAMASHITA E., OSHIMA A., FUJIYOSHI Y., TSUKIHARA T., 2009 Structure of the connexin 26 gap junction channel at 3.5 A resolution. Nature **458**: 597–602.

MAHAUT-SMITH M. P., JONES S., EVANS R. J., 2011 The P2X1 receptor and platelet function. Purinergic Signal. **7**: 341–56.

MALEY F., TRIMBLE R. B., TARENTINO A. L., PLUMMER T. H., 1989 Characterization of glycoproteins and their associated oligosaccharides through the use of endoglycosidases. Anal. Biochem. **180**: 195–204.

MANDAL S., MOUDGIL M., MANDAL S. K., 2009 Rational drug design. Eur. J. Pharmacol. **625**: 90–100.

MARKSTEIN M., PITSOULI C., VILLALTA C., CELNIKER S. E., PERRIMON N., 2008 Exploiting position effects and the gypsy retrovirus insulator to engineer precisely expressed transgenes. Nat. Genet. **40**: 476–83.

MARQUEZ-KLAKA B., RETTINGER J., BHARGAVA Y., EISELE T., NICKE A., 2007 Identification of an intersubunit cross-link between substituted cysteine residues located in the putative ATP binding site of the P2X1 receptor. J. Neurosci. **27**: 1456–66.

MARQUEZ-KLAKA B., RETTINGER J., NICKE A., 2009 Inter-subunit disulfide cross-linking in homomeric and heteromeric P2X receptors. Eur. Biophys. J. **38**: 329–38.

MARUYAMA T., KANAJI T., NAKADE S., KANNO T., MIKOSHIBA K., 1997 2APB, 2-aminoethoxydiphenyl borate, a membrane-penetrable modulator of Ins(1,4,5)P3-induced Ca2+ release. J. Biochem. **122**: 498–505.

MASLENNIKOV I., KLAMMT C., HWANG E., KEFALA G., OKAMURA M., ESQUIVIES L., MÖRS K., GLAUBITZ C., KWIATKOWSKI W., JEON Y. H., CHOE S., 2010 Membrane domain structures of three classes of histidine kinase receptors by cell-free expression and rapid NMR analysis. Proc. Natl. Acad. Sci. U. S. A. **107**: 10902–7.

MIGITA K., HAINES W. R., VOIGT M. M., EGAN T. M., 2001 Polar residues of the second transmembrane domain influence cation permeability of the ATP-gated P2X(2) receptor. J. Biol. Chem. **276**: 30934–41.

MILLER P. S., ARICESCU A. R., 2014 Crystal structure of a human GABAA receptor. Nature **512**: 270–275.

MINSKAIA E., RYAN M. D., 2013 Protein coexpression using FMDV 2A: effect of “linker” residues. Biomed Res. Int. **2013**: 291730.

MIO K., KUBO Y., OGURA T., YAMAMOTO T., SATO C., 2005 Visualization of the trimeric P2X2 receptor with a crown-capped extracellular domain. Biochem. Biophys. Res. Commun. **337**: 998–1005.

MIO K., OGURA T., YAMAMOTO T., HIROAKI Y., FUJIYOSHI Y., KUBO Y., SATO C., 2009 Reconstruction of the P2X(2) receptor reveals a vase-shaped structure with lateral tunnels above the membrane. Structure **17**: 266–75.

MIROUX B., WALKER J. E., 1996 Over-production of proteins in Escherichia coli: mutant hosts that allow synthesis of some membrane proteins and globular proteins at high levels. J. Mol. Biol. **260**: 289–98.

MIRZABEKOV T., BANNERT N., FARZAN M., HOFMANN W., KOLCHINSKY P., WU L., WYATT R., SODROSKI J., 1999 Enhanced expression, native purification, and characterization of CCR5, a principal HIV-1 coreceptor. J. Biol. Chem. **274**: 28745–50.

MITCHELL B. K., ITAGAKI H., RIVET M. P., 1999 Peripheral and central structures involved in insect gustation. Microsc. Res. Tech. **47**: 401–15.

MOHANTY A. K., WIENER M. C., 2004 Membrane protein expression and production: effects of polyhistidine tag length and position. Protein Expr. Purif. **33**: 311–25.

MONTELL C., 2009 A taste of the Drosophila gustatory receptors. Curr Opin Neurobiol **19**: 345–353.

MOREMEN K. W., TIEMEYER M., NAIRN A. V, 2012 Vertebrate protein glycosylation: diversity, synthesis and function. Nat. Rev. Mol. Cell Biol. **13**: 448–62.

MORTH J. P., PEDERSEN B. P., TOUSTRUP-JENSEN M. S., SØRENSEN T. L.-M., PETERSEN J., ANDERSEN J. P., VILSEN B., NISSEN P., 2007 Crystal structure of the sodium-potassium pump. Nature **450**: 1043–9.

MÜLLER B. A., 2009 Imatinib and its successors--how modern chemistry has changed drug development. Curr. Pharm. Des. **15**: 120–33.

MULRYAN K., GITTERMAN D. P., LEWIS C. J., VIAL C., LECKIE B. J., COBB A. L., BROWN J. E., CONLEY E. C., BUELL G., PRITCHARD C. A., EVANS R. J., 2000 Reduced vas deferens contraction and male infertility in mice lacking P2X1 receptors. Nature **403**: 86–9.

MURGIA M., HANAU S., PIZZO P., RIPPA M., VIRGILIO F. DI, 1993 Oxidized ATP. An irreversible inhibitor of the macrophage purinergic P2Z receptor. J. Biol. Chem. **268**: 8199–203.

MUS-VETEAU I., 2010 Heterologous expression of membrane proteins for structural analysis. Methods Mol. Biol. **601**: 1–16.

NAGAE M., YAMAGUCHI Y., 2012 Function and 3D Structure of the N-Glycans on Glycoproteins. Int. J. Mol. Sci. **13**: 8398–429.

NEER E. J., 1995 Heterotrimeric C proteins: Organizers of transmembrane signals. Cell **80**: 249–257.

NELSON D. W., GREGG R. J., KORT M. E., PEREZ-MEDRANO A., VOIGHT E. A., WANG Y., GRAYSON G., NAMOVIC M. T., DONNELLY-ROBERTS D. L., NIFORATOS W., HONORE P., JARVIS M. F., FALTYNEK C. R., CARROLL W. A., 2006 Structure-activity relationship studies on a series of novel, substituted 1-benzyl-5-phenyltetrazole P2X7 antagonists. J. Med. Chem. **49**: 3659–66.

NEWBOLT A., STOOP R., VIRGINIO C., SURPRENANT A., NORTH R. A., BUELL G., RASSENDREN F., 1998 Membrane topology of an ATP-gated ion channel (P2X receptor). J. Biol. Chem. **273**: 15177–82.

NEWSTEAD S., KIM H., HEIJNE G. VON, IWATA S., DREW D., 2007 High-throughput fluorescent-based optimization of eukaryotic membrane protein overexpression and purification in Saccharomyces cerevisiae. Proc. Natl. Acad. Sci. U. S. A. **104**: 13936–41.

NÖRENBERG W., ILLES P., 2000 Neuronal P2X receptors: localisation and functional properties. Naunyn. Schmiedebergs. Arch. Pharmacol. **362**: 324–39.

NORTH R. A., 2002 Molecular physiology of P2X receptors. Physiol. Rev. **82**: 1013–67.

NORTH R. A., JARVIS M. F., 2013 P2X receptors as drug targets. Mol. Pharmacol. **83**: 759–69.

ORMOND S. J., BARRERA N. P., QURESHI O. S., HENDERSON R. M., EDWARDSON J. M., MURRELL-LAGNADO R. D., 2006 An uncharged region within the N terminus of the P2X6 receptor inhibits its assembly and exit from the endoplasmic reticulum. Mol. Pharmacol. **69**: 1692–700.

OTT C. M., LINGAPPA V. R., 2002 Integral membrane protein biosynthesis: why topology is hard to predict. J. Cell Sci. **115**: 2003–9.

PALCZEWSKI K., KUMASAKA T., HORI T., BEHNKE C. A., MOTOSHIMA H., FOX B. A., TRONG I. LE, TELLER D. C., OKADA T., STENKAMP R. E., YAMAMOTO M., MIYANO M., 2000 Crystal structure of rhodopsin: A G protein-coupled receptor. Science **289**: 739–45.

PALCZEWSKI K., 2006 G protein-coupled receptor rhodopsin. Annu. Rev. Biochem. **75**: 743–67.

PALMER E., FREEMAN T., 2004 Investigation into the use of C- and N-terminal GFP fusion proteins for subcellular localization studies using reverse transfection microarrays. Comp. Funct. Genomics **5**: 342–53.

PALMER I., WINGFIELD P. T., 2004 Preparation and extraction of insoluble (inclusion-body) proteins from Escherichia coli. Curr. Protoc. Protein Sci. **Chapter 6**: Unit 6.3.

PANCHIN Y., KELMANSON I., MATZ M., LUKYANOV K., USMAN N., LUKYANOV S., 2000 A ubiquitous family of putative gap junction molecules. Curr Biol **10**: R473–4.

PANNEELS V., KOCK I., KRIJNSE-LOCKER J., REZGAOUI M., SINNING I., 2011 Drosophila photoreceptor cells exploited for the production of eukaryotic membrane proteins: receptors, transporters and channels. PLoS One **6**: e18478.

PEDERSEN B. P., BUCH-PEDERSEN M. J., MORTH J. P., PALMGREN M. G., NISSEN P., 2007 Crystal structure of the plasma membrane proton pump. Nature **450**: 1111–4.

PELEGRIN P., SURPRENANT A., 2006 Pannexin-1 mediates large pore formation and interleukin-1beta release by the ATP-gated P2X7 receptor. EMBO J **25**: 5071–5082.

PELEGRIN P., SURPRENANT A., 2007 Pannexin-1 couples to maitotoxin- and nigericin-induced interleukin-1beta release through a dye uptake-independent pathway. J. Biol. Chem. **282**: 2386–94.

PELEGRIN P., SURPRENANT A., 2009 The P2X(7) receptor-pannexin connection to dye uptake and IL-1beta release. Purinergic Signal **5**: 129–137.

PENUELA S., BHALLA R., GONG X.-Q., COWAN K. N., CELETTI S. J., COWAN B. J., BAI D., SHAO Q., LAIRD D. W., 2007 Pannexin 1 and pannexin 3 are glycoproteins that exhibit many distinct characteristics from the connexin family of gap junction proteins. J. Cell Sci. **120**: 3772–83.

PENUELA S., BHALLA R., NAG K., LAIRD D. W., 2009 Glycosylation regulates pannexin intermixing and cellular localization. Mol Biol Cell **20**: 4313–4323.

PENUELA S., GEHI R., LAIRD D. W., 2012 The biochemistry and function of pannexin channels. Biochim Biophys Acta **1828**: 15–22.

PENUELA S., GEHI R., LAIRD D. W., 2013 The biochemistry and function of pannexin channels. Biochim. Biophys. Acta **1828**: 15–22.

PFEIFFER B. D., NGO T.-T. B., HIBBARD K. L., MURPHY C., JENETT A., TRUMAN J. W., RUBIN G. M., 2010 Refinement of tools for targeted gene expression in Drosophila. Genetics **186**: 735–55.

PICHAUD F., DESPLAN C., 2001 A new visualization approach for identifying mutations that affect differentiation and organization of the Drosophila ommatidia. Development **128**: 815–26.

PIERRE SE, PONTING L, STEFANCSIK R M. P. ST., 2014 FlyBase 102 - advanced approaches to interrogating FlyBase. Nucleic Acids Res. 42(D1)D780-D788.

PINTOR J., KING B. F., MIRAS-PORTUGAL M. T., BURNSTOCK G., 1996 Selectivity and activity of adenine dinucleotides at recombinant P2X2 and P2Y1 purinoceptors. Br. J. Pharmacol. **119**: 1006–12.

PRIVÉ G. G., 2007 Detergents for the stabilization and crystallization of membrane proteins. Methods **41**: 388–97.

QURESHI O. S., PARAMASIVAM A., YU J. C. H., MURRELL-LAGNADO R. D., 2007 Regulation of P2X4 receptors by lysosomal targeting, glycan protection and exocytosis. J. Cell Sci. **120**: 3838–49.

RADFORD K. M., VIRGINIO C., SURPRENANT A., NORTH R. A., KAWASHIMA E., 1997 Baculovirus expression provides direct evidence for heteromeric assembly of P2X2 and P2X3 receptors. J. Neurosci. **17**: 6529–33.

RALEVIC V., BURNSTOCK G., 1998 Receptors for purines and pyrimidines. Pharmacol. Rev. **50**: 413–92.

RAMAN P., CHEREZOV V., CAFFREY M., 2006 The Membrane Protein Data Bank. Cell. Mol. Life Sci. **63**: 36–51.

RAMJEESINGH M., HUAN L. J., GARAMI E., BEAR C. E., 1999 Novel method for evaluation of the oligomeric structure of membrane proteins. Biochem. J. **342 (Pt 1**: 119–23.

RASSENDREN F., BUELL G., NEWBOLT A., NORTH R. A., SURPRENANT A., 1997 Identification of amino acid residues contributing to the pore of a P2X receptor. EMBO J. **16**: 3446–54.

RECKEL S., SOBHANIFAR S., DURST F., LÖHR F., SHIROKOV V. A., DÖTSCH V., BERNHARD F., 2010 Strategies for the cell-free expression of membrane proteins. Methods Mol. Biol. **607**: 187–212.

REES D. C., DEANTONIO L., EISENBERG D., 1989 Hydrophobic organization of membrane proteins. Science **245**: 510–3.

REITER L. T., POTOCKI L., CHIEN S., GRIBSKOV M., BIER E., 2001 A systematic analysis of human disease-associated gene sequences in Drosophila melanogaster. Genome Res. **11**: 1114–25.

RENDIĆ D., WILSON I. B. H., PASCHINGER K., 2008 The Glycosylation Capacity of Insect Cells. Croat. Chem. Acta **81**: 7–21.

RETTINGER J., SCHMALZING G., DAMER S., MÜLLER G., NICKEL P., LAMBRECHT G., 2000a The suramin analogue NF279 is a novel and potent antagonist selective for the P2X1 receptor. Neuropharmacology **39**: 2044–2053.

RETTINGER J., ASCHRAFI A., SCHMALZING G., 2000b Roles of individual N-glycans for ATP potency and expression of the rat P2X1 receptor. J. Biol. Chem. **275**: 33542–7.

RETTINGER J., BRAUN K., HOCHMANN H., KASSACK M. U., ULLMANN H., NICKEL P., SCHMALZING G., LAMBRECHT G., 2005 Profiling at recombinant homomeric and heteromeric rat P2X receptors identifies the suramin analogue NF449 as a highly potent P2X1 receptor antagonist. Neuropharmacology **48**: 461–8.

RICHARDS S., LIU Y., BETTENCOURT B. R., HRADECKY P., LETOVSKY S., NIELSEN R., THORNTON K., HUBISZ M. J., CHEN R., MEISEL R. P., COURONNE O., HUA S., SMITH M. A., ZHANG P., LIU J., BUSSEMAKER H. J., BATENBURG M. F. VAN, HOWELLS S. L., SCHERER S. E., SODERGREN E., MATTHEWS B. B., CROSBY M. A., SCHROEDER A. J., ORTIZ-BARRIENTOS D., RIVES C. M., METZKER M. L., MUZNY D. M., SCOTT G., STEFFEN D., WHEELER D. A., WORLEY K. C., HAVLAK P., DURBIN K. J., EGAN A., GILL R., HUME J., MORGAN M. B., MINER G., HAMILTON C., HUANG Y., WALDRON L., VERDUZCO D., CLERC-BLANKENBURG K. P., DUBCHAK I., NOOR M. A. F., ANDERSON W., WHITE K. P., CLARK A. G., SCHAEFFER S. W., GELBART W., WEINSTOCK G. M., GIBBS R. A., 2005 Comparative genome sequencing of Drosophila pseudoobscura: chromosomal, gene, and cis-element evolution. Genome Res. **15**: 1–18.

ROBERTS J. A., EVANS R. J., 2007 Cysteine substitution mutants give structural insight and identify ATP binding and activation sites at P2X receptors. J. Neurosci. **27**: 4072–82.

ROBERTS J. A., DIGBY H. R., KARA M., AJOUZ S. EL, SUTCLIFFE M. J., EVANS R. J., 2008 Cysteine substitution mutagenesis and the effects of methanethiosulfonate reagents at P2X2 and P2X4 receptors support a core common mode of ATP action at P2X receptors. J. Biol. Chem. **283**: 20126–36.

ROBERTSON H. M., WARR C. G., CARLSON J. R., 2003 Molecular evolution of the insect chemoreceptor gene superfamily in Drosophila melanogaster. Proc Natl Acad Sci U S A **100 Suppl** : 14537–14542.

ROBINSON L. E., MURRELL-LAGNADO R. D., 2013 The trafficking and targeting of P2X receptors. Front Cell Neurosci **7**: 233.

ROGER S., MEI Z.-Z., BALDWIN J. M., DONG L., BRADLEY H., BALDWIN S. A., SURPRENANT A., JIANG L.-H., 2010 Single nucleotide polymorphisms that were identified in affective mood disorders affect ATP-activated P2X7 receptor functions. J. Psychiatr. Res. **44**: 347–55.

ROLF M. G., BREARLEY C. A., MAHAUT-SMITH M. P., 2001 Platelet shape change evoked by selective activation of P2X1 purinoceptors with alpha,beta-methylene ATP. Thromb. Haemost. **85**: 303–8.

ROMANOV R. A., BYSTROVA M. F., ROGACHEVSKAYA O. A., SADOVNIKOV V. B., SHESTOPALOV V. I., KOLESNIKOV S. S., 2012 The ATP permeability of pannexin 1 channels in a heterologous system and in mammalian taste cells is dispensable. J. Cell Sci. **125**: 5514–23.

ROOSILD T. P., GREENWALD J., VEGA M., CASTRONOVO S., RIEK R., CHOE S., 2005 NMR structure of Mistic, a membrane-integrating protein for membrane protein expression. Science **307**: 1317–21.

ROYLE S. J., BOBANOVIĆ L. K., MURRELL-LAGNADO R. D., 2002 Identification of a non-canonical tyrosine-based endocytic motif in an ionotropic receptor. J. Biol. Chem. **277**: 35378–85.

ROYLE S. J., QURESHI O. S., BOBANOVIĆ L. K., EVANS P. R., OWEN D. J., MURRELL-LAGNADO R. D., 2005 Non-canonical YXXGPhi endocytic motifs: recognition by AP2 and preferential utilization in P2X4 receptors. J. Cell Sci. **118**: 3073–80.

RUBIO M. E., SOTO F., 2001 Distinct Localization of P2X receptors at excitatory postsynaptic specializations. J. Neurosci. **21**: 641–53.

SAMWAYS D. S. K., KHAKH B. S., DUTERTRE S., EGAN T. M., 2011 Preferential use of unobstructed lateral portals as the access route to the pore of human ATP-gated ion channels (P2X receptors). Proc. Natl. Acad. Sci. U. S. A. **108**: 13800–5.

SAMWAYS D. S. K., KHAKH B. S., EGAN T. M., 2012 Allosteric modulation of Ca2+ flux in ligand-gated cation channel (P2X4) by actions on lateral portals. J. Biol. Chem. **287**: 7594–602.

SANDILOS J. K., BAYLISS D. A., 2012 Physiological mechanisms for the modulation of pannexin 1 channel activity. J. Physiol. **590**: 6257–66.

SANZ J. M., CHIOZZI P., FERRARI D., COLAIANNA M., IDZKO M., FALZONI S., FELLIN R., TRABACE L., VIRGILIO F. DI, 2009 Activation of microglia by amyloid {beta} requires P2X7 receptor expression. J. Immunol. **182**: 4378–85.

SATO K., PELLEGRINO M., NAKAGAWA T., NAKAGAWA T., VOSSHALL L. B., TOUHARA K., 2008 Insect olfactory receptors are heteromeric ligand-gated ion channels. Nature **452**: 1002–6.

SATO K., TANAKA K., TOUHARA K., 2011 Sugar-regulated cation channel formed by an insect gustatory receptor. Proc. Natl. Acad. Sci. U. S. A. **108**: 11680–5.

SCHMIDT T. G., SKERRA A., 1994 One-step affinity purification of bacterially produced proteins by means of the “Strep tag” and immobilized recombinant core streptavidin. J. Chromatogr. A **676**: 337–45.

SCHWEISGUTH F., NERO P., POSAKONY J. W., 1994 The sequence similarity of the Drosophila suppressor of hairless protein to the integrase domain has no functional significance in vivo. Dev. Biol. **166**: 812–4.

SCOTT K., BRADY R., CRAVCHIK A., MOROZOV P., RZHETSKY A., ZUKER C., AXEL R., 2001 A chemosensory gene family encoding candidate gustatory and olfactory receptors in Drosophila. Cell **104**: 661–73.

SEDDON A. M., CURNOW P., BOOTH P. J., 2004 Membrane proteins, lipids and detergents: not just a soap opera. Biochim. Biophys. Acta **1666**: 105–17.

SELLIER M.-J., REEB P., MARION-POLL F., 2011 Consumption of bitter alkaloids in Drosophila melanogaster in multiple-choice test conditions. Chem. Senses **36**: 323–34.

SILVERMAN W. R., RIVERO VACCARI J. P. DE, LOCOVEI S., QIU F., CARLSSON S. K., SCEMES E., KEANE R. W., DAHL G., 2009 The pannexin 1 channel activates the inflammasome in neurons and astrocytes. J. Biol. Chem. **284**: 18143–51.

SIM J. A., YOUNG M. T., SUNG H.-Y., NORTH R. A., SURPRENANT A., 2004 Reanalysis of P2X7 receptor expression in rodent brain. J. Neurosci. **24**: 6307–14.

SKUBE S. B., CHAVERRI J. M., GOODSON H. V, 2010 Effect of GFP tags on the localization of EB1 and EB1 fragments in vivo. Cytoskeleton (Hoboken). **67**: 1–12.

SMITH T. M., HICKS-BERGER C. A., KIM S., KIRLEY T. L., 2002 Cloning, expression, and characterization of a soluble calcium-activated nucleotidase, a human enzyme belonging to a new family of extracellular nucleotidases. Arch. Biochem. Biophys. **406**: 105–15.

SOBOLEVSKY A. I., ROSCONI M. P., GOUAUX E., 2009 X-ray structure, symmetry and mechanism of an AMPA-subtype glutamate receptor. Nature **462**: 745–56.

SOTO F., LAMBRECHT G., NICKEL P., STÜHMER W., BUSCH A. E., 1999 Antagonistic properties of the suramin analogue NF023 at heterologously expressed P2X receptors. Neuropharmacology **38**: 141–9.

STEVENS T. J., ARKIN I. T., 2000 Do more complex organisms have a greater proportion of membrane proteins in their genomes? Proteins **39**: 417–20.

STOCKER R. F., 2004 Taste perception: Drosophila - a model of good taste. Curr Biol **14**: R560–1.

STOKES L., JIANG L.-H., ALCARAZ L., BENT J., BOWERS K., FAGURA M., FURBER M., MORTIMORE M., LAWSON M., THEAKER J., LAURENT C., BRADDOCK M., SURPRENANT A., 2006 Characterization of a selective and potent antagonist of human P2X(7) receptors, AZ11645373. Br. J. Pharmacol. **149**: 880–7.

STOKES L., SCURRAH K., ELLIS J. A., CROMER B. A., SKARRATT K. K., GU B. J., HARRAP S. B., WILEY J. S., 2011 A loss-of-function polymorphism in the human P2X4 receptor is associated with increased pulse pressure. Hypertension **58**: 1086–92.

SURPRENANT A., RASSENDREN F., KAWASHIMA E., NORTH R. A., BUELL G., 1996 The cytolytic P2Z receptor for extracellular ATP identified as a P2X receptor (P2X7). Science **272**: 735–8.

SWAYNE L. A., SORBARA C. D., BENNETT S. A., 2010 Pannexin 2 is expressed by postnatal hippocampal neural progenitors and modulates neuronal commitment. J Biol Chem **285**: 24977–24986.

TATE C. G., 2001 Overexpression of mammalian integral membrane proteins for structural studies. FEBS Lett. **504**: 94–8.

TAVOULARIS S., SCAZZOCCHIO C., SOPHIANOPOULOU V., 2001 Functional expression and cellular localization of a green fluorescent protein-tagged proline transporter in Aspergillus nidulans. Fungal Genet. Biol. **33**: 115–25.

TAYLOR A. L., SCHWIEBERT L. M., SMITH J. J., KING C., JONES J. R., SORSCHER E. J., SCHWIEBERT E. M., 1999 Epithelial P2X purinergic receptor channel expression and function. J. Clin. Invest. **104**: 875–84.

TERPE K., 2003 Overview of tag protein fusions: from molecular and biochemical fundamentals to commercial systems. Appl. Microbiol. Biotechnol. **60**: 523–33.

THORNE N., CHROMEY C., BRAY S., AMREIN H., 2004 Taste perception and coding in Drosophila. Curr Biol **14**: 1065–1079.

THORPE H. M., SMITH M. C., 1998 In vitro site-specific integration of bacteriophage DNA catalyzed by a recombinase of the resolvase/invertase family. Proc. Natl. Acad. Sci. U. S. A. **95**: 5505–10.

TONDI D., POWERS R. A., CASELLI E., NEGRI M. C., BLÁZQUEZ J., COSTI M. P., SHOICHET B. K., 2001 Structure-based design and in-parallel synthesis of inhibitors of AmpC beta-lactamase. Chem. Biol. **8**: 593–611.

TORRES G. E., EGAN T. M., VOIGT M. M., 1998 N-Linked glycosylation is essential for the functional expression of the recombinant P2X2 receptor. Biochemistry **37**: 14845–51.

TOTH-ZSAMBOKI E., OURY C., CORNELISSEN H., VOS R. DE, VERMYLEN J., HOYLAERTS M. F., 2003 P2X1-mediated ERK2 activation amplifies the collagen-induced platelet secretion by enhancing myosin light chain kinase activation. J. Biol. Chem. **278**: 46661–7.

TSUDA M., SHIGEMOTO-MOGAMI Y., KOIZUMI S., MIZOKOSHI A., KOHSAKA S., SALTER M. W., INOUE K., 2003 P2X4 receptors induced in spinal microglia gate tactile allodynia after nerve injury. Nature **424**: 778–83.

UENO K., KOHATSU S., CLAY C., FORTE M., ISONO K., KIDOKORO Y., 2006 Gsalpha is involved in sugar perception in Drosophila melanogaster. J. Neurosci. **26**: 6143–52.

UNWIN N., 2005 Refined structure of the nicotinic acetylcholine receptor at 4A resolution. J. Mol. Biol. **346**: 967–89.

URSU D., EBERT P., LANGRON E., RUBLE C., MUNSIE L., ZOU W., FIJAL B., QIAN Y.-W., MCNEARNEY T. A., MOGG A., GRUBISHA O., MERCHANT K., SHER E., 2014 Gain and loss of function of P2X7 receptors: mechanisms, pharmacology and relevance to diabetic neuropathic pain. Mol. Pain **10**: 37.

VACCA F., GIUSTIZIERI M., CIOTTI M. T., MERCURI N. B., VOLONTÉ C., 2009 Rapid constitutive and ligand-activated endocytic trafficking of P2X receptor. J. Neurochem. **109**: 1031–41.

VACCA F., D'AMBROSI N., NESTOLA V., AMADIO S., GIUSTIZIERI M., CUCCHIARONI M. L., TOZZI A., VELLUZ M. C., MERCURI N. B., VOLONTÉ C., 2011 N-Glycans mutations rule oligomeric assembly and functional expression of P2X3 receptor for extracellular ATP. Glycobiology **21**: 634–43.

VALENTE M., WATTERSON S. J., PARKER M. D., FORD R. C., YOUNG M. T., 2011 Expression, purification, electron microscopy, N-glycosylation mutagenesis and molecular modeling of human P2X4 and Dictyostelium discoideum P2XA. Biochim. Biophys. Acta **1808**: 2859–66.

VALERA S., HUSSY N., EVANS R. J., ADAMI N., NORTH R. A., SURPRENANT A., BUELL G., 1994 A new class of ligand-gated ion channel defined by P2x receptor for extracellular ATP. Nature **371**: 516–9.

VIRGILIO F. DI, FERRARI D., ADINOLFI E., 2009 P2X(7): a growth-promoting receptor-implications for cancer. Purinergic Signal. **5**: 251–6.

VIRGINIO C., ROBERTSON G., SURPRENANT A., NORTH R. A., 1998 Trinitrophenyl-substituted nucleotides are potent antagonists selective for P2X1, P2X3, and heteromeric P2X2/3 receptors. Mol. Pharmacol. **53**: 969–73.

VULCHANOVA L., ARVIDSSON U., RIEDL M., WANG J., BUELL G., SURPRENANT A., NORTH R. A., ELDE R., 1996 Differential distribution of two ATP-gated channels (P2X receptors) determined by immunocytochemistry. Proc. Natl. Acad. Sci. U. S. A. **93**: 8063–7.

WADA T., SHIMONO K., KIKUKAWA T., HATO M., SHINYA N., KIM S. Y., KIMURA-SOMEYA T., SHIROUZU M., TAMOGAMI J., MIYAUCHI S., JUNG K.-H., KAMO N., YOKOYAMA S., 2011 Crystal structure of the eukaryotic light-driven proton-pumping rhodopsin, Acetabularia rhodopsin II, from marine alga. J. Mol. Biol. **411**: 986–98.

WAGNER S., KLEPSCH M. M., SCHLEGEL S., APPEL A., DRAHEIM R., TARRY M., HÖGBOM M., WIJK K. J. VAN, SLOTBOOM D. J., PERSSON J. O., GIER J.-W. DE, 2008 Tuning Escherichia coli for membrane protein overexpression. Proc. Natl. Acad. Sci. U. S. A. **105**: 14371–6.

WALDRON J. B., SAWYNOK J., 2004 Peripheral P2X receptors and nociception: interactions with biogenic amine systems. Pain **110**: 79–89.

WALKER J. E., SARASTE M., RUNSWICK M. J., GAY N. J., 1982 Distantly related sequences in the alpha- and beta-subunits of ATP synthase, myosin, kinases and other ATP-requiring enzymes and a common nucleotide binding fold. EMBO J. **1**: 945–51.

WANG Z., SINGHVI A., KONG P., SCOTT K., 2004a Taste representations in the Drosophila brain. Cell **117**: 981–991.

WANG Z., SINGHVI A., KONG P., SCOTT K., 2004b Taste representations in the Drosophila brain. Cell **117**: 981–91.

WANG H., ELFERICH J., GOUAUX E., 2012 Structures of LeuT in bicelles define conformation and substrate binding in a membrane-like context. Nat. Struct. Mol. Biol. **19**: 212–9.

WATANABE T., ITO Y., YAMADA T., HASHIMOTO M., SEKINE S., TANAKA H., 1994 The roles of the C-terminal domain and type III domains of chitinase A1 from Bacillus circulans WL-12 in chitin degradation. J. Bacteriol. **176**: 4465–72.

WEISS L. A., DAHANUKAR A., KWON J. Y., BANERJEE D., CARLSON J. R., 2011 The molecular and cellular basis of bitter taste in Drosophila. Neuron **69**: 258–72.

WEN H., EVANS R. J., 2009 Regions of the amino terminus of the P2X receptor required for modification by phorbol ester and mGluR1alpha receptors. J. Neurochem. **108**: 331–40.

WEWERS M. D., SARKAR A., 2009 P2X(7) receptor and macrophage function. Purinergic Signal. **5**: 189–95.

WHITE N., BUTLER P. E. M., BURNSTOCK G., 2005 Human melanomas express functional P2 X(7) receptors. Cell Tissue Res. **321**: 411–8.

WHITE N., BURNSTOCK G., 2006 P2 receptors and cancer. Trends Pharmacol. Sci. **27**: 211–7.

WHITE C. W., CHOONG Y.-T., SHORT J. L., EXINTARIS B., MALONE D. T., ALLEN A. M., EVANS R. J., VENTURA S., 2013 Male contraception via simultaneous knockout of α1A-adrenoceptors and P2X1-purinoceptors in mice. Proc. Natl. Acad. Sci. U. S. A. **110**: 20825–30.

WICHER D., SCHÄFER R., BAUERNFEIND R., STENSMYR M. C., HELLER R., HEINEMANN S. H., HANSSON B. S., 2008 Drosophila odorant receptors are both ligand-gated and cyclic-nucleotide-activated cation channels. Nature **452**: 1007–11.

WICKI-STORDEUR L. E., SWAYNE L. A., 2014 The emerging Pannexin 1 signalome: a new nexus revealed? Front. Cell. Neurosci. **7**: 287.

WILDMAN S. S., BROWN S. G., KING B. F., BURNSTOCK G., 1999 Selectivity of diadenosine polyphosphates for rat P2X receptor subunits. Eur. J. Pharmacol. **367**: 119–23.

WILDMAN S. S., BROWN S. G., RAHMAN M., NOEL C. A., CHURCHILL L., BURNSTOCK G., UNWIN R. J., KING B. F., 2002 Sensitization by extracellular Ca(2+) of rat P2X(5) receptor and its pharmacological properties compared with rat P2X(1). Mol. Pharmacol. **62**: 957–66.

WILKINSON W. J., JIANG L.-H., SURPRENANT A., NORTH R. A., 2006 Role of ectodomain lysines in the subunits of the heteromeric P2X2/3 receptor. Mol. Pharmacol. **70**: 1159–63.

WILLEMSEN N. M., HITCHEN E. M., BODETTI T. J., APOLLONI A., WARRILOW D., PILLER S. C., HARRICH D., 2006 Protein methylation is required to maintain optimal HIV-1 infectivity. Retrovirology **3**: 92.

WISOTSKY Z., MEDINA A., FREEMAN E., DAHANUKAR A., 2011 Evolutionary differences in food preference rely on Gr64e, a receptor for glycerol. Nat. Neurosci. **14**: 1534–41.

WOLF C., ROSEFORT C., FALLAH G., KASSACK M. U., HAMACHER A., BODNAR M., WANG H., ILLES P., KLESS A., BAHRENBERG G., SCHMALZING G., HAUSMANN R., 2011 Molecular determinants of potent P2X2 antagonism identified by functional analysis, mutagenesis, and homology docking. Mol. Pharmacol. **79**: 649–61.

WOOD C., WILLIAMS C., WALDRON G. J., 2004 Patch clamping by numbers. Drug Discov. Today **9**: 434–41.

WORTHINGTON R. A., SMART M. L., GU B. J., WILLIAMS D. A., PETROU S., WILEY J. S., BARDEN J. A., 2002 Point mutations confer loss of ATP-induced human P2X(7) receptor function. FEBS Lett. **512**: 43–6.

WU J., HOLSTEIN J. D., UPADHYAY G., LIN D.-T., CONWAY S., MULLER E., LECHLEITER J. D., 2007 Purinergic receptor-stimulated IP3-mediated Ca2+ release enhances neuroprotection by increasing astrocyte mitochondrial metabolism during aging. J. Neurosci. **27**: 6510–20.

WUU J. J., SWARTZ J. R., 2008 High yield cell-free production of integral membrane proteins without refolding or detergents. Biochim. Biophys. Acta **1778**: 1237–50.

XU G.-Y., HUANG L.-Y. M., 2002 Peripheral inflammation sensitizes P2X receptor-mediated responses in rat dorsal root ganglion neurons. J. Neurosci. **22**: 93–102.

YAMAMOTO K., SOKABE T., MATSUMOTO T., YOSHIMURA K., SHIBATA M., OHURA N., FUKUDA T., SATO T., SEKINE K., KATO S., ISSHIKI M., FUJITA T., KOBAYASHI M., KAWAMURA K., MASUDA H., KAMIYA A., ANDO J., 2006 Impaired flow-dependent control of vascular tone and remodeling in P2X4-deficient mice. Nat. Med. **12**: 133–7.

YAN D., ZHU Y., WALSH T., XIE D., YUAN H., SIRMACI A., FUJIKAWA T., WONG A. C. Y., LOH T. L., DU L., GRATI M., VLAJKOVIC S. M., BLANTON S., RYAN A. F., CHEN Z.-Y., THORNE P. R., KACHAR B., TEKIN M., ZHAO H.-B., HOUSLEY G. D., KING M.-C., LIU X. Z., 2013 Mutation of the ATP-gated P2X(2) receptor leads to progressive hearing loss and increased susceptibility to noise. Proc. Natl. Acad. Sci. U. S. A. **110**: 2228–33.

YANG C.-H., BELAWAT P., HAFEN E., JAN L. Y., JAN Y.-N., 2008 Drosophila egg-laying site selection as a system to study simple decision-making processes. Science **319**: 1679–83.

YAO K. M., WHITE K., 1994 Neural specificity of elav expression: defining a Drosophila promoter for directing expression to the nervous system. J. Neurochem. **63**: 41–51.

YAO Z., MACARA A. M., LELITO K. R., MINOSYAN T. Y., SHAFER O. T., 2012 Analysis of functional neuronal connectivity in the Drosophila brain. J. Neurophysiol. **108**: 684–96.

YEN M. R., SAIER JR. M. H., 2007 Gap junctional proteins of animals: the innexin/pannexin superfamily. Prog Biophys Mol Biol **94**: 5–14.

YOUNG M. T., ZHANG Y.-H., CAO L., BROOMHEAD H., JIANG L.-H., 2008 Role of the domain encompassing Arg304-Ile328 in rat P2X2 receptor conformation revealed by alterations in complex glycosylation at Asn298. Biochem. J. **416**: 137–43.

ZEMKOVA H., HE M.-L., KOSHIMIZU T., STOJILKOVIC S. S., 2004 Identification of ectodomain regions contributing to gating, deactivation, and resensitization of purinergic P2X receptors. J. Neurosci. **24**: 6968–78.

ZEMKOVA H., YAN Z., LIANG Z., JELINKOVA I., TOMIC M., STOJILKOVIC S. S., 2007 Role of aromatic and charged ectodomain residues in the P2X(4) receptor functions. J. Neurochem. **102**: 1139–50.

ZHANG J., YUN J., SHANG Z., ZHANG X., PAN B., 2009 Design and optimization of a linker for fusion protein construction. Prog. Nat. Sci. **19**: 1197–1200.

ZHANG J., ZHANG K., GAO Z.-G., PAOLETTA S., ZHANG D., HAN G. W., LI T., MA L., ZHANG W., MÜLLER C. E., YANG H., JIANG H., CHEREZOV V., KATRITCH V., JACOBSON K. A., STEVENS R. C., WU B., ZHAO Q., 2014 Agonist-bound structure of the human P2Y12 receptor. Nature **509**: 119–22.

ZHAO X., LI G., LIANG S., 2013 Several Affinity Tags Commonly Used in Chromatographic Purification. J. Anal. Methods Chem. **2013**: 581093.

ZIMMER M., 2002 Green fluorescent protein (GFP): applications, structure, and related photophysical behavior. Chem. Rev. **102**: 759–81.

ZIMMERMANN H., 2000 Extracellular metabolism of ATP and other nucleotides. Naunyn. Schmiedebergs. Arch. Pharmacol. **362**: 299–309.

ZUKER C. S., 1996 The biology of vision of Drosophila. Proc. Natl. Acad. Sci. U. S. A. **93**: 571–6.

Publications

Grimes L.M., Young M.T., (2014) Purinergic P2X receptors: structural and functional features depicted by X-ray and molecular modelling studies. *Curr. Med. Chem.* (accepted; in press)